Developing an antisense oligonucleotide treatment for Spinocerebellar Ataxia Type 3

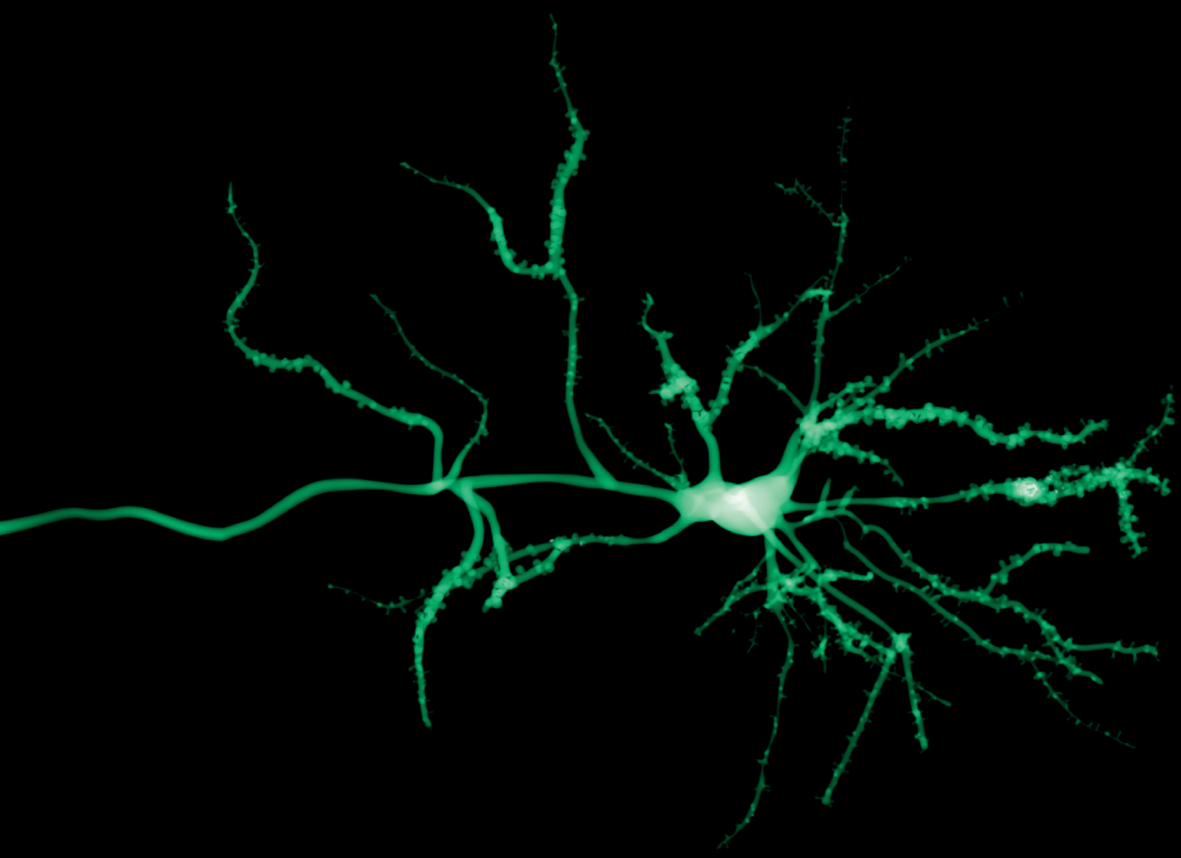

Lodewijk Toonen

DEVELOPING AN ANTISENSE OLIGONUCLEOTIDE TREATMENT FOR SPINOCEREBELLAR ATAXIA TYPE 3

Lodewijk J.A. Toonen

Cover design: Selvanegra, iStock photo

Layout and printing production: Off Page, Amsterdam

ISBN: 978-94-6182-883-5

Printing of this thesis was financially supported by ADCA vereniging Nederland

DEVELOPING AN ANTISENSE OLIGONUCLEOTIDE TREATMENT FOR SPINOCEREBELLAR ATAXIA TYPE 3

Proefschrift

ter verkrijging van
de graad van Doctor aan de Universiteit Leiden,
op gezag van Rector Magnificus prof.mr. C.J.J.M. Stolker,
volgens besluit van het College voor Promoties
te verdedigen op 31 mei 2018
klokke 15.00 uur

door

Lodewijk Julius Anton Toonen
geboren te 's-Hertogenbosch
in 1988

PROMOTOR:

Prof. Dr. J.T. den Dunnen

CO-PROMOTOR:

Dr. W.M.C. van Roon-Mom

LEDEN PROMOTIECOMMISSIE:

Prof. Dr. A.M. Aartsma-Rus
Prof. Dr. Harm H. Kampinga[1]
Dr. B. van de Warrenburg[2]

[1] Afdeling Celbiologie, Faculteit Medische Wetenschappen/Universitair Medisch Centrum Groningen
[2] Afdeling Neurologie, Donders Institute for Brain, Cognition and Behaviour, Radboud Universitair Medisch Centrum

TABLE OF CONTENTS

1

General introduction

Adapted from:
Evers, M. M.*, Toonen, L. J.*, & van Roon-Mom, W. M. (2014).
***authors contributed equally**
Mol Neurobiol, 49(3), 1513-1531.

POLYGLUTAMINE DISORDERS

The polyglutamine disorders are a group of 9 hereditary neurodegenerative disorders in which symptoms generally present around midlife. The disorders are caused by a similar type of genetic change, namely an abnormal expansion of a CAG repeat in the coding region of a gene [1]. The CAG repeat is translated into an expanded polyglutamine (polyQ) stretch in the protein and these disorders were hence termed polyQ disorders. The CAG expansion underlying the polyQ disorders occur in 9 otherwise unrelated genes, and the repeat lengths that result in disease vary between the different polyQ disorders (Table 1). There is however, in all cases, a clear correlation between the length of the CAG repeat and the age of onset of a polyQ disorder [2]. The involved proteins in which polyQ expansion is present are mostly ubiquitously expressed in all cells, but clinical features such as age of onset and most severely affected brain regions differ between the polyQ disorders. The research in this thesis is focused primarily on spinocerebellar ataxia type 3.

Table 1. Polyglutamine disorders (adapted from Riley and Orr [3])

Disease	Phenotype	Gene locus	Protein	protein mass (kDa)	Wild-type allele repeat length	Mutant allele repeat length
SBMA	Proximal muscle atrophy	Xq11-12	Androgen receptor	99.2	6–39	40–63
HD	Psychiatric, cognitive, motor abnormalities	4p16.3	Huntingtin	347.6	6–34	36–121
SCA1	Ataxia	6p22-23	Ataxin-1	86.9	8–44	39–83
SCA2	Ataxia	12q23-24	Ataxin-2	140.3	13–33	32–77
SCA3/MJD	Ataxia	14q24-31	Ataxin-3	41.8	12–40	54–89
SCA6	Ataxia	19p3	CACNA1A	282.4	4–18	19–33
SCA7	Ataxia, retinal degeneration	3p12-21	Ataxin-7	95.5	4–35	37–306
SCA17	Ataxia	2q13	TATA-BP	37.7	29–42	47–55
DRPLA	Epilepsy, ataxia, dementia	12q	Atrophin-1	125.4	6–36	49–84

DRPLA: Dentatorubral-pallidoluysian atrophy, HD: Huntington's disease, SCA: spinocerebellar ataxia, SBMA: Spinal and bulbar muscular atrophy.

The 9 polyQ disorders are all caused by a polyglutamine repeat expansion in proteins that are expressed ubiquitously throughout the brain. Yet, the most severely affected brain regions and symptoms vary substantially between the disorders.

1 SPINOCEREBELLAR ATAXIA TYPE 3

Spinocerebellar ataxia type 3 (SCA3), or Machado–Joseph disease (MJD)[4], is the most common spinocerebellar ataxia [5, 6] and the second most common polyglutamine (polyQ) disease after Huntington's disease (HD) [7]. Similar to the other polyQ disorders, SCA3 is inherited in an autosomal dominant fashion [8], is neurodegenerative and ultimately fatal. There are currently only therapeutic strategies to alleviate the symptoms, but not to counteract disease progression [9]. SCA3 is clinically heterogeneous, with the main feature being progressive ataxia that can affect balance, gait and speech. Other frequently described symptoms include pyramidal signs, progressive external ophthalmoplegia, dysarthria, dysphagia, rigidity, distal muscle atrophies and double vision [8, 10-12]. These symptoms usually start around midlife, with the exact age of onset being variable. Neuropathological studies have detected widespread neuronal loss in the cerebellum, thalamus, midbrain, pons, medulla oblongata and spinal cord of SCA3 patients, as reviewed by Riess et al [13]. Also, peripheral neuropathy with axonal and demyelinating characteristics were observed in 55% of SCA3 patients, though the contribution hereof to presented symptoms in SCA3 is not clear [14].

SCA3 is caused by an expanded stretch of CAG triplets in the coding region of the *ATXN3* gene on chromosome 14q32.1, encoding the ataxin-3 protein[15]. Healthy individuals have up to 40 CAG repeats, whilst affected individuals have between 54 and 89 glutamine repeats. A repeat range from 40 to 54 is associated with incomplete penetrance of the disease[15-17]. SCA3 patients with two mutant alleles show a more severe disease phenotype than those with a single mutant allele [18]. Also, there is a clear correlation between CAG repeat size and age of onset, though CAG repeat length only accounts for approximately 50% of the total variability in age of onset [19]. The expanded CAG repeat leads to formation of an expanded polyQ tract in the C-terminal region of the ataxin-3 protein, leading to toxic gain of function of the protein and formation of characteristic neuronal aggregates [20]. The neurotoxic properties of these aggregates are still under debate since the number of aggregates does not correlate to the level of neurodegeneration or the *ATXN3* CAG repeat length [21]. Involvement of proteolytic cleavage of the mutant ataxin-3 protein, liberating shorter protein fragments containing the expanded polyQ fragment, appears an important pathway to cellular toxicity and aggregate formation [22]. Observations in Drosophila models for polyQ disorders also hint towards possible involvement of the expanded CAG repeat itself inducing toxicity at the RNA level [23]. Despite being a monogenetic disease, SCA3 pathogenesis has proven to be complex. Over the last decade extensive studies in cell and animal have led to the identification of several cellular processes potentially involved in SCA3 pathology.

Nonetheless, much remains to be elucidated regarding the toxicity resulting from mutant ataxin-3 RNA and protein, and a more comprehensive understanding of the many cellular processes involved would be of great benefit for the development of therapeutic strategies.

ATAXIN-3: A DEUBIQUITINATING ENZYME

Two years following the discovery of the *ATXN3* gene, the ataxin-3 protein was detected, and was found to be expressed throughout the brain [24]. Today it is known that ataxin-3 is in fact expressed throughout the entire body, and 20 isoforms have been described which are all potentially protein-coding [25]. Of these, 2 isoforms have been extensively investigated, with the isoform most prominently expressed in brain being encoded by 11 exons (RefSeqNM_004993) and consisting of 361 amino acids (Fig.1) [26-28]. The ataxin-3 protein has a molecular weight of approximately 42 kDa, which increases depending on the size of the C-terminal polyQ repeat. Ataxin-3 is a deubiquitinating enzyme, with a total of 3 ubiquitin interacting motifs (UIMs) and with a catalytic Josephin domain located at the N-terminus[29, 30]. The UIMs can bind and position the ubiquitin chains in such a manner that the catalytic Josephin domain is then able to cleave these chains [30]. In this manner, ataxin-3 can either rescue proteins from degradation or stimulate breakdown by the removal of inhibitory poly-ubiquitin chains and by the regeneration of free and reusable ubiquitin[30, 31]. Besides protein degradation, the ubiquitin-proteasomal pathway is involved in various cellular processes such as endocytosis, transcriptional regulation and antigen presentation.

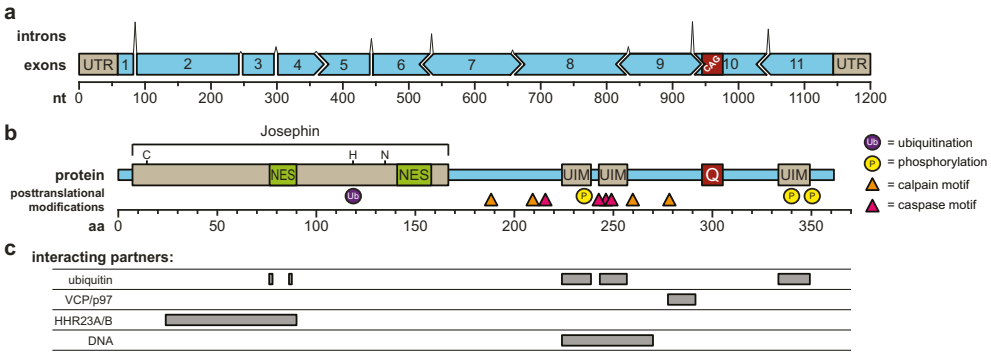

Figure 1. Schematic representation of *ATXN3* gene and protein with interacting partners (adapted from Evers *et al* [32]). a. The ATXN3 gene (Ensembl transcript ID: ENST00000558190.5) consists of 11 exons with the start codon in exon 1 and the CAG repeat in exon 10. The shape of the boxes depict the reading frame, nt: nucleotides. Based on CAG repeat of 10. The height of the introns are relative to their length. **b.** The ataxin-3 protein consists of 361 amino acids (aa), with an N-terminal Josephin domain that contains crucial amino acids for its isopeptidase activity [cysteine 14 (C), histidine 119 (H), and asparagine 134 (N)] and two nuclear export signals (NES). The C-terminal part contains three ubiquitin interacting motifs (UIMs) and the polyglutamine (polyQ) repeat. Specific amino acids known to undergo posttranslational modifications are indicated with circles. Preferential cleavage sites for calpain and caspases potentially generating toxic protein fragments are depicted with triangles. **c.** Binding domains of the main interacting partners: ubiquitin, VCP/p97 valosin-containing protein, hHR23A and hHR23B human homologues of yeast protein RAD23, and DNA binding.

Amino acid cysteine 14, histidine 119, and asparagine 134 of the Josephin domain of ataxin-3 are essential for its isopeptidase function and are highly conserved between Josephin and other ubiquitin C-terminal hydrolases and ubiquitin-specific proteases [33, 34]. The UIMs mediate selective binding to ubiquitin chains and restrict the types of chains that can be cleaved by the Josephin domain. Ataxin-3 is known to recognise poly-ubiquitin chains of four or more ubiquitins [31, 35] and binds the poly-ubiquitin linkages lysine 48, lysine 63 and mixed linkage ubiquitin chains, with preference for lysine 63-tagged ubiquitins [30, 36]. Editing and removal of poly-ubiquitin chains as well as recycling of ubiquitin is critical for cellular homeostasis. Polyubiquitin chains linked through lysines 6, 11, 27, 29, 33 and 48 target proteins for proteasomal degradation. In contrast, lysine 63 or linear polyubiquitin chains have non-proteolytic functions such as activation of kinases and autophagy, where it is proposed to be involved in the biogenesis of protein inclusions [37].

Ataxin-3 protein interactions

Ataxin-3 has been found to interact with the valosin-containing protein (VCP/p97) [38, 39] through a motif close to the polyQ repeat (Fig. 1) [40]. VCP/p97 has numerous functions, one of which is the regulation of misfolded protein degradation in a process named endoplasmic reticulum -associated degradation (ERAD)[38, 41]. The ataxin-3-VCP/p97 complex is involved in assisting targeted proteins to the proteasome [42]. Ataxin-3 is also known to interact with the human homologues of yeast protein RAD23, hHR23A and hHR23B. hHR23A and hHR23B are involved in DNA repair pathways as well as the delivery of ubiquitinated substrates to the proteasome for degradation[39]. The binding site of hHR23B to ataxin-3 is located in the second ubiquitin binding site of the Josephin domain, and in concordance, hHR23B was shown to compete with ubiquitin binding [34]. Cell stress resulted in altered interactions with both VCP/p97 and HR23B, which were found mainly in the cytoplasm, although no effect on protein degradation was reported [43]. Another association between ataxin-3 and the DNA damage repair pathway stems from the interaction between ataxin-3 and polynucleotide kinase 3′-phosphatase (PNKP). PNKP is an DNA end-processing enzyme, and it was found that wild-type ataxin-3 stimulates PNKP activity [44]. In addition, ataxin-3 is recruited to DNA double-strand breaks, and through its deubiquitinating activity was shown to regulate the chromatin dwell time of mediator of DNA damage checkpoint protein 1 (MDC1), which in turn recruits DNA repair proteins [45].

Ataxin-3 and transcriptional regulation

Besides the clear role of ataxin-3 in protein degradation, ataxin-3 has been shown to regulate transcription. Ataxin-3 is, for instance, able to repress matrix metalloproteinase-2 (MMP-2) transcription, and increased nuclear localisation of ataxin-3 through phosphorylation enhances this transcriptional repression [46]. Ataxin-3 can also regulate PTEN transcription, in turn influencing PI3K pathway activity [47]. In cells overexpressing wild-type ataxin-3, transcriptional repression of cell surface- and ECM-associated genes was observed [48]. These effects on transcription by ataxin-3 may occur through interactions with transcriptional regulators.

Indeed, ataxin-3 is known to interact with p300, p300/CBP-associated factor (PCAF)[49], histone deacetylases (HDAC) 3 and 6, nuclear receptor co-repressor (NCoR1) [48]. However, ataxin-3 can also directly bind to target DNA sequences in chromatin regions of MMP-2, after which transcription is repressed through recruitment of HDAC3 [50].Whether this direct DNA binding by ataxin-3 is an important pathway of gene regulation is currently still an open question.

Is ataxin-3 an essential protein?

Whether ataxin-3 is an essential protein for normal cellular function remains uncertain. On one hand ataxin-3 appears dispensable, as knockout of *ATXN3* in a *C. elegans* model did not negatively affect lifespan [51] and conferred a resistance to stress [52]. Downregulation of ataxin-3 in the striatum of rats using shRNA did not result in overt signs of toxicity [53]. In line with this, ataxin-3 knock-out mice did not present problems with viability or fertility [54, 55]. However, closer examination of the molecular phenotype of ataxin-3 knockout models has revealed subtle changes, particularly with regards to ubiquitination, that are important to consider. Firstly, depletion of ataxin-3 using siRNA in cultured non-neuronal human and mouse cells resulted in accumulation of ubiquitinated material in the cytoplasm, cytoskeletal disorganisation, loss of cell adhesion and increased cell death [56]. Additionally, increased levels of protein ubiquitination were observed in tissues of an ataxin-3 knockout mouse, and a subtle increase in anxiety of the mice was reported [54]. More recently, the role of ataxin-3 in the DNA damage response has been established, with ataxin-3 depletion compromising double-strand DNA break repair [45]. Taken together, it can be concluded that loss of ataxin-3 is tolerated in mice, but several subtle alterations in cellular homeostasis indicate that ataxin-3 may not be completely dispensable for cellular functioning in the long term.

PATHOGENIC MECHANISMS OF MUTANT ATAXIN-3

Wild-type ataxin-3 in the normal population has a polyQ stretch of between 13 and 44 [13]. Following mutational expansion to over 52 repeats, the ataxin-3 protein becomes toxic to brain cells. No correlation between ataxin-3 mRNA expression levels and the extent of neurodegeneration was found for the brain regions affected in SCA3 [57]. It hence appears that there is no difference in expression levels of mutant ataxin-3 to explain the regional differences in brain pathology and cytotoxicity in a straightforward manner. Rather, specific brain regions are more sensitive to the toxic effects of ataxin-3. It is currently unclear what factors are involved in conveying this specific toxicity, but several hypotheses regarding mutant ataxin-3 pathogenesis have been proposed and will be discussed below.

> Despite being ubiquitously expressed and well conserved among species, it is still unclear whether ataxin-3 is an essential protein for cellular functioning.

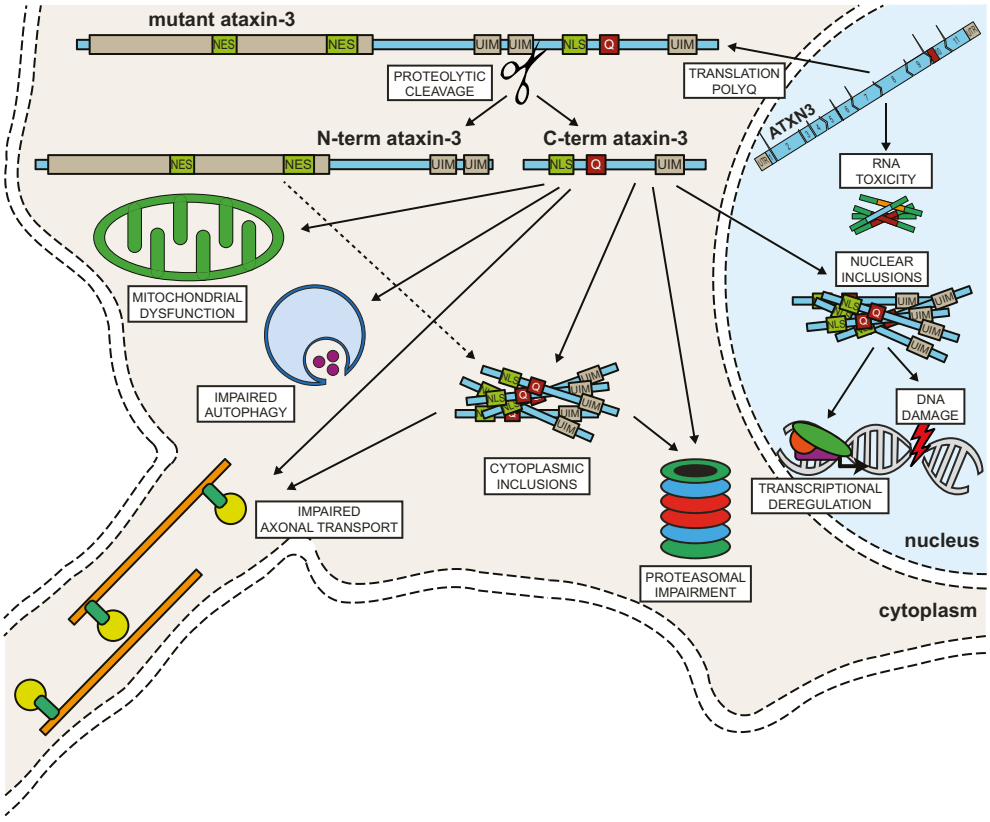

Figure 2. Cellular mechanisms of mutant ataxin-3 toxicity (adapted from [32]). In SCA3 the CAG repeat of the *ATXN3* gene is translated into a polyQ expansion in the mutant ataxin-3 protein. The expanded polyQ repeat causes misfolding of the protein. Proteolytic cleavage of ataxin-3 can generate C-terminal protein fragments containing the polyQ repeat. Full length and cleaved forms of ataxin-3 can form soluble monomers, oligomers or large insoluble aggregates, both in the nucleus and in the cytoplasm that cause toxicity. Other cellular disturbances in SCA3 pathogenesis include transcriptional deregulation, impaired autophagy, mitochondrial dysfunction, proteasomal impairment, compromised axonal transport and DNA damage. Finally, there is also evidence implicating RNA toxicity of the mutant *ATXN3* transcript in disease pathogenesis.

Mutant ataxin-3 aggregation

Similar to the other polyQ disorders, intracellular aggregates in neurons of brain material from SCA3 patients were observed as a hallmark of disease. Aggregates were observed in the substantia nigra, globus pallidus, dorsal medulla and dentate nucleus [20]. Using overexpression systems in cell- and animal models, mutant ataxin-3 was indeed found to accumulate in intracellular aggregates [58, 59].There is a clear correlation between the length of the polyQ stretch in ataxin-3 and its propensity to form aggregates [60, 61]. In particular, the nuclear accumulation of ataxin-3 appears to be important to induce toxicity, as targeting ataxin-3 to the nucleus worsens the SCA3 phenotype in mice [62]. Ubiquitinated ataxin-3 inclusions can be found in several brain regions

of SCA3 patients [20, 27]. During disease progression, SCA3 mice show a decrease in the level of soluble mutant atxin-3 in the cerebellum, whilst both nuclear aggregate formation and the ataxic phenotype progress [63]. Ataxin-3 aggregates are not exclusively found in the cell nucleus, however. Axonal ubiquitinated aggregates have been identified in SCA3 brain tissue fiber tracts [64] and cytoplasmic inclusions were also observed in several affected brain regions [65].The ataxin-3 inclusions in the cytoplasm have been proposed to interfere with axonal transport. However, there appears to be no direct correlation between the number of aggregates and severity of neurodegeneration [21, 64]. Additionally, it is currently not clear whether the observed ataxin-3 aggregates consist of full-length ataxin-3 protein, or are initiated by shorter polyQ containing ataxin-3 fragments.

The hallmark neuronal aggregates of SCA3 are closely associated with proteolytic cleavage of mutant ataxin-3.

Proteolytic cleavage and induction of toxicity

Proteolytic cleavage of proteins is a continuous process in a normally functioning cell, and serves many purposes from degradation of proteins to post-translational processing [66]. However, in the case of mutated proteins, proteolytic processing may contribute to disease. In the case of SCA3, research has shown that proteolytic cleavage of mutant ataxin-3 can generate shorter protein fragments containing the polyQ stretch. These protein fragments are more toxic to cells than the full length ataxin-3 protein, and in addition are more prone to aggregate [22, 67]. It is therefore thought that the proteolytic cleavage, which can generate short C-terminal ataxin-3 fragments containing the polyQ stretch, may be a driving force in SCA3 pathogenesis. The two main families of enzymes that have been investigated in this regard for ataxin-3 are the caspase and calpain families of proteases. Caspases cleave at defined motifs containing an aspartate residue, and at least 3 such sites located in ataxin-3 are in a position capable of generating a short polyQ containing fragment [68]. However, caspase cleavage of ataxin-3 occurs less efficiently than for huntingtin and atrophin-1[69] and inhibition of caspase cleavage did not reduce aggregate formation in SCA3 neuronal cell culture experiments [68].

Cleavage of ataxin-3 by the calpain-2 enzyme occurs throughout the protein, but a key cleavage site that is well investigated is the one just upstream of the polyQ repeat, at amino acid 260 [70, 71] (Fig.1). Cleavage at this site generates C-terminal ataxin-3 fragments that are highly prone to aggregation [70]. Inhibition of calpains in SCA3 mice results in a reduction of ataxin-3 proteolysis, nuclear localisation, aggregation and was successful in reducing toxicity [71, 72]. Conversely, stimulation of calpain activity *in vivo* worsened the ataxic phenotype of mice [70]. There is also evidence that ataxin-3 with longer polyQ stretches is more prone to calpain cleavage than ataxin-3 with shorter polyQ stretches, potentially exacerbating the formation of the toxic fragments [70]. It appears that during disease progression in mice,

soluble levels of mutant ataxin-3 in the brain decrease, possibly as a result of calpain cleavage, whilst the aggregate burden increases [63]. It has been suggested that calpains are involved in the neuronal specificity of SCA3 pathology, as excitation-mediated calcium influx in neuronal cells activated calpain-2 *in vitro*, and lead to ataxin-3 cleavage and aggregation [73]. A recent study, however, was unable to reproduce this excitation related ataxin-3 aggregation in similar neuronal cells [74], and further research is thus required to comprehensively establish ataxin-3 cleavage induced neuronal pathology.

Impairment of protein degradation

Ataxin-3 is involved in the proteasomal protein degradation pathway and this pathway is indeed found affected in SCA3 as mutant ataxin-3 appears to interfere with degradation of substrates [43, 75]. The mechanism behind this, however, appears to be more so the result of toxic gain of mutant ataxin-3 function rather than loss of function. For instance, a reduction in the level of protein deubiquitination was reported in a cell model expressing mutant ataxin-3, despite mutant ataxin-3 showing similar ubiquitin chain proteolysis as wild type ataxin-3 [30]. Mutant ataxin-3 was also shown to bind to VCP more efficiently [38, 43, 76]. For this reason, it is more likely that both mutant and wildtype ataxin-3 get trapped in the ubiquitin-rich aggregates together with components of the proteasomal machinery [20, 77]. The interaction with VCP is important, as expression of a N-terminal ataxin-3 fragment lacking the VCP binding site resulted in an impaired unfolded protein response and ER stress, without apparent changes in levels of ERAD components when tested in a mouse model [78].

Besides ERAD dysregulation, the process of autophagy also was shown impaired in SCA3 as observed in other neurodegenerative disorders[79]. Ataxin-3 aggregates in SCA3 were shown to contain components of autophagy machinery, such as beclin-1 [80]. Indeed, autophagy stimulation through beclin-1 overexpression was shown to alleviate disease pathogenesis in a SCA3 rat model [80], in parallel to previous research for HD [81]. Recent evidence shows that the polyQ repeat is required for the interaction between beclin-1 and ataxin-3, which is important to maintain adequate beclin-1 protein levels and thus normal initiation of autophagy. The polyQ expansion competes for this interaction, thereby contributing to impairment of autophagy [82]. Together, current research suggest SCA3 pathology to at least partly result from loss of function from ERAD and autophagy machinery, together culminating in impaired protein degradation and cellular stress.

SCA3 pathology is predominantly the result of gain of toxicity of mutant ataxin-3, rather than loss of ataxin-3 protein functioning.

Mitochondrial dysfunction

It has been suggested that increasing oxidative stress and inability to protect against free radicals with age could lead to mitochondrial dysfunction and cell damage in polyQ disorders [83-86]. For SCA3, a cell model overexpressing mutant ataxin-3 with 78 glutamines indeed showed reduced antioxidant enzyme levels, increased mitochondrial DNA damage, and reduced energy supply, which indicates impaired mitochondrial function [86]. In SCA3 mice, mitochondrial DNA damage was seen in affected brain regions [87], and evidence of moderate compromised mitochondrial complex II was found [88]. Finally, in brain tissue of SCA3 patients, downregulation of superoxide dismutase was detected, suggesting diminished antioxidant enzyme function. As damaged mitochondria will not be able to scavenge free radicals and prevent cell energy impairment as effectively, this process may therefore further increase oxidative stress in the cell. Oxidative stress is then able to modulate vital cellular functions, potentially resulting in activation of apoptosis or excitotoxicity, two of the main causes of neuronal death [89].

Transcriptional deregulation

Since ataxin-3 displays DNA-binding properties and interacts with transcriptional regulators, transcriptional deregulation has been suggested to play a central role in the SCA3 pathogenesis [3]. In SCA3 and other polyQ disorders, transcription factors are sequestered into nuclear aggregates, resulting in deregulation of their function as transcriptional co-repressor or activator [90, 91]. Transcription of genes involved in inflammatory processes, cell signalling and cell surface-associated proteins were found to be altered in SCA3 cell and mouse models [48, 92, 93]. Likewise, some corresponding proteins like MMP-2, amyloid β-protein and interleukins were found to be significantly increased in SCA3 patient brain material [92]. A second mode of transcriptional deregulation arises from impairment of ataxin-3 function. Wild-type ataxin-3 can repress transcription through recruitment of histone deacetylase 3 and nuclear receptor corepressor, resulting in histone deacetylation. However, mutant ataxin-3 results in reduced histone deacetylation in this context, allowing for aberrant transcription to take place [50].

RNA toxicity and repeat-associated non-ATG translation

Until recently, it was believed that polyQ disorders are solely the result of gain of toxic protein function and, to a lesser extent, loss of wild-type protein function. However, increasing evidence suggests involvement of the expanded CAG repeat at the RNA level in polyQ pathogenesis. This may occur through various mechanisms, including alternative splicing, bidirectional transcription, involvement of the RNA interference pathway, as well as repeat-associated non-ATG (RAN) initiated translation [32]. Evidence from toxicity of the CAG repeat itself stems from the observed neural dysfunction in *Drosophila melanogaster* models where the repeat was positioned in the 3′ untranslated region (UTR). Interspersing the repeat with CAA codons resulted in only a mild phenotype [23]. The pathways underlying RNA toxicity could be sequestration of proteins to the hairpin structure of the CAG repeat, like for

Table 2. Potential toxicity pathways involved in SCA3 pathogenesis

Pathway	Established in	contribution to pathology*	References
Nuclear ataxin-3 inclusions/ aggregates	cell and mouse models, patient brain material	++++	20, 27, 63, 73
Proteolytic ataxin-3 cleavage/ toxic protein fragments	cell culture, animal models	+++	22, 68, 70, 94
Proteasomal impairment	cell models, patient brain material	++	77, 95
Autophagy impairment	cell and mouse models	+++	80, 82
Axonal transport impairment	patient brain material	++	64
Transcriptional deregulation	cell and animal models	+++	48, 93, 96
RNA toxicity	Drosophila	+	23
RAN translation	indirect; evidence in HD	unknown	97

RAN = Repeat associated non-ATG translation, HD = Huntington disease *This scale is an arbitrary measure based on current evidence in literature and the interpretation of the author.

instance the transcription factor muscleblind-like 1 (MBNL1) [98], resulting in misregulation of splicing [99]. Additionally, MID1 protein is recruited to expanded CAG repeat containing RNA, which in turn results in aberrant translation of proteins from the CAG mRNAs [100, 101]. However, the actual contribution of this direct RNA toxicity may be limited in SCA3, since other research suggests that CAG repeats in the UTR are only toxic when considerably exceeding the repeat length normally found in SCA3 patients [98, 102].

For SCA3 and other polyQ disorders, reading frame shifts and subsequent translation of homopolymeric repeats such as polyalanine (polyA) have been established [103, 104]. The polyA repeat is associated with increased toxicity over the polyQ repeat, and may therefore be a substantial contributor to toxicity associated with the expanded CAG repeat [105]. Of note, expansion proteins from all three reading frames can be produced without an AUG start codon, in a process termed RAN translation [97]. Frameshifting and RAN translation are distinct translational steps, but are both dependent on the repeat sequence length [106]. RAN translation is usually associated with sequences that are considered to be non-coding, but may nonetheless be involved in polyQ disorder toxicity as well.

DNA damage

Ataxin-3 has recently been discovered to interact with, or modulate activity of, several DNA damage response associated proteins, such as HHR23A, HHR23B[39], MDC1[45], polynucleotide kinase 3′-phosphatase (PNKP)[44, 107], and checkpoint kinase 1 (Chk1) [108]. Interestingly, a large increase in DNA damage has been demonstrated in cells, mouse brain and human brain material of SCA3 [107], suggesting DNA damage may be involved in SCA3 pathogenesis. Indeed, defects in the DNA repair have been linked to several other neurological disorders [109]. In the case of SCA3, it was shown that wild-type ataxin-3 stimulates PNKP activity, whereas mutant ataxin-3 inhibits this activity [44]. The deactivation of PNKP by mutant ataxin-3 in

fact appears to be involved in inducing DNA damage and subsequent cell death underlying neurodegeneration [107], suggesting a direct pathologic link. It is currently unclear whether the interfering effect of mutant ataxin-3 on PNKP functioning is the result of PNKP inhibition through inclusions in aggregates or a more direct inhibition due to binding of mutant ataxin-3 [110]. Additionally, it will be of importance to determine whether the deubiquitinating activity of ataxin-3 is involved in the PKNP modulation, such as observed for the checkpoint mediator protein MDC1[45]. Mutant ataxin-3 is able to deubiquitinate and stabilize Chk1 protein at a comparable capacity as wild-type ataxin-3, arguing against involvement of altered enzymatic activity of mutant ataxin-3 as a initiator of DNA damage in this context [108].

Collectively, there is abundant evidence that ataxin-3 is involved in the DNA repair pathway, but it remains to be elucidated how mutant ataxin-3 relates to the increased DNA damage observed in SCA3, and to what extent this contributes to pathology.

THERAPIES

Currently no therapies are available to delay SCA3 disease progression and patients are only treated symptomatically. Nonetheless, several interesting new compounds and RNA targeting therapeutics are currently in preclinical development. Firstly, compounds resulting in increased clearance of mutant ataxin-3 are being investigated. Increasing intracellular protein degradation by various compounds have shown to be capable of improving the phenotype of SCA3 mice [111,112], but strong modulation of autophagy may cause neurotoxicity [113] and these compounds thus have to be implemented with great care. Additionally, several chemical chaperones capable of reducing ataxin-3 aggregation have been tested with success in cell culture experiments[114], and trehalose [115] is currently in phase II clinical trial for the treatment of SCA3. A screening of FDA-approved drugs has recently identified the serotonin reuptake inhibitor as a drug capable of improving the phenotype in *c.elegans* and SCA3 mice [116]. However, only the autophagy inhibitor lithium has been tested in SCA3 patients so far, but no beneficial effect on disease progression could be determined [117]. Various other compounds and strategies have been tested in SCA3 mouse models. Firstly, preventing SCA3 disease progression through modulation of calcium homeostasis has been investigated using Dantrolene [118] and caffeine [119,120] with promising results that warrant further investigation of these compounds. Additionally, the HDAC inhibitor sodium butyrate was capable of inducing beneficial effects on the phenotype of SCA3 mice, possibly by ameliorating transcriptional repression [121]. Thirdly, inhibition of ataxin-3 cleavage by treatment with the calpain inhibitor BDA-410 successfully prevented motor deficits in SCA3 mice [94]. Caloric restriction was found to reduce motor deficits in SCA3 mouse models, through rescue of sirtuin 1 (SIRT1) levels [122].

Recently there has been increased interest in stem cell transplantation as treatment strategy for neurodegenerative disorders. Transplantation of cerebellar neural stem cells in SCA3 mice led to differentiation of the cells into neurons and supportive cells, and alleviated motor behaviour impairment and neuropathy [123]. An exciting aspect of stem cell transplantation is that they can potentially induce cell replacement to compensate for the neuronal loss in SCA3.

Indeed, transplanted embryonic neurons were shown capable of integrating in pre-existing brain circuits in mice[124]. However, clinical success of stem cell use in for instance Alzheimer and Parkinson's disease have been modest thus far [125, 126], and some concerns regarding safety have been risen [127]. Due to the monogenetic nature, SCA3 is also an ideal candidate for therapies directly targeting the *ATXN3* transcript. Downregulation of ataxin-3 using shRNA and siRNA has shown success in mouse models [128-130]. Additionally, antisense oligonucleotides can be used to down regulate[131, 132] or modify ataxin-3 through exon skipping [133]. The use of antisense oligonucleotide therapies in neurodegenerative disorders is extensively reviewed in **Chapter 2.**

Scope of the thesis

In this thesis, antisense oligonucleotides (AONs) are investigated as a potential treatment for SCA3.

Chapter 2 describes the current state of development of AONs and their use as therapy for neurodegenerative disorders. In **Chapter 3,** an AON based strategy to reduce formation of toxic ataxin-3 cleavage fragments in cell models is described. **Chapter 4** describes pathogenic mechanisms and biomarkers in a SCA3 mouse model using a multi-omics approach. In **Chapter 5,** a novel AON based therapy to remove the toxic polyQ repeat from ataxin-3 in the SCA3 mouse model is investigated. **Chapter 6** provides an overview of potential side effects and toxicity related to 2'OMe AONs after intracerebroventricular injection in mice. **Chapter 7** discusses the main findings of the thesis, and how these relate to the current state of SCA3 research and AON based therapies.

REFERENCES

1. Gusella, JF, and MacDonald, ME (2000). Molecular genetics: unmasking polyglutamine triggers in neurodegenerative disease. *Nature reviews Neuroscience* **1**: 109-115.

2. Everett, CM, and Wood, NW (2004). Trinucleotide repeats and neurodegenerative disease. *Brain : a journal of neurology* **127**: 2385-2405.

3. Riley, BE, and Orr, HT (2006). Polyglutamine neurodegenerative diseases and regulation of transcription: assembling the puzzle. *Genes & development* **20**: 2183-2192.

4. Haberhausen, G, Damian, MS, Leweke, F, and Muller, U (1995). Spinocerebellar ataxia, type 3 (SCA3) is genetically identical to Machado-Joseph disease (MJD). *Journal of the neurological sciences* **132**: 71-75.

5. Ranum, LP, Lundgren, JK, Schut, LJ, Ahrens, MJ, Perlman, S, Aita, J, *et al.* (1995). Spinocerebellar ataxia type 1 and Machado-Joseph disease: incidence of CAG expansions among adult-onset ataxia patients from 311 families with dominant, recessive, or sporadic ataxia. *American journal of human genetics* **57**: 603-608.

6. Silveira, I, Lopes-Cendes, I, Kish, S, Maciel, P, Gaspar, C, Coutinho, P, *et al.* (1996). Frequency of spinocerebellar ataxia type 1, dentatorubropallidoluysian atrophy, and Machado-Joseph disease mutations in a large group of spinocerebellar ataxia patients. *Neurology* **46**: 214-218.

7. Pringsheim, T, Wiltshire, K, Day, L, Dykeman, J, Steeves, T, and Jette, N (2012). The incidence and prevalence of Huntington's disease: a systematic review and meta-analysis. *Movement disorders : official journal of the Movement Disorder Society* **27**: 1083-1091.

8. Coutinho, P, and Andrade, C (1978). Autosomal dominant system degeneration in Portuguese families of the Azores Islands. A new genetic disorder involving cerebellar, pyramidal, extrapyramidal and spinal cord motor functions. *Neurology* **28**: 703-709.

9. Bauer, PO, and Nukina, N (2009). The pathogenic mechanisms of polyglutamine diseases and current therapeutic strategies. *Journal of neurochemistry* **110**: 1737-1765.

10. Rosenberg, RN (1992). Machado-Joseph disease: an autosomal dominant motor system degeneration. *Movement disorders : official journal of the Movement Disorder Society* **7**: 193-203.

11. Soong, B, Cheng, C, Liu, R, and Shan, D (1997). Machado-Joseph disease: clinical, molecular, and metabolic characterization in Chinese kindreds. *Annals of neurology* **41**: 446-452.

12. Teive, HA, Munhoz, RP, Arruda, WO, Lopes-Cendes, I, Raskin, S, Werneck, LC, *et al.* (2012). Spinocerebellar ataxias: genotype-phenotype correlations in 104 Brazilian families. *Clinics (Sao Paulo, Brazil)* **67**: 443-449.

13. Riess, O, Rub, U, Pastore, A, Bauer, P, and Schols, L (2008). SCA3: neurological features, pathogenesis and animal models. *Cerebellum (London, England)* **7**: 125-137.

14. Linnemann, C, Tezenas du Montcel, S, Rakowicz, M, Schmitz-Hubsch, T, Szymanski, S, Berciano, J, *et al.* (2016). Peripheral Neuropathy in Spinocerebellar Ataxia Type 1, 2, 3, and 6. *Cerebellum (London, England)* **15**: 165-173.

15. Kawaguchi, Y, Okamoto, T, Taniwaki, M, Aizawa, M, Inoue, M, Katayama, S, *et al.* (1994). CAG expansions in a novel gene for Machado-Joseph disease at chromosome 14q32.1. *Nature genetics* **8**: 221-228.

16. Durr, A, Stevanin, G, Cancel, G, Duyckaerts, C, Abbas, N, Didierjean, O, *et al.* (1996). Spinocerebellar ataxia 3 and Machado-Joseph disease: clinical, molecular, and neuropathological features. *Annals of neurology* **39**: 490-499.

17. Padiath, QS, Srivastava, AK, Roy, S, Jain, S, and Brahmachari, SK (2005). Identification of a novel 45 repeat unstable allele associated with a disease phenotype at the MJD1/SCA3 locus. *American journal of medical genetics Part B, Neuropsychiatric genetics : the official publication of the International Society of Psychiatric Genetics* **133b**: 124-126.

18. Carvalho, DR, La Rocque-Ferreira, A, Rizzo, IM, Imamura, EU, and Speck-Martins, CE (2008). Homozygosity enhances severity in spinocerebellar ataxia type 3. *Pediatric neurology* **38**: 296-299.

19. Maciel, P, Gaspar, C, DeStefano, AL, Silveira, I, Coutinho, P, Radvany, J, *et al.* (1995). Correlation between CAG repeat length and clinical features in Machado-Joseph disease. *American journal of human genetics* **57**: 54-61.

20. Paulson, HL, Perez, MK, Trottier, Y, Trojanowski, JQ, Subramony, SH, Das, SS, *et al.* (1997). Intranuclear inclusions of expanded polyglutamine protein in spinocerebellar ataxia type 3. *Neuron* **19**: 333-344.

21. Rub, U, de Vos, RA, Brunt, ER, Sebesteny, T, Schols, L, Auburger, G, *et al.* (2006). Spinocerebellar ataxia type 3 (SCA3): thalamic neurodegeneration occurs independently from thalamic ataxin-3 immunopositive neuronal intranuclear inclusions. *Brain pathology (Zurich, Switzerland)* **16**: 218-227.

22. Haacke, A, Broadley, SA, Boteva, R, Tzvetkov, N, Hartl, FU, and Breuer, P (2006). Proteolytic cleavage of polyglutamine-expanded ataxin-3 is critical for aggregation and sequestration of non-expanded ataxin-3. *Human molecular genetics* **15**: 555-568.

23. Li, LB, Yu, Z, Teng, X, and Bonini, NM (2008). RNA toxicity is a component of ataxin-3 degeneration in Drosophila. *Nature* **453**: 1107-1111.

24. Paulson, HL, Das, SS, Crino, PB, Perez, MK, Patel, SC, Gotsdiner, D, *et al.* (1997). Machado-Joseph disease gene product is a cytoplasmic protein widely expressed in brain. *Annals of neurology* **41**: 453-462.

25. Bettencourt, C, Santos, C, Montiel, R, Costa Mdo, C, Cruz-Morales, P, Santos, LR, *et al.* (2010). Increased transcript diversity: novel splicing variants of Machado-Joseph disease gene (ATXN3). *Neurogenetics* **11**: 193-202.

26. Harris, GM, Dodelzon, K, Gong, L, Gonzalez-Alegre, P, and Paulson, HL (2010). Splice isoforms of the polyglutamine disease protein ataxin-3 exhibit similar enzymatic yet different aggregation properties. *PloS one* **5**: e13695.

27. Schmidt, T, Landwehrmeyer, GB, Schmitt, I, Trottier, Y, Auburger, G, Laccone, F, *et al.* (1998). An isoform of ataxin-3 accumulates in the nucleus of neuronal cells in affected brain regions of SCA3 patients. *Brain pathology (Zurich, Switzerland)* **8**: 669-679.

28. Trottier, Y, Cancel, G, An-Gourfinkel, I, Lutz, Y, Weber, C, Brice, A, *et al.* (1998). Heterogeneous intracellular localization and expression of ataxin-3. *Neurobiology of disease* **5**: 335-347.

29. Masino, L, Musi, V, Menon, RP, Fusi, P, Kelly, G, Frenkiel, TA, *et al.* (2003). Domain architecture of the polyglutamine protein ataxin-3: a globular domain followed by a flexible tail. *FEBS letters* **549**: 21-25.

30. Winborn, BJ, Travis, SM, Todi, SV, Scaglione, KM, Xu, P, Williams, AJ, *et al.* (2008). The deubiquitinating enzyme ataxin-3, a polyglutamine disease protein, edits Lys63 linkages in mixed linkage ubiquitin chains. *The Journal of biological chemistry* **283**: 26436-26443.

31. Burnett, B, Li, F, and Pittman, RN (2003). The polyglutamine neurodegenerative protein ataxin-3 binds polyubiquitylated proteins and has ubiquitin protease activity. *Human molecular genetics* **12**: 3195-3205.

32. Evers, MM, Toonen, LJ, and van Roon-Mom, WM (2014). Ataxin-3 protein and RNA toxicity in spinocerebellar ataxia type 3: current insights and emerging therapeutic strategies. *Mol Neurobiol* **49**: 1513-1531.

33. Mao, Y, Senic-Matuglia, F, Di Fiore, PP, Polo, S, Hodsdon, ME, and De Camilli, P (2005). Deubiquitinating function of ataxin-3: insights from the solution structure of the Josephin domain. *Proceedings of the National Academy of Sciences of the United States of America* **102**: 12700-12705.

34. Nicastro, G, Menon, RP, Masino, L, Knowles, PP, McDonald, NQ, and Pastore, A (2005). The solution structure of the Josephin domain of ataxin-3: structural determinants for molecular recognition. *Proceedings of the National Academy of Sciences of the United States of America* **102**: 10493-10498.

35. Berke, SJ, Chai, Y, Marrs, GL, Wen, H, and Paulson, HL (2005). Defining the role of ubiquitin-interacting motifs in the polyglutamine disease protein, ataxin-3. *The Journal of biological chemistry* **280**: 32026-32034.

36. Fang, S, and Weissman, AM (2004). A field guide to ubiquitylation. *Cellular and molecular life sciences: CMLS* **61**: 1546-1561.

37. Lim, KL, and Lim, GG (2011). K63-linked ubiquitination and neurodegeneration. *Neurobiology of disease* **43**: 9-16.

38. Zhong, X, and Pittman, RN (2006). Ataxin-3 binds VCP/p97 and regulates retrotranslocation of ERAD substrates. *Human molecular genetics* **15**: 2409-2420.

39. Wang, G, Sawai, N, Kotliarova, S, Kanazawa, I, and Nukina, N (2000). Ataxin-3, the MJD1 gene product, interacts with the two human homologs of yeast DNA repair protein RAD23, HHR23A and HHR23B. *Human molecular genetics* **9**: 1795-1803.

40. Boeddrich, A, Gaumer, S, Haacke, A, Tzvetkov, N, Albrecht, M, Evert, BO, *et al.* (2006). An arginine/lysine-rich motif is crucial for VCP/p97-mediated modulation of ataxin-3 fibrillogenesis. *The EMBO journal* **25**: 1547-1558.

41. Liu, Y, and Ye, Y (2012). Roles of p97-associated deubiquitinases in protein quality control at the endoplasmic reticulum. *Current protein & peptide science* **13**: 436-446.

42. Wang, Q, Li, L, and Ye, Y (2006). Regulation of retrotranslocation by p97-associated deubiquitinating enzyme ataxin-3. *The Journal of cell biology* **174**: 963-971.

43. Laco, MN, Cortes, L, Travis, SM, Paulson, HL, and Rego, AC (2012). Valosin-containing protein (VCP/p97) is an activator of wild-type ataxin-3. *PloS one* **7**: e43563.

44. Chatterjee, A, Saha, S, Chakraborty, A, Silva-Fernandes, A, Mandal, SM, Neves-Carvalho, A, *et al.* (2015). The role of the mammalian DNA end-processing enzyme polynucleotide kinase 3'-phosphatase in spinocerebellar ataxia type 3 pathogenesis. *PLoS genetics* **11**: e1004749.

45. Pfeiffer, A, Luijsterburg, MS, Acs, K, Wiegant, WW, Helfricht, A, Herzog, LK, *et al.* (2017). Ataxin-3 consolidates the MDC1-dependent DNA double-strand break response by counteracting the SUMO-targeted ubiquitin ligase RNF4. *The EMBO journal* **36**: 1066-1083.

46. Mueller, T, Breuer, P, Schmitt, I, Walter, J, Evert, BO, and Wullner, U (2009). CK2-dependent phosphorylation determines cellular localization and stability of ataxin-3. *Human molecular genetics* **18**: 3334-3343.

47. Sacco, JJ, Yau, TY, Darling, S, Patel, V, Liu, H, Urbe, S, *et al.* (2014). The deubiquitylase Ataxin-3 restricts PTEN transcription in lung cancer cells. *Oncogene* **33**: 4265-4272.

48. Evert, BO, Vogt, IR, Vieira-Saecker, AM, Ozimek, L, de Vos, RA, Brunt, ER, *et al.* (2003). Gene expression profiling in ataxin-3 expressing cell lines reveals distinct effects of normal and mutant ataxin-3. *Journal of neuropathology and experimental neurology* **62**: 1006-1018.

49. Li, F, Macfarlan, T, Pittman, RN, and Chakravarti, D (2002). Ataxin-3 is a histone-binding protein with two independent transcriptional corepressor activities. *The Journal of biological chemistry* **277**: 45004-45012.

50. Evert, BO, Araujo, J, Vieira-Saecker, AM, de Vos, RA, Harendza, S, Klockgether, T, *et al.* (2006). Ataxin-3 represses transcription via chromatin binding, interaction with histone deacetylase 3, and histone deacetylation. *The Journal of neuroscience : the official journal of the Society for Neuroscience* **26**: 11474-11486.

51. Rodrigues, AJ, Coppola, G, Santos, C, Costa Mdo, C, Ailion, M, Sequeiros, J, *et al.* (2007). Functional genomics and biochemical characterization of the C. elegans orthologue of the Machado-Joseph disease protein ataxin-3. *FASEB journal : official publication of the Federation of American Societies for Experimental Biology* **21**: 1126-1136.

52. Rodrigues, AJ, Neves-Carvalho, A, Teixeira-Castro, A, Rokka, A, Corthals, G, Logarinho, E, *et al.* (2011). Absence of ataxin-3 leads to enhanced stress response in C. elegans. *PloS one* **6**: e18512.

53. Alves, S, Nascimento-Ferreira, I, Dufour, N, Hassig, R, Auregan, G, Nobrega, C, *et al.* (2010). Silencing ataxin-3 mitigates degeneration in a rat model of Machado-Joseph disease: no role for wild-type ataxin-3? *Human molecular genetics* **19**: 2380-2394.

54. Schmitt, I, Linden, M, Khazneh, H, Evert, BO, Breuer, P, Klockgether, T, *et al.* (2007). Inactivation of the mouse Atxn3 (ataxin-3) gene increases protein ubiquitination. *Biochemical and biophysical research communications* **362**: 734-739.

55. Switonski, PM, Fiszer, A, Kazmierska, K, Kurpisz, M, Krzyzosiak, WJ, and Figiel, M (2011). Mouse ataxin-3 functional knock-out model. *Neuromolecular Med* **13**: 54-65.

56. Rodrigues, AJ, do Carmo Costa, M, Silva, TL, Ferreira, D, Bajanca, F, Logarinho, E, *et al.* (2010). Absence of ataxin-3 leads to cytoskeletal disorganization and increased cell death. *Biochimica et biophysica acta* **1803**: 1154-1163.

57. Schmitt, I, Brattig, T, Gossen, M, and Riess, O (1997). Characterization of the rat spinocerebellar ataxia type 3 gene. *Neurogenetics* **1**: 103-112.

58. Evert, BO, Wullner, U, Schulz, JB, Weller, M, Groscurth, P, Trottier, Y, *et al.* (1999). High level expression of expanded full-length ataxin-3 in vitro causes cell death and formation of intranuclear inclusions in neuronal cells. *Human molecular genetics* **8**: 1169-1176.

59. Ikeda, H, Yamaguchi, M, Sugai, S, Aze, Y, Narumiya, S, and Kakizuka, A (1996). Expanded polyglutamine in the Machado-Joseph disease protein induces cell death in vitro and in vivo. *Nature genetics* **13**: 196-202.

60. Teixeira-Castro, A, Ailion, M, Jalles, A, Brignull, HR, Vilaca, JL, Dias, N, *et al.* (2011). Neuron-specific proteotoxicity of mutant ataxin-3 in C. elegans: rescue by the DAF-16 and HSF-1 pathways. *Human molecular genetics* **20**: 2996-3009.

61. Scarff, CA, Almeida, B, Fraga, J, Macedo-Ribeiro, S, Radford, SE, and Ashcroft, AE (2015). Examination of Ataxin-3 (atx-3) Aggregation by Structural Mass Spectrometry Techniques: A Rationale for

Expedited Aggregation upon Polyglutamine (polyQ) Expansion. *Molecular & cellular proteomics : MCP* **14**: 1241-1253.

62. Bichelmeier, U, Schmidt, T, Hubener, J, Boy, J, Ruttiger, L, Habig, K, *et al.* (2007). Nuclear localization of ataxin-3 is required for the manifestation of symptoms in SCA3: in vivo evidence. *The Journal of neuroscience : the official journal of the Society for Neuroscience* **27**: 7418-7428.

63. Nguyen, HP, Hubener, J, Weber, JJ, Grueninger, S, Riess, O, and Weiss, A (2013). Cerebellar soluble mutant ataxin-3 level decreases during disease progression in Spinocerebellar Ataxia Type 3 mice. *PloS one* **8**: e62043.

64. Seidel, K, den Dunnen, WF, Schultz, C, Paulson, H, Frank, S, de Vos, RA, *et al.* (2010). Axonal inclusions in spinocerebellar ataxia type 3. *Acta neuropathologica* **120**: 449-460.

65. Hayashi, M, Kobayashi, K, and Furuta, H (2003). Immunohistochemical study of neuronal intranuclear and cytoplasmic inclusions in Machado-Joseph disease. *Psychiatry and clinical neurosciences* **57**: 205-213.

66. Ehrmann, M, and Clausen, T (2004). Proteolysis as a regulatory mechanism. *Annual review of genetics* **38**: 709-724.

67. Takahashi, T, Kikuchi, S, Katada, S, Nagai, Y, Nishizawa, M, and Onodera, O (2008). Soluble polyglutamine oligomers formed prior to inclusion body formation are cytotoxic. *Human molecular genetics* **17**: 345-356.

68. Berke, SJ, Schmied, FA, Brunt, ER, Ellerby, LM, and Paulson, HL (2004). Caspase-mediated proteolysis of the polyglutamine disease protein ataxin-3. *Journal of neurochemistry* **89**: 908-918.

69. Wellington, CL, Ellerby, LM, Hackam, AS, Margolis, RL, Trifiro, MA, Singaraja, R, *et al.* (1998). Caspase cleavage of gene products associated with triplet expansion disorders generates truncated fragments containing the polyglutamine tract. *The Journal of biological chemistry* **273**: 9158-9167.

70. Hubener, J, Weber, JJ, Richter, C, Honold, L, Weiss, A, Murad, F, *et al.* (2013). Calpain-mediated ataxin-3 cleavage in the molecular pathogenesis of spinocerebellar ataxia type 3 (SCA3). *Human molecular genetics* **22**: 508-518.

71. Haacke, A, Hartl, FU, and Breuer, P (2007). Calpain inhibition is sufficient to suppress aggregation of polyglutamine-expanded ataxin-3. *The Journal of biological chemistry* **282**: 18851-18856.

72. Simoes, AT, Goncalves, N, Koeppen, A, Deglon, N, Kugler, S, Duarte, CB, *et al.* (2012). Calpastatin-mediated inhibition of calpains in the mouse brain prevents mutant ataxin 3 proteolysis, nuclear localization and aggregation, relieving Machado-Joseph disease. *Brain : a journal of neurology* **135**: 2428-2439.

73. Koch, P, Breuer, P, Peitz, M, Jungverdorben, J, Kesavan, J, Poppe, D, *et al.* (2011). Excitation-induced ataxin-3 aggregation in neurons from patients with Machado-Joseph disease. *Nature* **480**: 543-546.

74. Hansen, SK, Stummann, TC, Borland, H, Hasholt, LF, Tumer, Z, Nielsen, JE, *et al.* (2016). Induced pluripotent stem cell - derived neurons for the study of spinocerebellar ataxia type 3. *Stem Cell Res* **17**: 306-317.

75. Doss-Pepe, EW, Stenroos, ES, Johnson, WG, and Madura, K (2003). Ataxin-3 interactions with rad23 and valosin-containing protein and its associations with ubiquitin chains and the proteasome are consistent with a role in ubiquitin-mediated proteolysis. *Molecular and cellular biology* **23**: 6469-6483.

76. Hirabayashi, M, Inoue, K, Tanaka, K, Nakadate, K, Ohsawa, Y, Kamei, Y, *et al.* (2001). VCP/p97 in abnormal protein aggregates, cytoplasmic vacuoles, and cell death, phenotypes relevant to neurodegeneration. *Cell death and differentiation* **8**: 977-984.

77. Chai, Y, Koppenhafer, SL, Shoesmith, SJ, Perez, MK, and Paulson, HL (1999). Evidence for proteasome involvement in polyglutamine disease: localization to nuclear inclusions in SCA3/MJD and suppression of polyglutamine aggregation in vitro. *Human molecular genetics* **8**: 673-682.

78. Hubener, J, Vauti, F, Funke, C, Wolburg, H, Ye, Y, Schmidt, T, *et al.* (2011). N-terminal ataxin-3 causes neurological symptoms with inclusions, endoplasmic reticulum stress and ribosomal dislocation. *Brain : a journal of neurology* **134**: 1925-1942.

79. Wong, E, and Cuervo, AM (2010). Autophagy gone awry in neurodegenerative diseases. *Nature neuroscience* **13**: 805-811.

80. Nascimento-Ferreira, I, Santos-Ferreira, T, Sousa-Ferreira, L, Auregan, G, Onofre, I, Alves, S, *et al.* (2011). Overexpression of the autophagic beclin-1 protein clears mutant ataxin-3 and alleviates Machado-Joseph disease. *Brain : a journal of neurology* **134**: 1400-1415.

81. Ravikumar, B, Vacher, C, Berger, Z, Davies, JE, Luo, S, Oroz, LG, *et al.* (2004). Inhibition of mTOR induces autophagy and reduces toxicity of polyglutamine expansions in fly and mouse models of Huntington disease. *Nature genetics* **36**: 585-595.

82. Ashkenazi, A, Bento, CF, Ricketts, T, Vicinanza, M, Siddiqi, F, Pavel, M, *et al.* (2017). Polyglutamine tracts regulate beclin 1-dependent autophagy. *Nature* **545**: 108-111.

83. Ajayi, A, Yu, X, Lindberg, S, Langel, U, and Strom, AL (2012). Expanded ataxin-7 cause toxicity by inducing ROS production from NADPH oxidase complexes in a stable inducible Spinocerebellar ataxia type 7 (SCA7) model. *BMC neuroscience* **13**: 86.

84. Goswami, A, Dikshit, P, Mishra, A, Mulherkar, S, Nukina, N, and Jana, NR (2006). Oxidative stress promotes mutant huntingtin aggregation and mutant huntingtin-dependent cell death by mimicking proteasomal malfunction. *Biochemical and biophysical research communications* **342**: 184-190.

85. Kim, SJ, Kim, TS, Hong, S, Rhim, H, Kim, IY, and Kang, S (2003). Oxidative stimuli affect polyglutamine aggregation and cell death in human mutant ataxin-1-expressing cells. *Neuroscience letters* **348**: 21-24.

86. Yu, YC, Kuo, CL, Cheng, WL, Liu, CS, and Hsieh, M (2009). Decreased antioxidant enzyme activity and increased mitochondrial DNA damage in cellular models of Machado-Joseph disease. *Journal of neuroscience research* **87**: 1884-1891.

87. Kazachkova, N, Raposo, M, Montiel, R, Cymbron, T, Bettencourt, C, Silva-Fernandes, A, *et al.* (2013). Patterns of mitochondrial DNA damage in blood and brain tissues of a transgenic mouse model of Machado-Joseph disease. *Neuro-degenerative diseases* **11**: 206-214.

88. Laco, MN, Oliveira, CR, Paulson, HL, and Rego, AC (2012). Compromised mitochondrial complex II in models of Machado-Joseph disease. *Biochimica et biophysica acta* **1822**: 139-149.

89. Emerit, J, Edeas, M, and Bricaire, F (2004). Neurodegenerative diseases and oxidative stress. *Biomedicine & pharmacotherapy = Biomedecine & pharmacotherapie* **58**: 39-46.

90. Perez, MK, Paulson, HL, Pendse, SJ, Saionz, SJ, Bonini, NM, and Pittman, RN (1998). Recruitment and the role of nuclear localization in polyglutamine-mediated aggregation. *The Journal of cell biology* **143**: 1457-1470.

91. van Roon-Mom, WM, Reid, SJ, Faull, RL, and Snell, RG (2005). TATA-binding protein in neurodegenerative disease. *Neuroscience* **133**: 863-872.

92. Evert, BO, Vogt, IR, Kindermann, C, Ozimek, L, de Vos, RA, Brunt, ER, *et al.* (2001). Inflammatory genes are upregulated in expanded ataxin-3-expressing cell lines and spinocerebellar ataxia type 3 brains. *The Journal of neuroscience : the official journal of the Society for Neuroscience* **21**: 5389-5396.

93. Chou, AH, Yeh, TH, Ouyang, P, Chen, YL, Chen, SY, and Wang, HL (2008). Polyglutamine-expanded ataxin-3 causes cerebellar dysfunction of SCA3 transgenic mice by inducing transcriptional dysregulation. *Neurobiology of disease* **31**: 89-101.

94. Simoes, AT, Goncalves, N, Nobre, RJ, Duarte, CB, and Pereira de Almeida, L (2014). Calpain inhibition reduces ataxin-3 cleavage alleviating neuropathology and motor impairments in mouse models of Machado-Joseph disease. *Human molecular genetics* **23**: 4932-4944.

95. Schmidt, T, Lindenberg, KS, Krebs, A, Schols, L, Laccone, F, Herms, J, *et al.* (2002). Protein surveillance machinery in brains with spinocerebellar ataxia type 3: redistribution and differential recruitment of 26S proteasome subunits and chaperones to neuronal intranuclear inclusions. *Annals of neurology* **51**: 302-310.

96. Ramani, B, Panwar, B, Moore, LR, Wang, B, Huang, R, Guan, Y, *et al.* (2017). Comparison of spinocerebellar ataxia type 3 mouse models identifies early gain-of-function, cell-autonomous transcriptional changes in oligodendrocytes. *Human molecular genetics* **26**: 3362-3374.

97. Banez-Coronel, M, Ayhan, F, Tarabochia, AD, Zu, T, Perez, BA, Tusi, SK, *et al.* (2015). RAN Translation in Huntington Disease. *Neuron* **88**: 667-677.

98. Wang, LC, Chen, KY, Pan, H, Wu, CC, Chen, PH, Liao, YT, *et al.* (2011). Muscleblind participates in RNA toxicity of expanded CAG and CUG repeats in Caenorhabditis elegans. *Cellular and molecular life sciences : CMLS* **68**: 1255-1267.

99. Mykowska, A, Sobczak, K, Wojciechowska, M, Kozlowski, P, and Krzyzosiak, WJ (2011). CAG repeats mimic CUG repeats in the misregulation of alternative splicing. *Nucleic acids research* **39**: 8938-8951.

100. Nalavade, R, Griesche, N, Ryan, DP, Hildebrand, S, and Krauss, S (2013). Mechanisms of RNA-induced toxicity in CAG repeat disorders. *Cell death & disease* **4**: e752.

101. Griesche, N, Schilling, J, Weber, S, Rohm, M, Pesch, V, Matthes, F, *et al.* (2016). Regulation of mRNA Translation by MID1: A Common Mechanism of Expanded CAG Repeat RNAs. *Frontiers in cellular neuroscience* **10**: 226.

102. McLeod, CJ, O'Keefe, LV, and Richards, RI (2005). The pathogenic agent in Drosophila models of 'polyglutamine' diseases. *Human molecular genetics* **14**: 1041-1048.

103. Davies, JE, and Rubinsztein, DC (2006). Polyalanine and polyserine frameshift products in Huntington's disease. *Journal of medical genetics* **43**: 893-896.

104. Gaspar, C, Jannatipour, M, Dion, P, Laganiere, J, Sequeiros, J, Brais, B, *et al.* (2000). CAG tract of MJD-1 may be prone to frameshifts causing polyalanine accumulation. *Human molecular genetics* **9**: 1957-1966.

105. Stochmanski, SJ, Therrien, M, Laganiere, J, Rochefort, D, Laurent, S, Karemera, L, *et al.* (2012). Expanded ATXN3 frameshifting events are toxic in Drosophila and mammalian neuron models. *Human molecular genetics* **21**: 2211-2218.

106. Wojciechowska, M, Olejniczak, M, Galka-Marciniak, P, Jazurek, M, and Krzyzosiak, WJ (2014). RAN translation and frameshifting as translational challenges at simple repeats of human neurodegenerative disorders. *Nucleic acids research* **42**: 11849-11864.

107. Gao, R, Liu, Y, Silva-Fernandes, A, Fang, X, Paulucci-Holthauzen, A, Chatterjee, A, *et al.* (2015). Inactivation of PNKP by mutant ATXN3 triggers apoptosis by activating the DNA damage-response pathway in SCA3. *PLoS genetics* **11**: e1004834.

108. Tu, Y, Liu, H, Zhu, X, Shen, H, Ma, X, Wang, F, *et al.* (2017). Ataxin-3 promotes genome integrity by stabilizing Chk1. *Nucleic acids research* **45**: 4532-4549.

109. Subba Rao, K (2007). Mechanisms of disease: DNA repair defects and neurological disease. *Nature clinical practice Neurology* **3**: 162-172.

110. Ward, JM, and La Spada, AR (2015). Ataxin-3, DNA damage repair, and SCA3 cerebellar degeneration: on the path to parsimony? *PLoS genetics* **11**: e1004937.

111. Menzies, FM, Huebener, J, Renna, M, Bonin, M, Riess, O, and Rubinsztein, DC (2010). Autophagy induction reduces mutant ataxin-3 levels and toxicity in a mouse model of spinocerebellar ataxia type 3. *Brain : a journal of neurology* **133**: 93-104.

112. Wang, HL, Hu, SH, Chou, AH, Wang, SS, Weng, YH, and Yeh, TH (2013). H1152 promotes the degradation of polyglutamine-expanded ataxin-3 or ataxin-7 independently of its ROCK-inhibiting effect and ameliorates mutant ataxin-3-induced neurodegeneration in the SCA3 transgenic mouse. *Neuropharmacology* **70**: 1-11.

113. Duarte-Silva, S, Silva-Fernandes, A, Neves-Carvalho, A, Soares-Cunha, C, Teixeira-Castro, A, and Maciel, P (2016). Combined therapy with m-TOR-dependent and -independent autophagy inducers causes neurotoxicity in a mouse model of Machado-Joseph disease. *Neuroscience* **313**: 162-173.

114. Yoshida, H, Yoshizawa, T, Shibasaki, F, Shoji, S, and Kanazawa, I (2002). Chemical chaperones reduce aggregate formation and cell death caused by the truncated Machado-Joseph disease gene product with an expanded polyglutamine stretch. *Neurobiology of disease* **10**: 88-99.

115. Tanaka, M, Machida, Y, Niu, S, Ikeda, T, Jana, NR, Doi, H, *et al.* (2004). Trehalose alleviates polyglutamine-mediated pathology in a mouse model of Huntington disease. *Nature medicine* **10**: 148-154.

116. Teixeira-Castro, A, Jalles, A, Esteves, S, Kang, S, da Silva Santos, L, Silva-Fernandes, A, *et al.* (2015). Serotonergic signalling suppresses ataxin 3 aggregation and neurotoxicity in animal models of Machado-Joseph disease. *Brain : a journal of neurology* **138**: 3221-3237.

117. Saute, JA, de Castilhos, RM, Monte, TL, Schumacher-Schuh, AF, Donis, KC, D'Avila, R, *et al.* (2014). A randomized, phase 2 clinical trial of lithium carbonate in Machado-Joseph disease. *Movement disorders : official journal of the Movement Disorder Society* **29**: 568-573.

118. Chen, X, Tang, TS, Tu, H, Nelson, O, Pook, M, Hammer, R, *et al.* (2008). Deranged calcium signaling and neurodegeneration in spinocerebellar ataxia type 3. *The Journal of neuroscience : the official journal of the Society for Neuroscience* **28**: 12713-12724.

119. Goncalves, N, Simoes, AT, Cunha, RA, and de Almeida, LP (2013). Caffeine and adenosine A(2A) receptor inactivation decrease striatal neuropathology in a lentiviral-based model of Machado-Joseph disease. *Annals of neurology* **73**: 655-666.

120. Goncalves, N, Simoes, AT, Prediger, RD, Hirai, H, Cunha, RA, and Pereira de Almeida, L (2017). Caffeine alleviates progressive motor deficits in a transgenic mouse model of spinocerebellar ataxia. *Annals of neurology* **81**: 407-418.

121. Chou, AH, Chen, SY, Yeh, TH, Weng, YH, and Wang, HL (2011). HDAC inhibitor sodium butyrate reverses transcriptional downregulation and ameliorates ataxic symptoms in a transgenic mouse model of SCA3. *Neurobiology of disease* **41**: 481-488.

122. Cunha-Santos, J, Duarte-Neves, J, Carmona, V, Guarente, L, Pereira de Almeida, L, and Cavadas, C (2016). Caloric restriction blocks neuropathology and motor deficits in Machado-Joseph disease mouse models through SIRT1 pathway. *Nature communications* **7**: 11445.

123. Mendonca, LS, Nobrega, C, Hirai, H, Kaspar, BK, and Pereira de Almeida, L (2015). Transplantation of cerebellar neural stem cells improves motor coordination and neuropathology in Machado-Joseph disease mice. *Brain : a journal of neurology* **138**: 320-335.

124. Falkner, S, Grade, S, Dimou, L, Conzelmann, KK, Bonhoeffer, T, Gotz, M, *et al.* (2016). Transplanted embryonic neurons integrate into adult neocortical circuits. *Nature* **539**: 248-253.

125. Duncan, T, and Valenzuela, M (2017). Alzheimer's disease, dementia, and stem cell therapy. *Stem cell research & therapy* **8**: 111.

126. Han, F, Baremberg, D, Gao, J, Duan, J, Lu, X, Zhang, N, *et al.* (2015). Development of stem cell-based therapy for Parkinson's disease. *Translational Neurodegeneration* **4**: 16.

127. Amariglio, N, Hirshberg, A, Scheithauer, BW, Cohen, Y, Loewenthal, R, Trakhtenbrot, L, *et al.* (2009). Donor-derived brain tumor following neural stem cell transplantation in an ataxia telangiectasia patient. *PLoS medicine* **6**: e1000029.

128. Liu, J, Yu, D, Aiba, Y, Pendergraff, H, Swayze, EE, Lima, WF, *et al.* (2013). ss-siRNAs allele selectively inhibit ataxin-3 expression: multiple mechanisms for an alternative gene silencing strategy. *Nucleic acids research* **41**: 9570-9583.

129. Nobrega, C, Nascimento-Ferreira, I, Onofre, I, Albuquerque, D, Hirai, H, Deglon, N, *et al.* (2013). Silencing mutant ataxin-3 rescues motor deficits and neuropathology in Machado-Joseph disease transgenic mice. *PloS one* **8**: e52396.

130. Alves, S, Nascimento-Ferreira, I, Auregan, G, Hassig, R, Dufour, N, Brouillet, E, *et al.* (2008). Allele-specific RNA silencing of mutant ataxin-3 mediates neuroprotection in a rat model of Machado-Joseph disease. *PloS one* **3**: e3341.

131. Moore, LR, Rajpal, G, Dillingham, IT, Qutob, M, Blumenstein, KG, Gattis, D, *et al.* Evaluation of Antisense Oligonucleotides Targeting ATXN3 in SCA3 Mouse Models. *Molecular Therapy - Nucleic Acids* **7**: 200-210.

132. Evers, MM, Pepers, BA, van Deutekom, JC, Mulders, SA, den Dunnen, JT, Aartsma-Rus, A, *et al.* (2011). Targeting several CAG expansion diseases by a single antisense oligonucleotide. *PloS one* **6**: e24308.

133. Evers, MM, Tran, HD, Zalachoras, I, Pepers, BA, Meijer, OC, den Dunnen, JT, *et al.* (2013). Ataxin-3 protein modification as a treatment strategy for spinocerebellar ataxia type 3: removal of the CAG containing exon. *Neurobiology of disease* **58**: 49-56.

2

Antisense oligonucleotides in therapy for neurodegenerative disorders

Melvin M. Evers, Lodewijk J. A. Toonen, Willeke M. C. van Roon-Mom (2015).
Adv Drug Deliv Rev, 87, 90-103

ABSTRACT

Antisense oligonucleotides are synthetic single stranded strings of nucleic acids that bind to RNA and thereby alter or reduce expression of the target RNA. They can reduce expression of mutant proteins by breakdown of the targeted transcript, but they can also restore protein expression or modify proteins through interference with pre-mRNA splicing. There has been a recent revival of interest in the use of antisense oligonucleotides to treat several neurodegenerative disorders using different approaches to prevent disease onset or halt disease progression and the first clinical trials for spinal muscular atrophy and amyotrophic lateral sclerosis showing promising results. For these trials, intrathecal delivery is being used but direct infusion into the brain ventricles and several methods of passing the blood brain barrier after peripheral administration are also under investigation.

INTRODUCTION

There has been a recent revival of interest in the use of antisense oligonucleotides to treat neurodegenerative disorders. Antisense oligonucleotides are synthetic single stranded strings of nucleic acids, between 8-50 nucleotides in length, that bind to RNA through standard Watson-Crick base pairing. Antisense oligonucleotides interfere with gene expression by altering RNA function. Depending on sequence and modifications, antisense oligonucleotides can alter RNA function through several distinct mechanisms, making them a diverse tool. They can be used to restore protein expression, reduce expression of a toxic protein, or modify mutant proteins to reduce their toxicity. Antisense-mediated gene inhibition was first introduced by Stephenson and Zamecnik in 1978 [1]. Using a DNA molecule of 13 nucleotides in length with modifications at the 3′ and 5′ OH moieties, they showed inhibition of replication and cell transformation of the Rous sarcoma virus. Since then, modifications to the backbone and sugar component have improved stability, binding strength and specificity which has made antisense oligonucleotides suitable for therapeutic application [2]. For several neurodegenerative disorders, antisense oligonucleotide therapy has now moved from the preclinical to the clinical stage, facilitated by the remarkable widespread distribution and cellular uptake of antisense oligonucleotides once delivered into the brain [3, 4].

There are many other types of nucleic acid molecules that can interfere at the RNA level using the RNA-induced silencing complex (reviewed in [5]) that promote selective degradation of homologous cellular mRNAs, but these will not be discussed. In this review we will outline the key characteristics of antisense oligonucleotides that make them very suitable for treating neurological disorders. We will discuss the delivery of antisense oligonucleotides to the nervous system and the available chemical modifications of antisense oligonucleotides that have been applied to neurodegenerative disorders. Finally different functional mechanisms to alter RNA function in the nervous system will be discussed, as well as several neurodegenerative disorders where these different antisense oligonucleotide mechanisms are being applied.

DELIVERY TO THE NERVOUS SYSTEM

In drug discovery, the aim is to find a substance which is potent, selective, and preferably bioavailable that needs to reach its target at sufficient concentrations [6]. For drugs to reach the nervous system they first have to cross the vascular barrier, which is made up of the blood brain barrier (BBB) or the blood-spinal cord barrier (BSCB). These vascular barriers prevent most molecules from entering the nervous system from the blood circulation. Despite this gate-controlling system, essential nutrients, such as glucose, are permitted to pass [7]. The vascular barriers of the nervous system are comprised of a monolayer of endothelial cells forming tight junctions through interactions of cell adhesion molecules [8]. Other structural components are astrocytes that surround the endothelial cells with their processes, pericytes located between the endothelial cells and astrocytes, macrophages, and finally the basement membrane. The endothelial cells of the BBB are characterized by only few fenestrae and pinocytic vesicles,

limiting transport to and from the brain. The BBB thus also largely separates the peripheral immune system from the brain. Although the BSCB is largely made up of the same components as the BBB, there are some functional and morphological differences [9]. For instance in the BSCB, the equivalent of the BBB endothelial cells are the choroid plexus epithelial cells [10] and the permeability of the two barriers are different probably due to differences in tight junction protein expression [11]. In neurodegenerative diseases, disruption of the vascular barrier is common [8, 12, 13] and it was shown in animal models that a compromised BBB barrier in itself can lead to neurodegeneration [12]. However, for most diseases of the nervous system that could be treated with antisense oligonucleotides, the antisense oligonucleotides will not be able to cross the vascular barrier when delivered systemically. Several methods have been used to deliver antisense oligonucleotides to the nervous system (see **Fig. 1**). Antisense oligonucleotide modifications will largely determine the most efficient route of delivery. In this chapter the different mechanisms for antisense oligonucleotides to enter the nervous system will be outlined. We will next review the different types of antisense oligonucleotide modifications used for neurodegenerative disorders in chapter 3.

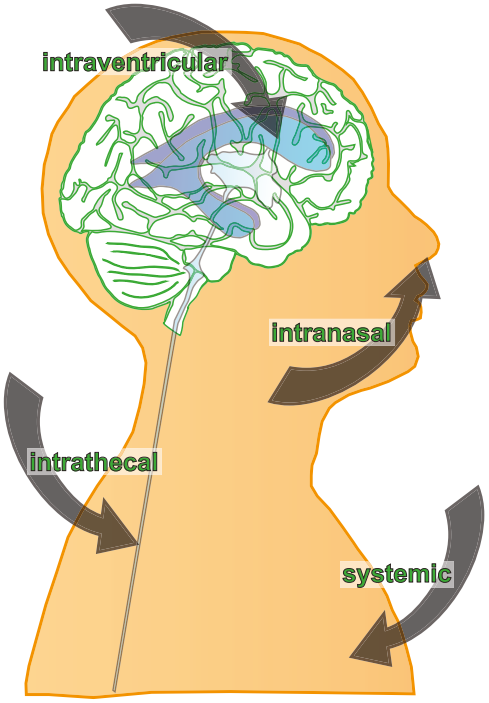

Figure 1. Routes for delivery of antisense oligonucleotides to the central nervous system. Next to systemic delivery, antisense oligonucleotides can be directly delivered into the cerebrospinal fluid through intracerebroventricular or intrathecal infusion using an implanted reservoir that is connected to the ventricles within the brain or spinal cord via an outlet catheter. An alternative less invasive route of delivery of antisense oligonucleotides could be conceivable via intranasal administration.

PERIPHERAL DELIVERY

Efforts are ongoing to deliver antisense oligonucleotides to the nervous system via the systemic route. In general, when a drug is administered systemically, a fraction will be bound to proteins (e.g. serum albumin, lipoprotein etc.) and a fraction will be unbound. The bound fraction is the pharmacologically relevant fraction, since it is available to cross the vascular barrier [8] depending on its physicochemical properties.

The first mechanism by which antisense oligonucleotides could cross the vascular barrier is simple diffusion. Small lipophilic substances which have a hydrogen bond are more likely to pass the vascular barrier [14] than compounds without hydrogen bonds and only molecules with a molecular weight smaller than 400 Dalton are able to cross the vascular barrier [15]. Antisense oligonucleotides generally have a molecular weight of approximately 6,000 to 10,000 Dalton and thus are too large to cross the vascular barrier by simple diffusion and reach an effective concentration in the nervous system. Indeed, early studies showed only limited brain uptake of peripherally administered radioactive antisense oligonucleotides with less than 1% of the injected oligonucleotide measured in brain [16-19]. The mechanism by which this antisense oligonucleotide crossed the BBB was named the saturable oligonucleotide transport system [17].

Another mechanism to cross the vascular barrier is via receptor-mediated endocytosis, which allows macromolecules, such as transferrin, insulin, leptin, and insulin-like growth factor 1, to enter the nervous system [20]. Studies by Lee and associates used biotinylated antisense oligonucleotides captured with a streptavidin conjugated radioactive labelled monoclonal antibody to the mouse transferrin receptor to quantify gene expression *in vivo* [21]. This radioactive labelled antisense oligonucleotide conjugate reached the brain through the endogenous transferrin transport pathway (receptor-mediated endocytosis) in a transgenic mouse model [21]. This same transferrin transport pathway was used to transport nanoparticles carrying antisense oligonucleotides targeting aquaporin 4 into the brain parenchyma [22].

More recent research has focussed on cell-penetrating peptide (CPP)-based delivery systems [23]. These have shown strong transmembrane capacity and great potential for therapeutic approaches for neurodegenerative disorders [24]. CPPs can be up to 30 amino acids in length and can carry a wide variety of cargos. Different CPPs use distinct cellular translocation pathways, which depend on cell types and cargos [25]. Systemically delivered antisense oligonucleotides tagged with arginine-rich CPPs were able to cross the BBB and were widely distributed throughout the brain of wild-type mice [26]. To note, not all types of antisense oligonucleotide modifications are suitable for coupling with CPPs. Although two promising CPP antisense oligonucleotides were abandoned as therapeutic agents since repetitive intravenous (IV) bolus injections of CPP antisense oligonucleotides caused lethargy and weight loss in rats [27] and tubular degeneration in the kidneys of monkeys [28], CPP systems are still a promising delivery system.

Although not tested thus far, antisense oligonucleotides encapsulated in exosomes would theoretically also be able to cross the vascular barrier after IV injection. Exosomes are a well-studied class of extracellular vesicles known to mediate communication between cells through transfer of proteins and nucleic acids [29, 30]. IV injection of exosomes transduced with short viral

peptides derived from rabies virus glycoprotein (RVG) resulted in crossing of the BBB and siRNA delivery to the brain [31]. These IV injected RVG-targeted exosomes bound to neurons, microglia and oligodendrocytes, resulting in a specific gene knockdown in the brain [29].

DIRECT DELIVERY TO THE NERVOUS SYSTEM

Besides mechanisms to cross the vascular barriers, there are also techniques that bypass them through direct infusion into the cerebrospinal fluid (CSF).

Antisense oligonucleotides can be infused intracerebroventricularly (ICV) after which the ASOs would have to pass the ependymal cell layer that lines the ventricular system to enter the parenchyma. Intrathecal (IT) delivery means delivery of the ASOs into the subarachnoid space of the spinal cord. From here it will have to pass the pia mater to enter the parenchyma. ASOs can be delivered ICT or IT through an outlet catheter that is connected to an implanted reservoir. Drugs can be injected into the reservoir and delivered directly to the CSF.

This route of delivery has several advantages over peripheral administration. It results in immediate high drug concentrations in the CSF meaning that a smaller dose can be used, potentially minimizing toxicity. Also, because there is free exchange between the CSF and brain parenchyma, and the BBB prevents transport of the antisense oligonucleotides into the peripheral circulation, direct delivery into the nervous system can relatively rapidly result in therapeutic drug concentrations. This infusion technique was used in antisense oligonucleotide applications in rodent models of neurodegenerative disorders as well as non-human primates [32]. Moreover, IT drug therapy has been applied to a wide variety of neurological conditions [33, 34]. To date there have been two phase I clinical trials completed using IT infusion of antisense oligonucleotides in amyotrophic lateral sclerosis (ALS) and spinal muscular atrophy (SMA) patients [35, 36] without any major adverse side effects [35].

INTRANASAL DELIVERY TO THE BRAIN

Although to date there have been very few studies showing delivery of antisense oligonucleotides to the brain via intranasal administration, this is a very promising alternative route of delivery. After intranasal administration, molecules can be transported along the olfactory and trigeminal nerve pathway and the rostral migratory stream [37]. It is less invasive compared to the above mentioned antisense oligonucleotide delivery methods and already was used successfully in clinical trials showing improved cognition after intranasal insulin application in Alzheimer disease patients [38]. Also intranasal delivery of small interfering RNA (siRNA) was shown to be very efficient. CPP conjugated to glycol-polycaprolactone copolymers were able to target siRNAs to the brain via the intranasal route [39]. In rats, intranasal delivery of antisense oligonucleotides was found to lead to good distribution throughout the brain, and was able to slow down intracerebral tumour growth [40]. These studies hence indicate that intranasal delivery may become a viable option for antisense oligonucleotide delivery in the future.

CHEMICAL MODIFICATIONS

Initially, antisense oligonucleotides were used in the form of synthetic unmodified DNA [41]. Though successful, these types of oligonucleotides proved very susceptible to degradation by endo- and exonucleases. It quickly became apparent that if antisense oligonucleotides were to be used for clinical applications, their pharmacological profile would have to be enhanced. Oligonucleotides have since benefited from technical advances in chemical modifications leading to significantly improved characteristics. Antisense oligonucleotides are available with a range of different modifications on the phosphate backbone and ribose sugar group in the case of RNA (see **Table 1**). The modifications used in studies of neurodegenerative disorders and their mode of actions will be discussed in the paragraphs below.

BACKBONE MODIFICATIONS: COUNTERACTING NUCLEASES

One of the main factors impeding antisense oligonucleotide efficacy is their rapid degradation by endo- and exonucleases. A 3′ to 5′ exonuclease is able to degrade unprotected antisense oligonucleotides within 30 minutes in serum [42], while intracellular exo- and endonucleases can lead to degradation in an even shorter timespan [43]. Brain associated α-exonuclease is likely responsible for degradation of antisense oligonucleotides in CSF [4]. One of the first successful modifications providing a good degree of protection from these nucleases is the phosphorothioate (PS) backbone. Termed the first generation of oligonucleotide modifications, the PS backbone is accomplished by replacement of one of the non-bridging oxygen atoms in the backbone with a sulphur atom [44]. Oligonucleotides with this modification are more stable with reported half-lives of 9 hours in human serum and 19 hours in rat CSF [45]. The negative charge of PS DNA furthermore allows for good uptake into various cell types *in vitro* [46] and into various brain cell types after microinjection into brain [47]. Another important characteristic of the PS backbone is its ability to activate ribonuclease H (RNase H), allowing for use in applications where target RNA downregulation is desired [48]. RNase H recognizes an RNA-DNA heteroduplex, and then cleaves the RNA strand, resulting in a 5-phosphate on the product and release of the intact DNA strand [49, 50]. A less favourable characteristic of the PS backbone is that it destabilize duplexes, leading to a decrease in melting temperature [51]. Cytotoxic effects of PS at high concentrations have been reported (reviewed in [52]), and are thought to be related to protein binding [53, 54] or complement activation [55]. PS modified antisense oligonucleotides have undergone extensive pharmacokinetic testing aimed at peripheral administration. In this context, it was found that PS oligonucleotides bind serum proteins, leading to reduced renal clearance and an increased circulation time [56, 57]. These favourable pharmacokinetic properties in the periphery are contrasted by the poor ability of PS oligonucleotides to cross the BBB [58].

Table 1. Chemical modifications of antisense oligonucleotides.

	Modification	Main features
Phosphate linkage	phosphodiester	Naturally occurring
		Inexpensive
	phosphoramidate	High affinity
		High nuclease resistance
		Does not support RNase H
	phosphorothioate (PS)	Improved nuclease resistance
		Improved binding to plasma proteins (preventing kidney clearance)
Sugar modification	LNA	Strong binding affinity
		Increased nuclease resistance
		Does not support RNase H
	2OMe	Improved binding affinity
		Improved nuclease resistance
		Inhibits immune stimulation of PS backbone
		Does not support RNase H
	MOE	Improved binding affinity
		Improved nuclease resistance
		Inhibits immune stimulation of PS backbone
		Does not support RNase H
	2'-Fluoro	Improved binding affinity
		Does not support RNase H cleavage
	cEt	Strong binding affinity
		Improved nuclease resistance
		Does not support RNase H
	tc-DNA	Improved nuclease resistance
		Improved binding affinity
		Does not support RNase H
Non-ribose modifications	PMO	Neutral charge
		Improved binding affinity
		Excellent nuclease resistance
		Does not support RNase H
	PNA	Uncharged
		High binding affinity
		Low toxicity
		High nuclease resistance

Sugar modifications are typically used together with the PS backbone modification. 2OMe: 2'-O-methyl, cEt: S-constrained-ethyl, LNA: Locked nucleic acid, MOE: 2'-O-methoxy-ethyl, PMO: phosphorodiamidate morpholino oligomer, PNA: peptide nucleic acid, Tc-DNA: Tricyclo-DNA

Main disadvantages	Application	Frequency of use	Refs
Rapidly degraded by nucleases	Steric hindrance	-	[44,105-107]
Quickly cleared by kidney	RNase H cleavage		
Quickly cleared by kidney	Steric hindrance	+	[37]
Can cause immune response/ cytotoxicity at high concentrations	Steric hindrance	+ + + + +	[108-110]
Slightly reduced binding affinity compared to phosphodiester	RNase H cleavage		
Higher toxicity than other modifications	Steric hindrance	+ + +	[74,111,112]
Higher risk of a-specific binding			
Higher propensity for self-annealing			
Lower affinity than most other modifications	Steric hindrance	+ + + +	[113,114]
Lower affinity than most other modifications	Steric hindrance	+ + + +	[28,33,115]
Little improvement for nuclease resistance	Steric hindrance	+	[116]
	Steric hindrance	+ +	[117-119]
Little research data available	Steric hindrance	+	[78,79]
Rapid clearance	Steric hindrance	+ + +	[98,120,121]
Poor uptake in cell nucleus			
Poor pharmacokinetic properties			
Rapid clearance	Steric hindrance	+ +	[92,112,122,123]
Poor uptake/ pharmacokinetic properties			

SUGAR GROUP MODIFICATIONS: IMPROVING AFFINITY AND REDUCING TOXICITY

2

In addition to the PS backbone, RNA oligonucleotides can be further modified at the 2' position of the ribose sugar. These types of modifications are termed the second generation oligonucleotide modification, and, in combination with the PS backbone, have been of great importance for advancing oligonucleotide safety and pharmacologic properties. In this class of modifications, the 2'-O-methyl (2OMe) and 2'-O-methoxy-ethyl (MOE) have proven most successful thus far. These modifications increase hybridization affinity to their target RNA compared to unmodified phosphorothioates [59-61], as well as increased resistance toward nuclease degradation [61, 62]. An additional key advantage of the 2' modifications is their ability to reduce sequence independent toxicity arising from the PS backbone [63], which also holds true in the CNS [64]. An important trait of 2'-modifications is their inability to recruit RNase H [65] and oligonucleotides that are fully modified in this fashion thus cannot induce RNase H-mediated target RNA downregulation.

For 2'-O-modified-PS antisense oligonucleotides only very mild toxicity has been reported, which did not interfere with their desired effects after ICV delivery in rodent brain [66], or in cultured neuronal cells [67]. Although it has been shown that PS antisense oligonucleotides can have an immunostimulatory effect via toll-like receptors, appropriate 2'-O modifications, such as 2OMe and MOE, can suppress these effects [68-70]. It is important to mention that possible toxic and immunostimulatory effects of 2OMe-PS antisense oligonucleotides may also be due to dosage, concentration, or duration of treatment [71].

Locked nucleic acids (LNA) are a 2'-modification where the 4'-carbon has been tethered to the 2'-hydroxyl group. LNAs provide resistance to nucleases [72] and show much improved hybridization compared to the other 2'-modifications [73, 74]. LNAs are also unable to induce RNase H-mediated target RNA downregulation [75, 76]. Though LNAs provide a better RNA binding affinity than most other 2'-modifications, there appear to be more severe toxicological problems with these oligonucleotides in systemic treatment [77]. Whether this also holds true for the CNS will remain to be determined, though one study reports that LNAs are tolerated in rat brain [78]. Additionally, the high affinity of LNAs can lead to a reduction in target specificity [74, 79]. For these reasons, a chimera design where LNA modified nucleosides are interspersed by unmodified or differently 2'O-modified nucleosides can be implemented [73]. LNAs can be further modified by addition of oligospermine nucleobases. The resulting antisense oligonculeotide-oligospermine conjugates are known as zip nucleic acids (ZNA) [80]. These conjugates lack the polyanionic nature and electrostatic repulsion of the negatively charged phosphate backbones, leading to increased binding affinities and improved cellular uptake. ZNA conjugates were found to reduce huntingtin expression in Huntington disease (HD) patient-derived cells [81]. Although ZNA conjugates are primarily used as probes for real-time PCR, they possess some therapeutically interesting properties.

Another conformationally constrained oligonucleotide modification available is tricyclo-DNA (tc-DNA). This modification is aimed at lessening the flexibility around the C3´-C4´ and

C4′-C5′ bonds by addition of an ethylene bridge fused with a cyclopropane unit. The result in a more stable duplex formation [82] that is not compatible with RNase H. Tc-DNA has been reported to be stable in serum and resulted in more potent splicing correction compared to a 2OMe-PS oligonucleotide when tested in cells [83]. To date, there have been very few studies performed making use of tc-DNA, but there has been one report stating splicing modulation in the brain occurred after peripheral administration of tc-DNA in a Duchenne muscular dystrophy mouse model [84]. Interestingly, dystrophin restoration in the mouse brain resulted in complete reversal of its behavioral phenotype [84].

Other sugar modifications less frequently used in CNS studies are the 2'-fluoro and S-constrained-ethyl (cEt) oligonucleotides. The 2'-fluoro, akin to OMe and MOE modifications, replaces the 2'-hydroxy with a fluoro group and provides a higher affinity than most other 2'-modifications [65], in addition to providing resistance to nucleases [85]. The cEt modified antisense oligonucleotides provide similar binding affinity as LNA, yet appear to have a more favourable toxicity profile [86], and have recently shown good promise in a humanized mouse model for HD [87].

Taken together, the second generation of oligonucleotide modifications have provided a good degree of improvement on the PS backbone, with enhancements in nuclease resistance, binding affinity and reduction of PS-induced toxicity. However, in light of the fact that most CNS research utilising oligonucleotides aims at downregulation of target RNA, the fact that these modifications are not compatible with RNAse H cleavage is an important consideration. For this reason, a RNAse H compatible gapmer strategy was conceived of (described in chapter 4), in which a PS oligonucleotide is not modified with 2'O-modifications over its entire length. Importantly, a MOE-PS gapmer oligonucleotide was the first to make it to clinical trials for a neurodegenerative disorder, and has shown favourable tolerability [35].

OTHER OLIGONUCLEOTIDE MODIFICATIONS

Besides the PS backbone and several ribose sugar modifications described above, efforts have been made with newer modifications that combine backbone, ribose and nucleosides modifications.

Peptide nucleic acids (PNA) are generated by replacement of the entire sugar phosphate backbone with polyamide linkages [88], but are still able to hybridize through Watson-Crick binding [89]. PNAs are uncharged, and provide a high resistance to nuclease and protease degradation [90]. Another important feature of PNAs is their high binding affinity for RNA [91]. In light of their inability to activate RNAse H, PNAs are mostly implemented in splicing modulation approaches or translation inhibition. A clear shortcoming of PNAs is their poor cellular uptake [92] and water insolubility [93]. However, both uptake and water solubility can be improved using peptide conjugates [94, 95]. Uptake in neuronal cells of unmodified PNA *in vivo* has been reported [96] but the use of PNA antisense oligonucleotides in neurodegenerative disorders

remains somewhat limited. When administered peripherally, PNAs are rapidly cleared [97] and these poor pharmacokinetic properties likely in part explain their limited *in vivo* use thus far.

Phosphorodiamidate morpholino oligomers (PMO) have a morpholine ring instead of the ribose ring, and have phosphoroamidate intersubunit linkages. Similar to PNAs, PMO backbones are neutrally charged and are not compatible with RNase H [98]. PMOs are highly resistant to nuclease and protease degradation [99]. In a phase 1 clinical trial using IV administration, PMOs were well tolerated, but were shown to suffer from the same pharmacokinetic shortcomings as PNAs since they are rapidly cleared from the blood [100]. Peptides can be conjugated to the PMO for improved cellular uptake and pharmacokinetics [101]. Also, bare PMO chemistry has been successfully used to modify splicing when administered directly in mouse brain [102], though toxicity at higher doses may occur [103]. Another interesting conjugated PMO is the vivo-morpholino, which features a terminal octaguanidinium dendrimer aimed at improving cell permeability and thus tissue uptake when administered peripherally [104]. Unfortunately, there have been reports of severe toxicity following IV administration of vivo-morpholino in mice [105]. Importantly, the increased toxicity of vivo-morpholino compared to bare PMOs also appears to hold true in the brain [103, 106]. Crossing of the BBB does not appear to occur efficiently for vivo-morpholinos [107], and, though microinjection in rat brain was effective, target protein downregulation lasted for only 14 days [108].

FUNCTIONAL MECHANISMS

Depending on the chemistry and target site, antisense oligonucleotides can be used in many different ways to modulate gene expression. Below we will discuss the major functional mechanisms that can be used in neurodegenerative disorders (for schematic representation **see Fig. 2**) where either the RNA is broken down or is altered with the use of antisense oligonucleotides.

RNASE H-MEDIATED DEGRADATION

As described in the previous paragraph, 2'-modifications enhance safety and pharmacologic properties of antisense oligonucleotides. However, RNase H requires a free 2'-oxygen and oligonucleotides that are fully 2'-modified cannot induce RNase H-mediated target RNA downregulation [65]. To induce gene knockdown through RNase H, an alternative strategy using gapmers has been developed **(Fig. 2A and B)**. A gapmer antisense oligonucleotide consists of a central DNA region with flanking 2'-modified nucleosides. Because the active site of an exonuclease only binds to two or three residues at the 3′- or 5′-end, a short stretch of 2'-modified RNA nucleosides at both ends is sufficient for the protection against exonucleases [109]. The gapmer molecule thus benefits from nuclease resistance and improved uptake from the wings, whilst activating RNAse H owing to the gap region [65].

If the target protein has important cellular functions general downregulation would be detrimental. In such case specific lowering of the mutation-containing protein is desired.

Selective RNase H-mediated degradation can be achieved using antisense oligonucleotide gapmers targeting (1) specific point mutations [110], (2) structural differences between wild-type and mutant mRNA [111-113], or (3) a single nucleotide polymorphism (SNP) that is unique to the mutant RNA [114] **(Fig. 2B)**.

STERIC HINDRANCE

Next to RNase H-mediated breakdown of mRNA, protein levels can also be reduced by preventing translation **(Fig. 2C)**. Here, all nucleotides of the antisense oligonucleotide have sugar modifications rendering them RNase H resistant. Suppressing RNA translation to reduce protein levels could be achieved by antisense oligonucleotides targeting the RNA translation start site or sterically blocking the binding of RNA binding protein complexes, such as ribosomal subunits [115] **(Fig. 2C)**.

Other antisense oligonucleotide applications that do not induce the lowering of transcript levels are gaining more interest. The best-known application is the manipulation of splicing [116] **(Fig. 2D)**. Most human genes express more than one mRNA through alternative splicing [117] and this is an important mechanism for gene regulation. In brain there is a very high level of alternative splicing [118] and disruption of normal splicing patterns can cause or modify human disease. Antisense oligonucleotides can be used to interfere with this naturally occurring regulatory mechanism by targeting splice sites or exonic/intronic inclusion signals that will result in skipping or inclusion of the targeted exon and altering the RNA and protein sequence **(Fig. 2D)**. For neurodegenerative disorders this can have multiple applications, e.g. switching from a harmful isoform to a less harmful isoform [119], skipping an aberrantly included exon to restore the normal transcript [120], removing disease-causing mutations from genes [119], or restoring the reading-frame by removing an exon with a mutation [121].

ANTISENSE OLIGONUCLEOTIDE APPROACHES FOR NEURODEGENERATIVE DISORDERS

For non-neurodegenerative disorders several antisense oligonucleotides therapies are under development with antisense-mediated exon skipping for Duchenne muscular dystrophy the closest to clinical application [122, 123]. Furthermore, one of the first repeat expansion diseases where antisense oligonucleotide mediated RNaseH dependent degradation of mutant RNA was developed for is Myotonic Dystrophy type 1 [124]. However, reaching sufficient concentrations of antisense oligonucleotides in the organ of interest and establishing sufficient high cellular uptake is a major issue. Here neurodegenerative disorders have the advantage. After reaching the nervous system, most antisense oligonucleotides are readily taken up by neurons and glia [3, 4]. It has been suggested that uptake occurs through nucleic acid channels [125] but the exact mechanism of cellular uptake is still poorly understood [126-128]. Once the antisense oligonucleotide has been delivered into the nervous system, the vascular barriers will prevent it from entering the periphery and there will be no rapid excretion or break down by the kidney and liver,

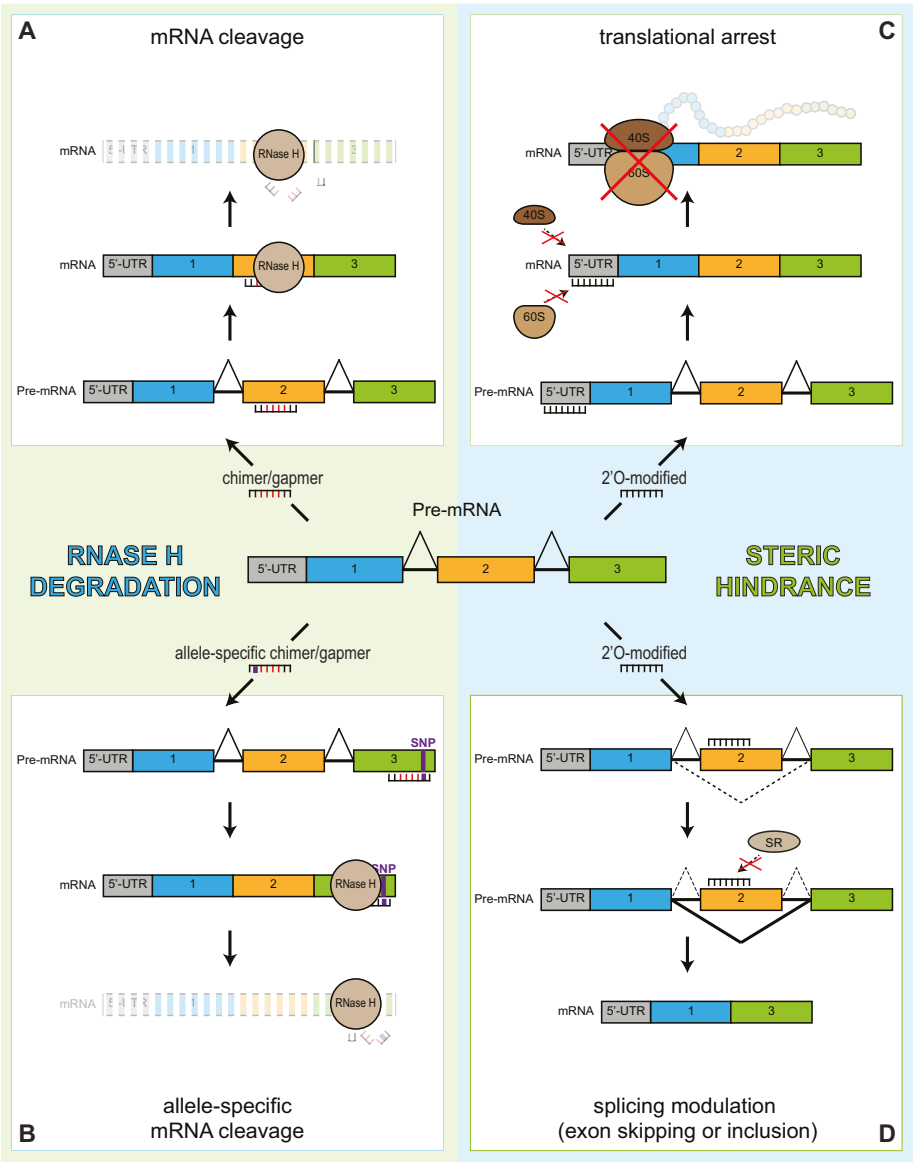

Figure 2. Functional mechanisms of antisense oligonucleotide for central nervous system disorders. Depending on the chemistry and target site, antisense oligonucleotides can be used in different ways to modulate gene expression: **A.** Antisense oligonucleotide gapmers induce RNase H-mediated breakdown of target RNA. **B.** RNase H-mediated breakdown by antisense oligonucleotide gapmers targeting specific point mutations, structural differences between wild-type and mutant mRNA or a single nucleotide polymorphism (SNP) that is unique to the mutant RNA. **C.** Suppressing RNA translation by antisense oligonucleotides targeting the RNA translation start site or sterically blocking the binding of RNA binding protein complexes, such as ribosomal subunits. **D.** Antisense oligonucleotides binding to targeting splice sites or exonic/intronic inclusion signals that will result in skipping or inclusion of the targeted exon. SR, pre-mRNA splicing machinery.

which means that it is easier to reach clinically effective concentrations. In rodents, it was shown that the tissue half-life of 2OMe-PS antisense oligonucleotides in peripheral tissue was around 10-65 days after IV injection [129, 130]. ICV infused MOE-PS antisense oligonucleotides can have a much longer tissue half-life of 71-206 days in the brain and 145-191 days in the spinal cord [131]. This striking difference in tissue half-life between neuronal and peripheral tissue could be explained by lower intrinsic nuclease activity in neuronal tissue compared to peripheral tissues [4], or by differences in endosome handling between neuronal and peripheral cell types [131]. Although antisense oligonucleotides have a long half-life they are eventually degraded, offering the possibility to discontinue treatment [132]. For clinical trials with long term administration it would be ideal to have the option to terminate the treatment effect if unwanted side effects occur. A so called antidote, or decoy, was recently applied in SMA mice initially treated with MOE-PS antisense oligonucleotides [131]. Administration of a fully complementary oligonucleotide three weeks after ICV injection of a therapeutic MOE-PS antisense oligonucleotide was reported to reverse the antisense oligonucleotide-mediated survival motor neuron 2 (SMN2) exon 7 inclusion in SMA mice [131].

For many neurodegenerative disorders it is known that certain proteins are specifically up regulated, either as a primary or secondary event in the disease process. In other disorders, proteins are not expressed due to mutations in a gene, or are aberrantly spliced and toxic protein isoforms are expressed. Mutant proteins can also aggregate, which can contribute to disease pathology. This paragraph will outline several neurodegenerative disorders where the use of antisense oligonucleotides is a promising therapeutic strategy. Examples are given where antisense oligonucleotide treatment resulted in therapeutic benefit in animal models and/or clinical trials (**Table 2**).

REDUCING PROTEIN EXPRESSION

Next to blocking translation, antisense oligonucleotides can also modulate splicing to introduce an out-of-frame deletion on transcript level, resulting in nonsense-mediated decay and knock down of target protein expression [133]. This approach is an alternative approach to RNase H-mediated degradation [134]. Alzheimer disease is the most common form of dementia where cleavage of amyloid precursor protein (APP) at the β-secretase and γ-secretase site causes elevated levels of β-amyloid peptide (Aβ). This is considered a key event in the pathogenesis of Alzheimer disease [135]. One of the first approaches to down regulate APP translation made use of PS antisense DNA oligonucleotides. After tail vein injections of PS antisense oligonucleotide there was a reduction in APP and modest behavioural improvement in a transgenic Alzheimer disease mouse model [19]. Whether these PS antisense DNA oligonucleotides consisted of modified 2' nucleosides or what the mechanism of action was has not been described. Next to Aβ plaque formation, another prominent feature of Alzheimer disease is aggregation of microtubule associated protein tau to form intracellular neurofibrillary tangles and glial tangles [136]. For Alzheimer disease and other tauopathies, antisense oligonucleotides have been applied to reduce expression of the tau protein [133]. Tau is encoded by the *MAPT* gene and several

Table 2. Antisense oligonucleotide approaches for neurodegenerative disorders.

Disease	Target gene	Oligonucleotide chemistry	Mechanism	Organism
SMA	SMN2	MOE-PS	Splicing modulation	SMA patients
	SMN2	MOE-PS, PMO and 2'OMe-PS	Splicing modulation	SMA mice and NH primates
	SMN2	PMO	Splicing modulation	SMA mouse
	SMN2	PMO and vivo-PMO	Splicing modulation	SMA mouse
	SMN2	PMO	Splicing modulation	SMA mouse
	SMN2	2OMe-PS, bifunctional	Splicing modulation + recruitment splicing factors	SMA mouse
	SMN2	MOE-PS	Splicing modulation	SMA mouse
ALS	SOD1	MOE-PS gapmer	RNase-H mediated degradation	ALS patients
	AChE	Oligodeoxynucleotide, 3 3'-nucleosides 2'Ome modified	RNAse-H mediated degradation	SOD1 mouse
	C9ORF72	MOE-PS gapmer and 2OMe-PS	RNase-H mediated degradation or steric hindrance of GGGGCC repeat	iPSC differentiated neurons
	C9ORF72	MOE-PS gapmer	RNase-H mediated degradation	Mouse
	SOD1	MOE-PS gapmer	RNase-H mediated degradation	SOD1 rats
	SOD1	MOE-PS gapmer	RNase-H mediated degradation	SOD1 rats and rhesus monkey
	GluR3	PNA	Not described	SOD1 mouse
	p75NTR	PNA	Translational arrest	SOD1 mouse
HD	Mutant HTT	MOE-PS and cEt-PS gapmers	RNase-H mediated degradation	neuronal culture
	Mutant HTT	MOE-PS and cEt-PS gapmers	RNase-H mediated degradation	HD mouse

Administration	Molecular effect	Phenotypic effect	Clinical/ preclinical	Reference
Intrathecal	Not tested. Good CSF distribution, no serious adverse events	NA	Phase 1 clinical	178
ICV in mice, intrathecal in NH primates	Mice: up to 3.5 fold change in transcript ratio Primate: predicted therapeutic dose	NA	Preclinical	131
ICV	8 fold increase SMN2 protein level	Lifespan extended from 13 to 54 days	Preclinical	179
ICV and SC	11 fold increase transcript ratio	Lifespan increased by 60 days	Preclinical	103
ICV	6 fold increase full length SMN2 transcript, and 3-fold increase protein	Lifespan extended from 15 to >100 days	Preclinical	102
ICV	3.5 fold increase SMN protein	Lifespan extended by 8 days	Preclinical	180
ICV and SC	ICV: 83% exon inclusion in brain SC: 47% exon inclusion in brain	ICV: lifespan extended to 16 days ICV+IP: lifespan extended to 173 days	Preclinical	181
Intrathecal	Not tested. No serious adverse events.	NA	Phase 1 clinical	35
IP	Higher motor neuron count	Lifespan extended by 10 days	Preclinical	182
NA	Reduction in RNA foci and RNA binding protein aggregation with both strategies	Mitigation excitotoxicity	Preclinical	141
ICV	Reduction C9ORF72 by 65% in brain and spinal cord.	No behavioural deficits induced	Preclinical	142
ICV	SOD1 protein reduction by ~40%	NA	Preclinical	183
ICV	Rat: 60% downregulation SOD1 protein	Lifespan extended by 10 days	Preclinical	132
IP	No effect seen at protein level in spinal cord	Lifespan extended by 10%	Preclinical	184
IP	Apparent p75NTR downregulation in spinal cord, though not quantified	Lifespan extended by ~10 days	Preclinical	185
bath application	Almost complete downregulation mutant htt protein	NA	Preclinical	156
ICV	90% reduction mutant htt protein	NA	Preclinical	87

Table 2. (continued)

Disease	Target gene	Oligonucleotide chemistry	Mechanism	Organism
	Mutant HTT	MOE-PS and cEt-PS gapmers	RNase-H mediated degradation	HD mouse
	HTT	MOE-PS gapmer	RNase-H mediated degradation	HD mouse
	HTT	MOE-PS gapmer	RNase-H mediated degradation	HD mice, Rhesus monkey
	HTT	MOE-PS and cEt-PS gapmers	RNase-H mediated degradation	HD mice
	HTT	PNA and LNA	Unknown mechanism, CAG repeat targeting	Fibroblasts
	HTT	2OMe-PS	Splicing modulation	Mouse
AD	Mutated APP	MOE gapmer	RNase-H mediated degradation	AD mouse
	GSK-3β	PS DNA	RNase-H mediated degradation	AD mouse
Creutzfeldt–Jakob	PrPc	MOE-PS gapmer	RNase-H mediated degradation	Prion infected mouse
SCA3	Ataxin-3	2OMe-PS	Splicing modulation	Mouse
Menkes disease	ATP7A	PMO	Splicing modulation	Zebrafish
FTD	Tau	2OMe-PS and PNA	Splicing modulation	Neuroblastoma cells with tau minigene

2OMe, 2'-O-methyl; AChE, acetylcholinesterase; AD, Alzheimer disease; ALS, amyotrophic lateral sclerosis; APP, amyloid precursor protein; ATP7A, copper-transporting ATPase 1; cEt, S-constrained-ethyl; CJD, Creutzfeldt-Jakob disease; CSF, cerebrospinal fluid; FTD, frontotemporal dementia; GluR3, glutamate receptor subunit 3; GSK-3β, glycogen synthase kinase 3; HD, Huntington disease; HTT, huntingtin; ICV, Intracerebroventricular; IP, intraperitoneal; iPSC, Induced pluripotent stem cells; LNA, locked nucleic acid; NA, not assessed; NH, non-human; MOE, 2'-O-methoxy-ethyl; p75NTR, p75 neurotrophin receptor; PMO, phosphorodiamidate morpholino oligomer; PNA, peptide nucleic acid; PrP^{c}, cellular prion protein; PS, phosphorothioate; SC, subcutaneous; SCA3, spinocerebellar ataxia type 3; SMA, spinal muscular atrophy; SMN2, survival of motor neuron 2; SOD1, superoxide dismutase 1

PMOs were designed to target MAPT transcripts. In human neuroblastoma cell lines a reduction of tau protein levels between 50% and 80% was achieved by exon skipping to induce an out-of-frame deletion in MAPT mRNA [133]. Antisense oligonucleotides resulting in steric blockage of the start codon to block translation initiation were also tested, but were found to be less efficient in reducing MAPT mRNA expression [133].

An antisense oligonucleotide therapeutic approach that is close to clinical application in a neurodegenerative disorder has been developed for ALS [35]. ALS is a progressive

Administration	Molecular effect	Phenotypic effect	Clinical/ preclinical	Reference
ICV	90% reduction mutant htt protein	NA	Preclinical	158
ICV	50% reduction mutant htt protein	Correction of motor and psychiatric phenotypes	Preclinical	186
ICV in mice, intrathecal in monkey	Mouse: up to 75% reduction htt protein Monkey: 60% reduction HTT RNA	Mouse: motor coordination reverted to normal levels	Preclinical	32
Locally in striatum	50% downregulation mutant htt protein	NA	Preclinical	157
Transfection	Up to ~80% allele specific downregulation mutant htt protein	NA	Preclinical	112
Locally in brain	25% exon skipping HTT mRNA	NA	Preclinical	174
ICV	AChE level almost back to normal	NA	Preclinical	110
ICV	~25% reduction GSK-3β	Improved learning and memory	Preclinical	187
ICV	Disease causing prion protein reduced by 90%	Incubation period prolonged by 2 months	Preclinical	152
ICV	40% exon skipping of ataxin-3 mRNA	NA	Preclinical	119
Microinjection	ATP7A protein restored to 35% of wildtype levels	Melanin pigmentation and notochord abnormalities rescued	Preclinical	167
Transfection	Up to 4 fold change in exon inclusion	NA	Preclinical	171

neurodegenerative disorder caused by degeneration of motor neurons in the brain and spinal cord. This eventually leads to muscle weakening, twitching, and an inability to move the arms, legs, and body [137]. Only 10% of ALS cases are familial and about 12% of all familial cases are caused by mutations in the gene that encodes for the enzyme superoxide dismutase 1 (SOD1) rendering the protein toxic and prone to aggregation [138]. The antisense oligonucleotides that have been used in ALS were designed to lower mRNA levels of the SOD1 transcripts. Continuous ventricular infusion of MOE-PS gapmer antisense oligonucleotides reduced levels of mutant

SOD1 in a rodent model of ALS and significantly slowed disease progression [132]. A phase I study to test the safety of this antisense oligonucleotide in subjects with familial ALS with a SOD1 mutation showed no serious adverse side effects after IT injection into the CSF [35]. A more recent development for ALS targets the hexanucleotide repeat expansion (GGGGCC) in the noncoding region of the *C9ORF72* gene. This repeat expansion is the most common cause of familial ALS [138] and although the underlying disease mechanism is not known, the repeat is transcribed and leads to accumulation of repeat-containing RNA foci in patient tissues [139]. This same repeat expansion also causes frontotemporal dementia (FTD). FTD is characterised by degeneration of frontal and temporal lobes, leading to changes in personality, behaviour, and language, resulting in death within 5 to 10 years. FTD and ALS are closely linked and share clinical, pathological, and genetic characteristics [140]. Various MOE-PS gapmer antisense oligonucleotides, targeting exon 2 common to all C9ORF72 transcripts, and others targeting the region in intron 1 adjacent to the repeat, reduced RNA foci formation in motor neurons differentiated from ALS/FTD patients-derived fibroblasts and induced pluripotent stem cells [141-143].

For HD, various antisense oligonucleotides with different modifications and backbones have been used to lower overall huntingtin protein levels [144]. HD is one of the nine known polyglutamine (polyQ) disorders, further consisting of the spinocerebellar ataxias (SCAs) 1, 2, 3, 6, 7, and 17), spinal and bulbar muscular atrophy (SBMA) and dentatorubro-pallidoluysian atrophy (DRPLA). PolyQ disorders are caused by a CAG triplet repeat expansion in different genes and result in progressive neurodegeneration with psychiatric, cognitive and motor symptoms [145]. A prominent pathological hallmark of these diseases is the accumulation of aggregated polyQ proteins in the brain [146, 147]. In HD, a generic reduction of huntingtin RNA of up to 75% using MOE-PS gapmer antisense oligonucleotides was found to be well tolerated in rodents and non-human primates [32]. ICV infusion of MOE-PS antisense oligonucleotides in transgenic BACHD mice for two weeks targeting both the human huntingtin transgene and endogenous murine huntingtin resulted in reduced toxicity, extended survival, and significant improved motor performance up to 8 months post treatment [32]. For most of the polyQ disorders, it is known that the wild-type polyQ-containing proteins have important cellular functions, and therefore specific lowering of the mutant polyQ protein levels leaving wild-type levels unchanged, would be favoured over a generic downregulation.

Antisense oligonucleotide-mediated reduction of disease-specific upregulated proteins has been proposed as potential treatment for multiple sclerosis (MS). MS is an autoimmune disease of the CNS where multifocal infiltration of autoreactive T lymphocytes across the BBB takes place. Lymphocytes in MS patients display high levels of α-4 integrin on their surface [148] and this plays an important role in lymphocyte migration to sites of inflammation [49]. Decreasing leukocyte trafficking into various organs has been successful using monoclonal antibodies against α-4 integrin [150]. In a commonly used mouse model of MS, the experimental autoimmune encephalomyelitis model, antisense oligonucleotide-induced blocking of α-4 integrin expression reduced the incidence and severity of paralytic symptoms [151]. The 20-mer antisense oligonucleotides with MOE modifications and a PS backbone were designed to target a sequence just 3´ of the translation start site of the murine

α-4 integrin mRNA to block its translation. Subcutaneous daily injections reduced α-4 integrin surface expression. Although the site of action of this particular antisense oligonucleotide is unknown, it is thought that α-4 integrin levels are reduced in peripheral lymphoid tissue and this prevents trafficking of activated mononuclear cells into brain and spinal cord [151].

Reducing protein expression by antisense oligonucleotides was recently also shown as proof-of-principle for patients with Creutzfeldt-Jakob disease (CJD) [152]. CJD is caused by a conformational change of the harmless cellular prion protein (PrP^{c}) into an infectious and pathogenic insoluble isoform scrapie PrP (PrP^{Sc}) and subsequent deposition of extracellular aggregated prion proteins. The infectious PrP^{Sc} has the unique characteristic that it spreads throughout the brain and can be transmitted between people as well as between different species [153]. ICV infusion in PrP^{Sc} infected mice of MOE-PS gapmer antisense oligonucleotides for 14 days resulted in reduced PrP^{c} as well as reduced disease-causing PrP^{Sc} levels [152]. This reduction in disease-causing PrP^{Sc} is probably not due to decreased PrP^{c}, but due to a, yet unknown, anti-prion action of PS modified antisense oligonucleotides [154, 155].

SPECIFICALLY TARGETING THE MUTANT TRANSCRIPT

If a therapeutic target protein has important cellular functions and general downregulation would be detrimental, a specific lowering of the mutation-containing protein is desired. As described previously, there are several ways to specifically lower mutant transcript and/or mutant protein levels using antisense oligonucleotides.

Targeting the repeat expansion directly has been proposed as potential treatment for ALS/FTD [141, 142]. Binding of antisense oligonucleotides to intronic sequences exclusively linked to the GGGGCC hexanucleotide repeat expansion [142] or to the repeat directly [141] resulted in reduced RNA foci formation in ALS/FTD patient-derived neuronal cells. To achieve GGGGCC repeat specific targeting two mechanisms were proposed: 1) 2OMe-PS antisense oligonucleotides that disrupt the hairpin structure of the expansion and prevents RNA binding proteins to sequester to the GGGGCC repeat, and 2) MOE-PS gapmer antisense oligonucleotides that bind to the repeat and target the mutant C9ORF72 transcripts for RNase H-mediated RNA degradation [141].

For polyQ disorders the method that has frequently been used is targeting of the common denominator, the expanded CAG repeat. The mechanism behind this selective silencing is either due to structural differences between wild-type and expanded CAG-enclosing mRNA, or because a larger number of CAGs in the expanded repeat provides more binding possibilities for CAG-targeting oligonucleotides. Single stranded PNAs, LNAs, 2OMe-PS, and PMO antisense oligonucleotides targeting CAG repeats have all been used to specifically reduce expanded CAG-containing transcripts *in vitro* in patient-derived fibroblasts [111-113] and *in vivo* in a transgenic and a knock-in HD mouse model [113]. Although results look promising, some of the antisense oligonucleotides described here only show proper allele-specificity at longer CAG repeat lengths that are not very frequent in the patient population. Furthermore, although initial results do not show unwanted downregulation of other CAG-containing transcripts [111], this needs to be investigated further.

Another way to design a molecule that can distinguish between the wild-type and expanded CAG-containing mRNA is to target a SNP that is located on the mutant transcript [114, 156]. Chimeric MOE-PS DNA and cEt antisense oligonucleotides were shown to selectively reduce mutant huntingtin expression in patient-derived cells [157, 158]. A single ICV injection of chimeric cEt antisense oligonucleotides in a humanized HD mouse model resulted in reduction in mutant huntingtin expression up to 36 weeks post treatment [87]. Although the allele specificity with SNP targeting antisense oligonucleotides is very promising, there are some limitations. The diversity of SNPs within patient populations would make it necessary to develop multiple oligonucleotides. Furthermore, this approach is not applicable for HD patients that do not exhibit heterozygosity for the most frequent SNPs in the coding region of the *HTT* gene.

Another mutant-specific reduction of neurodegenerative disease-causing protein expression makes use of antisense oligonucleotides that target point mutations. For instance, point mutations near the β-secretase site in the human gene for APP lead to a dominantly inherited form of Alzheimer disease [159]. In a transgenic mouse model of Alzheimer disease containing this mutation, translation of the APP mRNA was blocked by MOE-PS gapmer antisense oligonucleotides that bind specifically to the mutated β-secretase site [110]. Repeated injections into the third ventricle (once a week for 4 weeks) reduced the levels of toxic Aβ, indicating that this could be a possible strategy to treat familial Alzheimer disease [110].

RESTORING PROTEIN EXPRESSION – INTERFERING WITH PRE-MRNA SPLICING

The most prominent application of protein modification through antisense oligonucleotides interfering with pre-mRNA splicing has been researched for SMA. SMA is an autosomal recessive neuromuscular disorder caused by dysfunction and loss of motor neurons in the anterior horn of the spinal cord and lower brain stem. The underlying cause of SMA is a homozygous deletion of SMN1. SMN1 depletion is not lethal because of the presence of the almost identical *SMN2* gene. However, the majority of SMN2 mRNA transcripts lack exon 7, due to a silent mutation within this exon. This reduces the inclusion of exon 7 which results in a truncated protein and reduced expression of functional SMN protein [160]. Current therapeutic strategies are aimed at modulating the splicing of SMN2 by blocking exonic splicing silencers (ESS) or intronic splicing silencers (ISS), thereby increasing exon 7 inclusion. Transfecting fibroblasts with an antisense oligonucleotide (termed ISS-N1) blocking an ISS in intron 7 of SMN2 resulted in inclusion of SMN2 exon 7 [120]. Improved efficacy of the antisense oligonucleotide was achieved by incorporation of a uniform MOE chemistry. A single injection of this MOE-PS antisense oligonucleotide into the cerebral ventricles in a severe mouse model of SMA showed increased exon 7 inclusion and SMN protein levels in the spinal cord resulting in increased muscle size and strength [161]. An increased exon 7 inclusion has also been achieved by 2OMe-PS antisense oligonucleotides targeting the 3′ splice site region of exon 8 [162]. These 2OMe-PS antisense oligonucleotides were found to result in exon 7 inclusion and elevated SMN protein expression

levels *in vivo* [71, 163]. A phase I clinical trial has been completed for SMA using IT injections of the MOE-PS antisense oligonucleotide targeting exon 7 inclusion [36]. In the high dose treated patients, SMN protein levels in the CSF more than doubled and these children showed increased muscle function scores up to 14 months after the injection [164], although these results should be interpreted with caution because this was an open label study. Currently a phase 2 trial is ongoing with 6 mg or 12 mg doses of MOE-PS antisense oligonucleotide administered IT on days 1, 15 and 85 [165]. Interim results show that the MOE-modified antisense oligonucleotide is also well tolerated after repeated injections [165].

Restoration of protein expression using antisense oligonucleotides is also applied to ataxia-telangiectasia. The most debilitating feature of ataxia-telangiectasia is the progressive loss of Purkinje cells in the cerebellum and the accompanying progressive ataxia due to mutations in the *ATM* gene (ataxia-telangiectasia mutated). The majority of mutations in the *ATM* gene are splice site substitutions that result in the absence of full-length ATM protein [166]. CPP PMOs targeting prototypic ATM splicing mutations that activated cryptic splicing sites restored ATM protein expression in cells [121]. Whilst the CPP PMO was shown to distribute throughout the mouse brain following repeated IV injection, no phenotypical changes were observed [26].

In a Menkes disease zebrafish model, correction of the disease phenotype was observed after PMO microinjection [167]. The fatal neurodegenerative disorder Menkes disease is caused by varied mutations in the *ATP7A* gene, resulting in loss-of-function of the transmembrane copper-transporting P-type ATPase [168]. The Menkes disease zebrafish had mutations at the 3′ and 5′ splice sites of the *ATP7A* orthologue, resulting in activation of cryptic splice sites and loss of the protein's ATPase function [167]. Various PMOs were investigated for their ability to rescue aberrant splicing [167]. However, mutations are distributed throughout the *ATP7A* gene [169] meaning that many different antisense oligonucleotides would have to be developed to treat all patients and the clinical use of antisense oligonucleotides for Menkes disease patients is currently limited.

MODIFYING PROTEIN - REMOVING DISEASE-CAUSING MUTATION

Antisense oligonucleotides are also used to remove neurodegenerative disease-causing mutations from genes at the RNA level. Antisense oligonucleotides have been applied to correct the ratio of tau protein isoforms as potential treatment for FTD [170, 171]. Tau interacts with microtubules through its microtubule binding repeat domains encoded by exons 9 to 12 [172]. Alternative splicing of exon 10 produces tau isoforms without exon 10 (3R) or with exon 10 (4R). In healthy human brain the ratio of 4R to 3R tau is generally around 1. Due to 5′ splice site mutations in FTD patients, the ratio 4R to 3R tau is shifted towards more exon 10-containing 4R [173], resulting in the formation of intracellular neurofibrillary tangles. Co-transfecting MAPT minigenes with 2OMe-PS [170] or PNA [171] antisense oligonucleotides directed against the 5′ splice site of exon 10 prevented exon 10 inclusion and shifted the 4R to 3R tau ratio towards more 3R tau levels.

In polyQ disorders, exon skipping is applied to modify polyQ proteins to prevent their toxic gain-of-function. In SCA3, reduction of polyQ toxicity was proposed by removal of the toxic polyQ repeat from the ataxin-3 protein [119]. By exclusion of exon 9 and the CAG-enclosing exon 10 from the ataxin-3 pre-mRNA using 2OMe-PS antisense oligonucleotides, a modified ataxin-3 protein was formed that lacked the polyQ repeat and retained important wild-type functions [119]. For HD, a more indirect antisense oligonucleotide approach to reduce protein toxicity was proposed [174]. Several studies have implicated the importance of proteolytic cleavage of mutant huntingtin in HD pathogenesis and it is generally accepted that N-terminal huntingtin fragments are more toxic than full-length protein [175-177]. Transfection of 2OMe-PS antisense oligonucleotides resulted in skipping of exon 12 in huntingtin pre-mRNA and the appearance of a shorter huntingtin protein [174]. In the 2OMe-PS antisense oligonucleotide treated fibroblasts, after proteolytic cleavage less 586 amino acid N-terminal huntingtin fragments implicated in HD toxicity was formed [174]. After a single ICV injection of murine 2OMe-PS antisense oligonucleotides, exon skipping of huntingtin and ataxin-3 was shown in the cerebellum [119] and striatum [174] of control mice. The advantage of this exon skipping approach is that there is no reduction in protein levels and the wild-type functions of the proteins likely remain largely unchanged.

CONCLUSION

The recent advances towards the clinical application of antisense oligonucleotides for neurodegenerative disorders are encouraging but safe delivery, long term efficacy and side effects of prolonged treatment still need to be assessed. Also, most studies have been performed in small animals and delivering high enough doses of antisense oligonucleotides throughout the much larger human brain will be a challenge. However, the widespread cellular uptake into brain cells is a major advantage over peripheral antisense oligonucleotide applications. The ease of delivery of modified antisense oligonucleotides seems to be linked with a lack of any major adverse side effects, making antisense oligonucleotides suitable candidates as potential treatment for neurodegenerative diseases. Completed clinical trials on antisense oligonucleotide-mediated therapies into the CSF reported thus far have been successful and no major adverse events were reported [35, 164] bringing this application closer to offer relief to many patients and families that so far had to do without effective treatment.

ACKNOWLEDGEMENTS

The authors would like to acknowledge Annemieke Aartsma-Rus for critically reading the manuscript. We also thank the following agencies for their funding support: AFMTéléthon (France), ZonMw (the Netherlands), Hersenstichting (the Netherlands), The Brugling Fund (the Netherlands), AtaxiaUK (United Kingdom), patiëntenvereniging Autosomaal Dominante Cerebellaire Ataxia (ADCA) (the Netherlands), and Integrated European Project in Omics Research of Rare Neuromuscular and Neurodegenerative Diseases (Neuromics).

REFERENCES

1. Stephenson, ML, and Zamecnik, PC (1978). Inhibition of Rous sarcoma viral RNA translation by a specific oligodeoxyribonucleotide. *Proc Natl Acad Sci U S A* **75**: 285-288.

2. Jarver, P, O'Donovan, L, and Gait, MJ (2014). A chemical view of oligonucleotides for exon skipping and related drug applications. *Nucleic Acid Ther* **24**: 37-47.

3. Butler, M, Hayes, CS, Chappell, A, Murray, SF, Yaksh, TL, and Hua, XY (2005). Spinal distribution and metabolism of 2'-O-(2-methoxyethyl)-modified oligonucleotides after intrathecal administration in rats. *Neuroscience* **131**: 705-715.

4. Whitesell, L, Geselowitz, D, Chavany, C, Fahmy, B, Walbridge, S, Alger, JR, *et al.* (1993). Stability, clearance, and disposition of intraventricularly administered oligodeoxynucleotides: implications for therapeutic application within the central nervous system. *Proc Natl Acad Sci U S A* **90**: 4665-4669.

5. Maxwell, MM (2009). RNAi applications in therapy development for neurodegenerative disease. *Curr Pharm Des* **15**: 3977-3991.

6. Alavijeh, MS, Chishty, M, Qaiser, MZ, and Palmer, AM (2005). Drug metabolism and pharmacokinetics, the blood-brain barrier, and central nervous system drug discovery. *NeuroRx* **2**: 554-571.

7. Bernacki, J, Dobrowolska, A, Nierwinska, K, and Malecki, A (2008). Physiology and pharmacological role of the blood-brain barrier. *Pharmacol Rep* **60**: 600-622.

8. Palmer, AM (2010). The blood-brain barrier. *Neurobiol Dis* **37**: 1-2.

9. Bartanusz, V, Jezova, D, Alajajian, B, and Digicaylioglu, M (2011). The blood-spinal cord barrier: morphology and clinical implications. *Ann Neurol* **70**: 194-206.

10. Engelhardt, B, and Sorokin, L (2009). The blood-brain and the blood-cerebrospinal fluid barriers: function and dysfunction. *Semin Immunopathol* **31**: 497-511.

11. Ge, S, and Pachter, JS (2006). Isolation and culture of microvascular endothelial cells from murine spinal cord. *J Neuroimmunol* **177**: 209-214.

12. Tomkins, O, Friedman, O, Ivens, S, Reiffurth, C, Major, S, Dreier, JP, *et al.* (2007). Blood-brain barrier disruption results in delayed functional and structural alterations in the rat neocortex. *Neurobiol Dis* **25**: 367-377.

13. Winkler, EA, Sengillo, JD, Sagare, AP, Zhao, Z, Ma, Q, Zuniga, E, *et al.* (2014). Blood-spinal cord barrier disruption contributes to early motor-neuron degeneration in ALS-model mice. *Proc Natl Acad Sci U S A* **111**: E1035-E1042.

14. Gerebtzoff, G, and Seelig, A (2006). In silico prediction of blood-brain barrier permeation using the calculated molecular cross-sectional area as main parameter. *J Chem Inf Model* **46**: 2638-2650.

15. Pardridge, WM (2010). Biopharmaceutical drug targeting to the brain. *J Drug Target* **18**: 157-167.

16. Agrawal, S, Temsamani, J, and Tang, JY (1991). Pharmacokinetics, biodistribution, and stability of oligodeoxynucleotide phosphorothioates in mice. *Proc Natl Acad Sci U S A* **88**: 7595-7599.

17. Banks, WA, Farr, SA, Butt, W, Kumar, VB, Franko, MW, and Morley, JE (2001). Delivery across the blood-brain barrier of antisense directed against amyloid beta: reversal of learning and memory deficits in mice overexpressing amyloid precursor protein. *J Pharmacol Exp Ther* **297**: 1113-1121.

18. Cossum, PA, Sasmor, H, Dellinger, D, Truong, L, Cummins, L, Owens, SR, *et al.* (1993). Disposition of the 14C-labeled phosphorothioate oligonucleotide ISIS 2105 after intravenous administration to rats. *J Pharmacol Exp Ther* **267**: 1181-1190.

19. Farr, SA, Erickson, MA, Niehoff, ML, Banks, WA, and Morley, JE (2014). Central and peripheral administration of antisense oligonucleotide targeting amyloid-beta protein precursor improves learning and memory and reduces neuroinflammatory cytokines in Tg2576 (AbetaPPswe) mice. *J Alzheimers Dis* **40**: 1005-1016.

20. Pardridge, WM (2007). Blood-brain barrier delivery. *Drug Discov Today* **12**: 54-61.

21. Lee, HJ, Boado, RJ, Braasch, DA, Corey, DR, and Pardridge, WM (2002). Imaging gene expression in the brain in vivo in a transgenic mouse model of Huntington's disease with an antisense radiopharmaceutical and drug-targeting technology. *J Nucl Med* **43**: 948-956.

22. Kozlu, S, Caban, S, Yerlikaya, F, Fernandez-Megia, E, Novoa-Carballal, R, Riguera, R, *et al.* (2014). An aquaporin 4 antisense oligonucleotide loaded, brain targeted nanoparticulate system design. *Pharmazie* **69**: 340-345.

23. Derossi, D, Joliot, AH, Chassaing, G, and Prochiantz, A (1994). The third helix of the Antennapedia homeodomain translocates through biological membranes. *J Biol Chem* **269**: 10444-10450.

24. Kang, T, Gao, X, and Chen, J (2014). Harnessing the Capacity of Cell-Penetrating Peptides for Drug Delivery to the Central Nervous System. *Curr Pharm Biotechnol*.

25. El-Andaloussi, S, Holm, T, and Langel, U (2005). Cell-penetrating peptides: mechanisms and applications. *Curr Pharm Des* **11**: 3597-3611.

26. Du, L, Kayali, R, Bertoni, C, Fike, F, Hu, H, Iversen, PL, *et al.* (2011). Arginine-rich cell-penetrating peptide dramatically enhances AMO-mediated ATM aberrant splicing correction and enables delivery to brain and cerebellum. *Hum Mol Genet* **20**: 3151-3160.

27. Amantana, A, Moulton, HM, Cate, ML, Reddy, MT, Whitehead, T, Hassinger, JN, *et al.* (2007). Pharmacokinetics, biodistribution, stability and toxicity of a cell-penetrating peptide-morpholino oligomer conjugate. *Bioconjug Chem* **18**: 1325-1331.

28. Moulton, HM, and Moulton, JD (2010). Morpholinos and their peptide conjugates: therapeutic promise and challenge for Duchenne muscular dystrophy. *Biochim Biophys Acta* **1798**: 2296-2303.

29. Alvarez-Erviti, L, Seow, Y, Yin, H, Betts, C, Lakhal, S, and Wood, MJ (2011). Delivery of siRNA to the mouse brain by systemic injection of targeted exosomes. *Nat Biotechnol* **29**: 341-345.

30. Valadi, H, Ekstrom, K, Bossios, A, Sjostrand, M, Lee, JJ, and Lotvall, JO (2007). Exosome-mediated transfer of mRNAs and microRNAs is a novel mechanism of genetic exchange between cells. *Nat Cell Biol* **9**: 654-659.

31. Kumar, P, Wu, H, McBride, JL, Jung, KE, Kim, MH, Davidson, BL, *et al.* (2007). Transvascular delivery of small interfering RNA to the central nervous system. *Nature* **448**: 39-43.

32. Kordasiewicz, HB, Stanek, LM, Wancewicz, EV, Mazur, C, McAlonis, MM, Pytel, KA, *et al.* (2012). Sustained therapeutic reversal of Huntington's disease by transient repression of huntingtin synthesis. *Neuron* **74**: 1031-1044.

33. Margetis, K, Korfias, S, Boutos, N, Gatzonis, S, Themistocleous, M, Siatouni, A, *et al.* (2014). Intrathecal baclofen therapy for the symptomatic treatment of hereditary spastic paraplegia. *Clin Neurol Neurosurg* **123**: 142-145.

34. Ver Donck, A, Vranken, JH, Puylaert, M, Hayek, S, Mekhail, N, and Van Zundert, J (2014). Intrathecal drug administration in chronic pain syndromes. *Pain Pract* **14**: 461-476.

35. Miller, TM, Pestronk, A, David, W, Rothstein, J, Simpson, E, Appel, SH, *et al.* (2013). An antisense oligonucleotide against SOD1 delivered intrathecally for patients with SOD1 familial amyotrophic lateral sclerosis: a phase 1, randomised, first-in-man study. *Lancet Neurol* **12**: 435-442.

36. Pharmaceuticals, I (2011). An Open-label Safety, Tolerability, and Dose-range Finding Study of ISIS SMNRx in Patients With Spinal Muscular Atrophy. *ClinicalTrials gov* **NCT01494701**.

37. Curtis, MA, Kam, M, Nannmark, U, Anderson, MF, Axell, MZ, Wikkelso, C, *et al.* (2007). Human neuroblasts migrate to the olfactory bulb via a lateral ventricular extension. *Science* **315**: 1243-1249.

38. Claxton, A, Baker, LD, Wilkinson, CW, Trittschuh, EH, Chapman, D, Watson, GS, *et al.* (2013). Sex and ApoE genotype differences in treatment response to two doses of intranasal insulin in adults with mild cognitive impairment or Alzheimer's disease. *J Alzheimers Dis* **35**: 789-797.

39. Kanazawa, T, Akiyama, F, Kakizaki, S, Takashima, Y, and Seta, Y (2013). Delivery of siRNA to the brain using a combination of nose-to-brain delivery and cell-penetrating peptide-modified nano-micelles. *Biomaterials* **34**: 9220-9226.

40. Hashizume, R, Ozawa, T, Gryaznov, SM, Bollen, AW, Lamborn, KR, Frey, WH, *et al.* (2008). New therapeutic approach for brain tumors: Intranasal delivery of telomerase inhibitor GRN163. *Neuro Oncol* **10**: 112-120.

41. Dias, N, and Stein, CA (2002). Antisense oligonucleotides: basic concepts and mechanisms. *Mol Cancer Ther* **1**: 347-355.

42. Eder, PS, DeVine, RJ, Dagle, JM, and Walder, JA (1991). Substrate specificity and kinetics of degradation of antisense oligonucleotides by a 3' exonuclease in plasma. *Antisense Res Dev* **1**: 141-151.

43. Dagle, JM, Weeks, DL, and Walder, JA (1991). Pathways of degradation and mechanism of action of antisense oligonucleotides in Xenopus laevis embryos. *Antisense Res Dev* **1**: 11-20.

44. De Clercq, E, Eckstein, E, and Merigan, TC (1969). Interferon induction increased through chemical modification of a synthetic polyribonucleotide. *Science* **165**: 1137-1139.

45. Campbell, JM, Bacon, TA, and Wickstrom, E (1990). Oligodeoxynucleoside phosphorothioate stability in subcellular extracts, culture media, sera and cerebrospinal fluid. *J Biochem Biophys Methods* **20**: 259-267.

46. Iversen, PL, Zhu, S, Meyer, A, and Zon, G (1992). Cellular uptake and subcellular distribution of phosphorothioate oligonucleotides into cultured cells. *Antisense Res Dev* **2**: 211-222.

47. Ogawa, S, Brown, HE, Okano, HJ, and Pfaff, DW (1995). Cellular uptake of intracerebrally administered oligodeoxynucleotides in mouse brain. *Regul Pept* **59**: 143-149.

48. Wu, H, Lima, WF, Zhang, H, Fan, A, Sun, H, and Crooke, ST (2004). Determination of the role of the human RNase H1 in the pharmacology of DNA-like antisense drugs. *J Biol Chem* **279**: 17181-17189.

49. Bennett, CF, and Swayze, EE (2010). RNA targeting therapeutics: molecular mechanisms of antisense oligonucleotides as a therapeutic platform. *Annu Rev Pharmacol Toxicol* **50**: 259-293.

50. Cerritelli, SM, and Crouch, RJ (2009). Ribonuclease H: the enzymes in eukaryotes. *FEBS J* **276**: 1494-1505.

51. Jaroszewski, JW, Clausen, V, Cohen, JS, and Dahl, O (1996). NMR investigations of duplex stability of phosphorothioate and phosphorodithioate DNA analogues modified in both strands. *Nucleic Acids Res* **24**: 829-834.

52. Levin, AA (1999). A review of the issues in the pharmacokinetics and toxicology of phosphorothioate antisense oligonucleotides. *Biochim Biophys Acta* **1489**: 69-84.

53. Brown, DA, Kang, SH, Gryaznov, SM, DeDionisio, L, Heidenreich, O, Sullivan, S, *et al.* (1994). Effect of phosphorothioate modification of oligodeoxynucleotides on specific protein binding. *J Biol Chem* **269**: 26801-26805.

54. Guvakova, MA, Yakubov, LA, Vlodavsky, I, Tonkinson, JL, and Stein, CA (1995). Phosphorothioate oligodeoxynucleotides bind to basic fibroblast growth factor, inhibit its binding to cell surface receptors, and remove it from low affinity binding sites on extracellular matrix. *J Biol Chem* **270**: 2620-2627.

55. Galbraith, WM, Hobson, WC, Giclas, PC, Schechter, PJ, and Agrawal, S (1994). Complement activation and hemodynamic changes following intravenous administration of phosphorothioate oligonucleotides in the monkey. *Antisense Res Dev* **4**: 201-206.

56. Rifai, A, Brysch, W, Fadden, K, Clark, J, and Schlingensiepen, KH (1996). Clearance kinetics, biodistribution, and organ saturability of phosphorothioate oligodeoxynucleotides in mice. *Am J Pathol* **149**: 717-725.

57. Watanabe, TA, Geary, RS, and Levin, AA (2006). Plasma protein binding of an antisense oligonucleotide targeting human ICAM-1 (ISIS 2302). *Oligonucleotides* **16**: 169-180.

58. Phillips, JA, Craig, SJ, Bayley, D, Christian, RA, Geary, R, and Nicklin, PL (1997). Pharmacokinetics, metabolism, and elimination of a 20-mer phosphorothioate oligodeoxynucleotide (CGP 69846A) after intravenous and subcutaneous administration. *Biochem Pharmacol* **54**: 657-668.

59. Freier, SM, and Altmann, KH (1997). The ups and downs of nucleic acid duplex stability: structure-stability studies on chemically-modified DNA:RNA duplexes. *Nucleic Acids Res* **25**: 4429-4443.

60. Lubini, P, Zurcher, W, and Egli, M (1994). Stabilizing effects of the RNA 2'-substituent: crystal structure of an oligodeoxynucleotide duplex containing 2'-O-methylated adenosines. *Chem Biol* **1**: 39-45.

61. McKay, RA, Miraglia, LJ, Cummins, LL, Owens, SR, Sasmor, H, and Dean, NM (1999). Characterization of a potent and specific class of antisense oligonucleotide inhibitor of human protein kinase C-alpha expression. *J Biol Chem* **274**: 1715-1722.

62. Geary, RS, Watanabe, TA, Truong, L, Freier, S, Lesnik, EA, Sioufi, NB, *et al.* (2001). Pharmacokinetic properties of 2'-O-(2-methoxyethyl)-modified oligonucleotide analogs in rats. *J Pharmacol Exp Ther* **296**: 890-897.

63. Zhao, Q, Temsamani, J, Iadarola, PL, Jiang, Z, and Agrawal, S (1996). Effect of different chemically modified oligodeoxynucleotides on immune stimulation. *Biochem Pharmacol* **51**: 173-182.

64. Peng, HS, Livanov, V, Zhang, W, Li, J, and Lesher, T (1998). Modification of phosphorothioate oligonucleotides yields potent analogs with minimal toxicity for antisense experiments in the CNS. *Brain Res Mol Brain Res* **62**: 1-11.

65. Monia, BP, Lesnik, EA, Gonzalez, C, Lima, WF, McGee, D, Guinosso, CJ, *et al.* (1993). Evaluation of 2'-modified oligonucleotides containing 2'-deoxy gaps as antisense inhibitors of gene expression. *J Biol Chem* **268**: 14514-14522.

66. Liebsch, G, Landgraf, R, Engelmann, M, Lorscher, P, and Holsboer, F (1999). Differential behavioural effects of chronic infusion of CRH 1 and CRH 2 receptor antisense oligonucleotides into the rat brain. *J Psychiatr Res* **33**: 153-163.

67. Muller, YL, Reitstetter, R, and Yool, AJ (2000). Antisense knockdown of calcium-dependent K+ channels in developing cerebellar Purkinje neurons. *Brain Res Dev Brain Res* **120**: 135-140.

68. Hamm, S, Latz, E, Hangel, D, Muller, T, Yu, P, Golenbock, D, *et al.* (2010). Alternating 2'-O-ribose methylation is a universal approach for generating non-stimulatory siRNA by acting as TLR7 antagonist. *Immunobiology* **215**: 559-569.

69. Ma, L, Wang, DD, Zhang, TY, Yu, H, Wang, Y, Huang, SH, *et al.* (2011). Region-specific involvement of BDNF secretion and synthesis in conditioned taste aversion memory formation. *J Neurosci* **31**: 2079-2090.

70. Robbins, M, Judge, A, Liang, L, McClintock, K, Yaworski, E, and MacLachlan, I (2007). 2'-O-methyl-modified RNAs act as TLR7 antagonists. *Mol Ther* **15**: 1663-1669.

71. Hua, Y, Sahashi, K, Hung, G, Rigo, F, Passini, MA, Bennett, CF, *et al.* (2010). Antisense correction of SMN2 splicing in the CNS rescues necrosis in a type III SMA mouse model. *Genes Dev* **24**: 1634-1644.

72. Frieden, M, Hansen, HF, and Koch, T (2003). Nuclease stability of LNA oligonucleotides and LNA-DNA chimeras. *Nucleosides Nucleotides Nucleic Acids* **22**: 1041-1043.

73. Braasch, DA, Liu, Y, and Corey, DR (2002). Antisense inhibition of gene expression in cells by oligonucleotides incorporating locked nucleic acids: effect of mRNA target sequence and chimera design. *Nucleic Acids Res* **30**: 5160-5167.

74. Elayadi, AN, Braasch, DA, and Corey, DR (2002). Implications of high-affinity hybridization by locked nucleic acid oligomers for inhibition of human telomerase. *Biochemistry* **41**: 9973-9981.

75. Kurreck, J, Wyszko, E, Gillen, C, and Erdmann, VA (2002). Design of antisense oligonucleotides stabilized by locked nucleic acids. *Nucleic Acids Res* **30**: 1911-1918.

76. Sorensen, MD, Kvaerno, L, Bryld, T, Hakansson, AE, Verbeure, B, Gaubert, G, *et al.* (2002). alpha-L-ribo-configured locked nucleic acid (alpha-L-LNA): synthesis and properties. *J Am Chem Soc* **124**: 2164-2176.

77. Swayze, EE, Siwkowski, AM, Wancewicz, EV, Migawa, MT, Wyrzykiewicz, TK, Hung, G, *et al.* (2007). Antisense oligonucleotides containing locked nucleic acid improve potency but cause significant hepatotoxicity in animals. *Nucleic Acids Res* **35**: 687-700.

78. Wahlestedt, C, Salmi, P, Good, L, Kela, J, Johnsson, T, Hokfelt, T, *et al.* (2000). Potent and nontoxic antisense oligonucleotides containing locked nucleic acids. *Proc Natl Acad Sci U S A* **97**: 5633-5638.

79. Gruegelsiepe, H, Brandt, O, and Hartmann, RK (2006). Antisense inhibition of RNase P: mechanistic aspects and application to live bacteria. *J Biol Chem* **281**: 30613-30620.

80. Noir, R, Kotera, M, Pons, B, Remy, JS, and Behr, JP (2008). Oligonucleotide-oligospermine conjugates (zip nucleic acids): a convenient means of finely tuning hybridization temperatures. *J Am Chem Soc* **130**: 13500-13505.

81. Gagnon, KT, Watts, JK, Pendergraff, HM, Montaillier, C, Thai, D, Potier, P, *et al.* (2011). Antisense and antigene inhibition of gene expression by cell-permeable oligonucleotide-oligospermine conjugates. *J Am Chem Soc* **133**: 8404-8407.

82. Renneberg, D, and Leumann, CJ (2002). Watson-Crick base-pairing properties of tricyclo-DNA. *J Am Chem Soc* **124**: 5993-6002.

83. Renneberg, D, Bouliong, E, Reber, U, Schumperli, D, and Leumann, CJ (2002). Antisense properties of tricyclo-DNA. *Nucleic Acids Res* **30**: 2751-2757.

84. Goyenvalle, A, Griffith, G, Babbs, A, Andaloussi, SE, Ezzat, K, Avril, A, *et al.* (2015). Functional correction in mouse models of muscular dystrophy using exon-skipping tricyclo-DNA oligomers. *Nat Med*.

85. Kawasaki, AM, Casper, MD, Freier, SM, Lesnik, EA, Zounes, MC, Cummins, LL, *et al.* (1993). Uniformly modified 2'-deoxy-2'-fluoro phosphorothioate oligonucleotides as nuclease-resistant antisense compounds with high affinity and specificity for RNA targets. *J Med Chem* **36**: 831-841.

86. Seth, PP, Siwkowski, A, Allerson, CR, Vasquez, G, Lee, S, Prakash, TP, *et al.* (2008). Design, synthesis and evaluation of constrained methoxyethyl (cMOE) and constrained ethyl (cEt) nucleoside analogs. *Nucleic Acids Symp Ser (Oxf)*: 553-554.

87. Southwell, AL, Skotte, NH, Kordasiewicz, HB, Ostergaard, ME, Watt, AT, Carroll, JB, *et al.* (2014). In vivo evaluation of candidate allele-specific mutant huntingtin gene silencing antisense oligonucleotides. *Mol Ther*.

88. Nielsen, PE, Egholm, M, Berg, RH, and Buchardt, O (1991). Sequence-selective recognition of DNA by strand displacement with a thymine-substituted polyamide. *Science* **254**: 1497-1500.

89. Egholm, M, Buchardt, O, Christensen, L, Behrens, C, Freier, SM, Driver, DA, *et al.* (1993). PNA hybridizes to complementary oligonucleotides obeying the Watson-Crick hydrogen-bonding rules. *Nature* **365**: 566-568.

90. Demidov, VV, Potaman, VN, Frank-Kamenetskii, MD, Egholm, M, Buchard, O, Sonnichsen, SH, *et al.* (1994). Stability of peptide nucleic acids in human serum and cellular extracts. *Biochem Pharmacol* **48**: 1310-1313.

91. Schwarz, FP, Robinson, S, and Butler, JM (1999). Thermodynamic comparison of PNA/DNA and DNA/DNA hybridization reactions at ambient temperature. *Nucleic Acids Res* **27**: 4792-4800.

92. Wittung, P, Kajanus, J, Edwards, K, Haaima, G, Nielsen, PE, Norden, B, *et al.* (1995). Phospholipid membrane permeability of peptide nucleic acid. *FEBS Lett* **375**: 27-29.

93. Hyrup, B, and Nielsen, PE (1996). Peptide nucleic acids (PNA): synthesis, properties and potential applications. *Bioorg Med Chem* **4**: 5-23.

94. Aldrian-Herrada, G, Desarmenien, MG, Orcel, H, Boissin-Agasse, L, Mery, J, Brugidou, J, *et al.* (1998). A peptide nucleic acid (PNA) is more rapidly internalized in cultured neurons when coupled to a retro-inverso delivery peptide. The antisense activity depresses the target mRNA and protein in magnocellular oxytocin neurons. *Nucleic Acids Res* **26**: 4910-4916.

95. Turner, Y, Wallukat, G, Saalik, P, Wiesner, B, Pritz, S, and Oehlke, J (2010). Cellular uptake and biological activity of peptide nucleic acids conjugated with peptides with and without cell-penetrating ability. *J Pept Sci* **16**: 71-80.

96. Tyler, BM, McCormick, DJ, Hoshall, CV, Douglas, CL, Jansen, K, Lacy, BW, *et al.* (1998). Specific gene blockade shows that peptide nucleic acids readily enter neuronal cells in vivo. *FEBS Lett* **421**: 280-284.

97. McMahon, BM, Mays, D, Lipsky, J, Stewart, JA, Fauq, A, and Richelson, E (2002). Pharmacokinetics and tissue distribution of a peptide nucleic acid after intravenous administration. *Antisense Nucleic Acid Drug Dev* **12**: 65-70.

98. Summerton, J, and Weller, D (1997). Morpholino antisense oligomers: design, preparation, and properties. *Antisense Nucleic Acid Drug Dev* **7**: 187-195.

99. Hudziak, RM, Barofsky, E, Barofsky, DF, Weller, DL, Huang, SB, and Weller, DD (1996). Resistance of morpholino phosphorodiamidate oligomers to enzymatic degradation. *Antisense Nucleic Acid Drug Dev* **6**: 267-272.

100. Devi, GR, Beer, TM, Corless, CL, Arora, V, Weller, DL, and Iversen, PL (2005). In vivo bioavailability and pharmacokinetics of a c-MYC antisense phosphorodiamidate morpholino oligomer, AVI-4126, in solid tumors. *Clin Cancer Res* **11**: 3930-3938.

101. Wu, B, Moulton, HM, Iversen, PL, Jiang, J, Li, J, Li, J, *et al.* (2008). Effective rescue of dystrophin improves cardiac function in dystrophin-deficient mice by a modified morpholino oligomer. *Proc Natl Acad Sci U S A* **105**: 14814-14819.

102. Porensky, PN, Mitrpant, C, McGovern, VL, Bevan, AK, Foust, KD, Kaspar, BK, *et al.* (2012). A single administration of morpholino antisense oligomer rescues spinal muscular atrophy in mouse. *Hum Mol Genet* **21**: 1625-1638.

103. Nizzardo, M, Simone, C, Salani, S, Ruepp, MD, Rizzo, F, Ruggieri, M, *et al.* (2014). Effect of combined systemic and local morpholino treatment on the spinal muscular atrophy Delta7 mouse model phenotype. *Clin Ther* **36**: 340-356.

104. Morcos, PA, Li, Y, and Jiang, S (2008). Vivo-Morpholinos: a non-peptide transporter delivers Morpholinos into a wide array of mouse tissues. *Biotechniques* **45**: 613-614, 616, 618.

105. Ferguson, DP, Dangott, LJ, and Lightfoot, JT (2014). Lessons learned from vivo-morpholinos: How to avoid vivo-morpholino toxicity. *Biotechniques* **56**: 251-256.

106. Zhou, H, Janghra, N, Mitrpant, C, Dickinson, RL, Anthony, K, Price, L, *et al.* (2013). A novel morpholino oligomer targeting ISS-N1 improves rescue of severe spinal muscular atrophy transgenic mice. *Hum Gene Ther* **24**: 331-342.

107. Ferguson, DP, Schmitt, EE, and Lightfoot, JT (2013). Vivo-morpholinos induced transient knockdown of physical activity related proteins. *PLoS One* **8**: e61472.

108. Reissner, KJ, Sartor, GC, Vazey, EM, Dunn, TE, Aston-Jones, G, and Kalivas, PW (2012). Use of vivo-morpholinos for control of protein expression in the adult rat brain. *J Neurosci Methods* **203**: 354-360.

109. Teplova, M, Wallace, ST, Tereshko, V, Minasov, G, Symons, AM, Cook, PD, *et al.* (1999). Structural origins of the exonuclease resistance of a zwitterionic RNA. *Proc Natl Acad Sci U S A* **96**: 14240-14245.

110. Chauhan, NB, and Siegel, GJ (2007). Antisense inhibition at the beta-secretase-site of beta-amyloid precursor protein reduces cerebral amyloid and acetyl cholinesterase activity in Tg2576. *Neuroscience* **146**: 143-151.

111. Evers, MM, Pepers, BA, van Deutekom, JC, Mulders, SA, den Dunnen, JT, Aartsma-Rus, A, *et al.* (2011). Targeting several CAG expansion diseases by a single antisense oligonucleotide. *PLoS One* **6**: e24308.

112. Hu, J, Matsui, M, Gagnon, KT, Schwartz, JC, Gabillet, S, Arar, K, *et al.* (2009). Allele-specific silencing of mutant huntingtin and ataxin-3 genes by targeting expanded CAG repeats in mRNAs. *Nat Biotechnol* **27**: 478-484.

113. Sun, X, Marque, LO, Cordner, Z, Pruitt, JL, Bhat, M, Li, PP, *et al.* (2014). Phosphorodiamidate morpholino oligomers suppress mutant huntingtin expression and attenuate neurotoxicity. *Hum Mol Genet* **23**: 6302-6317.

114. Miller, VM, Xia, H, Marrs, GL, Gouvion, CM, Lee, G, Davidson, BL, *et al.* (2003). Allele-specific silencing of dominant disease genes. *Proc Natl Acad Sci U S A* **100**: 7195-7200.

115. Kole, R, Krainer, AR, and Altman, S (2012). RNA therapeutics: beyond RNA interference and antisense oligonucleotides. *Nat Rev Drug Discov* **11**: 125-140.

116. van Ommen, GJ, and Aartsma-Rus, A (2013). Advances in therapeutic RNA-targeting. *N Biotechnol* **30**: 299-301.

117. Lander, ES, Linton, LM, Birren, B, Nusbaum, C, Zody, MC, Baldwin, J, *et al.* (2001). Initial sequencing and analysis of the human genome. *Nature* **409**: 860-921.

118. Yeo, G, Holste, D, Kreiman, G, and Burge, CB (2004). Variation in alternative splicing across human tissues. *Genome Biol* **5**: R74.

119. Evers, MM, Tran, HD, Zalachoras, I, Pepers, BA, Meijer, OC, den Dunnen, JT, *et al.* (2013). Ataxin-3 protein modification as a treatment strategy for spinocerebellar ataxia type 3: removal of the CAG containing exon. *Neurobiol Dis* **58**: 49-56.

120. Singh, NK, Singh, NN, Androphy, EJ, and Singh, RN (2006). Splicing of a critical exon of human Survival Motor Neuron is regulated by a unique silencer element located in the last intron. *Mol Cell Biol* **26**: 1333-1346.

121. Du, L, Pollard, JM, and Gatti, RA (2007). Correction of prototypic ATM splicing mutations and aberrant ATM function with antisense morpholino oligonucleotides. *Proc Natl Acad Sci U S A* **104**: 6007-6012.

122. Mendell, JR, Rodino-Klapac, LR, Sahenk, Z, Roush, K, Bird, L, Lowes, LP, *et al.* (2013). Eteplirsen for the treatment of Duchenne muscular dystrophy. *Ann Neurol* **74**: 637-647.

123. Voit, T, Topaloglu, H, Straub, V, Muntoni, F, Deconinck, N, Campion, G, *et al.* (2014). Safety and efficacy of drisapersen for the treatment of Duchenne muscular dystrophy (DEMAND II): an exploratory, randomised, placebo-controlled phase 2 study. *Lancet Neurol* **13**: 987-996.

124. Wheeler, TM, Leger, AJ, Pandey, SK, MacLeod, AR, Nakamori, M, Cheng, SH, *et al.* (2012). Targeting nuclear RNA for in vivo correction of myotonic dystrophy. *Nature* **488**: 111-115.

125. Shi, F, Gounko, NV, Wang, X, Ronken, E, and Hoekstra, D (2007). In situ entry of oligonucleotides into brain cells can occur through a nucleic acid channel. *Oligonucleotides* **17**: 122-133.

126. Geary, RS, Wancewicz, E, Matson, J, Pearce, M, Siwkowski, A, Swayze, E, *et al.* (2009). Effect of dose and plasma concentration on liver uptake and pharmacologic activity of a 2'-methoxyethyl modified chimeric antisense oligonucleotide targeting PTEN. *Biochem Pharmacol* **78**: 284-291.

127. Juliano, RL, Ming, X, and Nakagawa, O (2012). Cellular uptake and intracellular trafficking of antisense and siRNA oligonucleotides. *Bioconjug Chem* **23**: 147-157.

128. Koller, E, Vincent, TM, Chappell, A, De, S, Manoharan, M, and Bennett, CF (2011). Mechanisms of single-stranded phosphorothioate modified antisense oligonucleotide accumulation in hepatocytes. *Nucleic Acids Res* **39**: 4795-4807.

129. Heemskerk, H, de, WC, van, KP, Heuvelmans, N, Sabatelli, P, Rimessi, P, *et al.* (2010). Preclinical PK and PD studies on 2'-O-methyl-phosphorothioate RNA antisense oligonucleotides in the mdx mouse model. *Mol Ther* **18**: 1210-1217.

130. Verhaart, IE, Dool, vV-vd, Sipkens, JA, de Kimpe, SJ, Kolfschoten, IG, van Deutekom, JC, *et al.* (2014). The Dynamics of Compound, Transcript, and Protein Effects After Treatment With 2OMePS Antisense Oligonucleotides in mdx Mice. *Mol Ther Nucleic Acids* **3**: e148.

131. Rigo, F, Chun, SJ, Norris, DA, Hung, G, Lee, S, Matson, J, *et al.* (2014). Pharmacology of a central nervous system delivered 2'-O-methoxyethyl-modified survival of motor neuron splicing oligonucleotide in mice and nonhuman primates. *J Pharmacol Exp Ther* **350**: 46-55.

132. Smith, RA, Miller, TM, Yamanaka, K, Monia, BP, Condon, TP, Hung, G, *et al.* (2006). Antisense oligonucleotide therapy for neurodegenerative disease. *J Clin Invest* **116**: 2290-2296.

133. Sud, R, Geller, ET, and Schellenberg, GD (2014). Antisense-mediated Exon Skipping Decreases Tau Protein Expression: A Potential Therapy For Tauopathies. *Mol Ther Nucleic Acids* **3**: e180.

134. Aartsma-Rus, A, van, VL, Hirschi, M, Janson, AA, Heemskerk, H, de Winter, CL, *et al.* (2009). Guidelines for antisense oligonucleotide design and insight into splice-modulating mechanisms. *Mol Ther* **17**: 548-553.

135. Van Broeck, B, Van Broeckhoven, C, and Kumar-Singh, S (2007). Current insights into molecular mechanisms of Alzheimer disease and their implications for therapeutic approaches. *Neurodegener Dis* **4**: 349-365.

136. Ittner, LM, and Gotz, J (2011). Amyloid-beta and tau--a toxic pas de deux in Alzheimer's disease. *Nat Rev Neurosci* **12**: 65-72.

137. Al-Chalabi, A, and Leigh, PN (2000). Recent advances in amyotrophic lateral sclerosis. *Curr Opin Neurol* **13**: 397-405.

138. Renton, AE, Chio, A, and Traynor, BJ (2014). State of play in amyotrophic lateral sclerosis genetics. *Nat Neurosci* **17**: 17-23.

139. DeJesus-Hernandez, M, Mackenzie, IR, Boeve, BF, Boxer, AL, Baker, M, Rutherford, NJ, *et al.* (2011). Expanded GGGGCC hexanucleotide repeat in noncoding region of C9ORF72 causes chromosome 9p-linked FTD and ALS. *Neuron* **72**: 245-256.

140. Lashley, T, Hardy, J, and Isaacs, AM (2013). RANTing about C9orf72. *Neuron* **77**: 597-598.

141. Donnelly, CJ, Zhang, PW, Pham, JT, Haeusler, AR, Mistry, NA, Vidensky, S, *et al.* (2013). RNA toxicity from the ALS/FTD C9ORF72 expansion is mitigated by antisense intervention. *Neuron* **80**: 415-428.

142. Lagier-Tourenne, C, Baughn, M, Rigo, F, Sun, S, Liu, P, Li, HR, *et al.* (2013). Targeted degradation of sense and antisense C9orf72 RNA foci as therapy for ALS and frontotemporal degeneration. *Proc Natl Acad Sci U S A* **110**: E4530-E4539.

143. Riboldi, G, Zanetta, C, Ranieri, M, Nizzardo, M, Simone, C, Magri, F, *et al.* (2014). Antisense Oligonucleotide Therapy for the Treatment of C9ORF72 ALS/FTD Diseases. *Mol Neurobiol*.

144. Sah, DW, and Aronin, N (2011). Oligonucleotide therapeutic approaches for Huntington disease. *J Clin Invest* **121**: 500-507.

145. Fischbeck, KH (2001). Polyglutamine expansion neurodegenerative disease. *Brain Res Bull* **56**: 161-163.

146. Davies, SW, Turmaine, M, Cozens, BA, DiFiglia, M, Sharp, AH, Ross, CA, *et al.* (1997). Formation of neuronal intranuclear inclusions underlies the neurological dysfunction in mice transgenic for the HD mutation. *Cell* **90**: 537-548.

147. Seidel, K, Siswanto, S, Brunt, ER, den, DW, Korf, HW, and Rub, U (2012). Brain pathology of spinocerebellar ataxias. *Acta Neuropathol* **124**: 1-21.

148. Cannella, B, and Raine, CS (1995). The adhesion molecule and cytokine profile of multiple sclerosis lesions. *Ann Neurol* **37**: 424-435.

149. Rose, DM, Alon, R, and Ginsberg, MH (2007). Integrin modulation and signaling in leukocyte adhesion and migration. *Immunol Rev* **218**: 126-134.

150. Lobb, RR, and Hemler, ME (1994). The pathophysiologic role of alpha 4 integrins in vivo. *J Clin Invest* **94**: 1722-1728.

151. Myers, KJ, Witchell, DR, Graham, MJ, Koo, S, Butler, M, and Condon, TP (2005). Antisense oligonucleotide blockade of alpha 4 integrin prevents and reverses clinical symptoms in murine experimental autoimmune encephalomyelitis. *J Neuroimmunol* **160**: 12-24.

152. Nazor Friberg, K, Hung, G, Wancewicz, E, Giles, K, Black, C, Freier, S, *et al.* (2012). Intracerebral Infusion of Antisense Oligonucleotides Into Prion-infected Mice. *Mol Ther Nucleic Acids* **1**: e9.

153. Puoti, G, Bizzi, A, Forloni, G, Safar, JG, Tagliavini, F, and Gambetti, P (2012). Sporadic human prion diseases: molecular insights and diagnosis. *Lancet Neurol* **11**: 618-628.

154. Karpuj, MV, Giles, K, Gelibter-Niv, S, Scott, MR, Lingappa, VR, Szoka, FC, *et al.* (2007). Phosphorothioate oligonucleotides reduce PrP levels and prion infectivity in cultured cells. *Mol Med* **13**: 190-198.

155. Kocisko, DA, Vaillant, A, Lee, KS, Arnold, KM, Bertholet, N, Race, RE, *et al.* (2006). Potent antiscrapie activities of degenerate phosphorothioate oligonucleotides. *Antimicrob Agents Chemother* **50**: 1034-1044.

156. Skotte, NH, Southwell, AL, Ostergaard, ME, Carroll, JB, Warby, SC, Doty, CN, *et al.* (2014). Allele-specific suppression of mutant huntingtin using antisense oligonucleotides: providing a therapeutic option for all huntington disease patients. *PLoS One* **9**: e107434.

157. Carroll, JB, Warby, SC, Southwell, AL, Doty, CN, Greenlee, S, Skotte, N, *et al.* (2011). Potent and selective antisense oligonucleotides targeting single-nucleotide polymorphisms in the Huntington disease gene / allele-specific silencing of mutant huntingtin. *Mol Ther* **19**: 2178-2185.

158. Ostergaard, ME, Southwell, AL, Kordasiewicz, H, Watt, AT, Skotte, NH, Doty, CN, *et al.* (2013). Rational design of antisense oligonucleotides targeting single nucleotide polymorphisms for potent and allele selective suppression of mutant Huntingtin in the CNS. *Nucleic Acids Res* **41**: 9634-9650.

159. Selkoe, D, and Kopan, R (2003). Notch and Presenilin: regulated intramembrane proteolysis links development and degeneration. *Annu Rev Neurosci* **26**: 565-597.

160. Lorson, CL, Rindt, H, and Shababi, M (2010). Spinal muscular atrophy: mechanisms and therapeutic strategies. *Hum Mol Genet* **19**: R111-R118.

161. Passini, MA, Bu, J, Richards, AM, Kinnecom, C, Sardi, SP, Stanek, LM, *et al.* (2011). Antisense oligonucleotides delivered to the mouse CNS ameliorate symptoms of severe spinal muscular atrophy. *Sci Transl Med* **3**: 72ra18.

162. Lim, SR, and Hertel, KJ (2001). Modulation of survival motor neuron pre-mRNA splicing by inhibition of alternative 3' splice site pairing. *J Biol Chem* **276**: 45476-45483.

163. Williams, JH, Schray, RC, Patterson, CA, Ayitey, SO, Tallent, MK, and Lutz, GJ (2009). Oligonucleotide-mediated survival of motor neuron protein expression in CNS improves phenotype in a mouse model of spinal muscular atrophy. *J Neurosci* **29**: 7633-7638.

164. Rigo, F, Hua, Y, Krainer, AR, and Bennett, CF (2012). Antisense-based therapy for the treatment of spinal muscular atrophy. *J Cell Biol* **199**: 21-25.

165. Pharmaceuticals, I (2012). An Open-label Safety, Tolerability and Dose-range Finding Study of Multiple Doses of ISIS SMNRx in Patient With Spinal Muscular Atrophy (SMNRx - CS2). *ClinicalTrials gov* **NCT01703988**.

166. Sandoval, N, Platzer, M, Rosenthal, A, Dork, T, Bendix, R, Skawran, B, *et al.* (1999). Characterization of ATM gene mutations in 66 ataxia telangiectasia families. *Hum Mol Genet* **8**: 69-79.

167. Madsen, EC, Morcos, PA, Mendelsohn, BA, and Gitlin, JD (2008). In vivo correction of a Menkes disease model using antisense oligonucleotides. *Proc Natl Acad Sci U S A* **105**: 3909-3914.

168. Vulpe, C, Levinson, B, Whitney, S, Packman, S, and Gitschier, J (1993). Isolation of a candidate gene for Menkes disease and evidence that it encodes a copper-transporting ATPase. *Nat Genet* **3**: 7-13.

169. Tumer, Z, and Moller, LB (2010). Menkes disease. *Eur J Hum Genet* **18**: 511-518.

170. Donahue, CP, Muratore, C, Wu, JY, Kosik, KS, and Wolfe, MS (2006). Stabilization of the tau exon 10 stem loop alters pre-mRNA splicing. *J Biol Chem* **281**: 23302-23306.

171. Peacey, E, Rodriguez, L, Liu, Y, and Wolfe, MS (2012). Targeting a pre-mRNA structure with bipartite antisense molecules modulates tau alternative splicing. *Nucleic Acids Res* **40**: 9836-9849.

172. Gustke, N, Trinczek, B, Biernat, J, Mandelkow, EM, and Mandelkow, E (1994). Domains of tau protein and interactions with microtubules. *Biochemistry* **33**: 9511-9522.

173. Hutton, M, Lendon, CL, Rizzu, P, Baker, M, Froelich, S, Houlden, H, *et al.* (1998). Association of missense and 5'-splice-site mutations in tau with the inherited dementia FTDP-17. *Nature* **393**: 702-705.

174. Evers, MM, Tran, HD, Zalachoras, I, Meijer, OC, den Dunnen, JT, van Ommen, GJ, *et al.* (2014). Preventing formation of toxic N-terminal huntingtin fragments through antisense oligonucleotide-mediated protein modification. *Nucleic Acid Ther* **24**: 4-12.

175. Cooper, JK, Schilling, G, Peters, MF, Herring, WJ, Sharp, AH, Kaminsky, Z, *et al.* (1998). Truncated N-terminal fragments of huntingtin with expanded glutamine repeats form nuclear and cytoplasmic aggregates in cell culture. *Hum Mol Genet* **7**: 783-790.

176. Graham, RK, Deng, Y, Slow, EJ, Haigh, B, Bissada, N, Lu, G, *et al.* (2006). Cleavage at the caspase-6 site is required for neuronal dysfunction and degeneration due to mutant huntingtin. *Cell* **125**: 1179-1191.

177. Mende-Mueller, LM, Toneff, T, Hwang, SR, Chesselet, MF, and Hook, VY (2001). Tissue-specific proteolysis of Huntingtin (htt) in human brain: evidence of enhanced levels of N- and C-terminal htt fragments in Huntington's disease striatum. *J Neurosci* **21**: 1830-1837.

178. Pharmaceuticals, I (2009). Safety, Tolerability, and Activity Study of ISIS SOD1Rx to Treat Familial Amyotrophic Lateral Sclerosis (ALS) Caused by SOD1 Gene Mutations (SOD-1). *ClinicalTrials gov* **NCT01041222**.

179. Osman, EY, Miller, MR, Robbins, KL, Lombardi, AM, Atkinson, AK, Brehm, AJ, *et al.* (2014). Morpholino antisense oligonucleotides targeting intronic repressor Element1 improve phenotype in SMA mouse models. *Hum Mol Genet* **23**: 4832-4845.

180. Osman, EY, Yen, PF, and Lorson, CL (2012). Bifunctional RNAs targeting the intronic splicing silencer N1 increase SMN levels and reduce disease severity in an animal model of spinal muscular atrophy. *Mol Ther* **20**: 119-126.

181. Hua, Y, Sahashi, K, Rigo, F, Hung, G, Horev, G, Bennett, CF, *et al.* (2011). Peripheral SMN restoration is essential for long-term rescue of a severe spinal muscular atrophy mouse model. *Nature* **478**: 123-126.

182. Marc, G, Leah, R, Ofira, E, Oded, A, Zohar, A, and Hanna, R (2013). Presymptomatic treatment with acetylcholinesterase antisense oligonucleotides prolongs survival in ALS (G93A-SOD1) mice. *Biomed Res Int* **2013**: 845345.

183. Winer, L, Srinivasan, D, Chun, S, Lacomis, D, Jaffa, M, Fagan, A, *et al.* (2013). SOD1 in cerebral spinal fluid as a pharmacodynamic marker for antisense oligonucleotide therapy. *JAMA Neurol* **70**: 201-207.

184. Rembach, A, Turner, BJ, Bruce, S, Cheah, IK, Scott, RL, Lopes, EC*, et al.* (2004). Antisense peptide nucleic acid targeting GluR3 delays disease onset and progression in the SOD1 G93A mouse model of familial ALS. *J Neurosci Res* **77**: 573-582.

185. Turner, BJ, Cheah, IK, Macfarlane, KJ, Lopes, EC, Petratos, S, Langford, SJ*, et al.* (2003). Antisense peptide nucleic acid-mediated knockdown of the p75 neurotrophin receptor delays motor neuron disease in mutant SOD1 transgenic mice. *J Neurochem* **87**: 752-763.

186. Stanek, LM, Yang, W, Angus, S, Sardi, PS, Hayden, MR, Hung, GH*, et al.* (2013). Antisense oligonucleotide-mediated correction of transcriptional dysregulation is correlated with behavioral benefits in the YAC128 mouse model of Huntington's disease. *J Huntingtons Dis* **2**: 217-228.

187. Farr, SA, Ripley, JL, Sultana, R, Zhang, Z, Niehoff, ML, Platt, TL*, et al.* (2014). Antisense oligonucleotide against GSK-3beta in brain of SAMP8 mice improves learning and memory and decreases oxidative stress: Involvement of transcription factor Nrf2 and implications for Alzheimer disease. *Free Radic Biol Med* **67**: 387-395.

3

Antisense oligonucleotide-mediated exon skipping as a strategy to reduce proteolytic cleavage of ataxin-3

Lodewijk J.A. Toonen, Iris Schmidt, Martijn S. Luijsterburg, Haico van Attikum, Willeke M.C. van Roon-Mom (2016).
Sci Rep, 6, 35200

ABSTRACT

Spinocerebellar ataxia type-3 (SCA3) is a neurodegenerative disorder caused by a polyglutamine repeat expansion in the ataxin-3 protein. Cleavage of mutant ataxin-3 by proteolytic enzymes yields ataxin-3 fragments containing the polyglutamine stretch. These shorter ataxin-3 fragments are thought to be involved in SCA3 pathogenesis due to their increased cellular toxicity and their involvement in formation of the characteristic neuronal aggregates.

As a strategy to prevent formation of toxic cleavage fragments, we investigated an antisense oligonucleotide-mediated modification of the ataxin-3 pre-mRNA through exon skipping of exon 8 and 9, resulting in the removal of a central 88 amino acid region of the ataxin-3 protein. This removed protein region contains several predicted cleavage sites and two ubiquitin-interacting motifs. In contrast to unmodified mutant ataxin-3, the internally truncated ataxin-3 protein did not give rise to potentially toxic cleavage fragments when incubated with caspases. In vitro experiments did not show cellular toxicity of the modified ataxin-3 protein. However, the modified protein was incapable of binding poly-ubiquitin chains, which may interfere with its normal deubiquitinating function. Low exon skipping efficiencies combined with reduction in important ataxin-3 protein functions suggest that skipping of exon 8 and 9 is not a viable therapeutic option for SCA3.

INTRODUCTION

Spinocerebellar ataxia type 3 (SCA3), or Machado-Joseph disease, is a dominantly inherited neurodegenerative disorder with an onset around midlife and is characterized mainly by progressive ataxia affecting balance and gait [1]. SCA3 belongs to the polyglutamine (polyQ) family of disorders, which are all caused by expansion of a CAG repeat in the coding region of several different genes. In SCA3, the CAG repeat expansion is located in exon 10 of the *ATXN3* gene. Healthy individuals have a CAG repeat ranging from 10 to 51, whereas SCA3 patients have an expansion of 55 repeats or more [2]. The expanded CAG repeat is translated into a polyglutamine tract in the C-terminal region of the ataxin-3 protein.

Ataxin-3 is ubiquitously expressed, and though peripheral toxicity has been shown in recent years for polyQ disorders [3], ataxin-3 toxicity occurs mainly in the brain. Neuronal loss is most prominent in cerebellum, pons and spinal cord [1]. Ataxin-3 is a deubiquitinating enzyme involved in the regulation of protein degradation. The C-terminally located ubiquitin-interacting motifs (UIMs) of ataxin-3 can bind ubiquitin chains and the N-terminal Josephin domain is able to cleave these bound chains [4]. The ataxin-3 isoform most abundantly expressed in brain contains a total of 3 UIMs [5]. Though the exact cellular mechanisms leading to pathogenesis have not been fully elucidated, the general consensus is that a gain of toxic function, rather than loss of wild-type function, is the driving force behind SCA3 disease progression pathology [6].

A key role for the initiation of intracellular toxicity in polyglutamine disorders has been suggested to lie in the proteolytic cleavage of the mutant protein. Proteolytic cleavage can result in formation of shorter polyglutamine-containing protein fragments that are more toxic than the full-length protein and are prone to aggregation. Involvement of mutant ataxin-3 fragments has been suggested for several pathological processes such as: transcriptional deregulation, proteasomal and mitochondrial impairment, hindered axonal transport and impairment of autophagy [7]. Studies have shown that ataxin-3 can be cleaved by caspases [8, 9] and calpains [10]. These enzymes have several predicted cleavage motifs distributed throughout the ataxin-3 protein, and can hence generate protein fragments of varying sizes. C-terminal ataxin-3 fragments containing the polyQ expansion were detected in a SCA3 mouse model, as well as in patient brain areas most affected in SCA3, while they were not observed in unaffected regions or control brain [11]. Inhibition of calpain-mediated cleavage resulted in an alleviation of toxicity in neuroblastoma cells [12] as well as in mouse brain, where reduced ataxin-3 aggregation and nuclear localisation were also observed [13]. These results imply that preventing proteolytic cleavage of the mutant ataxin-3 protein could reduce its toxicity. However, such general inhibition of proteolytic enzymes also affects many other pathways in which these enzymes are involved. A more specific approach to prevent generation of toxic polyQ fragments may therefore be to render the ataxin-3 protein more resistant to cleavage. One way to achieve this protein modification is through use of antisense oligonucleotides (AONs).

AONs are short synthetic strands of DNA or RNA that can interact with RNA transcripts. AONs can act through different mechanisms, depending on the chemical modifications and design. For instance, transcripts can be broken down through RNAse H-mediated mechanisms.

Alternatively, by targeting AONs to mask specific splicing signals within exons or introns, exons can be hidden from the splicing machinery by steric hindrance of SR proteins [14]. In this manner, exons can be targeted for exclusion from the pre-mRNA, resulting in exon skipping [15]. When the RNA reading frame is maintained, a new internally truncated protein can be generated with this strategy. Use of AONs for disorders of the central nervous system has gained interest in recent years due to favourable distribution throughout the brain, widespread cellular uptake and the ability to specifically target single transcripts in monogenic neurodegenerative diseases [16]. Additionally, phase 1 clinical trial using intrathecally delivered AONs for amyotrophic lateral sclerosis and spinal muscular atrophy showed encouraging results on tolerability and distribution of AONs in the central nervous system [17, 18].

In the current study we induce skipping of *ATXN3* exons that encode the region of the protein containing several proteolytic cleavage sites. The aim is to form an internally truncate ataxin-3 protein that is less susceptible to proteolytic cleavage and the formation of toxic protein fragments. As an assessment of protein function, we determined the ubiquitin-binding capacity of the modified ataxin-3 protein and established the effect on DNA strand breaks.

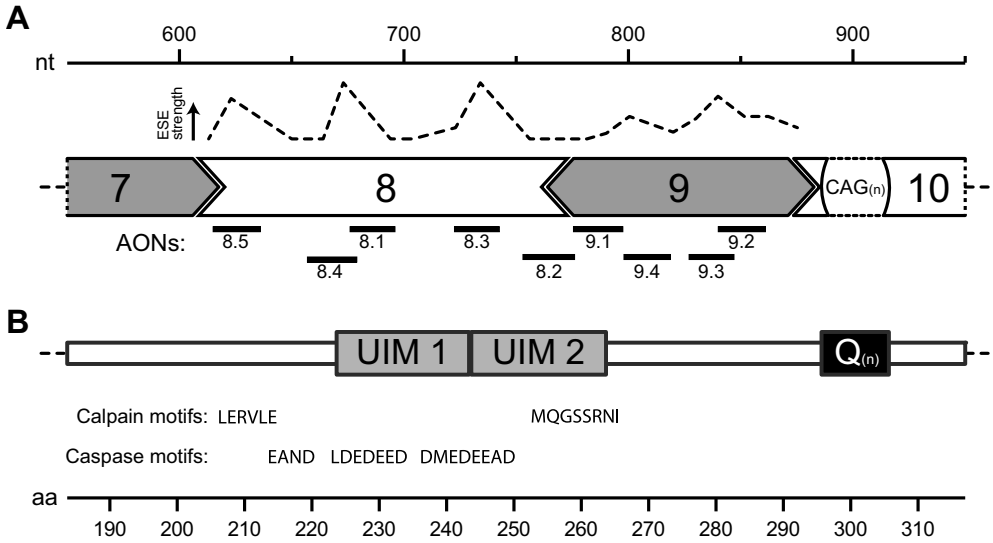

Figure 1. *ATXN3* exon structure and predicted cleavage motifs of ataxin-3. Based on Ensemble transcript ENST00000558190. **(A)** Depicted is the exonic splicing enhancer signal (ESE) strength as predicted by the human splicing finder. The shape of exons represents the influence on the RNA reading frame. Location of designed antisense oligonucleotides (AONs) against exon 8 and 9 to promote exon-skipping are drawn to scale. **(B)** The corresponding ataxin-3 protein region contains ubiquitin interacting motifs (UIMs) 1 and 2. Predicted cleavage sites N-terminal of the polyQ tract as detected for calpain [12] and predicted for caspases [8] are shown (not to scale). nt = nucleotides, aa = amino acids.

MATERIAL AND METHODS

All experiments described here are based on the ataxin-3 isoform RefSeq NM_004993.

Antisense oligonucleotides

Uniformly modified single stranded 2'O-methyl phosphorothioate AONs of 20 to 23 nucleotides in length were designed according to previously described guidelines [38] and are listed in table 1. AONs were targeted against the most potent exonic splicing enhancer sites as predicted by the Human Splicing Finder software [39]. Care was taken to target a partially open secondary RNA structure of the relevant exon based on m-fold [40]. When possible, RNA hybridization strength, melting temperature, self-annealing and guanine-cytosine content were kept within previously described parameters [41].

Cell culture

Control or SCA3 patient-derived fibroblasts (GM02153 and GM06153 respectively) were obtained from Coriell Cell Repositories (Camden, USA). Fibroblasts were maintained in Minimal Essential Medium (MEM) (Gibco, Invitrogen, Carlsbad, USA), containing 15% fetal bovine serum (FBS) (Clontech, Palo Alto, USA), 1% Glutamax (Gibco), and 100 U/ml penicillin/streptomycin (Gibco).

Human U2OS 2-6-3 cells (kind gift from Dr. S. Janicki) containing 200 copies of a LacO (256 ×)/TetO (96 ×)-containing cassette of ~4Mbp [21] were cultured in Dulbecco's Modified Eagle's Medium (DMEM) (Gibco), supplemented with 10% FBS, 1% glutamax, and 100 U/ml penicillin/streptomycin. All cells were grown at 37°C and 5% CO_2.

Human neuroblast SH-SY5Y cells were maintained in a 1:1 mixture of DMEM and HAM's F12 medium (Gibco) containing 15% FBS, 1% glutamax and 100 U/ml penicillin/streptomycin.

Table 1. Antisense oligonucleotide sequences.

AON name	Sequence (5′ to 3′)
AON 8.1	GCCCUCUGCAAAUCCUCCUC
AON 8.2	CUUGCAUACUUAGCUGAAUAGCC
AON 8.3	CUGCUUCCUCAUCUUCCAUG
AON 8.4	CCUCAUCUUCGUCUAACAUUCC
AON 8.5	CACUCGUUCCAGGUCUGUUUU
AON 9.1	GAGAUAUGUUUCUGGAACUACC
AON 9.2	GCUUCUCGUCUCUUCCGAAGC
AON 9.3	CCGAAGCUCUUCUGAAGUAA
AON 9.4	CCUGAUGUCUGUGUCAUAUCU

Transfection and RNA analysis

AON transfections were performed as previously described [42]. In brief, Lipofectamine transfection reagent (Life Technologies, Paisley, UK) was diluted to 0.3% in MEM without supplements. A concentration of 200 nM of each AON was added to Optimem transfection medium (Life technologies) and incubated on cells for 4 hours, after which a 2-4 fold volume of growth medium containing 5% FBS was added. Plasmid transfections were transfected similarly to the AONs, but using 0.6% lipofectamine and 1 – 1.5 µg of plasmid DNA per 9.6 cm^2 well. RNA was typically isolated 24 hours after transfection by trypsinizing (Life Technologies) cells and collecting the cell pellet. Cells were subsequently lysed and RNA was extracted using the Reliaprep RNA Cell Miniprep kit (Promega, Madison, USA) according to the manufacturer's protocol. Between 200-400 ng RNA was used as input for cDNA synthesis using the Transcriptor First Strand cDNA Synthesis Kit (Roche, Mannheim, Germany). cDNA was synthesized according to manufacturer's instructions using oligo-dT primers for 45 min at 50°C. PCR to assess exon skipping was performed using the Expand High Fidelity PCR kit (Roche), with 1 µl of cDNA as template, 200 µM of each deoxynucleotide, 500 nM forward (exon 4) and reverse primer (exon 11) (see table 2) (Eurogentec, Liege, Belgium), 1.7 units expand high-fidelity polymerase and PCR-grade water to a volume of 30 µl. PCR was performed with a 94°C denaturation step of 2 min., followed by 36 cycles of 15 sec denaturation at 94°C, 30 sec. annealing at 59°C and 80 sec. of elongation at 72°C, followed by a final extension step of 7 min. at 72°C. To confirm exon skipping, Sanger sequencing was performed by extracting PCR products from gel using the NucleoSpin Gel & PCR Clean-up kit (Machery Nagel, Düren, Germany). The extracted PCR products were subsequently re-amplified, purified and submitted for Sanger sequencing (Macrogen, Amsterdam, the Netherlands).

Quantitative PCR analysis of exon skip efficiency was performed on exons of the *ATXN3* transcript using the SensiMix SYBR & Fluorescein Kit (Bioline, Taunton, USA), with 2 µl of 10x diluted cDNA, 100nM forward and reverse primer and 4 µl 2x SensiMix SYBR & Fluorescein in a final reaction volume of 10 µl. The qPCR reaction was performed on the LightCycler 480 (Roche). Initial denaturation was 10 min. at 95°C, followed by 40 cycles of 10 sec. denaturation at 95°C, annealing at 60°C for 30 sec and elongation at 72°C for 20 sec. Reference genes used were: B-actin, hypoxanthine-guanine phosphoribosyltransferase (HPRT) and ribosomal protein L22 (Rpl22). All samples were ran in triplicate. Primers were designed with the help of Primer3 software [43] and are listed in table 2. Primer efficiencies were established using LinRegPCR v2014.0, using raw data amplification curves from the LightCycler software as input. After baseline correction, transcript level expression values (N0) were calculated and corrected for reference gene expression as described before [44].

Protein isolation and Western blotting

Fibroblasts were harvested 48 hours after AON transfection using 0.5% tripsin/EDTA solution and pelleted by centrifugation. After washing twice, cells were resuspended in lysis buffer [42] supplemented with cOmplete EDTA-free protease inhibitors (Roche). Cells were disrupted by

sonicating three times at an amplitude of 60hz for 5 sec., followed by 30 minutes incubation in a head-over-head rotor at 4°C. Protein concentrations were determined using the bicinchoninic acid kit (Thermo Fisher Scientific, Walthma, USA), with bovine serum albumin as a standard.

Protein samples were separated using 10% sodium dodecyl sulfate polyacrylamide gel electrophoresis (SDS-PAGE). Proteins were blotted onto a nitrocellulose membrane using the Transblot Turbo system (Bio-Rad, Hercules, USA), for 10 min. at 1.3 A. Blocking of membranes was performed using 5% low fat milk in tris buffered saline (TBS) for 1 hour. Blots were probed using an antibody specific for the C-terminal region of ataxin-3 (a kind gift from Dr. T. Schmidt) [45] at a 1:1000 dilution. As loading control, GAPDH was used and detected using ab181602 (Abcam, Cambridge, UK) at 1:50.000 dilution. After washing, membranes were incubated for 1 hour with Odyssey secondary antibodies, goat-anti-mouse IRDye 680RD or goat-anti-rabbit IRDye 800CW (LI-COR Biosciences, Lincoln, USA) at a 1:5000 dilution. Bands were visualised using an Odyssey infrared imaging system (LI-COR). Protein bands were quantified with the Odyssey software version 3.0 using the integrated intensity method.

Plasmids and mutations

Full length and exon 8 and 9 skipped products were obtained by performing PCR using primers (table 2) specific for the full length *ATXN3* transcript. After extracting the PCR products of interest from agarose gel, the fragments were purified and ligated into the pGEM-T Easy vector (Promega), using the 5´-A overhangs on the PCR products. Constructs for mutant ataxin-3 were obtained by gene synthesis (Genscript, Piscataway, USA), using a mixture of 71 CAG and CAA codons instead of the pure CAG tract to improve stability during the sub cloning process. Plasmids were subsequently digested with NotI and inserted into the PspOMI digested PacGFP-C1 (Clontech, Mountain View, USA) vector for GFP transfection experiments, or into the NotI digested Pet28a vector (Merck Millipore, Billerica, USA) for recombinant protein production.

Mutations of UIMs and cleavage sites were introduced using the QuickChange II Site Directed Mutagenesis kit (Agilent Technologies, Waldbronn, Germany) according to manufacturer's instructions using primers (table 2) containing the desired mutation or deletion. Mutations of UIMs 1 and 2 have been described previously [46]. Predicted caspase sites encoded by exon 8 of ataxin-3 [8] were inactivated by replacing aspartic acid amino acids by aspargines. Altered aspartic acids were: D208, D217, D223, D225, D228, D241, D244 and D248. These 9 mutations were obtained by gBlock gene synthesis (Integrated DNA technologies, Coralville, USA) of the *ATXN3* cDNA sequence, which was subsequently amplified by PCR and sub-cloned into the Pet28a vector. mCherry-LacR-RNF8 was generated as described previously [20]. All constructs were Sanger sequenced to verify correctness.

Recombinant protein production and purification

Hexa-HIS-tagged ataxin-3 proteins were produced using the Pet28a plasmid in a BL21 *E.coli* culture (New England BioLabs, Ipswich, USA). After 4 hours of protein production, bacteria

Table 2. Primer sequences used for cloning, mutagenesis and (quantitative) RT-PCR. Abbreviations: ACTB, beta actin; ATXN3, ataxin-3; HPRT1, hypoxanthine phosphoribosyltransferase 1; RPL22, ribosomal protein L22

Target gene	Primer name	Application	Sequence (5′ to 3′)
ATXN3	hATXN3_FL_Fw1	cloning	ATGGAGTCCATCTTCCACGA
ATXN3	hATXN3_FL_Rev	cloning	CGCATTGTTCCACTTTCCCA
ATXN3	hATXN3_L340A_Fw	mutagenesis	TATGAGTGAAGAAGACATGGCTCAGGCAGCTGTGACCATG
ATXN3	hATXN3_L340A_Rev	mutagenesis	CATGGTCACAGCTGCCTGAGCCATGTCTTCTTCACTCATA
ATXN3	hATXN3_del_L255-S260-Fw	mutagenesis	CTCCGCAGGGCTATTCAGTCCAGAAACATATCTCAA
ATXN3	hATXN3_del_L255-S260-Rev	mutagenesis	TTGAGATATGTTTCTGGACTGAATAGCCCTGCGGAG
ATXN3	hATXN3ex4Fw1	RT-PCR	GCCTTGAAAGTTTGGGGTTT
ATXN3	hATXN3ex11Rev1	RT-PCR	ACAGCTGCCTGAAGCATGTC
ATXN3	hATXN3-Qex3/4Fw1	qRT-PCR	GCCTTCTGGAAATATGGATGAC
ATXN3	hATXN3-Qex3/4Rev1	qRT-PCR	ATCGATCCTGAGCCTCTGATAC
ATXN3	hATXN3-Qex10/11Fw1	qRT-PCR	TCAGGACAGAGTTCACATCCA
ATXN3	hATXN3-Qex10/11Rev1	qRT-PCR	TTCAGGCAGCTGTGACCAT
ATXN3	hATXN3-Qex7/10Fw1	qRT-PCR	ATTGCGAAGCTGACCAACTC
ATXN3	hATXN3-Qex7/10Rev1	qRT-PCR	TTTTGCTGCTGTCTTTGCTC
ATXN3	hATXN3-Int11/11Fw1	qRT-PCR	AAATGTGGTTTTGTTTCCCAAC
ATXN3	hATXN3-Int11/11Rev1	qRT-PCR	ATGGTCACAGCTGCCTGAAG
ACTB	hACTBex4Fw1	qRT-PCR	AGCAAGCAGGAGTATGACGA
ACTB	hACTBex4Fw1	qRT-PCR	AGAAAGGGTGTAACGCAACTAA
HPRT1	hHPRT1ex3Fw1	qRT-PCR	GGGAGGCCATCACATTG
HPRT1	hHPRT1ex3Fw1	qRT-PCR	GTAATCCAGCAGGTCAGAAA
RPL22	hRPL22ex1Fw1	qRT-PCR	TCGCTCACCTCCCTTTCTAA
RPL22	hRPL22ex3Rev1	qRT-PCR	TCACGGTGATCTTGCTCTTG

were harvested by centrifugation and resuspended in BugBuster Plus (Merck Millipore) protein extraction reagent. HIS-tagged proteins were then bound using TALON slurry (Clontech) and finally dialysed overnight against PBS at 4°C.

Proteolytic cleavage assays

Calpain-2 cleavage assays were performed using 75 pmol of HIS-ataxin-3 protein with 15 to 200 ng calpain-2 (Calbiochem, Merck, Darmstadt, Germany) in reaction buffer containing 20 mM HEPES/KOH, pH 7.6, 10 mM KCl, 1.5 mM $MgCl_2$, 1 mM dithiothreitol, and 1 mM $CaCl_2$ [12], for a total volume of 50 µl. Caspase cleavage assays were performed with 50 pmol HIS-ataxin-3 protein with 200 U caspase 1 or caspase 6 (Enzo Life Sciences, Farmingdale, USA) in a buffer containing 50 mM Hepes, 50 mM NaCl, 10 mM EDTA, 10 mM DTT and 0.1% CHAPS. Cleavage reactions were incubated for 15 minutes at room temperature, after which reactions were stopped by addition of 4x Laemmli sample buffer (Bio-Rad) and heating to 100°C for 5 min. Cleavage fragments were identified by 10% SDS-PAGE and PageBlue protein staining (Thermo-Fisher-Scientific) or Western blotting.

RNF8-based chromatin tethering to assess ubiquitin binding of ATXN3 mutants

U2OS 2-6-3 cells [21] containing the LacO repeat array were co-transfected with mCherry-LacR-RNF8 [20] in combination with GFP-tagged ataxin-3 constructs and grown on 18 mm glass cover slips (Thermo Fisher Scientific). Cells were fixed after 24 hours using 4% paraformaldehyde, and washed for 30 minutes using 0.2% Triton X-100 (Sigma-Aldrich, St. Louis, USA) in PBS. Cover slips were subsequently mounted on microscope slides using 0.002% 4',6-diamidino-2-phenylindole (DAPI) in 1.3% 1,4-diazabicyclo[2.2.2]octane (DABCO) and stored overnight at 4°C prior to imaging on a Leica DM-5500B fluorescent microscope (Leica Microsystems, Buffalo Grove, USA) at 63x magnification. Fluorescent images were obtained from 2 replicate transfections of a minimum of 50 cells positive for both mCherry-RNF8 and GFP-ataxin-3. The increase of GFP-ataxin-3 localization at the LacO array was determined by drawing a line region of interest across the array using LAS AF Lite software (Leica Microsystems), and subtracting green background fluorescence around the array from the maximum fluorescence intensity at the LacO array. The obtained value is reported as the increase of GFP signal at the array for the different GFP ataxin-3 constructs upon tethering of RNF8.

Assessment DNA double-strand breaks

GFP-tagged ataxin-3 constructs were transfected in SH-SY5Y neuroblasts grown on collagen-coated 18 mm glass cover slips. 24 Hours after transfection, cells were fixed with 4% paraformaldehyde for 10 minutes and washed with PBS containing 0.5% bovine serum albumin (Sigma-Aldrich) and 0.15% glycine (Thermo Fisher Scientific) for 15 minutes. Slides were then incubated with rabbit anti-53BP1 at 1:1000 (Novus Biologicals, Littleton, USA) for 1.5 hours. After washing, detection was performed by incubation with anti-rabbit IgG Alexa 546 1:1000 (Invitrogen) for 1 hour and mounted with EverBrite hardset mounting medium containing DAPI

(Biotium, Hayward, USA). Images of >50 cells were obtained the next day using an AxioImager M2 (Zeiss, Oberkochen, Germany) equipped with a 63x PLAN APO (1.4 NA) oil-immersion objective and an HXP 120 metal-halide lamp used for excitation. Foci were quantified using an ImageJ custom-made macro as described previously [47]. Only cells expressing the GFP proteins were included for analysis.

Statistical analysis and calculations

Percentage of protein modification was calculated using the protein band mean Odyssey application software integrated intensity as follows: intensity modified protein / intensity all ataxin-3 bands * 100%. Ubiquitin-binding assays and calpain cleavage experiments were compared using 1 way ANOVA with Dunnet's multiple comparisons test. A minimum of 50 cells from 2 replicates per construct were included for the ubiquitin-binding assays. Analysis of calpain-2 cleavage efficiency was derived from a total of 3 replicates. A P value of <0.05 was considered statistically significant.

RESULTS

Combined exon 8 and 9 skipping results in a modified ataxin-3 Δ88aa protein lacking predicted cleavage sites

Here, we devised a therapeutic strategy to remove exons 8 and 9 from ataxin-3 pre-mRNA, thereby eliminating 5 known or predicted proteolytic cleavage sites from ataxin-3 as depicted in Figure 1. A total of 9 AONs were designed targeting *ATXN3* exon 8 and 9 (table 1) and transfected in human fibroblasts in order to assess exon skipping efficiency. Using RT-PCR analysis with primers flanking the targeted exons, we determined that candidate AON 8.3 and 9.1 produced the most efficient skipping of exon 8 or 9, respectively (Figure 2a). These AONs were subsequently tested in combination to induce simultaneous skipping of both exons. Sanger sequencing confirmed an in-frame *ATXN3* fragment where exon 7 was linked to exon 10. qPCR analysis showed that the most efficient AON combination, AON 8.3 and 9.1, induced up to 25% RNA modification (Figure 2a) following a single transfection. Transfection of AONs 8.3 and 9.1 did not only result in a double skip of exon 8 and 9, but also in a single skip of exon 8 (167 bp). This is predicted to be a target for nonsense-mediated decay [19] and therefore likely does not result in protein production. Single skipping of exon 9 (97 bp) was also observed for both alleles. This would lead to a reading-frame shift of exon 10 and potentially a novel protein product, but we did not detect this hypothetical protein in our western blot analysis (data not shown).

To determine the percentage of ataxin-3 protein modification after AON transfection in human fibroblasts, protein was isolated 48 hours after transfection. Following SDS-PAGE and western blotting, ataxin-3 protein was detected using an antibody specific to the C-terminal ataxin-3 region containing UIM3 (Figure 2b). Two modified ataxin-3 proteins (ataxin-3 Δ88aa) of the expected size were detected at 34 and 40 kDa, corresponding to ataxin-3 derived from both alleles and lacking 88 amino acids (V204 to K291) with a maximum of 14% ataxin-3

protein modification. The C-terminal antibody was still capable of binding the modified protein, showing that there was no shift in the RNA reading frame after skipping of the two exons. Additionally, the modified protein was not detected with antibody 1H9, that recognizes ataxin-3 amino acids E214 to L233. This epitope is in the region of ataxin-3 that is not present after exon skipping again confirming exon skipping after AON transfection.

Modified ataxin-3 Δ88aa protein is still cleaved by calpain-2

A total of 3 caspase and 2 calpain cleavage motifs associated with polyQ toxicity are predicted to be located in the 88 amino acid region encoded by *ATXN3* exon 8 and 9 (Figure 1). We hypothesized that the ataxin-3 Δ88aa protein lacking these 5 cleavage sites would be resistant to cleavage by caspases and calpains. In order to assess cleavage of ataxin-3 Δ88aa by caspases and calpains, we incubated purified recombinant ataxin-3 Δ88aa with caspases 1, 3 and 6 and calpain-2. Calpain-2 cleavage of ataxin-3 was more efficient compared to the caspases tested (Figure 3a). Within 15 minutes of incubating 15 pmol ataxin-3 with calpain-2 at room temperature, all full-length protein was cleaved. Despite this efficient cleavage, few ataxin-3 fragments were detectable with PageBlue staining. This indicates that under these conditions calpain-2 does not generate a specific preferential cleavage fragment, or generates many fragments too small for detection. No difference in the rate of proteolytic cleavage between ataxin-3 Δ88aa and unmodified ataxin-3 was observed (Figure 3b). Together, this shows that ataxin-3 Δ88aa, despite lacking predicted calpain-2 motifs ^{209}LERVLE^{214} and ^{257}MQGSSRNI^{264}, is efficiently cleaved by calpain-2.

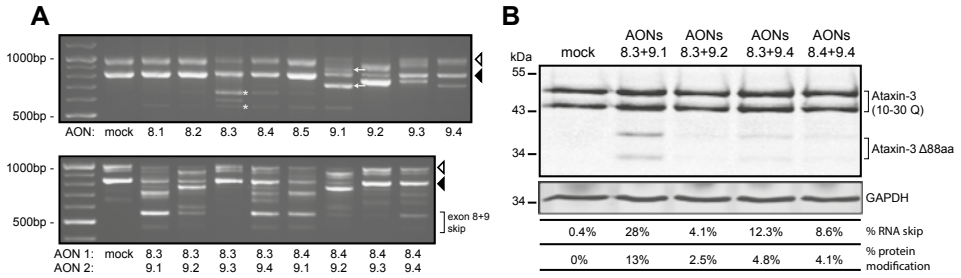

Figure 2. Ataxin-3 exon skipping in human fibroblasts. Control and SCA3 patient derived human fibroblasts were transfected with AONs complementary to exon 8 or 9 of *ATXN3*. (**A**) Screening of individual AONs for exon skipping activity at RNA level in SCA3 derived fibroblasts (white arrowhead = *ATXN3* 71 CAG, black arrowhead = *ATXN3* 10 CAG). For both the mutant and wild-type allele, the PCR product representing the single exon 8 skip is indicated with an asterix. Single exon 9 skip is indicated with an arrow. Combination of AONs for exon 8 and 9 were tested for simultaneous exon skipping (lower panel). (**B**) AON induced ataxin-3 protein modification. The most optimal AONs identified by the RNA screening were transfected in control fibroblasts and subjected to western blot analysis and anti-ataxin-3 probing. Percentage of exon skipping on RNA level as determined by qPCR and corresponding percentage of modification on protein level are indicated below.

Upon overnight incubation with caspase-1, similar cleavage fragments were observed for wild-type ataxin-3 (10Q) and mutant ataxin-3 (71Q), with the most prominent fragment corresponding to a ~28 kDa N-terminal fragment of ataxin-3 (Figure 3c). This finding was confirmed by western blotting with an antibody that recognizes the N-terminal T7 tag of the proteins. In case of ataxin-3 71Q, an additional ~42 kDa protein fragment was observed, likely corresponding to the C-terminal polyQ-containing fragment. Importantly, in the caspase-1 assay the corresponding ~28 and 42 kDa fragments were not observed for ataxin-3 Δ88aa with either 10 or 71 glutamines, indicating that the caspase-1 cleavage site was absent in the modified ataxin-3 protein.

The caspase-6 assay yielded similar results compared to caspase-1, with the N-terminal ~28 kDa fragment being the most prominent (Figure 3d). The caspase-3 assay yielded different protein fragments. In this case, an N-terminal fragment of ~39 kDa was most evident (Figure 3e). Probing with either a C-terminal antibody or 1C2, specific for the polyQ repeat, did not reveal the corresponding C-terminal protein fragment indicating the C-terminal fragment might be subject to further cleavage by caspase-3, rendering the fragment too small to be visible on the gel. However, due to inefficient cleavage by caspase-3 resulting only in small amounts of cleavage product, it is also possible that the C-terminal polyQ containing fragment was not abundant enough to be detected in these experiments.

Absence of ataxin-3 UIMs 1 and 2 shows reduced binding of ubiquitin chains

In order to establish whether ataxin-3 Δ88aa was able to bind ubiquitin chains through UIM3, we used a tethering approach to assess binding of ataxin-3 to locally induced ubiquitin moieties

Figure 3. Modified ataxin-3 is cleaved less efficient by several caspases. (A) Formation of smaller ataxin-3 protein fragments are observed with increasing doses of calpain-2. Wild-type (10Q) and mutant (71Q) ataxin-3 were used either unmodified or lacking the targeted 88-amino acid region (Δ88aa). Ataxin-3 with a deletion of the previously identified calpain cleavage site (ΔL255-G260) was used as a control protein. There is a rapid decrease in full length protein and appearance of shorter protein fragments with increasing concentrations of calpain-2. After calpain-2 incubation, ataxin-3 Δ88aa with 10 and 71Q gives rise to a ~4 kDa smaller N-terminal fragment with PageBlue staining that is not observed for the wild-type protein. All fragments identified with Page Blue were positive when stained with an antibody against the N-terminal T7 tag (lower panels). Ataxin-3 ΔL255-G260 was cleaved similar to wild-type ataxin-3. **(B)** Quantification of uncleaved band intensity from (A) using Odyssey software. No significant differences were observed between rate of cleavage of ataxin-3 Δ88aa and the full length ataxin-3 protein variants. **(C)** Caspase-1 mediated cleavage of ataxin-3 resulted in a similar ~30 kDa N-terminal fragment for 10Q and 71Q ataxin-3 as indicated with the arrow. The corresponding C-terminal polyQ containing fragment (indicated with asterix) was detectable for ataxin-3 71Q. Upon removal of the 88aa neither cleavage fragment was observed for both 10Q and 71Q proteins, indicating the responsible caspases cleavage site is located in the targeted 88aa region. Bars depict mean and SE. **(D)** Overnight incubation with caspase-3 results in the appearance of a faint fragment of similar size for unmodified ataxin-3 10Q and 71Q, but also the proteins lacking 88aa. **(E)** Fragments of similar size for ataxin-3 10Q and 71Q were observed after incubation with caspase-6. Removal of 88aa prevented formation of this fragment, similar to ataxin-3 where the caspase cleavage sites were individually mutated.

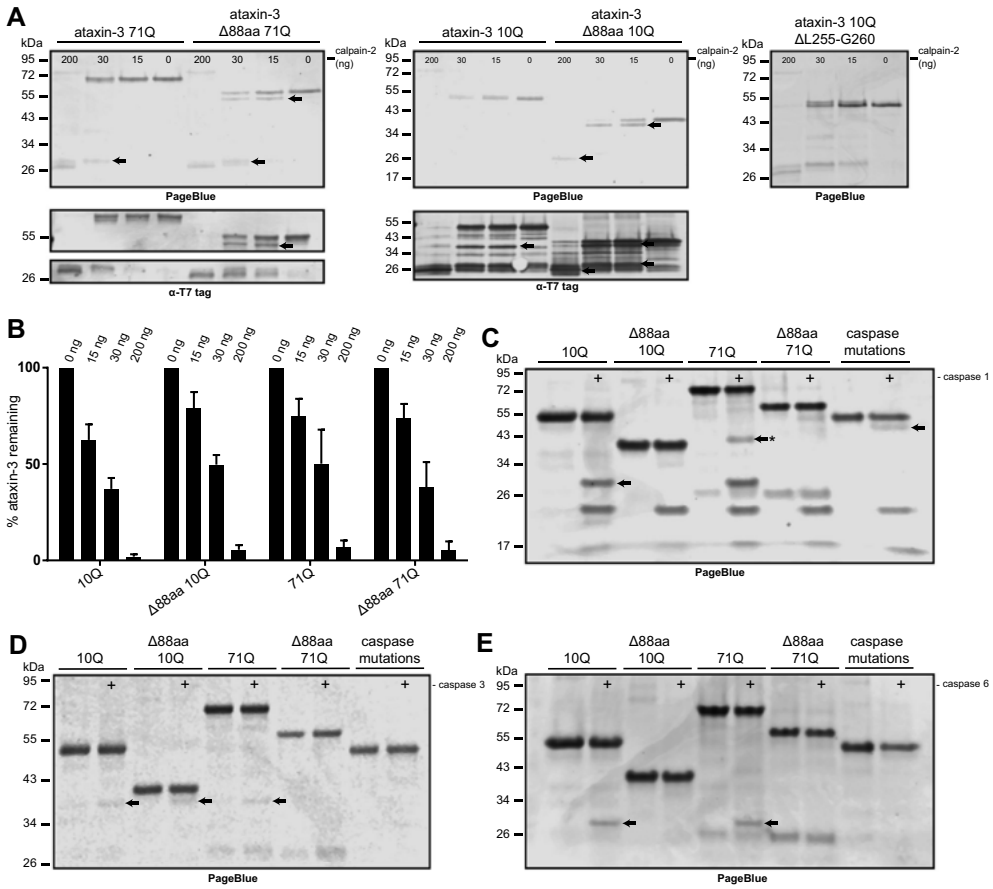

on chromatin [20]. To this end, 2-6-3 U2OS cells containing a stably integrated repeat array of the bacterial lactose operator (LacO) sequence [21] were used. A fusion protein consisting of red-fluorescent protein mCherry, the RNF8 E3 ubiquitin ligase and the *Escherichia coli* lactose repressor (LacR) protein (mCherry-LacR-RNF8) was expressed in these cells, resulting in the tethering of the LacR-fusion protein to the LacO array and the local ubiquitylation of chromatin (Figure 4b) [20]. Co-expression of GFP-tagged wild-type ataxin-3 (10Q) in these cells revealed recruitment of ataxin-3 (Figure 4c-d) to ubiquitin conjugates at the LacO array. In contrast, ataxin-3 that contained point mutations in all 3 UIMs (L229A, L249A and L340A) was unable to associate with RNF8-mediated ubiquitin chains in this cell system, indicating that the recruitment of ataxin-3 to the array is mediated by its binding to poly-ubiquitin chains. Ataxin-3 containing the 71Q expansion associated with RNF8-mediated ubiquitin chains with similar efficiency as wild-type ataxin-3 (10Q), indicating that the expanded polyQ stretch does not affect the ubiquitin-binding activity of ataxin-3. However, ataxin-3 Δ88aa with either 10Q or 71Q, failed to associate with RNF8-induced ubiquitin chains, indicating that the Δ88aa region containing UIMs 1 and 2 is essential for ubiquitin binding.

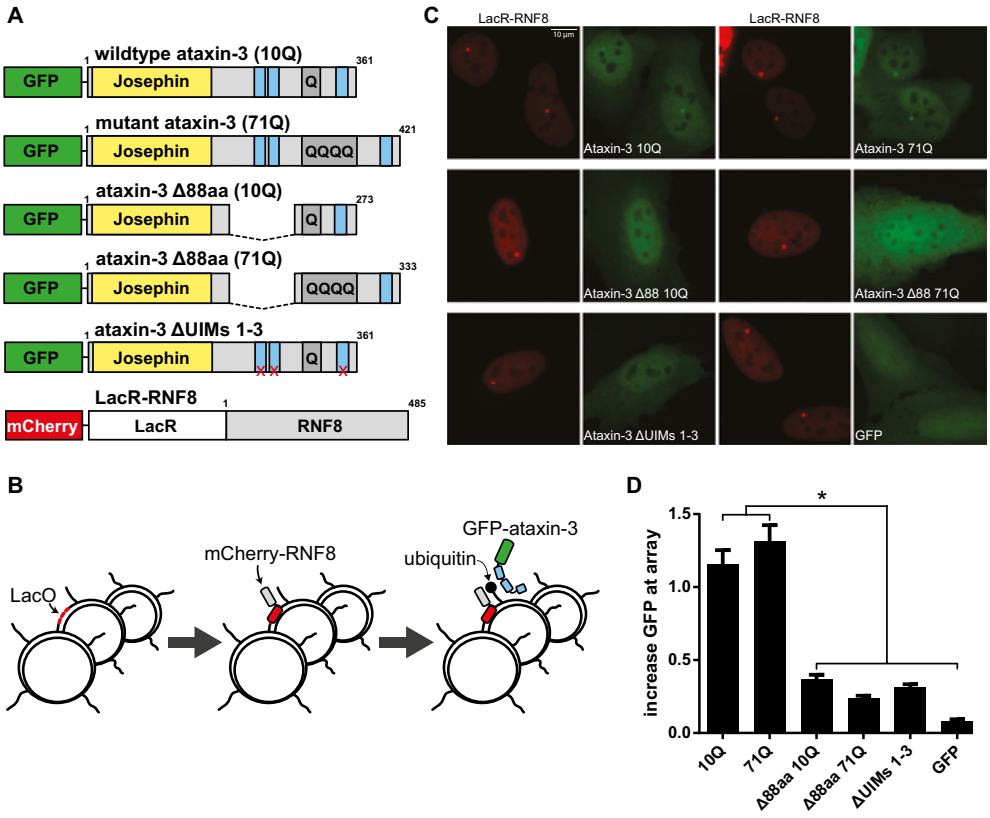

Figure 4. Modified ataxin-3 shows reduced binding of ubiquitin chains. **(A)** Schematic representation of ataxin-3 GFP-tagged proteins used for assessment of ubiquitin-binding with relevant functional domains depicted (not drawn to scale). For ataxin-3 ΔUIMs 1-3, the three UIMs were inactivated by point mutations. RFN8 ubiquitin ligase contained an N-terminal mCherry-LacR tag to enable visualization and targeting to the LacO array. **(B)** Representation of the histone ubiquitylation approach. A lacO repeat integrated into the genome of 2-6-3 U2OS cells allows targeting of the LacR-RNF8 fusion protein to the genomic LacO array, leading to localized chromatin ubiquitylation, which is bound by Ataxin-3. **(C)** Representative fluorescent images from transfected 2-6-3 U2OS cells expressing mCherry-LacR-RNF8 (red) and GFP-tagged Ataxin-3 proteins (green) . Scale bar 10 µm **(D)** Quantification of ataxin-3 localisation at the LacO repeat. Increase in GFP signal at the site of mCherry signal signifies association of ataxin-3 with ubiquitin chains. Displayed values are the mean of 2 independent experiments in more than 50 cells per condition. * $P \leq 0.0001$, bars depict mean and SE.

Ataxin-3 Δ88aa does not result in increased double stranded DNA breaks

Recently it was shown that the expression of polyQ-expanded ataxin-3 can lead to genomic DNA damage in neuroblasts through inactivation of polynucleotide kinase 3'-phosphatase (PNKP) [22]. It was established that PNKP directly interacts with ataxin-3, but PNKP activity was specifically inhibited when ataxin-3 contained a 84 polyQ stretch. PNKP has a function

in the repair of DNA double-strand breaks (DSBs) [23], and its inactivation led to an increase in the accumulation of 53BP1 and γH2AX, which are key factors involved in the DSB response, into cytologically discernable foci containing DNA breaks [22]. In order to assess whether this DNA damage phenotype could be alleviated by removal of the 88aa, we expressed GFP tagged full-length ataxin-3 and ataxin-3 Δ88aa with either 10Q or 71Q in SH-SY-5Y neuroblasts and quantitatively assessed the number of 53BP1 foci in GFP-positive cells. The number of 53BP1 foci was not increased in cells expressing ataxin-3 71Q compared to ataxin-3 10Q, indicating a similar level of DSBs (Figure 5b). Proper expression of the GFP-tagged ataxin-3 proteins was confirmed by western blot analysis (data not shown), showing that the expressed proteins contained both GFP and the polyQ stretch. For cells expressing the ataxin-3 Δ88aa with either 10Q or 71Q, no significant increase in 53BP1 foci was observed, indicating that there was no gain of toxic function for these proteins with regards to triggering genomic DNA damage.

DISCUSSION

Calpain-2 and caspase-mediated cleavage of ataxin-3 has been extensively investigated and is suggested to play a central role in polyQ mediated toxicity [8-10, 12, 13, 24]. In the current study we confirmed the proteolytic cleavage of ataxin-3 by caspases and calpain-2, which is known to result in the formation of ataxin-3 fragments that can result in toxic and aggregation-prone expanded polyQ-containing fragments [25]. Indeed, *in vivo* experiments in which a mutant ataxin-3 fragment corresponding to a cleavage fragment around amino acids 221 or 260 was expressed in mice resulted in an aggravated neurologic phenotype [10, 11]. AON-mediated removal of a central 88 amino acids region from ataxin-3 yielded a modified ataxin-3 protein predicted

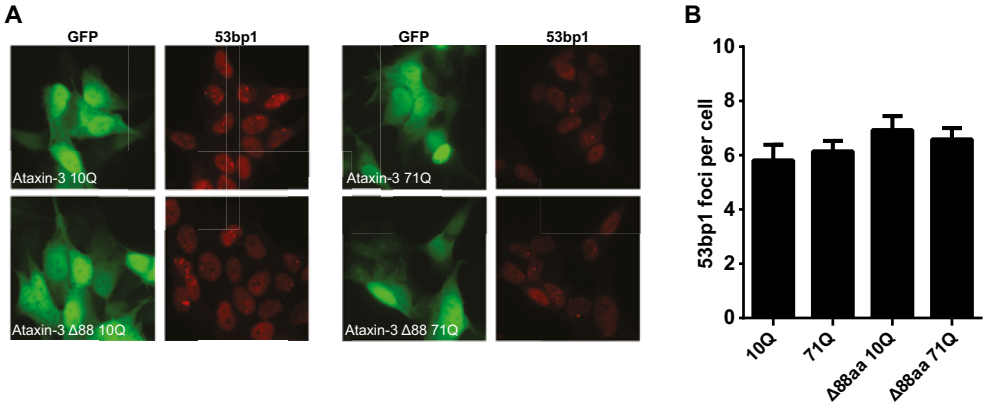

Figure 5. Expanded and modified ataxin-3 do not induce DNA strand breaks in neuroblasts. (A) SH-SY-5Y neuroblast cells transfected with GFP-ataxin-3 constructs were stained for the DNA double strand break marker 53BP1. **(B)** Quantification of 53BP1 foci in cells from A (> 50 cells per condition), mean and SE depicted.

to be less prone to proteolytic cleavage and thus less toxic. When tested in proteolytic cleavage assays, the Δ88aa ataxin-3 protein did not prove more resistant to calpain-2 cleavage. However, Δ88aa ataxin-3 did prove less sensitive to cleavage by caspases 1, 3 and 6, and formation of the polyQ-containing fragment was abolished.

The Δ88aa ataxin-3 protein lacks 5 out of the 9 predicted caspase cleavage sites [8]. Pinpointing the exact calpain cleavage sites is more difficult because the mechanisms underlying substrate recognition by calpains are currently poorly understood. Based on experimental evidence, an important calpain cleavage site is thought to be located around amino acid 260 [12]. Due to their close upstream proximity to the polyQ repeat, both the calpain and caspase cleavage sites in the central 88 amino acids region of ataxin-3 are in a key position to generate a truncated polyQ containing fragment.

The calpain-2 cleavage assays performed here showed complete proteolysis of all tested ataxin-3 proteins at relatively low calpain concentrations, indicating that other cleavage motifs in the protein are used by calpain-2 when the central 88 amino acids are absent. We did not observe the toxic calpain-derived C-terminal fragment previously described in a cellular context [24, 25], but this could be due to methodological differences since we used purified proteins in our cleavage assay while Haacke and colleagues used a cell model. Using *in vitro* cleavage assays with purified caspases 1 and 6, we observed a different cleavage profile for ataxin-3 Δ88aa when compared to wild-type ataxin-3. Specifically, a prominent N-terminal fragment of approximately 30 kDa in size was no longer generated when incubated with caspase-1 and 6. Importantly, a 43 kDa polyQ-containing fragment was also abrogated in the case of the mutant ataxin-3 protein containing 71 glutamines. An ataxin-3 protein in which all predicted caspase cleavage sites were mutated also did not generate ataxin-3 cleavage fragments, indicating that the observed differences in proteolysis are likely the result of absence of cleavage motifs. In line with previous research, there was no increased caspase-mediated cleavage of expanded ataxin-3 compared to non-expanded ataxin-3. Whether caspase-mediated ataxin-3 cleavage is indeed a major contributor to SCA3 pathogenesis remains to be determined through future *in vivo* experiments.

In silico predictions using Cascleave [26] software for Δ88aa ataxin-3 did not reveal generation of novel caspase cleavage motifs. In line with the increased resistance to caspase cleavage, we expected Δ88aa ataxin-3 to be less prone to calpain-2 cleavage as it lacks two key experimentally confirmed calpain-2 cleavage sites (Figure 1a) [12]. It is therefore unexpected that the calpain-2 cleavage rates of Δ88aa ataxin-3 were identical to ataxin-3 13Q (Figure 3b). This discrepancy between the two families of proteolytic enzymes can likely be explained by their mechanisms of substrate recognition. Substrate specificity of caspases has been extensively investigated, and is known to be highly dependent on specific peptide sequences [26]. In contrast to caspases, amino acid sequences around calpain cleavage sites are very diverse, and cleavage is likely also reliant on secondary and higher order structures [29], making *in silico* prediction of calpain cleavage difficult. The comparable calpain-2 cleavage efficiency of Δ88aa ataxin-3 and wildtype ataxin-3 may hence be explained by previous observations, where amino acid substitutions at key positions in calpain substrates led to cleavage of adjacent sites [30].

The Δ88aa ataxin-3 protein we describe here lacks UIMs 1 and 2, which are known to play a key role in the ubiquitin-binding function and specificity of ataxin-3 [4, 27]. We show that the remaining third UIM is unable to bind poly-ubiquitin chains using a cell system with localised chromatin ubiquitylation [20] This observation is in line with a previously proposed functional model of ataxin-3, where the first 2 UIMs position ubiquitin chains to the catalytic Josephin domain in a linear fashion [28]. Additionally, as the valosin-containing protein (VCP) binding site is absent in Δ88aa ataxin-3, it may be useful to assess the effect of loss of VCP interaction in future experiments. VCP is described to be involved in ataxin-3 fibrillogenesis [29], but also likely has a functional effect on the retrotranslocation of endoplasmic reticulum-associated degradation (ERAD) substrates [30] as well as ataxin-3 activation [31].

Recently it was shown that ataxin-3 interacts with the DNA end-processing enzyme PNKP. Interestingly, it was shown that wild-type ataxin-3 led to stimulation of PNKP, whereas expanded ataxin-3 led to inhibition [22, 32]. PNKP has a crucial role in the initiation of DNA strand breaks through catalysing the restoration of 5'-phosphate and 3'-hydroxyl termini and interacting with other DNA repair proteins [23, 33]. Hence, PNKP inactivation by expanded ataxin-3 may serve an important role in SCA3 pathogenesis, especially given the fact that the nervous system is particularly sensitive to DNA damage compared to other tissues [34]. It has been suggested that the PNKP inactivation by mutant ataxin-3 might in part be explained by its recruitment in polyQ aggregates [22]. Formation of polyQ aggregates, in turn, may be dependent on ataxin-3 cleavage and formation of short protein fragments containing the polyQ tract.

When expressing the Δ88aa ataxin-3 proteins, we did not observe an increase in the spontaneous formation of 53BP1 foci, which is a marker for DNA damage. However, we could not reproduce the previously reported ataxin-3-induced DNA damage phenotype in neuroblast cells [22]. One explanation for this discrepancy may lie in the fact that Gao and colleagues used an ataxin-3 protein with a slightly longer polyQ stretch (84Q) and used differentiated SY5Y neuroblast cells. Differentiation leads to alteration in cellular bioenergetics and oxidative stress response [35] with increased oxidative vulnerability [36] in these cells. It may therefore be useful to test the effect of ataxin-3 Δ88aa expression in differentiated neuroblasts in future experiments.

Our initial aim was to assess the therapeutic potential of AON-mediated removal of proteolytic cleavage sites of ataxin-3 for SCA3. Several advantages for the therapeutic use of AONs in the brain and central nervous system have been found over the years. These include: good distribution following infusion in the cerebrospinal fluid, excellent uptake in neurons and glial cells, high stability with half-lives of several months in the rodent brain and no adverse events in the clinical trials conducted thus far [18, 37]. The AONs we describe in the current study likely do not provide a high enough level of ataxin-3 protein modification to be able to assess the influence of removal of these proteolytic cleavage sites from ataxin-3 on SCA3 neuropathology *in vivo*. Future studies could optimise the AON sequences against *ATXN3* exons 8 and 9 to provide a higher level of splicing modification prior to testing *in vivo*. AON potency may further benefit from more recent chemical modifications, which especially *in vivo* may yield significantly improved stability and potency (reviewed in [16]). Furthermore, the effect of the proposed protein modification on ataxin-3 functioning is an important consideration.

Taken together, the fact that the AONs provide a low level of protein modification combined with the fact that ataxin-3 ubiquitin-binding function is reduced show that this approach is likely not an optimal therapeutic strategy for SCA3.

ACKNOWLEDGEMENTS

The authors are grateful to Susan Janicki for kindly providing U2OS 2-6-3 cells, to Thorsten Schmidt for providing antibodies and to Linda Switzar for technical assistance and advice. This work was financially supported by a VENI grant from The Netherlands Organisation for Scientific Research (NWO; to M.S.L.) and ZonMw 40-41900-98-018, Hersenstichting/Brugling Fund BG2013-03 and European Union Seventh Framework Programme (FP7/2007–2013) under grant agreement No. 305,121 (Neuromics) (to W.M.C.vR-M).

CONTRIBUTIONS

Study conception and design: W.M.C.vR-M., L.J.A.T., H.v.A. and M.S.L. Experiments were performed by L.J.A.T and I.S. The data analysis and drafting of manuscript was performed by L.J.A.T. Manuscript was revised by W.M.C.vR-M, H.v.A. and M.S.L.

COMPETING INTERESTS

W.M.C.vR-M is applicant of patent US 14/047,876 on antisense oligonucleotide directed removal of proteolytic cleavage sites for neurodegenerative diseases. The other authors declare no conflict of interest.

REFERENCES

1. Riess, O, Rub, U, Pastore, A, Bauer, P, and Schols, L (2008). SCA3: neurological features, pathogenesis and animal models. *Cerebellum (London, England)* **7**: 125-137.

2. Cummings, CJ, and Zoghbi, HY (2000). Trinucleotide repeats: mechanisms and pathophysiology. *Annual review of genomics and human genetics* **1**: 281-328.

3. Bradford, JW, Li, S, and Li, XJ (2010). Polyglutamine toxicity in non-neuronal cells. *Cell research* **20**: 400-407.

4. Winborn, BJ, Travis, SM, Todi, SV, Scaglione, KM, Xu, P, Williams, AJ, *et al.* (2008). The deubiquitinating enzyme ataxin-3, a polyglutamine disease protein, edits Lys63 linkages in mixed linkage ubiquitin chains. *The Journal of biological chemistry* **283**: 26436-26443.

5. Bettencourt, C, Santos, C, Montiel, R, Costa Mdo, C, Cruz-Morales, P, Santos, LR, *et al.* (2010). Increased transcript diversity: novel splicing variants of Machado-Joseph disease gene (ATXN3). *Neurogenetics* **11**: 193-202.

6. Matos, CA, de Macedo-Ribeiro, S, and Carvalho, AL (2011). Polyglutamine diseases: the special case of ataxin-3 and Machado-Joseph disease. *Prog Neurobiol* **95**: 26-48.

7. Evers, MM, Toonen, LJ, and van Roon-Mom, WM (2014). Ataxin-3 protein and RNA toxicity in spinocerebellar ataxia type 3: current insights and emerging therapeutic strategies. *Mol Neurobiol* **49**: 1513-1531.

8. Berke, SJ, Schmied, FA, Brunt, ER, Ellerby, LM, and Paulson, HL (2004). Caspase-mediated proteolysis of the polyglutamine disease protein ataxin-3. *Journal of neurochemistry* **89**: 908-918.

9. Wellington, CL, Ellerby, LM, Hackam, AS, Margolis, RL, Trifiro, MA, Singaraja, R, *et al.* (1998). Caspase cleavage of gene products associated with triplet expansion disorders generates truncated fragments containing the polyglutamine tract. *J Biol Chem* **273**: 9158-9167.

10. Hubener, J, Weber, JJ, Richter, C, Honold, L, Weiss, A, Murad, F, *et al.* (2013). Calpain-mediated ataxin-3 cleavage in the molecular pathogenesis of spinocerebellar ataxia type 3 (SCA3). *Human molecular genetics* **22**: 508-518.

11. Goti, D, Katzen, SM, Mez, J, Kurtis, N, Kiluk, J, Ben-Haiem, L, *et al.* (2004). A mutant ataxin-3 putative-cleavage fragment in brains of Machado-Joseph disease patients and transgenic mice is cytotoxic above a critical concentration. *J Neurosci* **24**: 10266-10279.

12. Haacke, A, Hartl, FU, and Breuer, P (2007). Calpain inhibition is sufficient to suppress aggregation of polyglutamine-expanded ataxin-3. *J Biol Chem* **282**: 18851-18856.

13. Simoes, AT, Goncalves, N, Koeppen, A, Deglon, N, Kugler, S, Duarte, CB, *et al.* (2012). Calpastatin-mediated inhibition of calpains in the mouse brain prevents mutant ataxin 3 proteolysis, nuclear localization and aggregation, relieving Machado-Joseph disease. *Brain : a journal of neurology* **135**: 2428-2439.

14. Aartsma-Rus, A, De Winter, CL, Janson, AA, Kaman, WE, Van Ommen, GJ, Den Dunnen, JT, *et al.* (2005). Functional analysis of 114 exon-internal AONs for targeted DMD exon skipping: indication for steric hindrance of SR protein binding sites. *Oligonucleotides* **15**: 284-297.

15. Spitali, P, and Aartsma-Rus, A (2012). Splice modulating therapies for human disease. *Cell* **148**: 1085-1088.

16. Evers, MM, Toonen, LJ, and van Roon-Mom, WM (2015). Antisense oligonucleotides in therapy for neurodegenerative disorders. *Advanced drug delivery reviews* **87**: 90-103.

17. Chiriboga, CA, Swoboda, KJ, Darras, BT, Iannaccone, ST, Montes, J, De Vivo, DC, *et al.* (2016). Results from a phase 1 study of nusinersen (ISIS-SMNRx) in children with spinal muscular atrophy. *Neurology* **86**: 890-897.

18. Miller, TM, Pestronk, A, David, W, Rothstein, J, Simpson, E, Appel, SH, *et al.* (2013). An antisense oligonucleotide against SOD1 delivered intrathecally for patients with SOD1 familial amyotrophic lateral sclerosis: a phase 1, randomised, first-in-man study. *Lancet Neurol* **12**: 435-442.

19. Maquat, LE (2004). Nonsense-mediated mRNA decay: splicing, translation and mRNP dynamics. *Nature reviews Molecular cell biology* **5**: 89-99.

20. Luijsterburg, MS, Acs, K, Ackermann, L, Wiegant, WW, Bekker-Jensen, S, Larsen, DH, *et al.* (2012). A new non-catalytic role for ubiquitin ligase RNF8 in unfolding higher-order chromatin structure. *The EMBO Journal* **31**: 2511-2527.

21. Janicki, SM, Tsukamoto, T, Salghetti, SE, Tansey, WP, Sachidanandam, R, Prasanth, KV, *et al.* (2004). From Silencing to Gene Expression: Real-Time Analysis in Single Cells. *Cell* **116**: 683-698.

22. Gao, R, Liu, Y, Silva-Fernandes, A, Fang, X, Paulucci-Holthauzen, A, Chatterjee, A, *et al.* (2015). Inactivation of PNKP by mutant ATXN3 triggers apoptosis by activating the DNA damage-response pathway in SCA3. *PLoS genetics* **11**: e1004834.

23. Weinfeld, M, Mani, RS, Abdou, I, Aceytuno, RD, and Glover, JN (2011). Tidying up loose ends: the role of polynucleotide kinase/phosphatase in DNA strand break repair. *Trends in biochemical sciences* **36**: 262-271.

24. Koch, P, Breuer, P, Peitz, M, Jungverdorben, J, Kesavan, J, Poppe, D, *et al.* (2011). Excitation-induced ataxin-3 aggregation in neurons from patients with Machado-Joseph disease. *Nature* **480**: 543-546.

25. Haacke, A, Broadley, SA, Boteva, R, Tzvetkov, N, Hartl, FU, and Breuer, P (2006). Proteolytic cleavage of polyglutamine-expanded ataxin-3 is critical for aggregation and sequestration of non-expanded ataxin-3. *Human molecular genetics* **15**: 555-568.

26. Song, J, Tan, H, Shen, H, Mahmood, K, Boyd, SE, Webb, GI, *et al.* (2010). Cascleave: towards more accurate prediction of caspase substrate cleavage sites. *Bioinformatics (Oxford, England)* **26**: 752-760.

27. Burnett, B, Li, F, and Pittman, RN (2003). The polyglutamine neurodegenerative protein ataxin-3 binds polyubiquitylated proteins and has ubiquitin protease activity. *Human molecular genetics* **12**: 3195-3205.

28. Mao, Y, Senic-Matuglia, F, Di Fiore, PP, Polo, S, Hodsdon, ME, and De Camilli, P (2005). Deubiquitinating function of ataxin-3: insights from the solution structure of the Josephin domain. *Proceedings of the National Academy of Sciences of the United States of America* **102**: 12700-12705.

29. Boeddrich, A, Gaumer, S, Haacke, A, Tzvetkov, N, Albrecht, M, Evert, BO, *et al.* (2006). An arginine/lysine-rich motif is crucial for VCP/p97-mediated modulation of ataxin-3 fibrillogenesis. *The EMBO Journal* **25**: 1547-1558.

30. Zhong, X, and Pittman, RN (2006). Ataxin-3 binds VCP/p97 and regulates retrotranslocation of ERAD substrates. *Hum Mol Genet* **15**: 2409-2420.

31. Laco, MN, Cortes, L, Travis, SM, Paulson, HL, and Rego, AC (2012). Valosin-containing protein (VCP/p97) is an activator of wild-type ataxin-3. *PloS one* **7**: e43563.

32. Chatterjee, A, Saha, S, Chakraborty, A, Silva-Fernandes, A, Mandal, SM, Neves-Carvalho, A, *et al.* (2015). The role of the mammalian DNA end-processing enzyme polynucleotide kinase 3'-phosphatase in spinocerebellar ataxia type 3 pathogenesis. *PLoS genetics* **11**: e1004749.

33. Caldecott, KW (2008). Single-strand break repair and genetic disease. *Nature reviews Genetics* **9**: 619-631.

34. McKinnon, PJ (2009). DNA repair deficiency and neurological disease. *Nat Rev Neurosci* **10**: 100-112.

35. Schneider, L, Giordano, S, Zelickson, BR, M, SJ, G, AB, Ouyang, X, *et al.* (2011). Differentiation of SH-SY5Y cells to a neuronal phenotype changes cellular bioenergetics and the response to oxidative stress. *Free radical biology & medicine* **51**: 2007-2017.

36. Forster, JI, Koglsberger, S, Trefois, C, Boyd, O, Baumuratov, AS, Buck, L, *et al.* (2016). Characterization of Differentiated SH-SY5Y as Neuronal Screening Model Reveals Increased Oxidative Vulnerability. *Journal of biomolecular screening* **21**: 496-509.

37. Rigo, F, Chun, SJ, Norris, DA, Hung, G, Lee, S, Matson, J, *et al.* (2014). Pharmacology of a central nervous system delivered 2'-O-methoxyethyl-modified survival of motor neuron splicing oligonucleotide in mice and nonhuman primates. *The Journal of pharmacology and experimental therapeutics* **350**: 46-55.

38. Aartsma-Rus, A (2012). Overview on AON design. *Methods Mol Biol* **867**: 117-129.

39. Desmet, FO, Hamroun, D, Lalande, M, Collod-Beroud, G, Claustres, M, and Beroud, C (2009). Human Splicing Finder: an online bioinformatics tool to predict splicing signals. *Nucleic Acids Res* **37**: e67.

40. Zuker, M (2003). Mfold web server for nucleic acid folding and hybridization prediction. *Nucleic Acids Res* **31**: 3406-3415.

41. Aartsma-Rus, A, van Vliet, L, Hirschi, M, Janson, AA, Heemskerk, H, de Winter, CL, *et al.* (2009). Guidelines for antisense oligonucleotide design and insight into splice-modulating mechanisms. *Molecular therapy : the journal of the American Society of Gene Therapy* **17**: 548-553.

42. Evers, MM, Tran, HD, Zalachoras, I, Meijer, OC, den Dunnen, JT, van Ommen, GJ, *et al.* (2014). Preventing formation of toxic N-terminal huntingtin fragments through antisense oligonucleotide-mediated protein modification. *Nucleic Acid Ther* **24**: 4-12.

43. Rozen, S, and Skaletsky, H (2000). Primer3 on the WWW for general users and for biologist programmers. *Methods Mol Biol* **132**: 365-386.

44. Ruijter, JM, Ramakers, C, Hoogaars, WM, Karlen, Y, Bakker, O, van den Hoff, MJ, *et al.* (2009). Amplification efficiency: linking baseline and bias in the analysis of quantitative PCR data. *Nucleic Acids Res* **37**: e45.

45. Schmidt, T, Landwehrmeyer, GB, Schmitt, I, Trottier, Y, Auburger, G, Laccone, F, *et al.* (1998). An isoform of ataxin-3 accumulates in the nucleus of neuronal cells in affected brain regions of SCA3 patients. *Brain pathology (Zurich, Switzerland)* **8**: 669-679.

46. Evers, MM, Tran, HD, Zalachoras, I, Pepers, BA, Meijer, OC, den Dunnen, JT, *et al.* (2013). Ataxin-3 protein modification as a treatment strategy for spinocerebellar ataxia type 3: removal of the CAG containing exon. *Neurobiol Dis* **58**: 49-56.

47. Typas, D, Luijsterburg, MS, Wiegant, WW, Diakatou, M, Helfricht, A, Thijssen, PE, *et al.* (2016). The de-ubiquitylating enzymes USP26 and USP37 regulate homologous recombination by counteracting RAP80. *Nucleic Acids Res* **44**: 2976.

4

Transcriptional profiling and biomarker identification reveal tissue specific effects of expanded ataxin-3 in a spinocerebellar ataxia type 3 mouse model

Lodewijk J.A. Toonen, Maurice Overzier, Melvin M. Evers, Leticia G. Leon, Sander A.J. van der Zeeuw, Hailiang Mei, Szymon M. Kielbasa, Jelle J. Goeman, Kristina M. Hettne, Olafur Th. Magnusson, Marion Poirel, Alexandre Seyer, Peter A. C. 't Hoen, Willeke M.C. van Roon-Mom (2018).
Molecular Neurodegeneration, in revision

ABSTRACT

Background

Spinocerebellar ataxia type 3 (SCA3) is a progressive neurodegenerative disorder caused by expansion of the polyglutamine repeat in the ataxin-3 protein. Expression of mutant ataxin-3 is known to result in transcriptional dysregulation, which can contribute to the cellular toxicity and neurodegeneration. Since the exact causative mechanisms underlying this process have not been fully elucidated, gene expression analyses in brains of transgenic SCA3 mouse models may provide useful insights.

Methods

Here we characterised the MJD84.2 SCA3 mouse model expressing the mutant human ataxin-3 gene using a multi-omics approach on brain and blood. Gene expression changes in brainstem, cerebellum, striatum and cortex were used to study pathological changes in brain, while blood gene expression and metabolites/lipids levels were examined as potential biomarkers for disease.

Results

Despite normal motor performance at 17.5 months of age, presymptomatic transcriptional changes in brain tissue of the SCA3 mice were observed. Most transcriptional changes occurred in brainstem and striatum, whilst cerebellum and cortex were only modestly affected. The most significantly altered genes in SCA3 mouse brain were *Tmc3*, *Zfp488*, *Car2*, and *Chdh*. Based on the transcriptional changes, α-adrenergic and CREB pathways were most consistently altered for combined analysis of the four brain regions. When examining individual brain regions, axon guidance and synaptic transmission pathways were most strongly altered in striatum, whilst brainstem presented with strongest alterations in the pi-3k cascade and cholesterol biosynthesis pathways. Similar to other neurodegenerative diseases, reduced levels of tryptophan and increased levels of ceramides, di- and triglycerides were observed in SCA3 mouse blood.

Conclusions

The observed presymptomatic transcriptional changes in SCA3 mouse brain reveal parallels with previous reported neuropathology in patients, but also shows brain region specific effects as well as involvement of adrenergic signalling and CREB pathway changes in SCA3.

Keywords

Spinocerebellar ataxia type 3, mouse model, RNA sequencing, metabolomics

BACKGROUND

Spinocerebellar ataxia type 3 (SCA3), also known as Machado Joseph Disease (MJD), is a progressive neurodegenerative disorder, with symptoms usually presenting around midlife. SCA3 is the most common of the dominantly inherited ataxias and is caused by a CAG repeat expansion in the *ATXN3* gene [1]. The CAG repeat is translated into a polyglutamine (polyQ) stretch in the ataxin-3 protein, which upon mutational expansion to 56 – 84 glutamines results in a gain of toxic protein function [2]. This protein toxicity mostly shows its effects in the brain, and neuronal loss in SCA3 has been reported predominantly in the brainstem, cerebellum (spinocerebellar pathways and dentate nucleus), striatum, thalamus, substantia nigra and pontine nuclei [3]. Over time, the neuronal loss causes clinical symptoms in SCA3 patients such as progressive ataxia, dystonia, spasticity, and various other symptoms (reviewed in [1]).

The molecular mechanisms of mutant ataxin-3 toxicity have been the subject of extensive research, and a range of cellular changes have been suggested to contribute to toxicity. These include aggregation and nuclear localisation of expanded ataxin-3 protein [4, 5], impaired protein degradation [6], mitochondrial dysfunction [7] and transcriptional deregulation [8]. Transcriptional deregulation may arise due to sequestration of transcription factors such as TATA-box binding protein [9] and CREB binding protein (CBP) [10] into the polyQ aggregates, thereby interfering with their function. Previous gene expression studies have identified altered inflammatory processes, cell signalling and cell surface associated genes in cell and conditional animal models of SCA3 [8, 11, 12]. Despite these recent advances in SCA3 pathogenicity, it is currently still not fully elucidated which molecular mechanisms are altered in response to mutant ataxin-3. For this reason, it is useful to examine genetic mouse models of SCA3 for transcriptional changes that occur in different regions of the brain to infer causative disease mechanisms [13].

Apart from gaining insight into disease mechanisms, transcriptional changes may also be potentially useful as biomarkers to track disease progression in SCA3. Since it is not possible to study longitudinal gene expression changes in human brain tissue, it is useful to establish potential transcriptional changes in peripheral tissues such as blood. In addition, metabolite and lipid changes in blood can also be used as easily obtainable biomarkers, and can potentially be used to track disease progression [14]. Previous research by our group has shown that there are common gene expression signatures in blood and brain of patients with Huntington disease [15]. Since patient material is not readily available, genetic SCA3 mouse models are a good starting point to identify such potential disease biomarkers.

In this study, we set out to identify the molecular mechanisms involved in SCA3 pathology. Current next-generation sequencing techniques provide an attractive means to objectively study the transcriptome and allow for very sensitive and accurate assessment of changes in gene expression. As such, we performed RNA sequencing of brain and blood from the hemizygous MJD84.2 mouse model of SCA3, which ubiquitously expresses the full human *ATXN3* gene with 84 CAGs [16] and gene expression analysis was performed in 4 different regions of the brain. Additionally, blood samples from the mice were subjected to RNA sequencing and serum

was used for metabolomic and lipidomic analysis to identify potential biomarkers capable of tracking disease progression.

We found that the MJD84.2 mice presented with reduced bodyweight compared to wild-type, but did not develop motor symptoms even at 17.5 months of age. Gene expression changes in blood were also not pronounced, with pathway analysis suggesting respiratory electron transport and mitochondrial function to be affected. In parallel to other neurodegenerative disorders, further metabolomic and lipidomic analyses of blood revealed decreased tryptophan and increased levels of a di- and triglycerides and ceramides in SCA3 mice. In contrast to blood, transcriptional changes were readily detected in brain, with the highest number of differentially expressed genes in brainstem and striatum. Somewhat surprisingly, the cerebellum was affected to a smaller extent compared to these two brain regions. The main deregulated pathways in brain were cellular signalling pathways (α-adrenergic and CREB signalling) and pathways related to synaptic transmission. This study hence provides additional evidence for affected CREB signalling in SCA3 and suggests affected neurotransmission pathways, particularly in striatum. These transcriptional changes most likely represent the early state molecular alterations associated with SCA3 pathology.

METHODS

SCA3 mice and tissue sampling

MJD84.2 transgenic SCA3 mice [16] and wild-type C57BL/6 mice were obtained from Jackson Laboratories (Bar Harbor, Maine, USA). All animal experiments were carried out in accordance with European Communities Council Directive 2010/63/EU and were approved by the Leiden University animal ethical committee. Breeding was performed by crossing hemizygous SCA3 mice with wild-types. ATXN3 CAG repeat lengths were verified for each mouse through gene fragment analysis, using human specific primers (Table S1) flanking the CAG repeat similar to described previously [17]. Human *ATXN3* repeat lengths were 76 or 77 for all transgenic mice. Only male mice were used, and a total of 8 transgenic and 8 wild-type mice were included in the experiment (Table 1), though 2 transgenic mice did not survive to the end of the study. Mice were group housed in individually ventilated cages with food and drinking water available *ad libitum*. Blood samples for metabolomic analyses were obtained at 4, 12 and 16 months of age from 4 wild-type and 4 SCA3 mice. Animals were fasted 4 hours prior to obtaining 200 µl blood through tail cut and collection in heparin lithium tubes. Tubes were immediately spun down at 18,000 x g and the supernatant (plasma) was stored at -80°C. For RNA sequencing, 200 µl of blood was obtained by tail cut at 9 months and 17.5 months of age. Blood samples for RNA sequencing were collected in RNAprotect animal blood tubes (Qiagen) following manufacturer's instructions, stored overnight at 4°C and subsequently frozen at -80°C until RNA isolation. At 17.5 months of age, mice were sacrificed and brainstem, cerebellum, striatum and cortex were dissected, snap-frozen in liquid nitrogen and stored at -80°C.

Behavioural testing

To assess the motor phenotype and coordination of the mice, rotarod and beamwalk tests were performed. The rotarod (Ugo Basile, Italy) accelerated from 5 to 45 rpm within 15 s and the latency to fall from the rod was used as measure of motor performance. On a testing day, the rotarod test was performed in 3 consecutive trials, and the average time to fall in seconds was reported. The beamwalk balance test consisted of 2 boxes (20 x 20 x 20 cm) elevated at 53 cm height and connected by a plastic cylindrical bar of ø 10 mm or ø 30 mm and 80 cm long. Mice were placed in the transparent elevated box and crossed the bar to an enclosed dark box. The average latency to cross from 3 trials per testing day is reported. The beamwalk test was performed when the mice were 4, 6, 7.5, 9 and 12 months of age. The rotarod test was performed at the same time points, with an extra assessment at 17.5 months.

Metabolite profiling in plasma

Analysis of the plasma samples was performed by Profilomics (Gif-sur-Yvette, France). For extraction of metabolites, 15 µL plasma sample was treated with 60 µL of methanol with a mixture of internal standards. Protein was precipitated at 4°C, centrifuged and supernatants were dried under nitrogen. Samples were then resuspended in ammonium carbonate 10mM pH10.5/AcN 40:60 (v/v). Chromatography settings for LC-HRMS were followed as outlined by Boudah *et al* [18]. Plasma extracts were separated on a HTC PAL-system (CTC Analytics AG, Zwingen, Switzerland) coupled with a Transcend 1250 liquid chromatographic system (ThermoFisher Scientific, Les Ulis, France) using an aSequant ZICpHILIC 5 µm, 2.1 × 150 mm at 15°C (Merck, Darmstadt, Germany). After injecting 10 µL of sample, the column effluent was directly introduced into the heated Electrospray (HESI) source of a Q-Exactive mass spectrometer (Thermo Scientific, San Jose, CA) and analysis was performed in both ionization modes. Identification of molecules was performed using TraceFinder3.1 software (ThermoFisher Scientific, Les Ulis, France). The dataset was filtered and cleaned based on quality control samples as described by Dunn *et al* [19].

Lipid profiling in plasma

Analysis of lipids in plasma was performed on identical samples as described for the metabolite analysis. Lipid analyses were performed at Profilomics (Gif-sur-Yvette, France), in accordance with previously described methods [20]. In brief, 50 µL of plasma was added to 245 µL of CHCl3/MeOH 1:1 (v/v) and 5 µL of internal standard mixture. Extraction was performed after 2 h at 4°C and centrifugation at 15,000 × g for 10 min at 4°C. The upper phase (aqueous phase), containing ganglioside species and several lysophospholipids, was transferred and dried under a stream of nitrogen. The protein interphase was discarded and the lower rich-lipid phase (organic phase) was pooled with the dried upper phase. Samples were then reconstituted in 50 µl CHCl3/MeOH 1:1, vortexed for 30 s, sonicated for 60 s and diluted 100 times in MeOH/IPA/H2O 65:35:5 (v/v/v) before injection. Similar to metabolite detection, plasma total lipid extracts were separated on HTC PAL-system (CTC Analytics AG) coupled with a Transcend 1250 liquid

chromatographic system (ThermoFisher Scientific) using a kinetex C8 2.6 µm 2.1 x 150 mm column (Phenomenex, Sydney, NSW, Australia). Mass spectrometry was performed similar as for the metabolites and data processing was done as previously described [20].

RNA isolation

After thawing, filled blood tubes were incubated for 4 hours at 25°C to ensure proper cell lysis. Isolation of RNA was subsequently performed using the RNeasy protect animal blood kit (Qiagen, Hilden, Germany) according to manufacturer's instructions for total RNA isolation including DNAse treatment, resulting in isolation of RNA molecules longer than approximately 200 nucleotides. Reduction of alpha and beta globin mRNA was performed on RNA samples using the GLOBINclear magnetic bead kit for mouse/rat (Qiagen) following manufacturer's instructions.

For isolation of RNA from brain tissue, approximately 30 mg of tissue was transferred to next advance pink bead tubes (Next Advance, Averill Park, US) containing 500 µl Trizol (Ambion, Thermo Fisher scientific, Waltham, MA, USA). Tissue was homogenised in a bullet blender BBX24 (Next Advance) for 3 minutes on setting 8. A total of 100 µl chloroform was added and samples were spun down at 10,000 x g for 15 min. The aqueous phase contining the RNA was removed and an equal volume of 70% ethanol was added. RNA purification was then performed using the PureLink RNA mini kit (Thermo Fisher scientific) in accordance with the manufacturer's protocol using provided RNA columns and a 15 min DNase step. RNA was eluted in 80 µl nuclease free water. Concentration and purity of RNA was measured using Nanodrop spectrophotometry and RNA was stored at -80°C.

RNA sequencing

Library preparation and RNA sequencing was performed at deCode Genetics (Reykjavik, Iceland). The quality of RNA was assessed with the LabChip GX using the 96-well RNA kit (Perkin Elmer). Approximately 1 µg of total RNA was used as starting material, and the average RIN values were 7.7 (SD ± 0.5) for brain tissue and 6.8 (SD ± 0.9) for blood. Non strand-specific sample preparation was performed using the TruSeq Poly-A v2 kit (Illumina, San Diego, USA) following manufacturer's instructions. In brief, mRNA was captured using magnetic poly-T oligo-attached magnetic beads, RNA molecules were fragmented, and cDNA synthesis was performed using SuperScript II (Invitrogen, Carlsbad CA, USA) with random hexamer primers. Subsequently, 2nd strand cDNA synthesis was performed in conjunction with RNAse-H treatment. End repair was performed to generate blunt ends and 3′ adenylation was performed, followed by ligation of indexing adapters to the ds-cDNA. PCR was performed to amplify the fragments. Quality of sequencing libraries was determined through pool sequencing on a MiSeq instrument (Illumina) to assess insert size, sample diversity and optimize cluster densities. Pooled samples (4 samples/pool) were clustered on paired-end (PE) flowcells (1 pool per lane) using a cBot instrument (Illumina). The sequencing was performed using a HiSeq 2500 with v4 SBS sequencing kits (read lengths 2x125 cycles). Primary processing and base

calling was performed with Illumina's HCS and RTA. Demultiplexing and generation of FASTQ files was done with Illumina scripts (bcl2fastq v1.8). The FASTQ files for the mouse brain RNA can be found in the GEO repository, accession GSE107958 and blood samples are listed under accession GSE108069.

Sequencing data processing

Analysis of sequencing data was performed using the BIOPET Gentrap in-house pipeline (http://biopet-docs.readthedocs.io/en/v0.7.0/pipelines/gentrap/) The fastqc toolkit (v0.11.2) was used to evaluate sequencing quality (http://www.bioinformatics.babraham.ac.uk/projects/fastqc/). Sickle (v1.33 with default settings) and Cutadapt (v1.10, with default settings except for "-m 20") were used to clean up reads. Cleaned reads were aligned to the mouse reference genome build 10 (GRCm38/mm10) using STAR aligner version 2.3.0e [21]. The non-default settings used by STAR are "--outFilterMultimapNmax 1 –outFilterMismatchNmax 10 –outSJfilterReads Unique". Average number of reads was 84 million (SD ± 18 million). On average, 66% of reads were aligned to known genes. Gene raw read counts are generated using *HTSeq* (v0.6.1) with the Refseq gene annotation extracted from UCSC on 11-09-2015. The non-default settings used by *HTSeq are* "--format bam –stranded no". Gene expression analysis was performed using edgeR (v 3.14.0) [22]. The normalization was performed using the trimmed mean of M-values (TMM) normalization method [23].

Differential gene expression and statistical analysis

Analysis of gene expression was performed on genes exceeding an average 4 counts per million (CPM) across all samples. Principle component analysis (PCA) was performed to confirm sample consistency (i.e. clustering per brain region). Additionally, correlation between genotype and GC percentage or 5′ - 3′ ratios was assessed for potential confounding effects. Differential gene expression was performed using the generalized linear model (GLM) likelihood ratio test functionality of edgeR [22]. Analyses were performed for the 4 brain regions separately, but also as a combined dataset, which is termed "brain data combined" data throughout the manuscript. For this combined analysis of all brain regions, we modelled the effect of strain and tissue (brain region) and the interaction between them to allow detection of strain effects that were either present in all brain regions or tissue-specific. For this, a design matrix was created with the function model.matrix(~ Tissue * Strain) and dispersion was estimated accounting for this design. A general linear model was fit using the glmFit function, and likelihood ratio test then performed with glmLRT on the combination of coefficients for Strain and the interaction term Tissue*Strain. The null hypothesis is that the gene shows no differential expression in any brain region. This analysis is powerful for finding genes with weak effects in several brain regions, but does not allow inference of differential expression in any specific brain regions. For differential gene expression analysis between SCA3 and wildtype mice within individual brain regions, one coefficient was assigned to each group using model.matrix(~0 + group). Likelihood ratiotest was then performed using glmLRT function with contrast argument to allow pairwise

genotype comparison for each brain region. Analysis of differential gene expression for blood was performed similar to brain, but due to observation of a confounding influence, GC-content correction was first performed using the conditional quantile normalization (CQN) package as previously described [24]. The GC-content correction offset obtained from CQN was then included when estimating dispersion in edgeR. The two time points (9 and 17.5 months) were included as contrasts for the likelihood ratiotest. Genes with a false discovery rate (FDR, Benjamini-Hochberg) below 0.05 were considered significant. Plots were generated using ggplot2 package [25] or graphpad Prism 7. Analysis of the metabolites and lipids in blood was performed using a Welch's t-test without multiple testing correction (due to 4 vs 4 sample size), and nominal p-values < 0.05 were considered significant.

Functional annotation of gene sets and pathway analysis

For identification of functional processes, sets of genes with a FDR of <0.05 were used, for each individual brain region and also for all brain regions combined. This led to inclusion of 585 genes from all brain regions combined, 195 genes for brainstem and 824 genes from striatum. Cerebellum and cortex did not present with enough differentially expressed genes to perform pathway analysis. Pathway analysis and exploration of metabolite-phenotype links was performed using Ingenuity Pathway Analysis (IPA) and the Euretos Knowledge Platform (EKP) [26]. Euretos allows for semantic search for biologically interesting connections between genes, proteins, metabolites and drugs based on an underlying database of 176 integrated data sources (January 2017) [27]. Pathway analysis was performed by the use of the Fisher exact test for gene set enrichment. Overlapping significantly altered pathways between the Euretos and Ingenuity analysis were considered as the most reliable signal, and are hence listed as top overrepresented pathways.

Validation with RT-qPCR

RNA sequencing results were validated on the same RNA samples using qPCR. cDNA synthesis was performed using oligo-dT primers for brain and random hexamer primers for blood RNA, with the Transcriptor First Strand cDNA Synthesis Kit (Roche, Mannheim, Germany) similar to described previously [28], but using an incubation step of 60 minutes at 50 °C . qPCR was performed with SensiMix SYBR & Fluorescein Kit (Bioline, Taunton, USA) similar to previously described [28], using 3 µl of 5x diluted cDNA for brain samples and 3 µl of 15x diluted cDNA for blood. Mouse reference genes used were β-actin (*Actb*), Hypoxanthine-guanine phosophoribosyltransferase (*Hprt*), and Ribosomal Protein L22 (*Rpl22*) for brain tissue and *Actb*, vinculin (*Vcl*) and *Hprt* for blood (Table S1). Primers were designed with Primer3 software [29] and PCR efficiencies and expression values (N0) were determined using LinRegPCR 2014.0 [19]. Transcript level expression was then divided by the geometric mean of the 3 reference genes expression [30]. Statistical tests were performed in graphpad (7.0) using the two-stage linear step-up multiple testing procedure of Benjamini, Krieger and Yekutieli, with Q = 5% and without assuming a consistent SD.

Western blotting

Protein isolation and western blotting of mouse brain tissue was performed following standard protocols. In brief, brain tissue was homogenized in RIPA buffer using a bullet blender BBX24 (Next Advance, Averill Park, US). Protein concentration was determined using the bicinchoninic acid kit (Thermo Fisher Scientific). A total of 30 μg protein was boiled for 5 min with 4x Laemmli sample buffer and separated on 10% Tris-glycine precast gel (Biorad, Veenendaal, the Netherlands) and transferred to a nitrocellulose membrane. Membranes were blocked in 5% low fat milk and incubated overnight at 4°C with primary antibodies: rabbit anti-carbonic anhydrase 2 (car2) 1:2000 (Novus Biologicals, Littleton, CO, USA), rabbit anti-psat1 1:1000 (Novus Biologicals) and as loading control mouse anti-β-actin 1:5000 (Abcam, Cambridge, UK). Detection was performed using secondary antibodies IRDye 680RD and 800CW (LI-COR Biosciences, Lincoln, USA) 1:5000, and membranes were imaged using Odyssey infrared imaging system (LI-COR). Quantification was performed with Odyssey software version 3.0 (Licor) using the integrated intensity method. Intensity of car2 and psat1 protein bands were divided by the β-actin intensity to correct for protein loading.

RESULTS

SCA3 mice do not present with overt motor symptoms at 17 months of age

The MJD84.2 mouse model ubiquitously expresses full-length mutant human ataxin-3 with 84 glutamines, under control of the human ataxin-3 promoter. During a 17.5 month period, the behavioural phenotype of the mice was assessed using motor tests, and blood was collected for assessment of biomarkers at transcript and metabolite/lipid level. To this end, blood RNA for sequencing was collected at two time points and blood plasma for mass-spec was collected at three time points (for experimental overview, see Fig. 1A). During the testing period, the MJD84.2 mice had a significantly lower body weight compared to control mice (Fig. 1B). Assessment of an ataxic phenotype using rotarod and beamwalk balance tests at 5 time points revealed only two significant differences. The first difference was a faster performance of SCA3 mice on the balance beam at 12 months of age (Fig. 1C), likely attributable to the lower bodyweight. The second significant difference was a shorter latency to fall on the rotarod at 4 months of age for SCA3 mice (Fig. 1D). However, given poorer performance of wild-type mice at the following time points, this suggests to a difference in learning rather than motor performance. The motor and balance performance of the SCA3 mice was identical to the wild-type mice at all other time points tested.

Individual brain regions are differently affected by mutant ataxin-3

To establish differential gene expression changes between wild-type and SCA3 mice, RNA sequencing of brain and blood tissue was performed (Table 1). After exclusion of RNA samples with low concentration (< 200 ng), a total of 53 samples were successfully sequenced. The average number of reads per sample was 84 million (SD ± 18 million) and on average

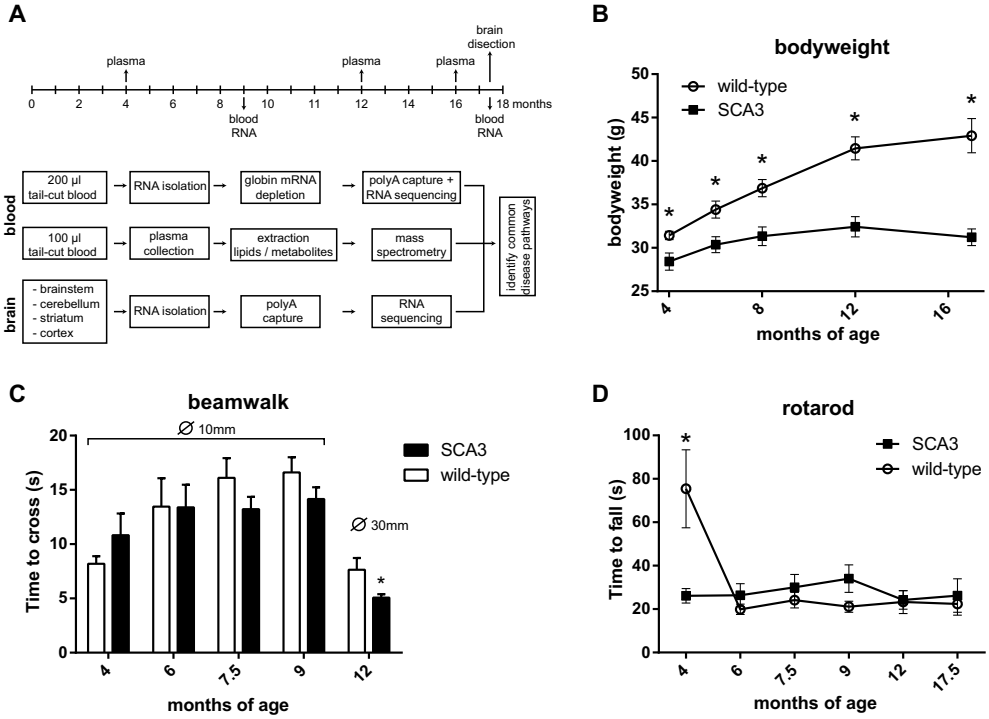

Figure 1. Experimental design and behavioural testing in SCA3 mice. A) MJD84.2 hemizygous mice were used as a model for SCA3. At indicated time points, plasma was collected for metabolic and lipidomic analyses, and whole blood was collected for RNA sequencing purposes. At 17.5 months of age, mice were sacrificed and 4 brain regions were isolated for RNA sequencing. **B)** SCA3 mice show significantly lower bodyweight compared to wild-type mice. **C)** The beamwalk balance test shows identical performance in coordination/balance performance of SCA3 and wild-type mice, apart from a better performance of SCA3 mice at 12 months of age. **D)** The rotarod motor performance shows a significant decrease in time to fall for SCA3 mice at 4 months of age. Depicted data represents 8 wild-type vs 8 SCA3 mice. Shown is mean +/- SEM, * = $p < 0.05$ using multiple t-test.

Table 1. RNA sequencing and metabolomic/lipidomic sample overview

Analysis	Tissue	Wild-type mice	SCA3 mice
RNA-seq	brainstem	8	6
RNA-seq	cerebellum	7	6
RNA-seq	cortex	7	6
RNA-seq	striatum	8	5
RNA-seq	blood (9 and 17.5 months)	6	5
Metabolomics	plasma (4 and 16 months)	4	4
Lipidomics	plasma (4 and 16 months)	4	4 (4 months), 3 (16 months)

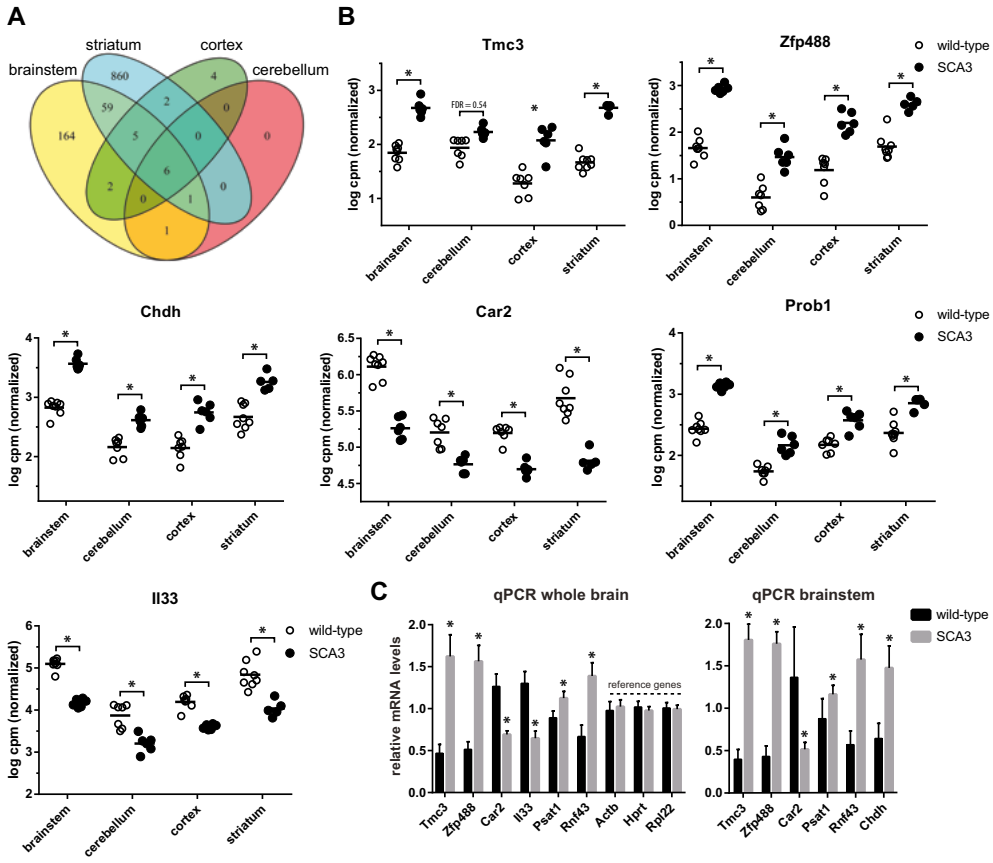

Figure 2. RNA sequencing results for SCA3 mouse brain. A) Venn diagram depicting overlap of significantly altered genes (FDR < 0.05) from RNA sequencing analysis between SCA3 and wild-type mice per brain region. Six genes were common to all four regions. **B)** Plots of the 6 most significantly altered genes in SCA3 mouse brain (combined regions). Expression values of genes are depicted separately for the 4 tested brain regions. * = FDR < 0.01 **C)** qPCR validation on equimolar cDNA from the 4 brain regions, as well as separately in brainstem confirms significant gene expression changes. Based on 7 wild-type vs 6 SCA3 mice at 17.5 months of age. * = FDR < 0.01. *Actb, Hprt* and *Rpl22* were used as reference genes.

66% of sequencing reads were aligned to exons of known genes (Fig. S1). Genes with average expression below 4 CPM were excluded, resulting in a total of 12,372 genes to be included for differential expression analysis. The brain RNA sequencing data can be accessed at GEO repository GSE107958. PCA plots showed good separation of samples based on brain region (Fig. S2) and using an FDR of < 0.05, a total of 585 genes were found significantly altered in the SCA3 brain regions combined analysis. The top 25 genes from the analysis of brain regions combined are listed in Table 2, with corresponding log2 fold change per brain region. When examining each brain region individually, the extent of differential gene expression in SCA3 mice differed greatly per brain region (Fig. 2A), with 238 genes differentially expressed in brainstem,

Table 2. Top 25 differentially expressed genes in SCA3 mice brains (regions combined). Noted with * are genes that are also differentially expressed in individual brain regions.

Gene symbol	Name	FDR	Brainstem log2 fold change	Cerebellum log2 fold change	Striatum log2 fold change	Cortex log2 fold change	Protein function (GO term mol function or biological process)
Tmc3	transmembrane channel-like gene family 3	1.30E-61	1.16*	0.42	1.47*	1.16*	ion transport
Zfp488	zinc finger protein 488	1.05E-56	1.79*	1.25*	1.29*	1.45*	transcription, oligodendrocyte specific
Car2	carbonic anhydrase 2	3.63E-44	-1.26*	-0.64*	-1.26*	-0.72*	carbonate dehydratase activity
Chdh	choline dehydrogenase	3.26E-40	1.04*	0.66*	0.85*	0.87*	choline dehydrogenase activity
Prob1	proline rich basic protein 1	9.30E-38	1*	0.62*	0.68*	0.59*	unknown
Il33	interleukin 33	9.98E-35	-1.3*	-0.98*	-1.2*	-0.87*	cytokine activity
Fbxw15	F-box and WD-40 domain protein 15	5.97E-27	-1.8*	-0.84	-1.44*	-0.79	unknown
Rnf43	ring finger protein 43	5.64E-21	1.06*	0.74*	0.65*	0.88*	ubiquitin-protein transferase activity
Polr2a	RNA polymerase II subunit A	2.00E-20	0.74*	0.16	0.47*	0.35	DNA-directed RNA polymerase activity
Ppl	periplakin	1.50E-19	2.14*	0.73	0.9*	0.62	cadherin binding involved in cell-cell adhesion
Arsb	arylsulfatase B	2.48E-16	0.53*	0.2	0.32*	0.18	sulphate hydrolysis
Kcnk13	potassium two pore domain channel subfamily k member 13	3.04E-16	-0.97*	-0.73*	-0.81*	-0.44	voltage-gated ion channel
Chil1	chitinase-3-like protein 1	7.24E-16	-0.75*	-0.28	-0.69*	-0.56*	carbohydrate metabolic process
Serpinb1a	serpin Family B Member 1	1.16E-15	-1.34*	-0.86	-1.21*	-0.81	negative regulation of endopeptidase activity
Tspan2	tetraspanin 2	5.27E-15	-0.87*	-0.3	-0.99*	-0.41	astrocyte and microglia development
Hist1h2be	Histone H2B type 1-C/E/G	2.39E-14	0.78*	0.18	0.77*	0.66*	antibacterial humoral response
Acot1	Acyl-coenzyme A thioesterase 1	1.90E-13	0.74*	0.35	0.28	0.29	acyl-CoA metabolic process
Erbb2ip	erbin	1.86E-12	-0.89*	-0.44	-0.54*	-0.30	cellular response to tumor necrosis factor

Table 2. (continued)

Gene symbol	Name	FDR	Brainstem log2 fold change	Cerebellum log2 fold change	Striatum log2 fold change	Cortex log2 fold change	Protein function (GO term mol function or biological process)
Glul	Glutamine synthetase	1.12E-11	-0.63*	-0.25	-0.45*	-0.21	glutamine biosynthetic process
Cbs	Cystathionine beta-synthase	1.68E-11	-0.41*	-0.06	-0.40*	-0.14	catalyzes first step of the transsulfuration pathway
Qdpr	Dihydropteridine reductase	2.10E-11	-0.64*	-0.39	-0.70*	-0.36	6,7-dihydropteridine reductase activity
Sox8	Transcription factor SOX-8	6.57E-11	0.58*	0.37	0.42*	0.38	enteric nervous system development
Psat1	Phosphoserine aminotransferase	6.63E-11	0.48*	0.39	0.40*	0.46*	L-serine biosynthetic process
Enpp6	Ectonucleotide pyrophosphatase/ phosphodiesterase family member 6	2.01E-10	0.20*	0.58	0.76*	1.25*	choline metabolic process
Ttyh1	Protein tweety homolog 1	1.37E-09	-0.44*	-0.12	-0.04	-0.14	chloride transport

8 in cerebellum, 19 in cortex and 933 in striatum (FDR < 0.05) compared to wild-type mice. This observation is consistent with smaller fold-changes observed for most genes in cerebellum and cortex. Of the differentially expressed genes, 6 (*Rnf43, Zfp488, Car2, Chdh, Prob1, Il33*) were consistently significantly altered in all 4 brain regions (Fig. 2B). For each brain region that we analysed, we ranked the genes based on p-value, and the majority of the genes in these 4 lists were unique to that particular brain region, thus revealing tissue specific gene expression patterns. For validation we selected 6 genes from the top 25 significant genes of the brain region combined analysis, based on FDR, fold change and expression level. Through qPCR on the same samples as used for RNA sequencing, we validated the significant change in expression level for all 6 genes (Fig. 2C). Finally, differential expression was confirmed at the protein level for carbonic anhydrase 2 (*Car2*) and phosphoserine aminotransferase 1 (*Psat1*), as these proteins were predicted to be differentially expressed in all 4 brain regions. Cortex and cerebellum of the SCA3 mice was available for validation of protein levels, and both brain regions showed a similar direction of protein change as was found on mRNA level and reached significance for *Car2* in both brain regions and for *Psat1* in cerebellum (Fig. 3 and Fig.S3).

Cellular signalling pathways are altered in SCA3 mouse brain

To establish gene expression changes in SCA3 mice at the gene function level, the Euretos knowledge platform and Ingenuity pathway analysis (IPA) tools were used to assess pathway enrichment. Both tools showed good overlap in the top significant pathways for brain region combined analysis. The top pathways associated with the 585 differentially expressed genes in SCA3 mouse brain (4 regions combined) are listed in Table 3. The top pathways are sorted on ingenuity p-value, the complete list of pathway analysis can be found in supplementary file 1. The combined region pathways signify alterations in pathways which are most consistent for the 4 brain regions, though effect size can differ per individual region. From this combined analysis, cellular signalling pathways were the most significantly enriched pathways, namely: α-adrenergic, CREB and protein kinase A (PKA) signalling, which are all predicted to be downregulated. CREB proteins can be activated by phosphorylation by kinases, including PKA [31], and can thus be involved in the same signalling cascade. Indeed, both CREB and PKA signalling have been implicated in Huntington disease [32, 33] and other neurodegenerative disorders [34], and CREB signalling is known to be required for long-term synaptic plasticity and axonal outgrowth [35], which was also found as one of the most significantly altered pathways. Similar to Huntington disease, sterol regulatory element binding proteins (SREBPs) and cholesterol biosynthesis [36, 37] were also among the top significantly altered pathways in the current SCA3 study. Finally, a total of 24 significantly altered genes were associated with the cellular process of myelination (go:0042552), suggesting a defect in myelin homeostasis in SCA3 brain as was also reported for Huntington disease [38].

Since ataxin-3 is ubiquitously expressed in brain, and in SCA3 patients there is no clear correlation between the affected brain regions and level of ataxin-3 expression [39], region specific pathological mechanisms are likely at play. Indeed, different pathways were observed when

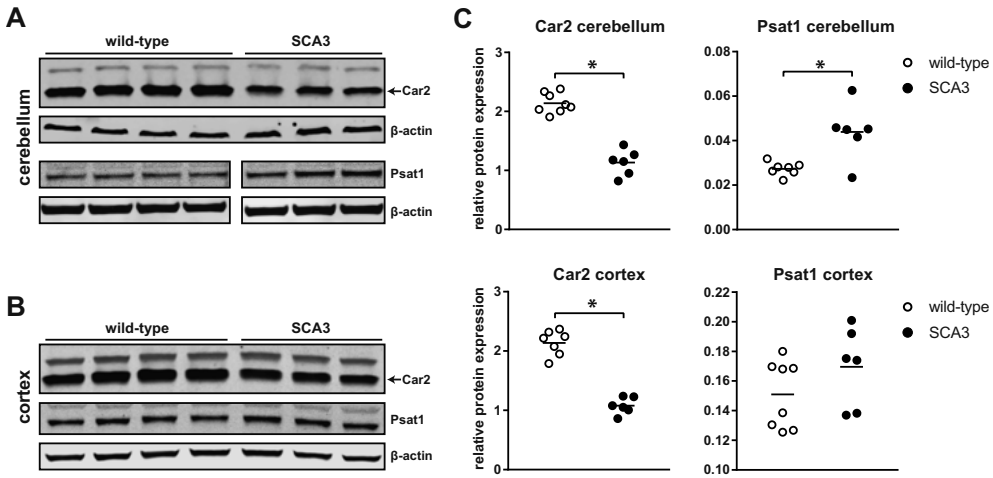

Figure 3. Protein validation of RNA sequencing results in SCA3 mouse brain. Western blot analysis of mouse brain lysates from cerebellum (**A**) and cortex (**B**) probed for Car2 and Psat1 protein. Depicted are results of 4 wild-type and 3 SCA3 mice. **C**) Quantification of band intensity reveals significant downregulation of Car2 protein in cerebellum and cortex of SCA3 mice, and significant upregulation of Psat1 in cerebellum. Protein expression was corrected per lane for β-actin levels. Based on 8 wild-type vs 6 SCA3 mice. * = p-value < 0.05 with student's *t*-test.

performing brain region combined analysis compared to brainstem and striatum individually (Table 3 and Fig. 4A). In striatum, the predominant effects were observed in axon guidance and synaptic transmission pathways (Fig. 4B) in addition to neurotransmitter receptor induced postsynaptic events. These pathways were however not apparently affected in brainstem (Fig. 4C). Of note, the affected neurotransmitter receptor pathway is most likely glutamate dependent based on involved genes (*Grind2d* and *Grik1*). Transcriptional analysis of SCA1 [40, 41] as well as SCA7 [42] mouse models have previously established a potential involvement of glutamate signalling, suggesting that this may be a signalling pathway that is more broadly affected in the polyQ cerebellar ataxias. Brainstem showed the most significant alterations in amino acid metabolism, cholesterol biosynthesis and the pi-3k cascade, though these pathways were also significantly altered in striatum. Due to the small number of differentially expressed genes, pathway analysis was not possible for cerebellum and cortex.

Differential gene expression in blood

Blood samples were collected at 9 and 17.5 months of age, RNA was isolated and sequenced after depletion of globin transcripts. Average number of reads was 57.5 million (SD ± 10.7 million), and on average 53% were aligned to known genes (Fig. S4A). The blood RNA sequencing data can be found under GEO accession GSE108069. A total of 9800 genes were used for gene expression analysis. Globin transcripts were successfully reduced (Fig. S4B), and were < 4 CPM. However, both average GC percentage and 5'-3' bias were significantly lower in the samples

Table 3. Top overrepresented pathways for genes differentially expressed in SCA3 mouse brain.

Pathway	Number of genes	p-value	Pathway database
Brain regions combined analysis (585 genes)			
α-adrenergic signalling	11	1.23E-05	Ing
CREB signalling in neurons	25	1.95E-05	Ing
protein kinase A signalling	25	2.57E-05	Ing
axon guidance	24	3.63E-05	Ing + Euretos
transmission across chemical synapses	13	5.50E-05	Ing + Euretos
superpathway of cholesterol biosynthesis (srebp)	6	6.03E-05	Ing + Euretos
myelination (cellular process)	24	8.02E-06	Ing + Euretos
Brainstem (195 genes)			
pi-3k cascade	6	1.20E-04	Ing + Euretos
amino acid metabolism	9	1.31E-04	Euretos
Superpathway of Cholesterol Biosynthesis	5	1.74E-04	Ing + Euretos
Striatum (824 genes)			
axon guidance	38	2.19E-07	Ing + Euretos
neurotransmitter receptor binding and downstream transmission in the postsynaptic cell	19	9.72E-06	Euretos
synaptic transmission/long term potentiation	23	3.02E-05	Ing + Euretos

Overrepresented pathways based on Ingenuity (Ing) and Euretos pathway analyses. Where applicable, Ingenuity obtained p-values are preferentially reported. The three top pathways in brainstem were also significantly altered in striatum.

from SCA3 mice (Fig. S4C and D). The GC content can have a confounding effect on differential gene expression in RNA sequencing analysis, because it may arise during PCR amplification before sequencing, and it is difficult to separate from a true signal [43]. For this reason, GC-content correction was performed prior to analysis [24]. At 9 months of age, only *Uba52* was significantly downregulated in blood of SCA3 mice, while at 17.5 months of age a total of 142 genes were found differentially expressed compared to wild-type mice. The top 10 differentially expressed genes at 17.5 months are listed in Table 4 and corresponding plots of the top 5 genes are shown in (Fig. 5A). Of the significantly altered genes in SCA3 mouse blood, Tnfsf14 (Tumor Necrosis Factor (Ligand) Superfamily, Member 14) has previously been reported to be upregulated in blood of SCA3 patients [44]. Tnfsf14 showed a log fold change of 0.8 in SCA3 mouse blood, with a FDR of 0.048. Through qPCR validation we were able to verify the expression changes in SCA3 mouse blood for protein scribble homolog (*Scrib,* log fold change -0.4, FDR 0.02) and cation-transporting ATPase 13A2 (*Atp13a2*, log fold change -0.4, FDR 0.037), and were able to confirm a trend for 4 other genes tested (Fig. 5B). Pathway analysis of the significantly altered genes revealed an effect on respiratory electron transport and mitochondria associated genes.

Metabolic and lipid changes in blood of SCA3 mice

Plasma samples from 4 wild-type and 4 transgenic mice were collected at 4, 12 and 16 months of age and used for LC-MS detection of metabolites (Profilomics, Gif-sur-Yvette, France). A total

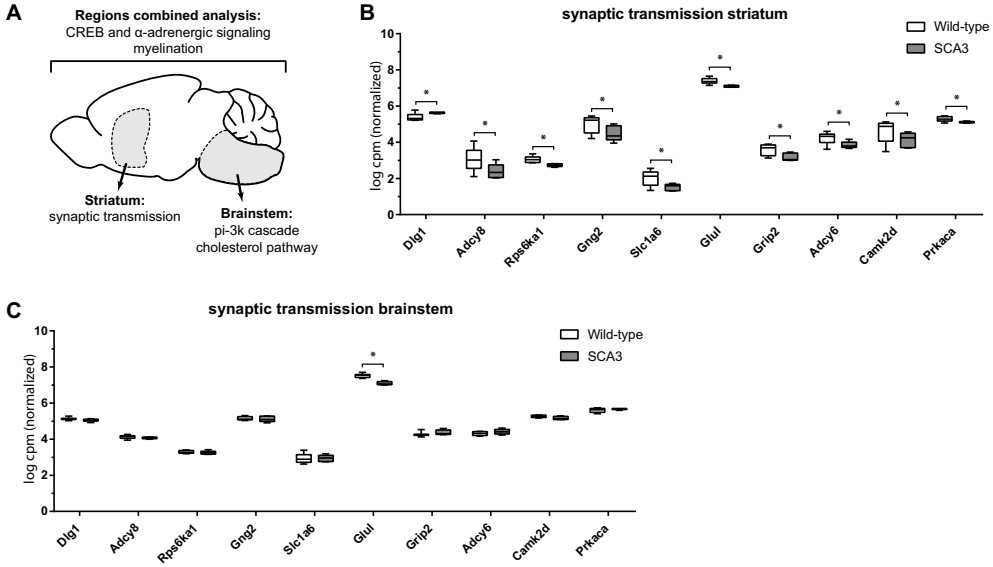

Figure 4. Affected pathways in SCA3 mouse brain. **(A)** Brainstem and striatum present with different top affected pathways based on gene expression analysis. Expression of synaptic transmission associated genes in striatum **(A)** and brainstem **(B)** of wild-type and SCA3 mice confirm that the transcriptional changes in this pathway are specific to striatum. Obtained from RNA sequencing of 8 wild-type and 6 SCA3 mice. Depicted are 10 out the 23 differentially expressed genes within synaptic transmission pathway.

Table 4. Top 10 differentially expressed genes in SCA3 mouse blood at 17.5 months old

Gene symbol	Name	FDR	Log fold change	Protein function (GO term mol. function or biological process)
Pdia6	protein disulfide isomerase associated 6	0.002	-0.6	apoptotic cell clearance
Hs3st3b1	heparan sulfate (glucosamine) 3-O-sulfotransferase 3B1	0.002	0.9	glycosaminoglycan biosynthetic process
Klk8	kallikrein related-peptidase 8	0.004	1.0	endopeptidase activity
Il18r1	interleukin 18 receptor 1	0.007	0.7	interleukin-18-mediated signaling pathway
Runx2	runt related transcription factor 2	0.007	0.8	ATP binding
Reck	reversion-inducing-cysteine-rich protein with kazal motifs	0.007	1.1	endopeptidase inhibitor activity
Tob1	transducer of ErbB-2.1	0.007	0.8	receptor tyrosine kinase binding
Phf13	PHD finger protein 13	0.007	0.6	chromatin binding
Rhoh	ras homolog family member H	0.007	-0.5	mast cell activation
Smad7	Mothers Against Decapentaplegic Homolog 7	0.010	0.7	activin binding

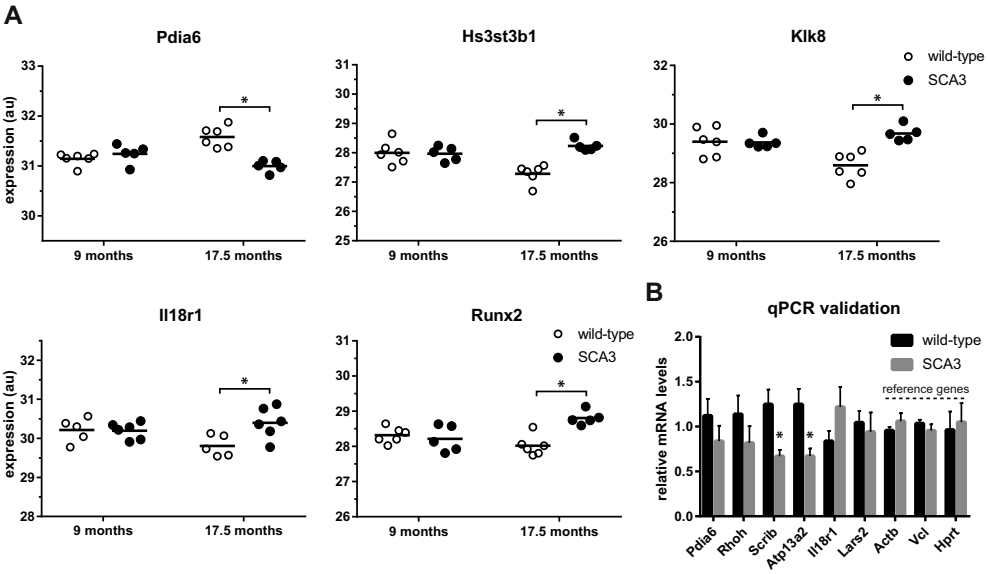

Figure 5. top 5 differentially expressed genes in blood of SCA3 mice. At 17.5 months 142 genes were differentially expressed (FDR < 0.05). **A)** Normalized expression of top 5 differentially expressed genes at 17.5 months of age in blood of wild-type and SCA3 mice as detected by RNA sequencing. **B)** qPCR validation of blood RNA confirms significant gene expression changes for *Scrib* and *Atp13a2*. Based on 8 wild-type vs 6 SCA3 mice at 17.5 months of age. * = FDR < 0.05. *Actb, Vcl* and *Hprt* (right columns) were used as reference genes.

of 195 variables were detected in both ionization modes, where 114 could be matched at a level 1 annotation (retention time, relative isotopic ratio and MS/MS spectra) and 81 with a level 2 annotation (no MS/MS data) to an in-house database of metabolites. Combining positive and negative ion modes led to detection of 148 unique metabolites. The corresponding chemical classes of the detected metabolites are depicted in (Fig. S5).

Alterations in metabolite levels were assessed between wild-type and SCA3 mice at individual time points using the Welch's unequal variances *t*-test procedure by comparing the area under the curve (AUC) using log10 areas. Due to the low sample number, there was no correction for multiple testing and nominal *p*-values are reported. A total of 32 metabolites were found to be significantly different ($p < 0.05$) between SCA3 and wild-type mice. The 10 most significantly altered metabolites, irrespective of testing time point, are listed in Table 5. At 4 months of age, DL-Dihydroorotic-acid was most significantly altered, whilst L-Threonic-acid was most significantly altered at 12 months of age, and DL-tryptophan at 16 months (Fig. 6A).

To assess alterations of the metabolome in SCA3 mice over time, a PCA was performed (Fig. S6). Age was weakly but significantly correlated with the first principal component (PC), which explains 57% of variance ($\rho = -0.586$, $p < 0.05$). Genotype also weakly but significantly correlated with PC3, explaining 7% of variance (Fig. S6B) ($\rho = -0.463$, $p < 0.05$), indicating that the effect

of mutant ataxin-3 expression in the mice did not induce a strong effect on blood metabolite levels. When comparing SCA3 to wild-type mice at 4, 12 and 16 months of age, the number of significantly altered metabolites in blood were 14, 20 and 4 respectively. From these metabolites, only DL-Tryptophan was altered at two of the time points, whilst the other metabolites were only found to be altered at a single time point. The full list of measured metabolites and comparisons between genotypes can be found in supplementary file 2.

On the same plasma samples, lipid levels were also examined. A total of 491 unique lipids were identified, divided over 26 classes (Fig. S5). To have an overview of the dataset, areas of all unique lipids from the same lipid class were summed. Differences in levels of the individual lipids and of the lipid classes at 4, 12 and 16 months were assessed using the Welch's unequal variance t-test without multiple testing correction (Table S2). Using this method, at 4 months of age no lipid classes were found significantly different in plasma between SCA3 and wild-type mice. At 12 months of age, glycerophosphoserine and sulfatides were decreased significantly in the SCA3 mouse. At 16 months of age, di- and triacylglycerols and ceramides were

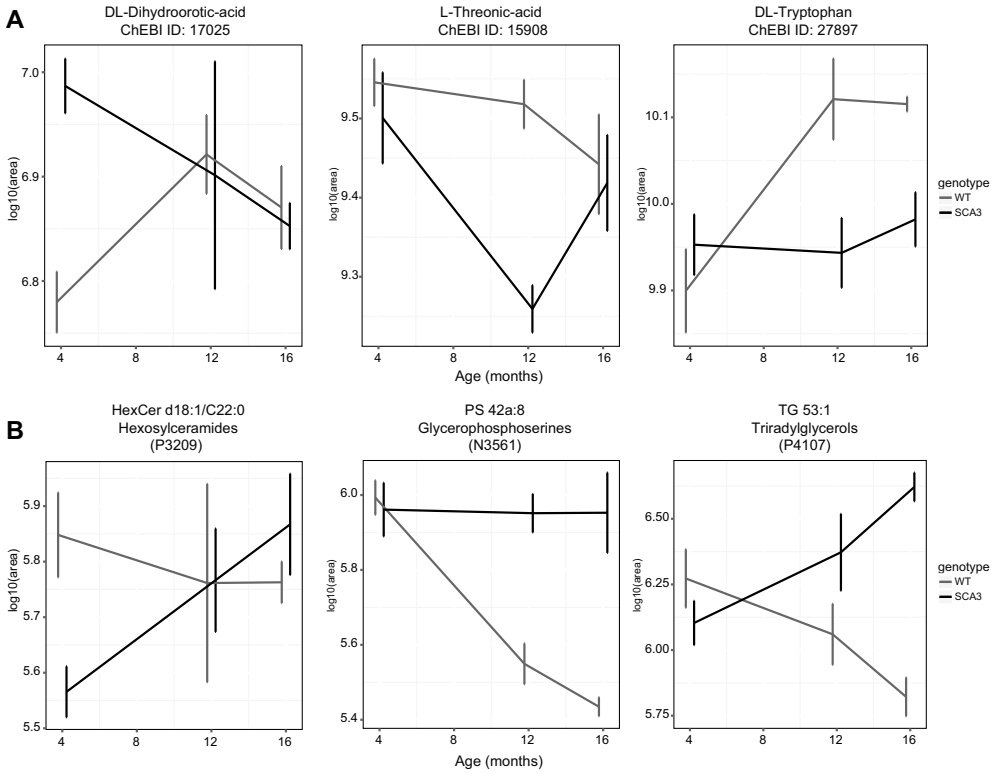

Figure 6. Significantly altered metabolites at 4, 12 and 16 months of age in the MJD84.2 mouse model. **A)** Levels of the 3 most significantly altered metabolites over time. **B)** Levels of 3 most significantly altered lipids over time. Listed profilomic ID can be found in supplementary files 1 and 2. Based on 4 wild-type vs 4 SCA3 mice. Depicted is mean log areas ±SD per time point.

significantly increased in plasma of SCA3 mice compared to wild-type. Both diacylglycerols and ceramides have been linked to the oxidative stress and stress signalling pathways [45, 46]. In contrast, glycerophosphoserine, lyso-phosphoinositols and sulfatide were found to be decreased in the SCA3 mice over time. Interestingly, 3 of the 4 NeuGC-GM2 gangliosides were found significantly altered at 16 months. The full list of measured lipids can be found in supplementary file 3. The most significantly altered individual lipids are shown in (Fig. 6B). Due to their association with disease progression, ceramides, sulfatides, glycerophosphoserine and triradylglycerol may be of potential interest as biomarkers of disease progression in these mice.

DISCUSSION

Here, we determined gene expression as well as metabolite and lipid changes in the SCA3 MJD84.2 mouse model [16]. Given the absence of motor symptoms and significant neurodegeneration, the reported alterations likely represent the early pathological changes that precede neurodegeneration. Transcriptional deregulation is a known pathogenic process in SCA3 [8], but so far few studies have been performed to establish which transcriptional changes occur and how these are involved in the molecular pathogenicity in SCA3. Furthermore, there is currently a requirement for reliable (pre)clinical biomarkers capable of tracking disease progression in SCA3.

Multi-omic biomarker identification in blood of SCA3 mice

Both metabolites [47] and gene transcripts [48] may serve as biomarkers to track neurodegenerative disease progression in blood. Sequencing of whole blood RNA revealed lower levels of *Uba52* at 9 months of age, whereas 142 genes were differentially expressed at 17.5 months of age in the SCA3 mice. A total of 10 genes have been reported as transcript biomarkers in blood of SCA3 patients [44]. Of these 10 genes, only upregulation of Tumor Necrosis Factor Superfamily Member 14 (*Tnfsf14)* was also observed significantly upregulated in our dataset of the SCA3 mice. Despite the modest overlap, this observation does solidify *Tnfsf14* as a potential blood biomarker for SCA3. Pathway analysis of the 142 altered genes in our blood dataset suggested affected respiratory electron transport pathways, in line with mitochondrial abnormalities and increased oxidative damage observed in peripheral blood of Huntington patients [49] and mitochondrial DNA damage previously reported in blood and brain of SCA3 mice [50]. Interestingly, whole blood RNA sequencing of SCA2 patients also suggested affected mitochondrial function [51], suggesting a potential commonality between the different polyQ disorders.

Metabolite analysis of blood revealed a range of altered metabolites in SCA3 mouse blood at all three time points tested. However, due to the small sample size used, the results must be interpreted with caution and the most relevant alterations in metabolites are those that are represented at multiple time points and show increasing fold change over time. In this regard, DL-Tryptophan (CHEBI: 27897) was identified as the most promising biomarker. DL-tryptophan levels were found to be altered at both 12 and 16 months of age, with lower levels in

Table 5. Top altered blood metabolites in SCA3 mice at 3 time points

Compound	ChEBI ID	Fold change	p-value	Altered at Time points	Associated pathway
4 months					
DL-Dihydroorotic-acid	17025	1.61 ± 0.19	0.002	4 months	Pyrimidine Metabolism
N-a-acetyl-L-arginine	40521	1.95 ± 0.39	0.003	4 months	NA
3-hydroxydecanoic-acid / 10-hydroxydecanoic-acid	17409	1.51 ± 0.21	0.005	4 months	Fatty Acid
12 months					
L-Threonic-acid	15908	0.55 ± 0.08	0.001	12 months	Ascorbate and aldarate metabolism
2-Aminoisobutyric-acid / Aminobutyric-acid	27971	2.58 ± 0.69	0.002	12 months	NA
Asparagine	17196	0.68 ± 0.08	0.003	12 months	Ammonia Recycling / Aspartate Metabolism / Transcription/Translation
16 months					
Methylhistamine	29009	0.87 ± 0.06	0.019	16 months	Histidine Metabolism
DL-Tryptophan	27897	0.74 ± 0.11	0.020	12 and 16 months	NA
Threonine / D-allo-Threonine	16857	0.77 ± 0.09	0.038	16 months	Glycine and Serine Metabolism / Threonine and 2-Oxobutanoate Degradation / Transcription/Translation

Nominal p-values reported, associated pathway obtained from Profilomics database.

SCA3 mice (fold change 0.7 +/- 0.11). Interestingly, blood tryptophan levels have been correlated with disease progression in blood of Huntington disease patients, with affected patients also showing lower levels [52, 53]. Indeed, tryptophan and its degradation products have been proposed as pathogenic factors in Huntington brain, with the tryptophan metabolite quinolinate reported to be elevated in Huntington disease brain, due to increased 3-hydroxyanthranilate oxygenase activity [54]. To our knowledge, tryptophan levels in blood of SCA3 patients have not been assessed yet, and would thus be a good starting point to establish a biomarker indicative of disease progression.

Lipidomic analyses revealed that at 16 months of age the di- and triglycerides and ceramides (CHEBI: 85812 and 85777) levels were increased considerably in the SCA3 mice (supplementary file 2). Interestingly, increased triglycerides levels have been detected in blood of SCA3 patients [55], but ceramides have not yet been assessed in a clinical setting. In a mouse model for Huntington disease, increased diacylglycerol kinase (DGK) activity has been observed, and a protective effect of DGK inhibition was suggested [56]. In line with the blood transcriptional changes, ceramides have been frequently reported in relation with neurodegenerative disorders, especially in the context of oxidative stress, inflammation and apoptosis [57-59]. For instance, in spinal cord tissue from amyotrophic lateral sclerosis spinal cord patients, increased levels of ceramides were detected and preceded the clinical phenotype in a mouse model [60]. The proposed mechanism is that the mutant protein leads to increased oxidative stress, thereby altering the sphingolipid metabolism to produce more ceramides and cholesterol esters, in turn sensitising motor neurons susceptible to excitotoxicity and oxidative stress, culminating in cell death [60]. A comparison between ceramides in blood and CNS tissue of the SCA3 mouse in future experiments may thus be useful to establish ceramides as a potential biomarker.

CREB and α-adrenergic signalling pathway transcripts are most consistently altered throughout the SCA3 mouse brain

A combined brain region differential gene expression analysis was performed in order to prioritise the most robust and consistent transcriptional alterations across all brain regions. The 75 week time point used for transcriptional analysis in this study corresponds to the early and minor loss of Purkinje cells in the MJD84.2 mouse model [61]. This early phase of cell loss at 75 weeks does not result in motor deficits of these mice as found in this study and by others [62]. Other molecular hallmarks of SCA3 are however present in these mice, including increased ataxin-3 nuclear localisation and insolubility [62-64]*, which is considered an early stage of aberrant protein aggregation,* deranged calcium signalling [63] and increased excitability in Purkinje cells [61].

In this manner, CREB and α-adrenergic signalling pathways were determined as most strongly affected in the SCA3 mouse brain. α-Adrenergic signalling has not yet been extensively investigated for SCA3, and further validation in other mouse models and patient brain material should thus be performed to more reliably establish this finding. However, adenosine homeostasis is reportedly changed in Huntington [65], suggestive of potential parallels between

the two polyQ disorders. Additionally, an adenosine A2A receptor agonist, though pleiotropic, was shown to have beneficial effects on neurodegeneration and transcriptional dysregulation in a SCA3 transgenic mouse [66].

Downregulation of CREB signalling was the second most affected pathway based on the RNA sequencing of brain tissue in the SCA3 mice. This finding is in good agreement with previous studies where ataxin-3 was found to interact with CREB-binding protein, and inhibits transcription by this coactivator [67].This inhibition likely takes place through sequestration of CREB-binding protein by the polyglutamine, as evidenced in the polyQ disease spinal and bulbar muscular atrophy (SBMA) [68]. Furthermore, an expanded polyglutamine stretch is also known to supress phosphorylation of CREB through binding of the coactivator TAFII130, interfering with CREB-dependent transcription and subsequently contributing to polyQ pathogenicity [69]. Also, CREB deficiency enhances polyQ induced lethality in *Drosophila,* which can be partly rescued by increased CREB expression [70]. As CBP regulates CREB[71] and SREBP transcriptional activity [72], these results suggest that loss of CBP function underlies at least part of the transcriptional dysregulation in the SCA3 brain, similar to what has been suggested for Huntington disease [73]. Consistent with the synaptic transmission related gene expression changes we observed in striatum of the SCA3 mice, CREB signalling is known to be required for long-term synaptic plasticity and axonal outgrowth [35]. Together, these findings suggest that CREB dependent transcription is indeed inhibited due to presence of expanded polyQ protein, and that the resulting transcriptional dysregulation contributes to the pathogenic mechanisms in SCA3 [34].

Mutant ataxin-3 affects synaptic transmission pathways more strongly in striatum

From the combined brain region transcriptional analysis, CREB and α-adrenergic signalling were found most strongly affected. However, it was clear that the contribution of each individual brain region to this list was not equal. We observed larger fold changes and more differentially expressed genes in striatum and brainstem than observed in cortex and cerebellum. As we and others have repeatedly shown similar expression of the mutant ataxin-3 transgene in the MJD84.2 mouse model in the brain regions tested here [16, 74, 75], it is unlikely that variations in expression levels can explain these differences. Since previous studies suggest that cellular *ATXN3* transcript and protein levels do not correlate well with neuronal degeneration in SCA3 [39, 76], these findings are indicative of differential effects of mutant ataxin-3 in each brain region. One of the more surprising findings in our dataset was the fact that the synaptic transmission pathways were more strongly affected in striatum compared to brainstem and cerebellum. Pathway analysis of the transcriptome in the brainstem showed that the pi-3k cascade and cholesterol biosynthesis pathways were most significantly altered in this brain region of the SCA3 mouse. It is not clear why different pathways are affected in brainstem compared to striatum in the SCA3 mouse. However, in a previous study we did note the strongest nuclear localisation of mutant ataxin-3 in the substantia nigra [75]. In SCA3 patients a marked reduction in dopamine transport was found in striatum [77]. Given that the dopaminergic innervation of

striatum originates from substantia nigra [78,79], pathogenic nuclear localisation of mutant ataxin-3 may interfere with this dopaminergic signalling. Indeed, in light of the requirement of CREB for dopamine dependent gene expression in the striatum [80], the observed alteration in CREB signalling in the striatum of the SCA3 mouse may reflect affected dopaminergic signalling from substantia nigra. Nonetheless, in a more severe SCA3 mouse model synaptic transmission and signal transduction pathways were found altered in cerebellum of symptomatic mice [8]. It will thus be interesting to determine whether these synaptic transmission deficiencies in cerebellum correlate with nuclear localisation or aggregation of mutant ataxin-3 and are a requirement for motor phenotype onset. The affected axon guidance pathway in striatum of SCA3 mice was also identified in a transcriptomic study with SCA2 mice, where weighted correlation network analysis of cerebellum found one module associated with axon guidance correlating to disease status (Pflieger et al., 2017).

Emerging role of white matter dysfunction in SCA3

In a recent study, RNAseq profiling was performed on pons of 22 week old MJD84.2 and two knock-in SCA3 models [81]. A total of 38 genes were found differentially expressed in pons of these mouse models. In our study, we were able to identify 32 of these reported genes, and indeed found significant differential expression for 23 of those genes in brainstem of the MJD84.2 mice. This overlap argues for the robustness of both studies, and since we observed altered expression for 11 genes associated with myelination (*Olig1, Olig 2, Ddx54, Fyn, Egfr, Cdkn1c, Pmp22, Klk6, Mal, Tspan2,* and *Aspa*), our findings further solidify *white matter changes as a potential disease process in brainstem of SCA3 mice.* The top downregulated protein identified in our study, Car2, accumulates on oligodendrocyte processes associated with myelinated axons and it is thought that Car2 may be involved in myelin formation in the central nervous system [82], though no major myelin abnormalities have been observed in Car2 deficient mice [83,84]. Furthermore, *Zfp488* (zinc finger protein 488) was significantly upregulated in SCA3 mice, and plays a role in the differentiation of neural progenitor cells to mature oligodendrocytes, thereby assisting in remyelination after injury [85]. *Together, these gene expression studies warrant further investigation of these white matter related processes in SCA3 pathogenicity.*

CONCLUSIONS

Taken together, we report here *Tnfs14* transcript, DL-tryptophan levels and spingolipids ceramides as potential blood biomarkers for SCA3. Mechanistically, we found alterations in transcript levels for CREB and α-adrenergic pathways most consistently affected throughout all brain regions of the MJD84.2 mice. In striatum, synaptic transmission pathways were most strongly affected, whilst brainstem showed largest changes in the pi-3k cascade.

DECLARATIONS

Acknowledgements

The authors want to thank Eleni Mina and Ioannis Moustakas for assisting with the analysis of RNA sequencing data, and want to thank Merel Boogaard for assistance with the CAG repeat sizing of the mice.

Funding

This research was supported by ZonMw 40-41900-98-018, Hersenstichting/Brugling Fund BG2013-03 and European Union Seventh Framework Programme (FP7/2007–2013) under grant agreement No. 305,121 (Neuromics) (to W.M.C.vR-M). Leticia G. Leon was supported by a fellowship by Associazione Italiana per la Ricerca sul Cancro (AIRC) co-funded by the European Union.

Availability of data and materials

Multi-omic data will be deposited in public repositories upon acceptance of manuscript.

Authors contributions

Experiments performed by: MO, LJAT and MME. RNA sequencing performed by OTM, quality control and alignment performed by SAJvdZ and HM. Analysis of RNA sequencing by PACtH, LGL, JJG, SMK and LJAT. Metabolomic/lipid analysis by MP and AS. Pathway analysis performed by KMH and MME. Design of experiments by LJAT and WvRM. Paper written by LJAT.

Competing interests

Kristina M. Hettne has performed paid consultancy since November 1, 2015, for Euretos b.v, a startup founded in 2012 that develops knowledge management and discovery services for the life sciences, with the Euretos Knowledge Platform as a marketed product.

Ethics approval

All animal experiments were approved by the Leiden University animal ethical committee.

Consent for publication

Not applicable

REFERENCES

1. Riess, O, Rub, U, Pastore, A, Bauer, P, and Schols, L (2008). SCA3: neurological features, pathogenesis and animal models. *Cerebellum (London, England)* **7**: 125-137.

2. Evers, MM, Toonen, LJ, and van Roon-Mom, WM (2014). Ataxin-3 protein and RNA toxicity in spinocerebellar ataxia type 3: current insights and emerging therapeutic strategies. *Molecular neurobiology* **49**: 1513-1531.

3. Matos, CA, de Macedo-Ribeiro, S, and Carvalho, AL (2011). Polyglutamine diseases: the special case of ataxin-3 and Machado-Joseph disease. *Prog Neurobiol* **95**: 26-48.

4. Bichelmeier, U, Schmidt, T, Hubener, J, Boy, J, Ruttiger, L, Habig, K, *et al.* (2007). Nuclear localization of ataxin-3 is required for the manifestation of symptoms in SCA3: in vivo evidence. *The Journal of neuroscience : the official journal of the Society for Neuroscience* **27**: 7418-7428.

5. Paulson, HL, Perez, MK, Trottier, Y, Trojanowski, JQ, Subramony, SH, Das, SS, *et al.* (1997). Intranuclear inclusions of expanded polyglutamine protein in spinocerebellar ataxia type 3. *Neuron* **19**: 333-344.

6. Chai, Y, Koppenhafer, SL, Shoesmith, SJ, Perez, MK, and Paulson, HL (1999). Evidence for proteasome involvement in polyglutamine disease: localization to nuclear inclusions in SCA3/MJD and suppression of polyglutamine aggregation in vitro. *Human molecular genetics* **8**: 673-682.

7. Yu, YC, Kuo, CL, Cheng, WL, Liu, CS, and Hsieh, M (2009). Decreased antioxidant enzyme activity and increased mitochondrial DNA damage in cellular models of Machado-Joseph disease. *Journal of neuroscience research* **87**: 1884-1891.

8. Chou, AH, Yeh, TH, Ouyang, P, Chen, YL, Chen, SY, and Wang, HL (2008). Polyglutamine-expanded ataxin-3 causes cerebellar dysfunction of SCA3 transgenic mice by inducing transcriptional dysregulation. *Neurobiology of disease* **31**: 89-101.

9. Perez, MK, Paulson, HL, Pendse, SJ, Saionz, SJ, Bonini, NM, and Pittman, RN (1998). Recruitment and the role of nuclear localization in polyglutamine-mediated aggregation. *The Journal of cell biology* **143**: 1457-1470.

10. Nucifora, FC, Jr., Sasaki, M, Peters, MF, Huang, H, Cooper, JK, Yamada, M, *et al.* (2001). Interference by huntingtin and atrophin-1 with cbp-mediated transcription leading to cellular toxicity. *Science (New York, NY)* **291**: 2423-2428.

11. Evert, BO, Vogt, IR, Kindermann, C, Ozimek, L, de Vos, RA, Brunt, ER, *et al.* (2001). Inflammatory genes are upregulated in expanded ataxin-3-expressing cell lines and spinocerebellar ataxia type 3 brains. *The Journal of neuroscience : the official journal of the Society for Neuroscience* **21**: 5389-5396.

12. Evert, BO, Vogt, IR, Vieira-Saecker, AM, Ozimek, L, de Vos, RA, Brunt, ER, *et al.* (2003). Gene expression profiling in ataxin-3 expressing cell lines reveals distinct effects of normal and mutant ataxin-3. *Journal of neuropathology and experimental neurology* **62**: 1006-1018.

13. Trancikova, A, Ramonet, D, and Moore, DJ (2011). Genetic mouse models of neurodegenerative diseases. *Progress in molecular biology and translational science* **100**: 419-482.

14. Mastrokolias, A, Pool, R, Mina, E, Hettne, KM, van Duijn, E, van der Mast, RC, *et al.* (2016). Integration of targeted metabolomics and transcriptomics identifies deregulation of phosphatidylcholine metabolism in Huntington's disease peripheral blood samples. *Metabolomics : Official journal of the Metabolomic Society* **12**: 137.

15. Mina, E, van Roon-Mom, W, Hettne, K, van Zwet, E, Goeman, J, Neri, C, *et al.* (2016). Common disease signatures from gene expression analysis in Huntington's disease human blood and brain. *Orphanet journal of rare diseases* **11**: 97.

16. Cemal, CK, Carroll, CJ, Lawrence, L, Lowrie, MB, Ruddle, P, Al-Mahdawi, S, *et al.* (2002). YAC transgenic mice carrying pathological alleles of the MJD1 locus exhibit a mild and slowly progressive cerebellar deficit. *Human molecular genetics* **11**: 1075-1094.

17. Gardiner, SL, van Belzen, MJ, Boogaard, MW, van Roon-Mom, WMC, Rozing, MP, van Hemert, AM, *et al.* (2017). Huntingtin gene repeat size variations affect risk of lifetime depression. *Translational psychiatry* **7**: 1277.

18. Boudah, S, Olivier, MF, Aros-Calt, S, Oliveira, L, Fenaille, F, Tabet, JC, *et al.* (2014). Annotation of the human serum metabolome by coupling three liquid chromatography methods to high-resolution mass spectrometry. *Journal of chromatography B, Analytical technologies in the biomedical and life sciences* **966**: 34-47.

19. Dunn, WB, Broadhurst, D, Begley, P, Zelena, E, Francis-McIntyre, S, Anderson, N, *et al.* (2011). Procedures for large-scale metabolic profiling of serum and plasma using gas chromatography and liquid chromatography coupled to mass spectrometry. *Nature protocols* **6**: 1060-1083.

20. Seyer, A, Boudah, S, Broudin, S, Junot, C, and Colsch, B (2016). Annotation of the human cerebrospinal fluid lipidome using high resolution mass spectrometry and a dedicated data processing workflow. *Metabolomics : Official journal of the Metabolomic Society* **12**: 91.

21. Dobin, A, Davis, CA, Schlesinger, F, Drenkow, J, Zaleski, C, Jha, S, *et al.* (2013). STAR: ultrafast universal RNA-seq aligner. *Bioinformatics (Oxford, England)* **29**: 15-21.

22. Robinson, MD, McCarthy, DJ, and Smyth, GK (2010). edgeR: a Bioconductor package for differential expression analysis of digital gene expression data. *Bioinformatics (Oxford, England)* **26**: 139-140.

23. Robinson, MD, and Oshlack, A (2010). A scaling normalization method for differential expression analysis of RNA-seq data. *Genome Biology* **11**: R25-R25.

24. Hansen, KD, Irizarry, RA, and Wu, Z (2012). Removing technical variability in RNA-seq data using conditional quantile normalization. *Biostatistics (Oxford, England)* **13**: 204-216.

25. Wickham, H (2009). ggplot2: Elegant Graphics for Data Analysis. Springer-Verlag New York.

26. Euretos (2017). Euretos platform http://www.euretos.com/.

27. Euretos (2017). Euretos platform databases http://www.euretos.com/files/EKPSources2017.pdf.

28. Toonen, LJ, Schmidt, I, Luijsterburg, MS, van Attikum, H, and van Roon-Mom, WM (2016). Antisense oligonucleotide-mediated exon skipping as a strategy to reduce proteolytic cleavage of ataxin-3. *Sci Rep* **6**: 35200.

29. Rozen, S, and Skaletsky, H (2000). Primer3 on the WWW for general users and for biologist programmers. *Methods Mol Biol* **132**: 365-386.

30. Ruijter, JM, Ramakers, C, Hoogaars, WM, Karlen, Y, Bakker, O, van den Hoff, MJ, *et al.* (2009). Amplification efficiency: linking baseline and bias in the analysis of quantitative PCR data. *Nucleic acids research* **37**: e45.

31. Shaywitz, AJ, and Greenberg, ME (1999). CREB: a stimulus-induced transcription factor activated by a diverse array of extracellular signals. *Annual review of biochemistry* **68**: 821-861.

32. Wyttenbach, A, Swartz, J, Kita, H, Thykjaer, T, Carmichael, J, Bradley, J, *et al.* (2001). Polyglutamine expansions cause decreased CRE-mediated transcription and early gene expression changes prior to cell death in an inducible cell model of Huntington's disease. *Human molecular genetics* **10**: 1829-1845.

33. Giralt, A, Saavedra, A, Carreton, O, Xifro, X, Alberch, J, and Perez-Navarro, E (2011). Increased PKA signaling disrupts recognition memory and spatial memory: role in Huntington's disease. *Human molecular genetics* **20**: 4232-4247.

34. Saura, CA, and Valero, J (2011). The role of CREB signaling in Alzheimer's disease and other cognitive disorders. *Reviews in the neurosciences* **22**: 153-169.

35. Alberini, CM (2009). Transcription factors in long-term memory and synaptic plasticity. *Physiological reviews* **89**: 121-145.

36. Leoni, V, and Caccia, C (2015). The impairment of cholesterol metabolism in Huntington disease. *Biochimica et biophysica acta* **1851**: 1095-1105.

37. Block, RC, Dorsey, ER, Beck, CA, Brenna, JT, and Shoulson, I (2010). Altered cholesterol and fatty acid metabolism in Huntington disease. *Journal of clinical lipidology* **4**: 17-23.

38. Bartzokis, G, Lu, PH, Tishler, TA, Fong, SM, Oluwadara, B, Finn, JP, *et al.* (2007). Myelin breakdown and iron changes in Huntington's disease: pathogenesis and treatment implications. *Neurochemical research* **32**: 1655-1664.

39. Nishiyama, K, Murayama, S, Goto, J, Watanabe, M, Hashida, H, Katayama, S, *et al.* (1996). Regional and cellular expression of the Machado-Joseph disease gene in brains of normal and affected individuals. *Annals of neurology* **40**: 776-781.

40. Ingram, M, Wozniak, EA, Duvick, L, Yang, R, Bergmann, P, Carson, R, *et al.* (2016). Cerebellar Transcriptome Profiles of ATXN1 Transgenic Mice Reveal SCA1 Disease Progression and Protection Pathways. *Neuron* **89**: 1194-1207.

41. Serra, HG, Byam, CE, Lande, JD, Tousey, SK, Zoghbi, HY, and Orr, HT (2004). Gene profiling links SCA1 pathophysiology to glutamate signaling in Purkinje cells of transgenic mice. *Human molecular genetics* **13**: 2535-2543.

42. Chou, AH, Chen, CY, Chen, SY, Chen, WJ, Chen, YL, Weng, YS, *et al.* (2010). Polyglutamine-expanded ataxin-7 causes cerebellar dysfunction by inducing transcriptional dysregulation. *Neurochemistry international* **56**: 329-339.

43. Benjamini, Y, and Speed, TP (2012). Summarizing and correcting the GC content bias in high-throughput sequencing. *Nucleic acids research* **40**: e72.

44. Raposo, M, Bettencourt, C, Maciel, P, Gao, F, Ramos, A, Kazachkova, N, *et al.* (2015). Novel candidate blood-based transcriptional biomarkers of Machado-Joseph disease. *Movement disorders : official journal of the Movement Disorder Society* **30**: 968-975.

45. Denis, U, Lecomte, M, Paget, C, Ruggiero, D, Wiernsperger, N, and Lagarde, M (2002). Advanced glycation end-products induce apoptosis of bovine retinal pericytes in culture: involvement of diacylglycerol/ceramide production and oxidative stress induction. *Free radical biology & medicine* **33**: 236-247.

46. Ruvolo, PP (2001). Ceramide regulates cellular homeostasis via diverse stress signaling pathways. *Leukemia* **15**: 1153-1160.

47. Kori, M, Aydin, B, Unal, S, Arga, KY, and Kazan, D (2016). Metabolic Biomarkers and Neurodegeneration: A Pathway Enrichment Analysis of Alzheimer's Disease, Parkinson's Disease, and Amyotrophic Lateral Sclerosis. *Omics : a journal of integrative biology* **20**: 645-661.

48. Mastrokolias, A, Ariyurek, Y, Goeman, JJ, van Duijn, E, Roos, RA, van der Mast, RC, *et al.* (2015). Huntington's disease biomarker progression profile identified by transcriptome sequencing in peripheral blood. *European journal of human genetics : EJHG* **23**: 1349-1356.

49. Chen, CM, Wu, YR, Cheng, ML, Liu, JL, Lee, YM, Lee, PW, *et al.* (2007). Increased oxidative damage and mitochondrial abnormalities in the peripheral blood of Huntington's disease patients. *Biochemical and biophysical research communications* **359**: 335-340.

50. Kazachkova, N, Raposo, M, Montiel, R, Cymbron, T, Bettencourt, C, Silva-Fernandes, A, *et al.* (2013). Patterns of mitochondrial DNA damage in blood and brain tissues of a transgenic mouse model of Machado-Joseph disease. *Neuro-degenerative diseases* **11**: 206-214.

51. Sen, NE, Drost, J, Gispert, S, Torres-Odio, S, Damrath, E, Klinkenberg, M, *et al.* (2016). Search for SCA2 blood RNA biomarkers highlights Ataxin-2 as strong modifier of the mitochondrial factor PINK1 levels. *Neurobiology of disease* **96**: 115-126.

52. Forrest, CM, Mackay, GM, Stoy, N, Spiden, SL, Taylor, R, Stone, TW, *et al.* (2010). Blood levels of kynurenines, interleukin-23 and soluble human leucocyte antigen-G at different stages of Huntington's disease. *Journal of neurochemistry* **112**: 112-122.

53. Widner, B, Leblhuber, F, Walli, J, Tilz, GP, Demel, U, and Fuchs, D (1999). Degradation of tryptophan in neurodegenerative disorders. *Advances in experimental medicine and biology* **467**: 133-138.

54. Schwarcz, R, Okuno, E, White, RJ, Bird, ED, and Whetsell, WO, Jr. (1988). 3-Hydroxyanthranilate oxygenase activity is increased in the brains of Huntington disease victims. *Proceedings of the National Academy of Sciences of the United States of America* **85**: 4079-4081.

55. Pacheco, LS, da Silveira, AF, Trott, A, Houenou, LJ, Algarve, TD, Bello, C, *et al.* (2013). Association between Machado-Joseph disease and oxidative stress biomarkers. *Mutation research* **757**: 99-103.

56. Zhang, N, Li, B, Al-Ramahi, I, Cong, X, Held, JM, Kim, E, *et al.* (2012). Inhibition of lipid signaling enzyme diacylglycerol kinase epsilon attenuates mutant huntingtin toxicity. *The Journal of biological chemistry* **287**: 21204-21213.

57. Adibhatla, RM, and Hatcher, JF (2008). Altered lipid metabolism in brain injury and disorders. *Sub-cellular biochemistry* **49**: 241-268.

58. Arboleda, G, Morales, LC, Benitez, B, and Arboleda, H (2009). Regulation of ceramide-induced neuronal death: cell metabolism meets neurodegeneration. *Brain research reviews* **59**: 333-346.

59. Posse de Chaves, EI (2006). Sphingolipids in apoptosis, survival and regeneration in the nervous system. *Biochimica et biophysica acta* **1758**: 1995-2015.

60. Cutler, RG, Pedersen, WA, Camandola, S, Rothstein, JD, and Mattson, MP (2002). Evidence that accumulation of ceramides and cholesterol esters mediates oxidative stress-induced death of motor neurons in amyotrophic lateral sclerosis. *Annals of neurology* **52**: 448-457.

61. Shakkottai, VG, do Carmo Costa, M, Dell'Orco, JM, Sankaranarayanan, A, Wulff, H, and Paulson, HL (2011). Early changes in cerebellar physiology accompany motor dysfunction in the polyglutamine disease spinocerebellar ataxia type 3. *The Journal of neuroscience : the official journal of the Society for Neuroscience* **31**: 13002-13014.

62. Costa Mdo, C, Luna-Cancalon, K, Fischer, S, Ashraf, NS, Ouyang, M, Dharia, RM, *et al.* (2013). Toward RNAi therapy for the polyglutamine disease Machado-Joseph disease. *Molecular therapy : the journal of the American Society of Gene Therapy* **21**: 1898-1908.

63. Chen, X, Tang, TS, Tu, H, Nelson, O, Pook, M, Hammer, R, *et al.* (2008). Deranged calcium signaling and neurodegeneration in spinocerebellar ataxia type 3. *The Journal of neuroscience : the official journal of the Society for Neuroscience* **28**: 12713-12724.

64. Toonen, LJA, Rigo, F, van Attikum, H, and van Roon-Mom, WMC (2017). Antisense Oligonucleotide-Mediated Removal of the Polyglutamine Repeat in Spinocerebellar Ataxia Type 3 Mice. *Molecular therapy Nucleic acids* **8**: 232-242.

65. Lee, CF, and Chern, Y (2014). Adenosine receptors and Huntington's disease. *International review of neurobiology* **119**: 195-232.

66. Chou, AH, Chen, YL, Chiu, CC, Yuan, SJ, Weng, YH, Yeh, TH, *et al.* (2015). T1-11 and JMF1907 ameliorate polyglutamine-expanded ataxin-3-induced neurodegeneration, transcriptional dysregulation and ataxic symptom in the SCA3 transgenic mouse. *Neuropharmacology* **99**: 308-317.

67. Li, F, Macfarlan, T, Pittman, RN, and Chakravarti, D (2002). Ataxin-3 is a histone-binding protein with two independent transcriptional corepressor activities. *The Journal of biological chemistry* **277**: 45004-45012.

68. McCampbell, A, Taylor, JP, Taye, AA, Robitschek, J, Li, M, Walcott, J, *et al.* (2000). CREB-binding protein sequestration by expanded polyglutamine. *Human molecular genetics* **9**: 2197-2202.

69. Shimohata, M, Shimohata, T, Igarashi, S, Naruse, S, and Tsuji, S (2005). Interference of CREB-dependent transcriptional activation by expanded polyglutamine stretches--augmentation of transcriptional activation as a potential therapeutic strategy for polyglutamine diseases. *Journal of neurochemistry* **93**: 654-663.

70. Iijima-Ando, K, Wu, P, Drier, EA, Iijima, K, and Yin, JC (2005). cAMP-response element-binding protein and heat-shock protein 70 additively suppress polyglutamine-mediated toxicity in Drosophila. *Proceedings of the National Academy of Sciences of the United States of America* **102**: 10261-10266.

71. Kwok, RP, Lundblad, JR, Chrivia, JC, Richards, JP, Bachinger, HP, Brennan, RG, *et al.* (1994). Nuclear protein CBP is a coactivator for the transcription factor CREB. *Nature* **370**: 223-226.

72. Oliner, JD, Andresen, JM, Hansen, SK, Zhou, S, and Tjian, R (1996). SREBP transcriptional activity is mediated through an interaction with the CREB-binding protein. *Genes & development* **10**: 2903-2911.

73. Steffan, JS, Kazantsev, A, Spasic-Boskovic, O, Greenwald, M, Zhu, YZ, Gohler, H, *et al.* (2000). The Huntington's disease protein interacts with p53 and CREB-binding protein and represses transcription. *Proceedings of the National Academy of Sciences of the United States of America* **97**: 6763-6768.

74. Moore, LR, Rajpal, G, Dillingham, IT, Qutob, M, Blumenstein, KG, Gattis, D, *et al.* (2017). Evaluation of Antisense Oligonucleotides Targeting ATXN3 in SCA3 Mouse Models. *Molecular therapy Nucleic acids* **7**: 200-210.

75. Toonen, LJA, Rigo, F, van Attikum, H, and van Roon-Mom, WMC. Antisense Oligonucleotide-Mediated Removal of the Polyglutamine Repeat in Spinocerebellar Ataxia Type 3 Mice. *Molecular Therapy - Nucleic Acids* **8**: 232-242.

76. Schmidt, T, Landwehrmeyer, GB, Schmitt, I, Trottier, Y, Auburger, G, Laccone, F, *et al.* (1998). An isoform of ataxin-3 accumulates in the nucleus of neuronal cells in affected brain regions of SCA3 patients. *Brain pathology (Zurich, Switzerland)* **8**: 669-679.

77. Wullner, U, Reimold, M, Abele, M, Burk, K, Minnerop, M, Dohmen, BM, *et al.* (2005). Dopamine transporter positron emission tomography in spinocerebellar ataxias type 1, 2, 3, and 6. *Archives of neurology* **62**: 1280-1285.

78. Nicola, SM, Surmeier, J, and Malenka, RC (2000). Dopaminergic modulation of neuronal excitability in the striatum and nucleus accumbens. *Annual review of neuroscience* **23**: 185-215.

79. Watabe-Uchida, M, Zhu, L, Ogawa, SK, Vamanrao, A, and Uchida, N (2012). Whole-brain mapping of direct inputs to midbrain dopamine neurons. *Neuron* **74**: 858-873.

80. Andersson, M, Konradi, C, and Cenci, MA (2001). cAMP response element-binding protein is required for dopamine-dependent gene expression in the intact but not the dopamine-denervated striatum. *The Journal of neuroscience : the official journal of the Society for Neuroscience* **21**: 9930-9943.

81. Ramani, B, Panwar, B, Moore, LR, Wang, B, Huang, R, Guan, Y, *et al.* (2017). Comparison of spinocerebellar ataxia type 3 mouse models identifies early gain-of-function, cell-autonomous transcriptional changes in oligodendrocytes. *Human molecular genetics* **26**: 3362-3374.

82. Kida, E, Palminiello, S, Golabek, AA, Walus, M, Wierzba-Bobrowicz, T, Rabe, A, *et al.* (2006). Carbonic anhydrase II in the developing and adult human brain. *Journal of neuropathology and experimental neurology* **65**: 664-674.

83. Cammer, W, Zhang, H, and Tansey, FA (1995). Effects of carbonic anhydrase II (CAII) deficiency on CNS structure and function in the myelin-deficient CAII-deficient double mutant mouse. *Journal of neuroscience research* **40**: 451-457.

84. Ghandour, MS, Skoff, RP, Venta, PJ, and Tashian, RE (1989). Oligodendrocytes express a normal phenotype in carbonic anhydrase II-deficient mice. *Journal of neuroscience research* **23**: 180-190.

85. Soundarapandian, MM, Selvaraj, V, Lo, UG, Golub, MS, Feldman, DH, Pleasure, DE, *et al.* (2011). Zfp488 promotes oligodendrocyte differentiation of neural progenitor cells in adult mice after demyelination. *Scientific reports* **1**: 2.

SUPPLEMENTARY FIGURES

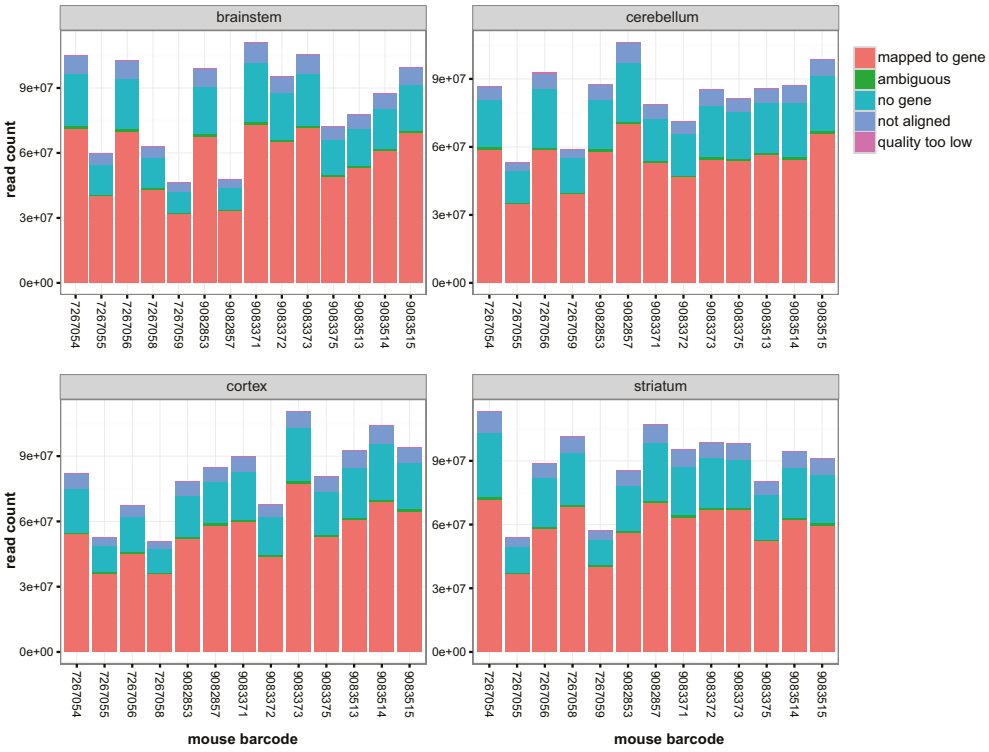

Supplementary figure 1. number of reads and alignment quality of brain RNA sequencing. Number of reads obtained for each mouse is depicted per brain region. RNA sequencing reads were aligned to mouse reference genome build 10 (GRCm38/mm10) using star aligner. Based on 8 wild-type vs 6 transgenic mice.

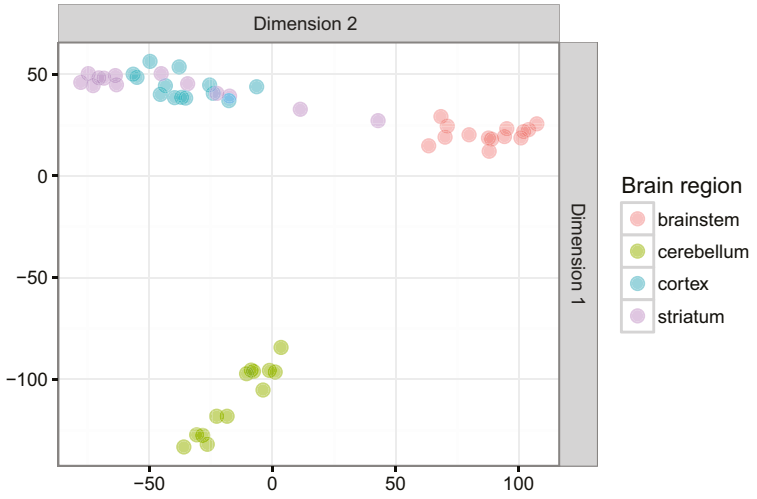

Supplementary figure 2. principal component analysis (PCA) of gene expression in brain regions. RNA sequencing based gene expression in mouse shows good clustering based on brain region. Based on 8 wild-type vs 6 transgenic mice.

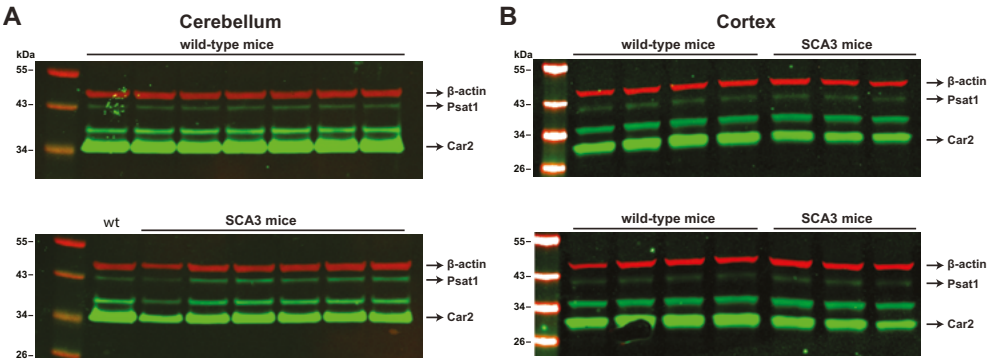

Supplementary figure 3. Protein validation of RNA sequencing results in SCA3 mouse brain. Western blot analysis of mouse brain lysates from cerebellum (**A**) and cortex (**B**) probed for Car2 and Psat1 proteins. Uncropped blots from those shown in Fig.3, showing all 8 wild-type and 6 SCA3 mice.

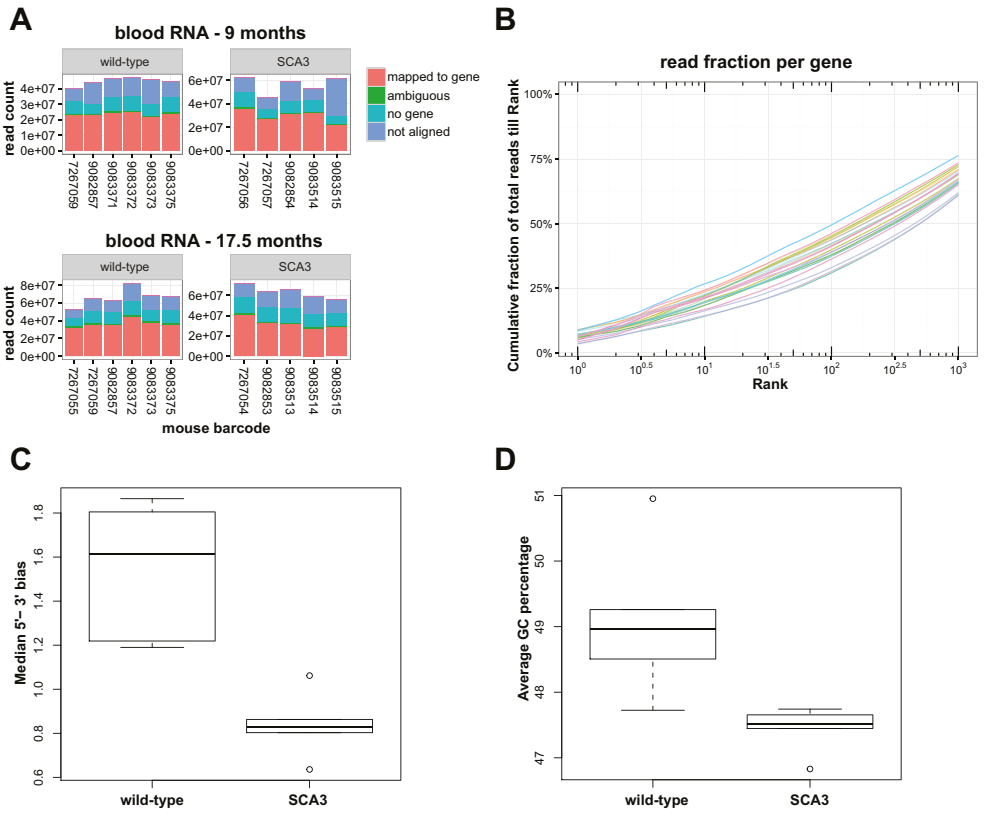

Supplementary figure 4. number of reads and quality of blood RNA sequencing. **A)** Number of reads obtained for each mouse is depicted per time point. RNA sequencing reads were aligned to mouse reference genome build 10 (GRCm38/mm10) using star aligner. **B)** Distribution of reads for blood RNA sequencing indicate that globin reduction was efficient (1st rank gene account for <10% of reads) and read distribution between samples was comparable. n = 22 **C)** Median 5'-3' bias in reads per genotype in blood at 17.5 months of age. SCA3 mice show significantly lower values ($p < 0.05$, Welch 2 sample t-test). **D)** Average GC percentage of all reads per genotype in blood at 17.5 months. Significantly lower values are seen in blood of SCA3 mice ($p < 0.05$, Welch 2 sample t-test) prior to GC-content correction.

Metabolite classes identified

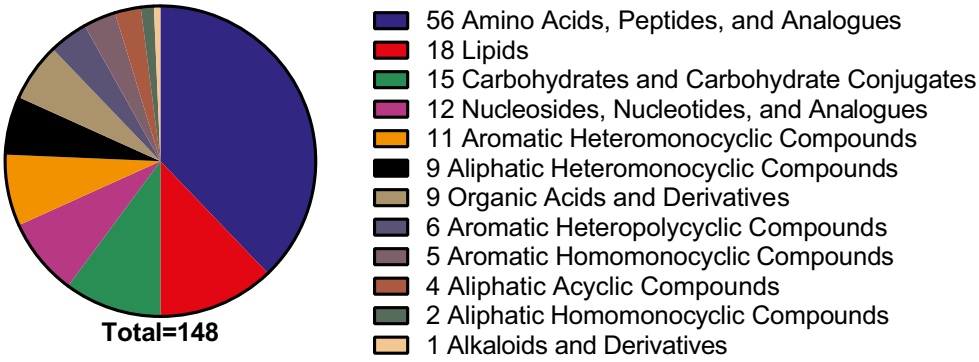

Lipid families identified

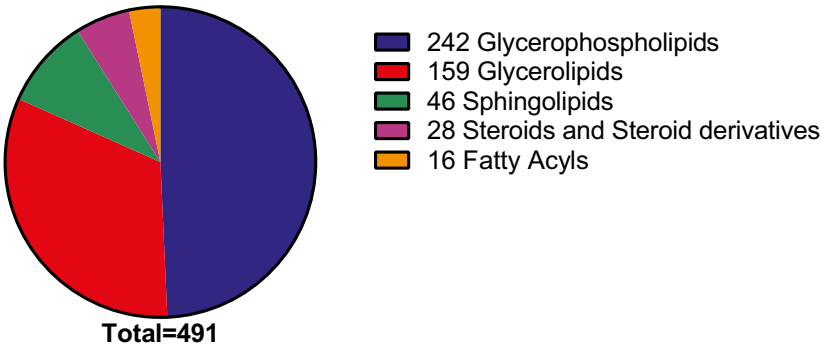

Supplementary figure 5. distribution of metabolite classes and lipid families identified from mass-spec analysis of plasma samples. LC-HRMS analysis of plasma samples led to identification of 148 unique metabolites and 491 lipids.

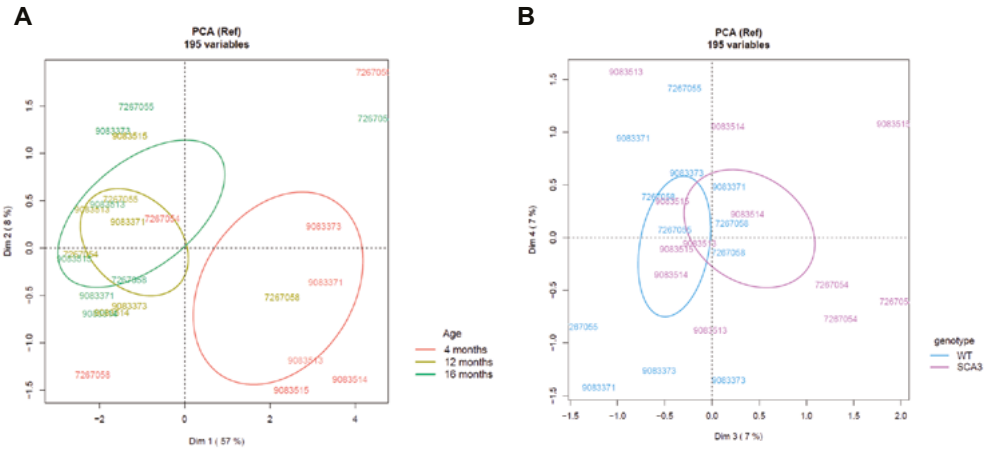

Supplementary figure 6. principal component analysis (PCA) of measured metabolites. Individual barcodes of mice are depicted, plasma was obtained for each mouse at 3 time points **A)** Age is significantly correlated with PC1 ($\rho = -0.586$, $p < 0.05$), hence explaining most of the variation between samples. SCA3 n = 4, wild-type (WT) n = 4. **B)** The third principal component (PC) is significantly correlated with genotype ($\rho = -0.463$, $p < 0.05$). PC3 and PC4 are shown.

SUPPLEMENTARY TABLES

Supplementary Table 1. Primers used for qPCR validation of RNA sequencing results

Target gene	Primer name	Application	Sequence (5′ to 3′)
Atxn3	hATXN3_int_9_fw_56FAM	repeat sizing	/56-FAM/GTAATCTGTATCAGACTAACTG CTCTTG
Atxn3	hATXN3_ex10_rev	repeat sizing	GATGTGAACTCTGTCCTGATAGGTC
Car2	mCar2_Qex3_Fw	qPCR	GCAGTGCTGAAAGGAGGACC
Car2	mCar2_Qex4_Rev	qPCR	CCCATATTTGGTGTTCCAGTGAA
Psat1	mPsat1_Qex1_Fw	qPCR	AAGCCACCAAGCAAGTGGTTA
Psat1	mPsat1_Qex2_Rev	qPCR	GATGCCGAGTCCTCTGTAGTC
Il33	mIl33_Qex2_Fw	qPCR	TCCAACTCCAAGATTTCCCCG
Il33	mIl33_Qex3_Rev	qPCR	CATGCAGTAGACATGGCAGAA
Tmc3	mTmc3_Qex4_Fw	qPCR	TCATCCCCTGGGAAATGAGGA
Tmc3	mTmc3_Qex5_Rev	qPCR	TCGGGAAGGACAACAAAGGC
Zfp488	mZfp488_Qex2_Fw	qPCR	GGCAGGGATGTTCAAGAAAATGA
Zfp488	mZfp488_Qex2_Rev	qPCR	CAGTCGAGGCTTGTTCGGT
Rnf43	mRnf43_Qex7_Fw	qPCR	CCGGGTCATTTCGTGCCTC
Rnf43	mRnf43_Qex8_Rev	qPCR	CCTGGTTCCTGGTAAGATGGAG
Pdia6	mPdia6_ex11_fw	qPCR blood	CTTCTCAAGGGGTCTTTCAGTG
Pdia6	mPdia6_ex12_rev	qPCR blood	GTGATGGTAGGAAAGGAACCAC
Rhoh	mRhoh_ex3_fw	qPCR blood	TTCACGAGTCATTCGCACAC
Rhoh	mRhoh_ex4_rev	qPCR blood	AGTAAGGAAACGGCAACCAG
Scrib	mScrib_ex9_fw	qPCR blood	AGCTGATCCTCACGGAGAAC
Scrib	mScrib_ex10_rev	qPCR blood	CAGGCGATTGTCTCTCAAAG
Atp13a2	mAtp13a2_Qex12_Fw	qPCR blood	TGACTCGGACAGGGTTCTG
Atp13a2	mAtp13a2_Qex13_Rev	qPCR blood	GCCACAAACTTCATGCTGTG
Il18r1	mIl18r1_Qex4_Fw	qPCR blood	TGAAGAGCTGATCCAGGACAC
Il18r1	mIl18r1_Qex5_Rev	qPCR blood	TCATCTCCAAACTCGGCATC
Lars2	mLars2_Qex11_Fw	qPCR blood	ATGGCACAGAGAGACTGAGTG
Lars2	mLars2_Qex12_Rev	qPCR blood	AGCCAGTCCTTCAGCTTGTTAC
Actb	mActb_Qex2_Fw	qPCR reference	GGCTGTATTCCCCTCCATCG
Actb	mActb_Qex3_Rev	qPCR reference	CCAGTTGGTAACAATGCCATGT
Hprt	m_Hprt_F	qPCR reference	TCCCTGGTTAAGCAGTACAGCC
Hprt	m_Hprt_R	qPCR reference	CGAGAGGTCCTTTTCACCAGC
Rpl22	mRpl22_ex3_fw1	qPCR reference	AGGAGTCGTGACCATCGAAC
Rpl22	mRpl22_ex3_rev1	qPCR reference	TTTGGAGAAAGGCACCTCTG
Vcl	mVcl_Qex1_Fw	qPCR reference	TGGACGGCAAAGCCATTCC
Vcl	mVcl_Qex2_Rev	qPCR reference	GCTGGTGGCATATCTCTCTTCAG

Table S2. Lipid classes altered at 4, 12 and 16 months in SCA3 mice. Only lipid classes with at least one significantly altered unique lipid at any time are shown.

		4 months		12 months		16 months		
Lipid Classes	**Total number of lipids per class**	**Number of significant lipids (p<0.05)**	**p-value***	**Number of significant lipids (p<0.05)**	**p-value***	**Number of significant lipids (p<0.05)**	**p-value***	**General trend**
Diacylglycerols (DG)	12	0	ns	0	ns	8	0.012	up
Triradylglycerols (TG)	147	0	ns	5	ns	104	0.005	up
Glycerophosphocholines (PC) - acids	68	0	ns	10	ns	6	ns	
Glycerophosphoethanolamines (PE) - acids	27	1	ns	1	ns	4	ns	
Glycerophosphoinositols (PI) - acyls	19	0	ns	4	ns	4	ns	
Glycerophosphoserines (PS) - acids	10	0	ns	3	0.046	4	0.006	down
Glycerophosphoserines (PS) - non-acids	6	0	ns	1	ns	1	ns	
Lyso-Glycerophosphocholines (LPC) - acids	29	1	ns	6	ns	2	ns	
Lyso-Glycerophosphoethanolamines (LPE) - acids	10	0	ns	1	ns	0	ns	
Lyso-Glycerophosphoinositols (LPI) - acids	3	0	ns	0	ns	0	0.045	down
Ceramides (Cer)	3	0	ns	0	ns	2	0.039	up
Hexosylceramides (HexCer)	2	1	ns	0	ns	0	ns	
Gangliosides - GM2	4	0	ns	0	ns	3	ns	
Sulfoglycosphingolipids (Su)	5	0	ns	0	ns	1	ns	
Hydroxylated Sulfoglycosphingolipids (Su-OH)	3	0	ns	1	0.041	3	0.003	down
Sphingomyelins (SM)	23	3	ns	0	ns	5	ns	
Cholesteryl Esters (Chol.Ester)	26	0	ns	1	ns	2	ns	

*p-value calculated from the sum of areas of each detected unique lipids of the same class. ns: non-significant

5

Antisense oligonucleotide-mediated removal of the polyglutamine repeat in spinocerebellar ataxia type 3 mice

Lodewijk J.A. Toonen, Frank Rigo, Haico van Attikum, Willeke M.C. van Roon-Mom (2017).
Mol Ther Nucleic Acids, 8, 232-242

ABSTRACT

Spinocerebellar ataxia type 3 (SCA3) is a currently incurable neurodegenerative disorder caused by a CAG triplet expansion in exon 10 of the *ATXN3* gene. The resultant expanded polyglutamine stretch in the mutant ataxin-3 protein causes a gain of toxic function, which eventually leads to neurodegeneration. One important function of ataxin-3 is its involvement in the proteasomal protein degradation pathway, and long-term downregulation of the protein may therefore not be desirable. In the current study, we made use of antisense oligonucleotides to mask predicted exonic splicing signals, resulting in exon 10 skipping from *ATXN3* pre-mRNA. This led to formation of a truncated ataxin-3 protein lacking the toxic polyglutamine expansion, but retaining its ubiquitin binding and cleavage function. Repeated intracerebroventricular injections of the antisense oligonucleotides in a SCA3 mouse model led to exon skipping and formation of the modified ataxin-3 protein throughout the mouse brain. Exon skipping was long lasting, with the modified protein being detectable for at least 2.5 months after antisense oligonucleotide injection. A reduction in insoluble ataxin-3 and nuclear accumulation was observed following antisense oligonucleotide treatment, indicating a beneficial effect on pathogenicity. Together, these data suggest that exon 10 skipping is a promising therapeutic approach for SCA3.

INTRODUCTION

Spinocerebellar ataxia type 3 (SCA3) is an hereditary neurodegenerative disorder characterized by ataxia, usually presenting in the third to sixth decade of life.[1] Pathoanatomical studies of SCA3 patient brains have shown neurodegeneration in the cerebellum, thalamus, midbrain, pons, medulla and spinal cord.[2] SCA3 is one of 9 known polyglutamine (polyQ) disorders. The causative mutation for polyQ disorders is a CAG codon repeat expansion in the coding region of a gene, which upon translation leads to an expanded glutamine amino acid stretch in the causative protein. It is thought that the polyQ expansion leads to a gain of toxic protein function.[3] In the case of SCA3, the CAG repeat expansion is located in exon 10 of the *ATXN3* gene, encoding the ataxin-3 protein.[4] In the normal population, an *ATXN3* CAG repeat length of 10 to 51 repeats is observed, whilst SCA3 patients have repeat lengths of 55 or longer.[5]

Ataxin-3 is a ubiquitously expressed deubiquitinating enzyme of around 42 kDa with its main function in the proteasomal protein degradation pathway.[6] Several ataxin-3 isoforms have been described[7] with the predominant ataxin-3 isoform (NM_004993) in human and mouse brain containing 3 ubiquitin interaction motifs (UIMs).[8, 9] It has been shown that the interaction between ataxin-3 and K48-linked poly-ubiquitin chains is dependent on the first two UIMs, whilst the third UIM located C-terminally of the polyQ stretch appears dispensable for this process.[10, 11] Upon binding of poly-ubiquitin chains by the UIMs, the N-terminal catalytic Josephin domain of ataxin-3 can cleave these chains. Through this process, ataxin-3 can facilitate substrate entry into the proteasome, as well as mediate other ubiquitin-dependent pathways.[11, 12]

Given the monogenetic nature, SCA3 is an ideal candidate for therapies that specifically target the *ATXN3* gene product. Indeed, several RNA interference (RNAi) strategies that downregulate ataxin-3 protein expression have been investigated over the last decade. Non-allele specific silencing of ataxin-3 was found to reduce neuropathology in a SCA3 rat model.[13] Additionally, by making use of a SNP associated with the mutant *ATXN3* allele (rs12895357), an allele specific RNAi-mediated reduction of mutant ataxin-3 decreased neuropathological abnormalities and/or motor deficits in both SCA3 rats and mice.[14-16] Antisense oligonucleotides (AONs) are another tool under investigation for therapeutic intervention in SCA3. Particularly for use in brain, AONs offer several favorable properties, including good distribution throughout the brain after infusion in the cerebrospinal fluid, excellent uptake by neurons and other brain cells, high stability with a half-life of several months, and a promising tolerability in clinical trials thus far.[17] Another advantage of using AONs is that they can also be used to redirect splicing by including or excluding specific exons.

Here we describe an AON based strategy to redirect splicing of the ataxin-3 pre-mRNA. The aim of this approach is to remove the toxic polyQ repeat from the mutant ataxin-3 protein thereby removing the cause of SCA3. Using an AON targeting exon 10 of *ATXN3* this exon is removed from the pre-mRNA, resulting in a truncated ataxin-3 protein consisting of 291 amino acids with a predicted mass of 34 kDa. Functional testing of the truncated protein lacking the polyQ domain and the third UIM showed that this modified ataxin-3 can still bind ubiquitin chains similar to wildtype ataxin-3. Finally, the AON was tested in the MJD84.2 SCA3 mouse

model using repeated bolus injection in the lateral ventricle of the brain. Remarkably, this lead to widespread distribution of the AON with ataxin-3 protein modification observed throughout the brain.

MATERIALS AND METHODS

Antisense oligonucleotides design and synthesis

Oligonucleotides targeting exon 10 (Table 1) of the human *ATXN3* transcript NM_004993 were designed according to previously described guidelines.[18, 19] AONs targeted predicted exonic splicing enhancer sites according to the Human Splicing Finder.[20] Specificity of the AONs was checked using BLAST analysis. The synthesis and purification of the oligonucleotides was performed as described previously.[21] AONs were fully modified with 2′-*O*-methoxyethylribose nucleotides and a phosphorothioate backbone. Cytosine residues were methylated to reduce immunostimulatory effects of the oligonucleotides *in vivo*.[22]

Cell culture

SCA3 fibroblast (GM06153) cell lines were obtained from Coriell Cell Repositories (Camden, USA) and maintained in Minimal Essential Medium (MEM) (Gibco, Invitrogen, Carlsbad, USA), containing 15% fetal bovine serum (FBS) (Clontech, Palo Alto, USA), 1% Glutamax (Gibco), and 100 U/ml penicillin/streptomycin (Gibco).

Human U2OS 2-6-3 cells containing 200 copies of a LacO (256 ×)/TetO (96 ×)-containing cassette of ~4Mbp,[23] were cultured in Dulbecco's Modified Eagle's Medium (DMEM) (Gibco), supplemented with 10% FBS, 1% glutamax, and 100 U/ml penicillin/streptomycin. All cells were grown at 37°C and 5% CO_2.

Transfections

Transfections of AONs was performed as described previously.[24] Briefly, fibroblasts were re-plated the day before transfection. AONs were diluted to 200nM in MEM medium without supplements containing 0.3% lipofectamine (Life Technologies, Paisley, UK). The cells were incubated with the transfection mixture for 4 hours, after which a three times volume of normal

Table 1. ATXN3 exon 10 antisense oligonucleotides

AON name	Sequence (5′ to 3′)
10.1	GCTGTTGCTGCTTTTGCTGCTG
10.1-2	CTGTTGCTGCTTTTGCTGCT
10.2	GAACTCTGTCCTGATAGGTC
10.3	CTAGATCACTCCCAAGTGCT
10.4	ATAGGTCCCGCTGCTGCT

growth medium was added. Cells were harvested one day after transfection for RNA analysis, or 2 days after transfection for protein analysis.

Plasmid transfections were performed similar to AON transfections using 1 to 1.5 µg of plasmid DNA (per 9.6 cm^2 well) in 0.6 ml MEM with 0.6% lipofectamine. Cells were imaged for GFP or mCherry protein expression the next day using a Leica DM-5500B fluorescent microscope (Leica Microsystems, Buffalo Grove, USA) at 63x magnification as previously described.[25]

Mice and oligonucleotide injections

MJD84.2 SCA3 mice[26] were obtained from Jackson laboratories (Bar Harbor, Maine, USA), stock number 012705. All animal experiments were carried out in accordance with European Communities Council Directive 2010/63/EU and were approved by the Leiden University animal ethical committee. Animals were housed singly after surgery in individually ventilated cages with a 12 hour light/dark cycle. Food and water were available *ad libitum*. Mice were bred with wildtype C57/BL6 mice (Charles River, Saint-Germain-Nuelles, France) to obtain wildtype or hemizygous SCA3 animals. Mice were genotyped using ear clip tissue material and a Phire animal tissue direct PCR kit (ThermoFisher scientific, Waltham, MA, USA), using forward primer hAtxn3int10fw1 and reverse primer hAtxn3int10rev1 (see Table 2) targeting the human *ATXN3* transcript, and mAtxn3int10fw1 and mAtxn3int10rev1 primers targeting mouse ataxin-3 as positive control for DNA isolation. Multiplex PCR was performed following manufacturer's instructions with an annealing temperature step of 61.5°C, 20 sec of extension at 72°C and a total of 35 PCR cycles.

For AON injections, a total of 34 male mice aged 2 to 2.5 months and weighing approximately 25 grams were anesthetized using 1.5% isoflurane gas anaesthesia and mounted on a Kopf

Table 2. Primer sequences

Target gene	Primer name	Application	Sequence (5′ to 3′)
ATXN3	hATXN3_FL_rev2	cDNA synthesis	TCCTACAACCGACGCATTGT
ATXN3	hATXN3_FL_Fw1	cloning	ATGGAGTCCATCTTCCACGA
ATXN3	hATXN3_FL_Rev	cloning	CGCATTGTTCCACTTTCCCA
ATXN3	hATXN3ex4Fw1	RT-PCR	GCCTTGAAAGTTTGGGGTTT
ATXN3	hATXN3ex11Rev1	RT-PCR	ACAGCTGCCTGAAGCATGTC
ATXN3	MJD_gen_fw1	genotyping PCR	ATACTTCACTTTTGAATGTTTCAGAC
ATXN3	MJD_gen_rev1	genotyping PCR	GAATGGTGAGCAGGCCTTAC
mATXN3	mAtxn3int10fw1	genotyping PCR	GCGTTGTTTTAACAGATATTCACG
mATXN3	mAtxn3int10rev1	genotyping PCR	TGTGAATGGACAGAAAGCAAA
ATNX3	hATXN3_ΔC14_fw	mutagenesis	GAAACAAGAAGGCTCACTTGCTCAACATT GCCTGAA
ATXN3	hATXN3_ΔC14_rev	mutagenesis	TTCAGGCAATGTTGAGCAAGTGAGCCTTC TTGTTTC

stereotactic device (David Kopf instruments, Tujunga, USA). Cannulas of 26 gauge and 3mm in length (Plastics1, Anaheim, CA, USA) were implanted in the right lateral ventricle, according to the following coordinates: 0.2 mm posterior and 1.0 mm lateral to bregma, and was lowered to a depth of 2.2 mm from the skull surface. The cannulas were subsequently fixed to the skull surface using dental cement, and closed with a screw-on internal dummy cannula. AONs for *in vivo* injections were dissolved in sterile PBS without calcium or magnesium to a concentration of 50 µg/µl as determined by UV spectrometry, and filtered using a 0.22 µm spin column filter. AONs or PBS were injected intracerebroventricular (ICV) through a 28 gauge needle placed in the guide cannula at a rate of 1 µl/min using a Hamilton syringe mounted in a syringe infusion pump (Stoelting, Wood Dale, IL, USA). The first AON injection consisting of 500 µg in 10 µl was performed under anaesthesia. Two additional ICV AON injections of 250 µg in 5 µl each were performed 2 and 3 weeks after surgery in freely moving mice, resulting in a total dose of 1 mg AON per mouse. Bodyweight was recorded every week post-surgery. Mice were sacrificed 3.5 months after surgery. The left hemisphere was dissected and snap frozen in liquid nitrogen, the right hemisphere was placed in 4% paraformaldehyde and fixed overnight at 4 ˚C. The fixed tissue was placed in 30% sucrose the next day and snap frozen in isopentane on dry ice.

RNA isolation and RT-PCR

Cells were detached by trypsinization (Life Technologies) and subsequently spun down. RNA was collected from the cell pellets using the Reliaprep RNA Cell Miniprep kit (Promega, Madison, USA) according to manufacturer's instructions. RNA from mouse brain tissue was obtained from fresh frozen material by homogenisation with a bullet blender BBX24 (Next Advance, Averill Park, US) for 3 minutes on setting 8, using pink beads (Next Advance), 500 µl Trizol (Ambion, Thermo Fisher scientific), and approximately 30 mg of tissue. After 5 minutes of incubation, 100 µl of chloroform was added and samples were spun down at 10.000g for 15 min. The aqueous phase was removed and added to an equal volume of 70% ethanol. Further RNA purification was performed using the PureLink RNA mini kit (Thermo Fisher scientific) in accordance with the manufacturer's protocol and using a 15 min DNase step. RNA was eluted in 80 µl nuclease free water.

For cDNA synthesis, 500 ng of RNA was used as input for the Transcriptor First Strand cDNA Synthesis Kit (Roche, Mannheim, Germany). The cDNA synthesis reaction was performed using oligoDT primers, or a gene-specific primer in the 3′ UTR region of human *ATXN3* for 45 min at 50˚C and stopped for 5 min at 85˚C, according to manufacturer's instructions. PCR was subsequently performed using primers in *ATXN3* exon 4 and 11 (see Table 2) with 1 µl cDNA as input. The PCR reaction contained 0.25mM dNTPs, 1U Faststart Taq DNA polymerase (Roche) and 10 pmol forward and reverse primers (Eurogentec, Liège, Belgium). PCR cycling was started with 4 min initial denaturation at 95˚C, followed by a total of 36 cycles with 30 sec. of denaturation at 95˚C, 30 sec of annealing at 59˚C, and 1 min extension at 72˚C. At the end of the program a final elongation step of 7 min at 72˚C was used. PCR products were separated by electrophoresis on a 1.5% agarose gel containing 0.002% ethidium bromide. Bands of skipped

products were excised from the gel, purified using a DNA extraction kit (Machery Nagel, Düren, Germany) according to manufacturer's instructions and the sequence was obtained by Sanger sequencing (Macrogen, Amsterdam, the Netherlands).

Protein isolation and western blotting

Protein from transfected cells was isolated by trypsinization and centrifugation of cells, after which the pellet was dissolved in Radioimmunoprecipitation assay (RIPA) buffer. Protein from ~30 mg mouse brain tissue was isolated by homogenisation with a bullet blender BBX24 for 3 min at intensity 8, in 500 µl RIPA buffer with 0.5 mm glass beads. Next, protein lysates were incubated in a head-over-head rotor at 4°C for 30 min. Protein concentration was determined using the bicinchoninic acid kit (Thermo Fisher Scientific), with bovine serum albumin as a standard. Protein samples were separated using 10% sodium dodecyl sulfate polyacrylamide gel electrophoresis (SDS-PAGE) with Laemmli sample buffer after boiling for 5 min at 100˚C. Proteins were blotted onto a nitrocellulose membrane using the Transblot Turbo system (Bio-Rad, Hercules, USA) for 10 min at 1.3 A. Blocking of membranes was done with 5% low fat milk powder in tris buffered saline (TBS) for 1 hour at room temperature. Membranes were stained using mouse anti-ataxin-3 1H9 (Abcam, Cambridge, UK) at 1:5000 dilution and rabbit anti-tubulin (Proteintech, Rosemont, IL, USA) 1:1000 overnight at 4°C. Blots were washed and incubated for 1 hour with Odyssey secondary antibodies, goat-anti-mouse IRDye 680RD or goat-anti-rabbit IRDye 800CW (LI-COR Biosciences, Lincoln, USA) at a 1:5000 dilution. Membranes were scanned using the Odyssey infrared imaging system (LI-COR). Protein bands were quantified with the Odyssey software version 3.0 using the integrated intensity method. Percentage of protein modification was calculated based on band intensities as follows: modified ataxin-3 / (modified ataxin-3 + human ataxin-3 84Q) * 100.

Cryosectioning and immunohistochemistry

Sectioning of paraformaldehyde fixed mouse brains from four control AON and three 10.4 AON treated mice was performed using a Leica CM3050 cryostat. Sagittal sections of 25 µm thickness from the right hemisphere were immediately transferred as free floating sections to PBS containing 0.02% sodium azide at room temperature. Sections were stored at 4°C until staining. Prior to staining, sections were washed three times in PBS with 0.2% triton-X100 for 10 min and incubated with M.O.M. mouse IgG blocking reagent (Vector Laboratories, Burlingame, USA) for 1 hour. Sections were washed and incubated overnight at 4 ˚C with primary antibodies diluted in M.O.M. protein concentrate diluent (Vector Laboratories). Primary antibodies used were: mouse anti-ataxin-3 1H9 1:1000 (Abcam, Cambridge, UK) and rabbit anti-tyrosine hydroxylase 1:500 (Santa Cruz biotechnology, Dallas, USA). For assessment of AON distribution, a rabbit antibody binding the phosphorothioate backbone of AONs was used at 1:10.000 diluted in 1% normal goat serum. After washing, sections were incubated with secondary antibodies, goat anti-mouse-alexa Fluor 594 or goat anti-rabbit-alexa Fluor 488 (Life technologies, Paisley, UK) at 1:500 dilution. Sections were mounted on superfrost plus coated

microscope slides (Fisher Emergo, Landsmeer, Netherlands), coverslipped using EverBrite hardset mounting medium containing DAPI (Biotium, Hayward, USA) and cured overnight prior to fluorescent microscopic examination using a Leica DM-5500 using 63x magnification for assessment of ubiquitin binding or Keyence Biorevo BZ-9000 fluorescent microscope for all other analyses at 10x magnification.

Image analysis of ataxin-3 nuclear intensity

Fluorescent images of substantia nigra were analysed using ImageJ (version 1.48).[27] Images were converted to 8 bit and the substantia nigra was automatically selected using a region of interest based on positive tyrosine hydroxylase green fluorescence (threshold 25-254). Within this region, ataxin-3 nuclear staining was determined using the analyse particles function (circularity 0.15-1.00) based on red fluorescent staining (threshold 35-254). Background fluorescence (intensity 35) was subtracted and the average fluorescence intensity per cell was subsequently used to represent intensity of nuclear ataxin-3. Identical analysis values were used to analyse all images. Between 400 and 1300 individual cells were assessed for 10.4 and control AON treated mice.

Dot-blot filter retardation assay

To detect aggregated ataxin-3 protein, mouse brain lysates in RIPA buffer were diluted in PBS to a final concentration of 0.15 µg/µl with 0.025% SDS. A total volume of 200 µl lysate was then passed through a cellulose acetate membrane of 0.2 µm (Whatman, Maidstone, UK) mounted in a 96-well vacuum manifold. Three additional washes were performed using PBS to remove unbound protein. The membrane was blocked using 5% non-fat milk and subsequently stained for 3 hours with mouse anti-ataxin-3 1H9 1:5000 (Abcam), and 1 hour with goat-anti-mouse IRDye 800CW 1:10.000 (LI-COR). Dots were quantified with the Odyssey software version 3.0 using the integrated intensity method.

Plasmids and mutations

Plasmids for transfection were obtained as previously described.[25] In short, PCR products for cloning were generated with primers flanking the full length *ATXN3* transcript (see Table 2) using AON transfected fibroblast cDNA as template. Full length or exon 10 skipped products were gel extracted, purified and ligated in the pGEM-T Easy vector (Promega) using the 5´-A overhangs. Mutations of the UIMs and deletion of cysteine 14 was generated using the QuickChange II Site Directed Mutagenesis kit (Agilent Technologies, Waldbronn, Germany) as described previously using primers containing the mutation (Table 2).[24] Expanded ataxin-3 with 71Q was obtained by genesynthesis (Genscript, Piscataway, USA), a mixture of CAG and CAA codons was generated to improve stability during the cloning process. Constructs were then subcloned into the PacGFP-C1 vector (Clontech, Mountain View, USA) using notI digestion, resulting in an N-terminally GFP tagged ataxin-3 protein expression. The mCherry-LacR-RNF8 construct has been described previously.[28] Purified ataxin-3 proteins were produced using the Pet28a vector (Merck Millipore, Billerica, USA) and BL21 *E.coli* (New England BioLabs, Ipswich, USA) as previously described.[25] All constructs were verified using Sanger sequencing.

Assessment of ubiquitin binding through RNF8 chromatin tethering

Ubiquitin binding assays were performed as previously described.[25] Briefly, human U2OS 2-6-3 cells with LacO repeats integrated in the genome[23] were grown on glass cover slips. Cells were transfected with both mCherry-LacR-RNF8[28] and GFP-ataxin-3 constructs. The cells were fixed in 4% paraformaldehyde the following day and glass slides were mounted on microscope slides with Everbrite mounting medium containing DAPI (Biotium, Corporate Place Hayward, US). Images were obtained for a minimum of 50 cells (2 replicate transfections) positive for both RNF8 and ataxin-3 fluorescent signals. Due to the LacR fusion, the RNF8 protein construct localises to the lacO repeat, resulting in local chromatin ubiquitination. Subsequently, ataxin-3 proteins localise to the ubiquitinated chromatin through their UIMs, resulting in colocalisation with the mCherry-RNF8. The GFP intensity, thus representing ubiquitin binding was quantified. By drawing a line region of interest across the mCherry-LacR-RNF8-marked array, the increase in GFP-ataxin-3 at the array was determined using the LAS AF Lite software (Leica Microsystems). The signal was background corrected by subtracting background GFP signal from the peak GFP intensity at the array.

Deubiquitination assay

The *in vitro* deubiquitination assay was performed as previously described.[29]

1.2 µg HIS-ataxin-3 proteins were incubated with 0.5 µg K63 linked hexa-ubiquitin chains (Boston Biochem, Cambridge, USA) in buffer containing 50 mM HEPES pH 8, 0.5 mM EDTA and 1 mM DTT. Incubations were performed for 16h at 37 ˚C. Reactions were stopped with 4x Laemmli sample buffer containing β-mercaptoethanol and by boiling the sample at 100 ˚C for 5 minutes. Samples were run on SDS-PAGE using 10% TGX gels (Biorad, Hercules, USA). After Western blotting, membranes were probed with anti-ataxin-3 1H9 (1:5000) and anti-ubiquitin 1:1000 (UG9511) (Enzo life sciences, Farmingdale, USA).

Statistical analyses

The percentage of ataxin-3 protein modification, filtertrap assay dot intensity, and ataxin-3 ubiquitin binding assays were analysed with one-way ANOVA using Tukey's posthoc multiple comparisons test. Raw intensity values obtained from Oyssey application software 'integrated intensity quantification' method were used for analyses of filtertrap assays and western blots. Western blot protein modification is reported as percentage modified ataxin-3 of the sum of all human ataxin-3 bands. Intensity of nuclear ataxin-3 accumulation in substantia nigra was compared using unpaired student t-test. Statistical analyses were performed using GraphPad Prism software version 6.02. P values < 0.05 were considered statistically significant.

RESULTS

Exon 10 skip leads to a truncated ataxin-3 protein lacking the polyQ repeat

Removal of exon 10 from the ataxin-3 pre-mRNA results in a stop codon right at the start of exon 11. As a consequence, the resulting ataxin-3 protein is truncated to amino acid 291 (Fig. 1A) and lacks the C-terminal region that contains the toxic polyQ repeat, as well as UIM 3. A total of five splice modulating AONs were designed targeting exon 10 (table 1) and were transfected in SCA3 patient-derived fibroblasts. RT-PCR and western blot analysis showed that three of the tested AONs induced exon 10 skipping as both expression of a shorter ataxin-3 transcript (Δ exon 10) and truncated protein (Δ C-terminus) were observed (Fig. 1B and C). Although AON 10.4 contained a SNP (rs12895357) associated with the expanded allele,[30, 31] we always observed modification of both wild type and mutant alleles.

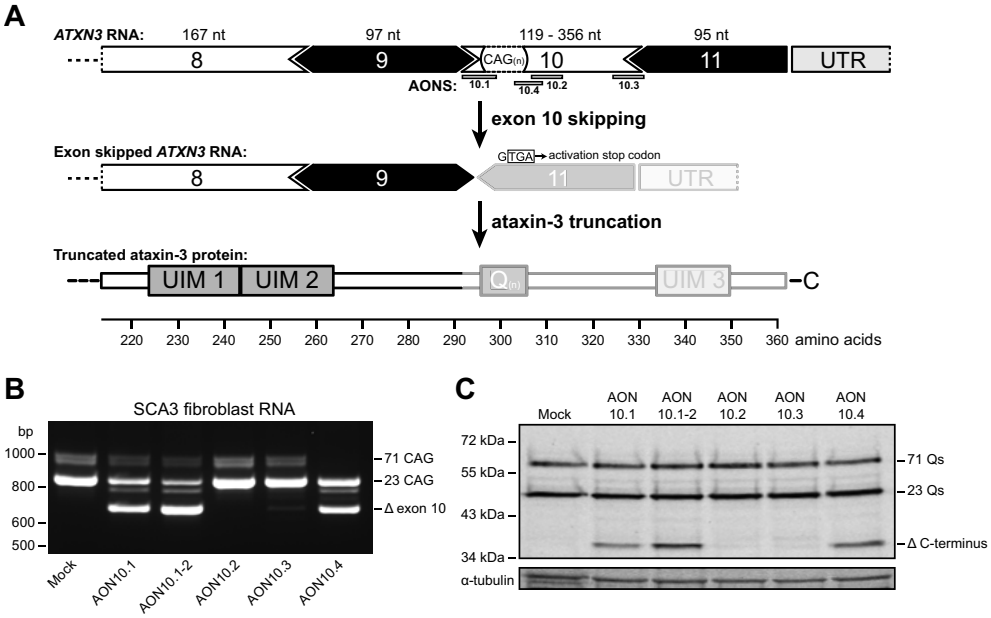

Figure 1. Antisense oligonucleotide mediated removal of the polyglutamine repeat from the ataxin-3 protein. (**A**) Schematic representation of the experimental approach to remove exon 10 from the ataxin-3 mRNA approach based on transcript ENST00000558190 (361 amino acids) using antisense oligonucleotides (AONs) targeting predicted splicing motifs within exon 10. Skipping of exon 10 leads to a novel stop codon at the start of exon 11. The resulting ataxin-3 protein contains 291 amino acids and lacks the polyQ repeat and C-terminus (depicted as transparent region). Five different AONs against exon 10 were tested for functionality by transfection in SCA3 patient derived fibroblasts. An internally truncated ataxin-3 RNA lacking the CAG repeat (Δ exon 10) (in (**B**)) and a truncated ataxin-3 protein lacking the polyQ-containing C-terminus (Δ C-terminus) (in (**C**)) were detected. Nt = nucleotides.

Ataxin-3 lacking polyQ binds and cleaves ubiquitin chains similar to wildtype

Due to the novel stop codon in exon 11 induced by exon 10 skipping, the ataxin-3 Δ C-terminus protein lacks the third UIM (Fig. 1A). To determine whether ataxin-3 Δ C-terminus was still capable of binding ubiquitin chains, we made use of a U2OS 2-6-3 cell line containing a large array of LacO repeats,[23] in which expression of mCherry-LacR-RNF8 fusion protein leads to localised ubiquitilation of the chromatin.[28] Ataxin-3 subsequently binds the ubiquitins as mediated by the UIMs, resulting in colocalisation between mCherry-RNF8 and GFP-ataxin-3. We have previously shown this colocalisation of ataxin-3 to the LacO array as a reliable marker for ubiquitin binding activity of ataxin-3.[25] Here, we tested several GFP-tagged ataxin-3 proteins for ubiquitin binding capacity (Fig. 2A). In line with previous observations, the ataxin-3 with either 10Q or 71Q can readily bind ubiquitin chains and hence colocalised with the ubiquitin moieties at the array (Fig. 2B-C). Ataxin-3 with all 3 UIMs inactivated by point mutations (L229A, L249A and L340A), termed UIMs L>A, colocalised with the ubiquitin conjugates to a significantly lower extent, confirming the specificity of the assay. Ataxin-3 Δ C-terminus colocalised with the ubiquitin conjugates at the array to a similar extent as wildtype ataxin-3, indicating that the ubiquitin chain binding capacity of the protein was retained despite lacking the third UIM.

To confirm the ubiquitin cleavage capacity of ataxin-3 Δ C-terminus, purified HIS-ataxin-3 proteins (Fig. 2D) were incubated with K63 linked hexa-ubiquitin chains. Similar to ataxin-3 10Q and 71Q, ataxin-3 Δ C-terminus was able to cleave ubiquitin chains as evidenced by the appearance of shorter ubiquitin fragments (penta- and tetra-ubiquitin) (Fig. 2E). In line with previous reports, deletion of a cysteine in the Josephin domain (ΔC14) abolished ataxin-3 ubiquitin protease activity.[32] Together, these results indicate that removal of the C-terminus from ataxin-3 does not interfere with ubiquitin binding and cleavage capacity.

Ataxin-3 exon skipping in mouse brain

To determine whether the ataxin-3 exon skip strategy is feasible *in vivo,* the four AONs against *ATXN3* RNA were tested in the MJD84.2 mouse model.[26] The MJD84.2 mouse contains the full human *ATXN3* gene with 84 CAGs including introns and flanking regions, making it a suitable SCA3 rodent model to assess human *ATXN3* splicing events *in vivo*. Sequencing analysis showed that the human *ATXN3* gene in this mouse also contains the SNP (rs12895357), and thus has full complementarity with AON 10.4 (data not shown). To assess AON efficacy, the AONs targeting exon 10 were injected as a single 500 μg ICV bolus in anesthetized hemizygous MJD84.2 mice. Two weeks after the injection, exon skipping was analysed in cortex and cerebellum (Fig. 3A). AON efficacy in both brain regions was similar to that observed in SCA3 fibroblasts transfections, with AON 10.4 being most efficient. Sanger sequencing confirmed that the shorter *ATXN3* RNA was the result of exon 10 skipping in the human transcript. In line with the transcript modification, a modified Δ C-terminus ataxin-3 protein of approximately 36 kDa in size was observed in the treated animals (Fig. 3B). Protein modification appeared more efficient in cortex than cerebellum. In the untreated animals, an ataxin-3 protein of similar size as Δ C-terminus

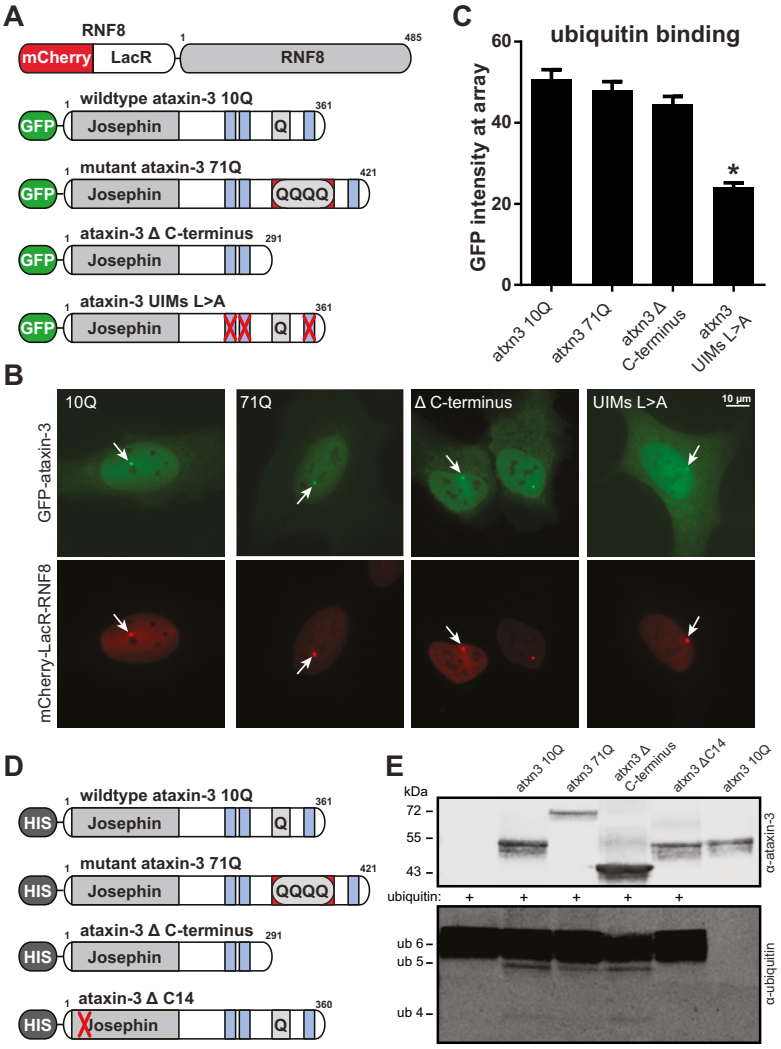

Figure 2. Ataxin-3 Δ C-terminus is capable of binding and cleaving ubiquitin chains. (**A**) Schematic representation of mCherry and GFP fusion proteins with their functional domains. The ubiquitin ligase RNF8 was fused to mCherry and LacR. Atatxin-3 was fused to GFP. Ubiquitin-interacting motifs (UIMs) of ataxin-3 are depicted in blue. Inactivating substitution mutations are indicated by red crosses (**B**) Tethering of the mCherry-LacR-RNF8 fusion protein to a LacO array in the chromatin in U2OS 2-6-3 cells (red signal) results in local chromatin ubiquitylation at the LacO array.[28] GFP-ataxin-3 proteins bind the RNF8-induced ubiquitin moieties at the the lacO array, thereby colocalizing with mCherry-LacR-RNF8 (green).[25] Representative images are shown. Arrows indicate the chromatin localised RNF8 and ataxin-3 where GFP intensity was quantified. (**C**) Quantification of increase in GFP-tagged ataxin-3 signal at the array after co-expression with mCherry-LacR-RNF8. Values represent the mean +SEM of >40 cells examined from two independent experiments. (**D**) Schematic representation of HIS-tagged ataxin-3 proteins used in ubiquitin cleavage reaction. The C14 deletion (ΔC14) is known to inactivate catalytic activity. (**E**) Purified HIS-ataxin-3 proteins were incubated for 16h with K63-linked hexa-ubiquitin to determine ubiquitin cleavage activity.

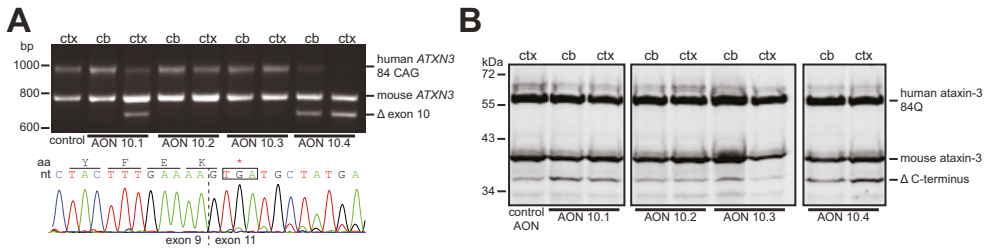

Figure 3. AON screening *in vivo*. 500µg AON was injected intracerebroventricularly in MJD84.2 mice. After 2 weeks, mice were sacrificed and RNA and protein was isolated from cortex and cerebellum. **(A)** RT-PCR using primers flanking *ATXN3* exon 10 shows the full length human ataxin-3 PCR product with 84 CAG repeats, the mouse ataxin-3 with 6 CAG repeats as well as the shorter ataxin-3 lacking exon 10 after injection of AON 10.1 and 10.4 (Δ exon 10). Sanger sequencing trace of Δ exon 10 RNA is shown below with corresponding reading frame. **(B)** Western blotting shows the full length human ataxin-3 protein with 84 Q repeats, the mouse ataxin-3 protein with 6 Qs and the truncated ataxin-3 protein lacking the C-terminus. Of the 4 AONs tested, AON 10.1 and 10.4 show the most efficient modification of the human ataxin-3 protein (Δ C-terminus). Ctx = cortex, cb = cerebellum.

ataxin-3 was observed as well, perhaps indicating the truncated ataxin-3 protein is a naturally occurring isoform or cleavage fragment in these mice.

AON effect lasts at least 2.5 months in mouse brain

Despite relatively high expression of mutant ataxin-3 throughout the brain, hemizygous MJD84.2 mice do not develop an ataxic phenotype on beamwalk tests,[33] but do develop a neuronal phenotype consisting of nuclear localisation of mutant human ataxin-3 in certain neuronal populations from around 2 months of age.[33, 34] To assess long term efficacy of AONs in the mouse brain and the effect on the neuronal phenotype, a total of 27 mice were treated with either PBS, scrambled control AON or AON 10.4 and sacrificed 2.5 months after the last injection. With repeated injections, a total ICV dose of 1 mg AON was achieved over a 3 week period (Fig. 4A). There was a clear dose dependent effect on protein modification, with a 500 µg dose resulting in 17% protein modification in cortex, and 1 mg AON resulting in 37% protein modification (supplementary Fig. 1). At the time of sacrifice, *ATXN3* exon 10 skipping was seen at RNA level in all tested brain regions (Fig. 4B and supplementary Fig. 2A), 40% ataxin-3 modification was seen in protein lysates from brainstem and cortex, while 20% ataxin-3 modification was seen in cerebellum (Fig. 4C-D and supplementary Fig. 2B). This indicates that the AONs have distributed throughout the brain, and are stable and effective for at least 2.5 months post injection. No deleterious effect of the AON on bodyweight or motor behaviour (supplementary Fig. 3) was observed during the course of the study.

AON treatment reduces insoluble ataxin-3 and prevents nuclear accumulation

Protein aggregation is considered a hallmark of polyQ disorders. It has been implicated as a pathogenic mechanism for these diseases[35, 36] and mutant ataxin-3 aggregates are found

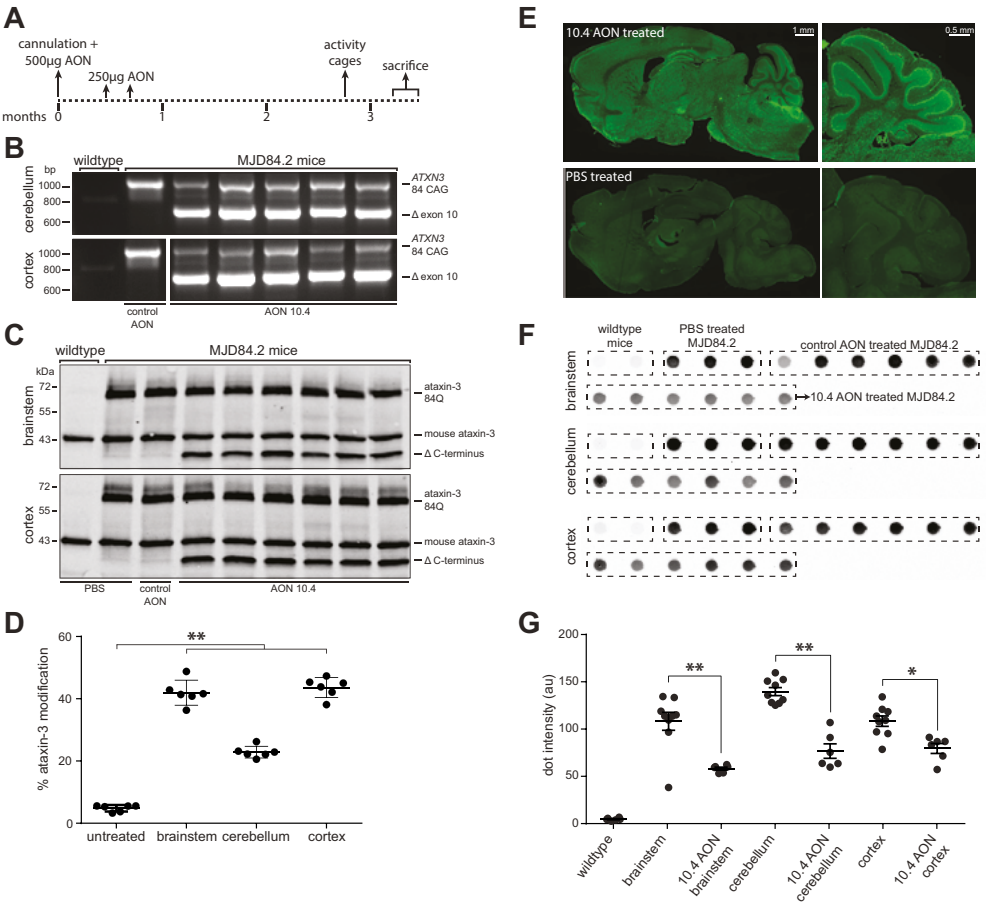

Figure 4. *in vivo* assesment of AON mediated removal of the ataxin-3 polyglutamine repeat in MJD84.2 mice. **(A)** Schematic representation of experimental design. At ~2.5 months of age (timepoint 0), mice were cannulated and 500 µg of AON 10.4 was injected ICV. Additional 250 µg injections were performed at week 3 and 4 resulting in a total dose of 1 mg. Mice were sacrificed after 3.5 months. n = 6 per group **(B)** RT-PCR specific for human *ATXN3* with primers flanking exon 10 shows full-length mutant ataxin-3 and ataxin-3 lacking exon 10 (Δ exon 10) in treated mice. **(C)** Modified ataxin-3 protein was seen for AON treated transgenic mice in all tested brain regions: brainstem and cortex are shown. Each lane represents one mouse. **(D)** Quantification of band intensity from C shows up to 40% ataxin-3 modification. Reported is modified ataxin-3 percentage of the sum of mutant and modified ataxin-3 band intensities. (E) Staining with an antibody against the phosphorothioate backbone shows that AONs are located throughout the entire mouse brain following ICV infusion. Upper panel shows a mouse sacrificed three months after injection with AON 10.4, lower panel depicts PBS injected mouse. Higher magnification of the cerebellum shows good AON uptake in the Purkinje cells. **(F)** Filter retardation assay indicates that mice carrying the transgene show insoluble ataxin-3 in all tested brain regions when stained with 1H9 anti-ataxin-3 antibody. A reduction in insoluble ataxin-3 is seen in AON 10.4 treated animals compared to PBS and control AON treated animals. **(G)** Quantification of dot intensity from F reveals significant reduction in filter trapped insoluble ataxin-3 protein in AON 10.4 treated mice. * $p < 0.05$ ** $p < 0.01$

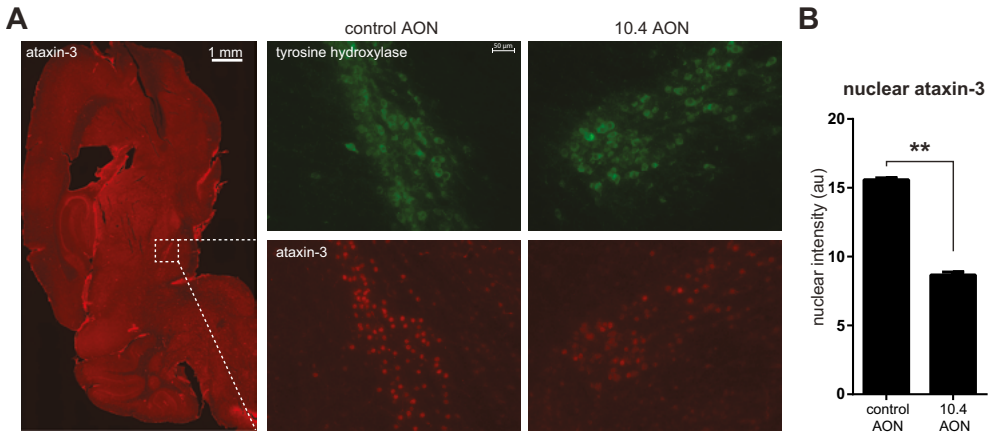

Figure 5. AON treatment reduces nuclear ataxin-3 accumulation in substantia nigra of SCA3 mice. (A) The nuclear accumulation of ataxin-3 was determined by staining with the 1H9 monoclonal antibody. Only cells of the substantia nigra expressing tyrosine hydroxylase were used in this analysis, as these showed the most intense nuclear ataxin-3 signal. **(B)** Quantification of staining intensity revealed that transgenic mice treated with 10.4 AON showed a decrease in nuclear ataxin-3 accumulation, likely due to the reduction in full length mutant ataxin-3 levels. Analysis performed on four control AON vs three 10.4 AON treated mice and four sections per mouse. Mean + SEM, evaluated with student t-test, ** $p < 0.01$

in the brain of SCA3 patients.[37] Using protein lysates from three different brain regions, we performed filter trap assays[38] to detect the level of insoluble ataxin-3 proteins (Fig. 4F). Insoluble ataxin-3 protein was detected in the transgenic MJD84.2 mice expressing mutant ataxin-3, but not in wildtype mice. The highest level of insoluble ataxin-3 was detected in the cerebellum. No significant difference in ataxin-3 insolubility was observed between scrambled AON and PBS treated SCA3 animals. Following AON 10.4 treatment, there was significantly less insoluble ataxin-3 detected compared to animals treated with scrambled AON or PBS (Fig. 4G).

To further assess the effect of AON treatment on expanded ataxin-3 pathogenicity, we performed immunofluorescent examination of SCA3 mouse brains in mice that were ~5.5 months of age at time of sacrifice. We observed strong nuclear ataxin-3 staining throughout the brainstem but specifically in the substantia nigra. Nuclear accumulation of expanded ataxin-3 has been shown to aggravate neurodegeneration and formation of aggregates *in vivo,*[39] and is therefore a useful marker to assess ataxin-3 toxicity. In fact, nuclear localisation of ataxin-3 appears to be required to induce symptoms of SCA3.[39] In the MJD84.2 mouse model, we observed strong nuclear localisation of ataxin-3 in the substantia nigra. Therefore, we used tyrosine hydroxylase staining to delineate the substantia nigra in sagittal brain sections (Fig. 5A). The intensity of ataxin-3 nuclear localisation in the substantia nigra was markedly reduced in mice treated with 10.4 AON when compared to animals treated with control AON (Fig. 5B).

DISCUSSION

In this work we describe an AON mediated exon skipping strategy for SCA3. Our therapeutic approach removes the polyQ repeat from the protein and therefore removes the cause of SCA3. This approach is superior to current treatments that only treat symptoms and not the cause of disease. It may also have some specific advantages over strategies that aim to lower expression of the ataxin-3 protein, since ataxin-3 has important cellular functions[40] in regulating protein degradation,[32] transcription[41] and DNA damage response.[29] Though ataxin-3 knockout appears tolerated in mice without major deficits,[42-44] it is currently unknown whether long-term downregulation will be tolerated in patients. Therefore, it is more prudent to avoid complete ataxin-3 downregulation. We provide evidence that repeated ICV injections of AONs in a transgenic SCA3 mouse model leads to substantial ataxin-3 RNA and protein modification (ataxin-3 Δ C-terminus) throughout the mouse brain, and is able to alleviate ataxin-3 nuclear accumulation and insolubility.

Ataxin-3 Δ C-terminus still contains the main known functional domains, namely the catalytic Josephin domain (aa 1-180) and the VCP interacting motif (aa 257–291).[45] The Josephin domain is required for ataxin-3 deubiquitinating activity,[46] in conjunction with UIM1 and 2 coordinating specific ubiquitin chain cleavage.[11, 12] The UIMs are required for the ubiquin binding capacity of ataxin-3, but the third UIM is not considered essential for this process.[10, 11, 24, 47] The current study confirms this by showing wildtype ubiquitin binding capacity of Δ C-terminus ataxin-3 in a cellular context (Fig. 2B-C). Previous experiments have shown that removing the C-terminus form ataxin-3 does not impair its de-ubiquitinating activity.[48] Our results are in line with these previous studies and show that ataxin-3 Δ C-terminus is capable of cleaving ubiquitin chains (Fig. 2E).

Ataxin-3 interaction with VCP is thought to be crucial for the activation of ataxin-3 and regulating the endoplasmic reticulum-associated degradation pathway through protein extraction from the endoplasmic reticulum.[49, 50] Ataxin-3 Δ C-terminus still contains the VCP binding motif. [45] Retainment of the VCP binding site in ataxin-3 Δ C-terminus may be of particular importance, as a mouse model expressing only the ataxin-3 N-terminus up to amino acid 259 resulted in extranuclear neuronal aggregates and premature death at 12 months of age.[51] This phenotype was associated with disturbances of endoplasmic reticulum-mediated unfolded protein response, possibly indicating the importance of ataxin-3 and VCP interaction in maintaining endoplasmic reticulum homeostasis.

A recent study by Liu and colleagues testing several different oligonucleotide chemistries found that *ATXN3* exon 10 could be skipped with CAG targeting oligonucleotides and the ataxin-3 Δ C-terminus protein was also observed in these experiments.[52] Both mutant and wildtype ataxin-3 alleles will be targeted by the AON, as the AON is complementary to the canonical exon 10 sequence. Indeed, we observed a similar level of exon skipping for the mutant and wildtype allele in SCA3 patient derived fibroblasts (Fig.1B and C). This observation underlines the importance of determining protein function of ataxin-3 Δ C-terminus in a neuronal context,

as the proposed AON treatment may lead to high protein modification levels throughout the brain.

Apart from retaining wild-type ataxin-3 function, an important concern is that the ataxin-3 Δ C-terminus protein should not result in a gain of toxic function. An ataxin-3 protein variant corresponding exactly to the Δ C-terminus protein resulting from exon 10 skipping has been tested in a yeast model and rat cerebellar granule cells, where it was shown that this protein indeed did not aggregate, but in some tests showed a mild increase in toxicity compared to the wildtype ataxin-3 protein.[53, 54] Whether these results can be extrapolated to the *in vivo* situation will have to be determined, but we did not observe overt signs of toxicity in the AON 10.4 treated mice expressing ataxin-3 Δ C-terminus based on bodyweight and locomotor activity (supplementary Fig. 3A and B). Additionally, no increase in cell death was observed in fibroblasts treated with AON 10.4 (Fig. 1C), or U2OS cells transfected with GFP- ataxin-3 Δ C-terminus (Fig. 2B), indicating that ataxin-3 Δ C-terminus is not toxic to these cells. Interestingly, a study investigating the transcript diversity of ataxin-3 in humans found two naturally occurring ataxin-3 isoforms generated by a stop codon after exon 9. Indeed, we observed an ataxin-3 protein of similar size to our Δ C-terminus protein in untreated SCA3 animals (Fig. 3B), perhaps indicating that this protein is also expressed in the transgenic mouse brain. If ataxin-3 Δ C-terminus is indeed a naturally occurring isoform, this may suggest that the protein is likely not a toxic variant. To more comprehensively test whether ataxin-3 Δ C-terminus is fully functional and not toxic to cells, it will be useful to express ataxin-3 Δ C-terminus in ataxin-3 knockout mice in future studies.

The current study used the MJD84.2 mouse model.[26] This mouse model contains the full human *ATXN3* gene, including flanking regions and introns which is essential when testing splice modulating AONs. Indeed, similar potency of the exon 10 targeting AONs were found when comparing patient derived fibroblast results with the *in vivo* ICV injections. Repeated bolus injections of AON 10.4 were tolerated and led to increased levels of ataxin-3 protein modification. No significant reduction in the level of soluble mutant ataxin-3 with western blot analysis (Fig. 4C), however a reduction in the amount of insoluble ataxin-3 was observed in the filtertrap assay (Fig. 4F).

We did not consistently observe strong nuclear accumulation of ataxin-3 in the deep cerebellar nuclei as previously reported in the MJD84.2 mice.[34] Though we were not able to detect clear aggregates in any brain regions, ataxin-3 nuclear localisation was readily seen in the substantia nigra, in line with previous reports.[55] The molecular SCA3 phenotype of the mice was beneficially effected by AON treatment, with a reduction of insoluble ataxin-3 species observed in filtertrap assays, and less nuclear ataxin-3 accumulation in the substantia nigra. The AONs were functionally active for at least 2.5 months, in line with previous studies using similar AON chemistries in spinal muscular atrophy mice reporting effects lasting for over 6 months after ICV injection.[56]

Clinical application of AONs currently seem promising. In clinical trials, intrathecal injection of MOE modified AONs in children with spinal muscular atrophy have shown AON half-lives in the CSF of 4-6 months, with good tolerability and improvement in patients motor

function.[57] This suggests that relatively infrequent dosing, such as intrathecal AON injections every 6 months, could be a feasible treatment regimen for SCA3. The removal of the polyQ repeat from ataxin-3 is likely to delay disease progression and restrict brain damage. In case of high efficacy of the treatment it could even stop disease progression completely. Since the mouse model used here does not present with ataxic symptoms, we were unable to assess an effect of our AON treatment on reversal of the motor phenotype. However, studies in mice where expression of mutant ataxin-3 was halted during early stage disease have shown that a reversal of the motor symptoms was possible.[58] A similar observation has been made when polyQ expanded Huntingtin protein was downregulated using AONs in a Huntington's disease mouse model.[59] This is a promising observation, but whether the same could be possible in humans is currently unknown. Because of the autosomal dominant nature of SCA3, patients can start therapy before onset of clinical symptoms, improving likelihood of a beneficial effect.

AUTHOR CONTRIBUTIONS

Research conception and experiment design by: W.M.C.vR-M, L.J.A.T., F.R. and H.v.A. Experiments performed and manuscript written by L.J.A.T. Revision to manuscript by W.M.C.vR-M, H.v.A and F.R.

ACKNOWLEDGEMENTS

The authors want to thank Maarten Schenke, Barry Pepers, Martijn Luijsterburg and Melvin Evers for advice on experimental setup and Maurice Overzier and Wouter Wiegant for practical assistance. The authors are grateful to Susan Janicki and Roger Greenberg for providing U2OS 2-6-3 cells. This work was financially supported by ZonMw 40-41900-98-018 and Hersenstichting/ Brugling Fund (BG2013-03) to W.M.C.vR-M.

REFERENCES

1. Rub, U, Schols, L, Paulson, H, Auburger, G, Kermer, P, Jen, JC, *et al.* (2013). Clinical features, neurogenetics and neuropathology of the polyglutamine spinocerebellar ataxias type 1, 2, 3, 6 and 7. *Prog Neurobiol* **104**: 38-66.
2. Riess, O, Rub, U, Pastore, A, Bauer, P, and Schols, L (2008). SCA3: neurological features, pathogenesis and animal models. *Cerebellum (London, England)* **7**: 125-137.
3. Orr, HT, and Zoghbi, HY (2007). Trinucleotide repeat disorders. *Annual review of neuroscience* **30**: 575-621.
4. Kawaguchi, Y, Okamoto, T, Taniwaki, M, Aizawa, M, Inoue, M, Katayama, S, *et al.* (1994). CAG expansions in a novel gene for Machado-Joseph disease at chromosome 14q32.1. *Nature genetics* **8**: 221-228.
5. Cummings, CJ, and Zoghbi, HY (2000). Trinucleotide repeats: mechanisms and pathophysiology. *Annual review of genomics and human genetics* **1**: 281-328.
6. Matos, CA, de Macedo-Ribeiro, S, and Carvalho, AL (2011). Polyglutamine diseases: the special case of ataxin-3 and Machado-Joseph disease. *Prog Neurobiol* **95**: 26-48.
7. Bettencourt, C, Raposo, M, Ros, R, Montiel, R, Bruges-Armas, J, and Lima, M (2013). Transcript diversity of Machado-Joseph disease gene (ATXN3) is not directly determined by SNPs in exonic or flanking intronic regions. *Journal of molecular neuroscience : MN* **49**: 539-543.
8. Harris, GM, Dodelzon, K, Gong, L, Gonzalez-Alegre, P, and Paulson, HL (2010). Splice isoforms of the polyglutamine disease protein ataxin-3 exhibit similar enzymatic yet different aggregation properties. *PloS one* **5**: e13695.
9. Schmidt, T, Landwehrmeyer, GB, Schmitt, I, Trottier, Y, Auburger, G, Laccone, F, *et al.* (1998). An isoform of ataxin-3 accumulates in the nucleus of neuronal cells in affected brain regions of SCA3 patients. *Brain pathology (Zurich, Switzerland)* **8**: 669-679.
10. Chai, Y, Berke, SS, Cohen, RE, and Paulson, HL (2004). Poly-ubiquitin binding by the polyglutamine disease protein ataxin-3 links its normal function to protein surveillance pathways. *J Biol Chem* **279**: 3605-3611.
11. Mao, Y, Senic-Matuglia, F, Di Fiore, PP, Polo, S, Hodsdon, ME, and De Camilli, P (2005). Deubiquitinating function of ataxin-3: insights from the solution structure of the Josephin domain. *Proceedings of the National Academy of Sciences of the United States of America* **102**: 12700-12705.
12. Winborn, BJ, Travis, SM, Todi, SV, Scaglione, KM, Xu, P, Williams, AJ, *et al.* (2008). The deubiquitinating enzyme ataxin-3, a polyglutamine disease protein, edits Lys63 linkages in mixed linkage ubiquitin chains. *The Journal of biological chemistry* **283**: 26436-26443.
13. Alves, S, Nascimento-Ferreira, I, Dufour, N, Hassig, R, Auregan, G, Nobrega, C, *et al.* (2010). Silencing ataxin-3 mitigates degeneration in a rat model of Machado-Joseph disease: no role for wild-type ataxin-3? *Hum Mol Genet* **19**: 2380-2394.
14. Alves, S, Nascimento-Ferreira, I, Auregan, G, Hassig, R, Dufour, N, Brouillet, E, *et al.* (2008). Allele-specific RNA silencing of mutant ataxin-3 mediates neuroprotection in a rat model of Machado-Joseph disease. *PLoS One* **3**: e3341.
15. Conceicao, M, Mendonca, L, Nobrega, C, Gomes, C, Costa, P, Hirai, H, *et al.* (2015). Intravenous administration of brain-targeted stable nucleic acid lipid particles alleviates Machado-Joseph disease neurological phenotype. *Biomaterials* **82**: 124-137.
16. Nobrega, C, Nascimento-Ferreira, I, Onofre, I, Albuquerque, D, Hirai, H, Deglon, N, *et al.* (2013). Silencing mutant ataxin-3 rescues motor deficits and neuropathology in Machado-Joseph disease transgenic mice. *PloS one* **8**: e52396.

17. Evers, MM, Toonen, LJ, and van Roon-Mom, WM (2015). Antisense oligonucleotides in therapy for neurodegenerative disorders. *Advanced drug delivery reviews* **87**: 90-103.

18. Aartsma-Rus, A (2012). Overview on AON design. *Methods Mol Biol* **867**: 117-129.

19. Aartsma-Rus, A, van Vliet, L, Hirschi, M, Janson, AA, Heemskerk, H, de Winter, CL, *et al.* (2009). Guidelines for antisense oligonucleotide design and insight into splice-modulating mechanisms. *Molecular therapy : the journal of the American Society of Gene Therapy* **17**: 548-553.

20. Desmet, FO, Hamroun, D, Lalande, M, Collod-Beroud, G, Claustres, M, and Beroud, C (2009). Human Splicing Finder: an online bioinformatics tool to predict splicing signals. *Nucleic Acids Res* **37**: e67.

21. Swayze, EE, Siwkowski, AM, Wancewicz, EV, Migawa, MT, Wyrzykiewicz, TK, Hung, G, *et al.* (2007). Antisense oligonucleotides containing locked nucleic acid improve potency but cause significant hepatotoxicity in animals. *Nucleic acids research* **35**: 687-700.

22. Bauer, S, Kirschning, CJ, Hacker, H, Redecke, V, Hausmann, S, Akira, S, *et al.* (2001). Human TLR9 confers responsiveness to bacterial DNA via species-specific CpG motif recognition. *Proceedings of the National Academy of Sciences of the United States of America* **98**: 9237-9242.

23. Janicki, SM, Tsukamoto, T, Salghetti, SE, Tansey, WP, Sachidanandam, R, Prasanth, KV, *et al.* (2004). From Silencing to Gene Expression: Real-Time Analysis in Single Cells. *Cell* **116**: 683-698.

24. Evers, MM, Tran, HD, Zalachoras, I, Pepers, BA, Meijer, OC, den Dunnen, JT, *et al.* (2013). Ataxin-3 protein modification as a treatment strategy for spinocerebellar ataxia type 3: removal of the CAG containing exon. *Neurobiology of disease* **58**: 49-56.

25. Toonen, LJ, Schmidt, I, Luijsterburg, MS, van Attikum, H, and van Roon-Mom, WM (2016). Antisense oligonucleotide-mediated exon skipping as a strategy to reduce proteolytic cleavage of ataxin-3. *Sci Rep* **6**: 35200.

26. Cemal, CK, Carroll, CJ, Lawrence, L, Lowrie, MB, Ruddle, P, Al-Mahdawi, S, *et al.* (2002). YAC transgenic mice carrying pathological alleles of the MJD1 locus exhibit a mild and slowly progressive cerebellar deficit. *Human molecular genetics* **11**: 1075-1094.

27. Schneider, CA, Rasband, WS, and Eliceiri, KW (2012). NIH Image to ImageJ: 25 years of image analysis. *Nature methods* **9**: 671-675.

28. Luijsterburg, MS, Acs, K, Ackermann, L, Wiegant, WW, Bekker-Jensen, S, Larsen, DH, *et al.* (2012). A new non-catalytic role for ubiquitin ligase RNF8 in unfolding higher-order chromatin structure. *The EMBO Journal* **31**: 2511-2527.

29. Pfeiffer, A, Luijsterburg, MS, Acs, K, Wiegant, WW, Helfricht, A, Herzog, LK, *et al.* (2017). Ataxin-3 consolidates the MDC1-dependent DNA double-strand break response by counteracting the SUMO-targeted ubiquitin ligase RNF4. *Embo j*.

30. Gaspar, C, Lopes-Cendes, I, Hayes, S, Goto, J, Arvidsson, K, Dias, A, *et al.* (2001). Ancestral origins of the Machado-Joseph disease mutation: a worldwide haplotype study. *American journal of human genetics* **68**: 523-528.

31. Michlewski, G, and Krzyzosiak, WJ (2004). Molecular architecture of CAG repeats in human disease related transcripts. *J Mol Biol* **340**: 665-679.

32. Burnett, B, Li, F, and Pittman, RN (2003). The polyglutamine neurodegenerative protein ataxin-3 binds polyubiquitylated proteins and has ubiquitin protease activity. *Human molecular genetics* **12**: 3195-3205.

33. Costa Mdo, C, Luna-Cancalon, K, Fischer, S, Ashraf, NS, Ouyang, M, Dharia, RM, *et al.* (2013). Toward RNAi therapy for the polyglutamine disease Machado-Joseph disease. *Molecular therapy : the journal of the American Society of Gene Therapy* **21**: 1898-1908.

34. Rodriguez-Lebron, E, Costa Mdo, C, Luna-Cancalon, K, Peron, TM, Fischer, S, Boudreau, RL, *et al.* (2013). Silencing mutant ATXN3 expression resolves molecular phenotypes in SCA3 transgenic mice. *Molecular therapy : the journal of the American Society of Gene Therapy* **21**: 1909-1918.

35. Chen, S, Ferrone, FA, and Wetzel, R (2002). Huntington's disease age-of-onset linked to polyglutamine aggregation nucleation. *Proceedings of the National Academy of Sciences of the United States of America* **99**: 11884-11889.

36. Holmes, WM, Klaips, CL, and Serio, TR (2014). Defining the limits: Protein aggregation and toxicity in vivo. *Critical reviews in biochemistry and molecular biology* **49**: 294-303.

37. Koch, P, Breuer, P, Peitz, M, Jungverdorben, J, Kesavan, J, Poppe, D, *et al.* (2011). Excitation-induced ataxin-3 aggregation in neurons from patients with Machado-Joseph disease. *Nature* **480**: 543-546.

38. Wanker, EE, Scherzinger, E, Heiser, V, Sittler, A, Eickhoff, H, and Lehrach, H (1999). Membrane filter assay for detection of amyloid-like polyglutamine-containing protein aggregates. *Methods in enzymology* **309**: 375-386.

39. Bichelmeier, U, Schmidt, T, Hubener, J, Boy, J, Ruttiger, L, Habig, K, *et al.* (2007). Nuclear localization of ataxin-3 is required for the manifestation of symptoms in SCA3: in vivo evidence. *The Journal of neuroscience : the official journal of the Society for Neuroscience* **27**: 7418-7428.

40. Evers, MM, Toonen, LJ, and van Roon-Mom, WM (2014). Ataxin-3 protein and RNA toxicity in spinocerebellar ataxia type 3: current insights and emerging therapeutic strategies. *Mol Neurobiol* **49**: 1513-1531.

41. Evert, BO, Araujo, J, Vieira-Saecker, AM, de Vos, RA, Harendza, S, Klockgether, T, *et al.* (2006). Ataxin-3 represses transcription via chromatin binding, interaction with histone deacetylase 3, and histone deacetylation. *The Journal of neuroscience : the official journal of the Society for Neuroscience* **26**: 11474-11486.

42. Moore, LR, Rajpal, G, Dillingham, IT, Qutob, M, Blumenstein, KG, Gattis, D, *et al.* (2017). Evaluation of Antisense Oligonucleotides Targeting ATXN3 in SCA3 Mouse Models. *Molecular therapy Nucleic acids* **7**: 200-210.

43. Schmitt, I, Linden, M, Khazneh, H, Evert, BO, Breuer, P, Klockgether, T, *et al.* (2007). Inactivation of the mouse Atxn3 (ataxin-3) gene increases protein ubiquitination. *Biochemical and biophysical research communications* **362**: 734-739.

44. Switonski, PM, Fiszer, A, Kazmierska, K, Kurpisz, M, Krzyzosiak, WJ, and Figiel, M (2011). Mouse ataxin-3 functional knock-out model. *Neuromolecular Med* **13**: 54-65.

45. Boeddrich, A, Gaumer, S, Haacke, A, Tzvetkov, N, Albrecht, M, Evert, BO, *et al.* (2006). An arginine/lysine-rich motif is crucial for VCP/p97-mediated modulation of ataxin-3 fibrillogenesis. *The EMBO journal* **25**: 1547-1558.

46. Nicastro, G, Todi, SV, Karaca, E, Bonvin, AM, Paulson, HL, and Pastore, A (2010). Understanding the role of the Josephin domain in the PolyUb binding and cleavage properties of ataxin-3. *PloS one* **5**: e12430.

47. Donaldson, KM, Li, W, Ching, KA, Batalov, S, Tsai, CC, and Joazeiro, CA (2003). Ubiquitin-mediated sequestration of normal cellular proteins into polyglutamine aggregates. *Proceedings of the National Academy of Sciences of the United States of America* **100**: 8892-8897.

48. Tzvetkov, N, and Breuer, P (2007). Josephin domain-containing proteins from a variety of species are active de-ubiquitination enzymes. *Biological chemistry* **388**: 973-978.

49. Laco, MN, Cortes, L, Travis, SM, Paulson, HL, and Rego, AC (2012). Valosin-containing protein (VCP/p97) is an activator of wild-type ataxin-3. *PloS one* **7**: e43563.

50. Zhong, X, and Pittman, RN (2006). Ataxin-3 binds VCP/p97 and regulates retrotranslocation of ERAD substrates. *Hum Mol Genet* **15**: 2409-2420.

51. Hubener, J, Vauti, F, Funke, C, Wolburg, H, Ye, Y, Schmidt, T, *et al.* (2011). N-terminal ataxin-3 causes neurological symptoms with inclusions, endoplasmic reticulum stress and ribosomal dislocation. *Brain : a journal of neurology* **134**: 1925-1942.

52. Liu, J, Yu, D, Aiba, Y, Pendergraff, H, Swayze, EE, Lima, WF, *et al.* (2013). ss-siRNAs allele selectively inhibit ataxin-3 expression: multiple mechanisms for an alternative gene silencing strategy. *Nucleic acids research* **41**: 9570-9583.

53. Bonanomi, M, Visentin, C, Invernizzi, G, Tortora, P, and Regonesi, ME (2015). The Toxic Effects of Pathogenic Ataxin-3 Variants in a Yeast Cellular Model. *PloS one* **10**: e0129727.

54. Pellistri, F, Bucciantini, M, Invernizzi, G, Gatta, E, Penco, A, Frana, AM, *et al.* (2013). Different ataxin-3 amyloid aggregates induce intracellular Ca(2+) deregulation by different mechanisms in cerebellar granule cells. *Biochimica et biophysica acta* **1833**: 3155-3165.

55. Chen, X, Tang, TS, Tu, H, Nelson, O, Pook, M, Hammer, R, *et al.* (2008). Deranged calcium signaling and neurodegeneration in spinocerebellar ataxia type 3. *The Journal of neuroscience : the official journal of the Society for Neuroscience* **28**: 12713-12724.

56. Rigo, F, Chun, SJ, Norris, DA, Hung, G, Lee, S, Matson, J, *et al.* (2014). Pharmacology of a central nervous system delivered 2'-O-methoxyethyl-modified survival of motor neuron splicing oligonucleotide in mice and nonhuman primates. *The Journal of pharmacology and experimental therapeutics* **350**: 46-55.

57. Chiriboga, CA, Swoboda, KJ, Darras, BT, Iannaccone, ST, Montes, J, De Vivo, DC, *et al.* (2016). Results from a phase 1 study of nusinersen (ISIS-SMN(Rx)) in children with spinal muscular atrophy. *Neurology* **86**: 890-897.

58. Boy, J, Schmidt, T, Wolburg, H, Mack, A, Nuber, S, Bottcher, M, *et al.* (2009). Reversibility of symptoms in a conditional mouse model of spinocerebellar ataxia type 3. *Hum Mol Genet* **18**: 4282-4295.

59. Kordasiewicz, HB, Stanek, LM, Wancewicz, EV, Mazur, C, McAlonis, MM, Pytel, KA, *et al.* (2012). Sustained therapeutic reversal of Huntington's disease by transient repression of huntingtin synthesis. *Neuron* **74**: 1031-1044.

SUPPLEMENTARY FIGURES

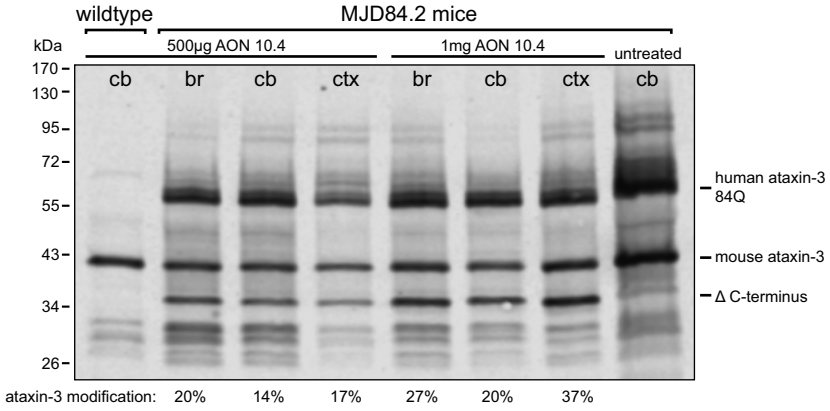

Supplementary Figure 1. Comparison of 500 µg and 1 mg AON 10.4 ICV bolus. AON 10.4 was tested *in vivo* by ICV injection in two mice to determine dose response. 500 µg AON was injected at 2.5 months of age, after which one of the mice was injected with a second 500 µg bolus 2 weeks later. Both mice were sacrificed 2 weeks after the last injection. Westernblot analysis and staining with 1H9 antibody shows ataxin-3 Δ C-terminus appearing in the three brainregions tested of the treated MJD84.2 mice. A clear increase in protein modifciation is seen with the 1 mg dose compared to the 500 µg dose. Cb = cerebellum, br = brainstem, ctx = cortex.

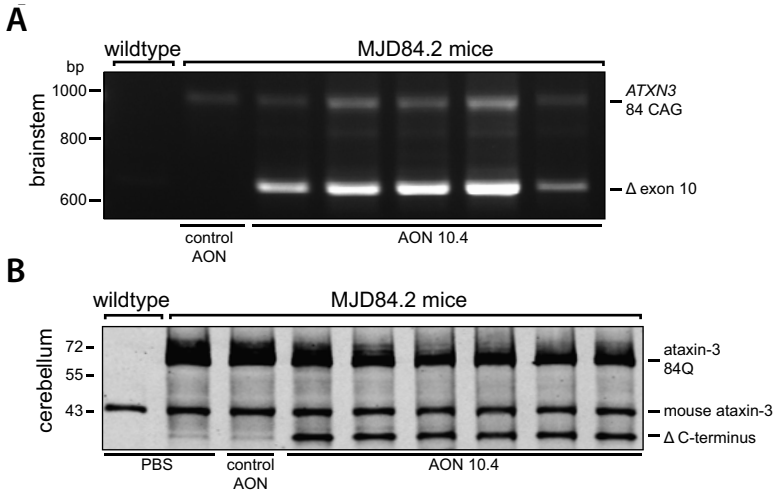

Supplementary Figure 2. In vivo assessment of exon skipping at RNA and protein level. Mice were treated with a total of 1 mg AON 10.4 or control AON, and sacrificed ~3.5 monhs after last injection. Results are obtained from mice depicted in figure 3. **(A)** RT-PCR with primers for human *ATXN3* show skipping of exon 10 in brainstem of AON 10.4 treated mice. **(B)** Modified ataxin-3 protein (Δ C-terminus) was observed in cerebellum of mice treated with AON 10.4.

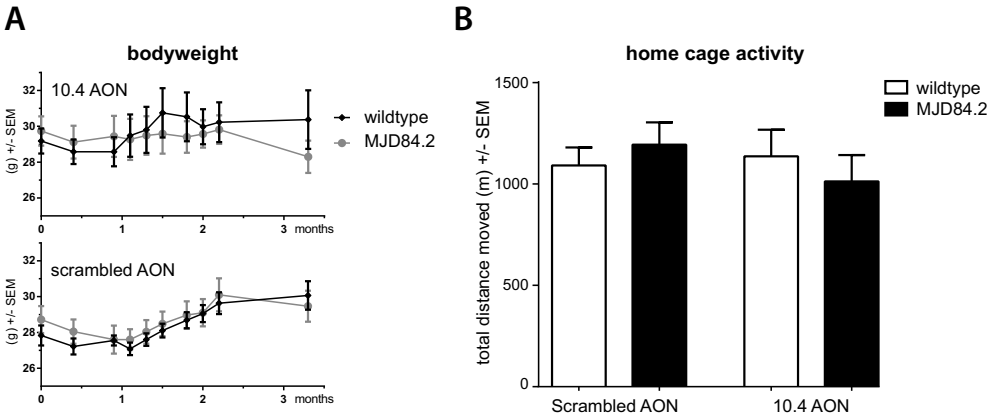

Supplementary Figure 3. MJD84.2 mouse does not present obvious ataxic phenotype at 5 months of age. (**A**) No significant difference in bodyweight between wildtype and transgenic mice was seen, or between scrambled and AON10.4 treated mice of both genotypes. (**B**) Wildtype and hemizygous MJD84.2 mice were tested for motor performance in a home cage activity system at around 5 months of age. Scrambled AON: 5 wildtype vs 5 SCA3 mice. 10.4 AON: 4 wildtype vs 6 SCA3 mice.

6

Intracerebroventricular administration of a 2-'O-methyl phosphorothioate antisense oligonucleotide results in activation of the innate immune system in mouse brain

Lodewijk J.A. Toonen*, João Casaca-Carreira*, Maria Pellisé-Tintoré, Hailiang Mei, Yasin Temel, Ali Jahanshahi#, Willeke M.C. van Roon-Mom# (2018).
***,# authors contributed equally**
Nucleic Acid Ther. doi:10.1089/nat.2017.0705

ABSTRACT

Antisense oligonucleotides (AONs) are versatile molecules that can be used to modulate gene expression by binding to RNA. The therapeutic potential of AONs appears particularly high in the central nervous system, due to excellent distribution and uptake in brain cells, as well as good tolerability in clinical trials thus far. Nonetheless, immune stimulation in response to AON treatment in the brain remains a concern. For this reason we performed RNA sequencing analysis of brain tissue from mice treated intracerebroventricularly with phosphorothioate, 2'O-methyl modified antisense oligonucleotides. A significant upregulation of immune system associated genes was observed in brains of AON treated mice, with the striatum showing largest transcriptional changes. Strongest upregulation was seen for the anti-viral enzyme 2'-5'-oligoadenylate synthase-like protein 2 (Oasl2) and Bone marrow stromal antigen 2 (Bst2). Histological analysis confirmed activation of microglia and astrocytes in striatum. The upregulation of immune system associated genes was detectable for at least two months after the last AON administration, consistent with a continuous immune response to the AON.

INTRODUCTION

Antisense oligonucleotides (AONs) are versatile molecules consisting of single strands of nucleic acids capable of binding to RNA through standard Watson-Crick interactions. AONs have been used since the 1960s [1], and a wide range of chemical modifications have been developed to tailor AONs to specific functions as well as improve their drug-like properties such as: binding energy, stability and tolerability [2]. Single-stranded AONs are mainly used for the down-regulation of target transcripts through an RNAse-H dependent mechanism, or to induce steric blocking for modulation of transcript splicing or translational inhibition [3]. Making use of these mechanisms, AONs are investigated as therapeutic agents for a wide range of diseases, and show particular promise for neurodegenerative disorders [3]. This is mainly due to the favourable distribution and excellent cellular uptake of AONs following administration in the cerebrospinal fluid (CSF) [4-6]. An AON approach based on redirecting splicing of SMN2 to induce protein expression as a treatment strategy for spinal muscular atrophy (SMA) [7, 8] has arguably been most successful thus far, with recent approval from the Food and Drug Administration (FDA) and European Medicines Agency (EMA) being achieved for the drug Spinraza [7]. AON-based therapies for other central nervous system (CNS) disorders have also shown very promising preclinical results in animal models, where for instance target downregulation for huntingtin [9] and SOD1 [10] protein was achieved very efficiently in mice. SOD1 downregulation was the first AON based therapy for the CNS to be successfully tested in phase 1 trial [11], and AON based downregulation of huntingtin as well as SOD1 are both in phase 2 clinical trial at the moment.

Most AONs currently in clinical development for CNS disorders contain a phosphorothioate (PS) backbone modification to provide protection from nuclease degradation, improve cellular uptake and to enhance AON stability [12]. Despite its many advantages, the main drawback of the PS backbone is its increased cellular toxicity compared to standard phosphodiester linkage [13]. These side effects may arise due to non-specific binding to proteins [14, 15] or complement activation [16]. Indeed, PS-AON are known to induce production of IL-6, TNF-α, IL-12 and CCL5 when added to splenocyte cultures [17]. At least some of these side effects also appear to occur in the CNS, where AON administration has been shown to induce an immune response in the rat brain [18]. This immune stimulation has a clear AON sequence dependent effect, which can be separate from RNA target engagement, as in particular the CpG motifs are known stimulants of the Toll-like receptor 9 (TLR) [19]. These immunostimulatory effects can fortunately be diminished by 2'-sugar and 5-methyl cytosine modifications [20-22], which also was shown to improve AON tolerability in the CNS [23].

Given the clinical advancement of AONs for disorders of the CNS, a comprehensive assessment of potential side effects is required. For this reason, we assessed the effect of a PS 2′-O-methyl modified AON when administered intracerebroventricularly (ICV) in the mouse brain. To assess changes induced at the transcript level, RNA sequencing analysis was performed for striatum, cortex and cerebellum. Furthermore, immunohistological examination was performed on striatal tissue to determine microglia and astrocyte activation after AON administration.

Table 1. overview of RNA sequencing samples from FVB test cohort

	PBS treated		AON treated	
cerebellum	n = 7	week 2: n = 4	n = 8	week 2: n = 6
		week 8: n = 3		week 8: n = 2
cortex	n = 8	week 2: n = 5	n = 7	week 2: n = 5
		week 8: n = 3		week 8: n = 2
striatum	n = 6	week 2: n = 2	n = 8	week 2: n = 5
		week 8: n = 4		week 8: n = 3

MATERIALS AND METHODS

Animals

Wild-type FVB mice and C57BL/6 mice were obtained from Jackson Laboratories (Bar Harbor, ME, USA). The test cohort of FVB mice used for RNA sequencing consisted of a total of 18 mice from 3 to 4 months of age, 3 of which received a total of 215 µg AON, 6 received 665 µg AON and 9 received PBS. The independent validation cohort consisted of 12 C57BL/6 mice, 8 of which received a total dose of 500 µg of the AON and 4 animals received PBS. Animal experiments were carried out in accordance with European Communities Council Directive 2010/63/EU and were approved by the Leiden University and Maastricht University animal ethical committees. Mice were housed individually during experimental procedures, with food and drinking water available *ad libitum* and with a reverse light/dark cycle of 12 h. Only male mice were used for experiments.

AON administration

The AON consisted of a 19-mer (5′- CUGAACUGGUCUACAGCUC –3′) [24, 25] and followed a steric blocking design with a full PS backbone and uniform 2'-O-methyl ribose modifications. Nucleotides were not 5-methyl modified. The AON was designed to be non-complementary to the mouse genome, with a maximum of 17/19 nucleotide complementarity. AONs were dissolved in sterile PBS without calcium or magnesium and diluted to a maximum concentration of 40 µg/µl for injection. Injections of AONs was performed ICV, following previously described procedures [24, 26]. In brief, mice were fixed in a stereotactic frame under isoflurane anaesthesia, and a burr hole was drilled in the skull. A 26 gauge cannula (Plastics1, Anaheim, CA, USA) was implanted at coordinates (relative to bregma) AP: –0.4, ML: 1.0, DV: –1.7 mm, and fixed with dental composite (OptiBond® All-In-One, Kerr Dental, Bioggio, Switzerland). AONs or PBS were administered under general anaesthesia at an infusion rate of ~ 1 µl/min for a total dose of 215 µg or 665 µg. The simplified administration scheme is depicted in (Fig. 1A). The 215 µg dose was achieved through a total of 6 injections (15 µg to 50 µg per injection) during a 2 month period. Animals dosed to 665 µg received 2 extra injection of 250 and 200 µg during a 1.5 month period. Animals from the C57Bl/6 validation cohort received repeated injections

of 5 µl of the same non-targeting AON at 20 µg/µl. Five injections for a total dose of 500 µg was performed in these mice during a 10 week period.

Tissue collection

Mice were sacrificed either 2 weeks (n = 11) or 8 weeks (n = 7) post injection (Fig. 1A). Mice from the C57Bl/6 validation cohort were sacrificed 4 months after the last AON injection (n = 12). Brains were removed, and striatum, cortex and cerebellum of the left hemisphere were snap frozen in liquid nitrogen and stored at -80 ˚C until RNA isolation. The entire right hemisphere was fixed in 4% paraformaldehyde overnight at 4 ˚C. Tissue was then placed in 30% sucrose for 1 or 2 days and stored in PBS containing 0.02% sodium azide at 4˚C until sectioning.

Immunofluorescent stainings and assessment of GFAP and Aif1 levels

Fixed mouse brain tissue was sectioned on a vibratome at 25 µm thickness, and coronal sections were collected in PBS containing 0.02% sodium azide. Sections were then washed with PBS containing 0.2% triton-X100 for 10 min and incubated overnight with one of the following primary antibodies diluted in 1% normal donkey serum: rabbit anti-PS-backbone (kind gift of Ionis Pharmaceuticals, Carlsbad, CA, USA; 1:1000), rabbit anti-glial fibrillary acidic protein (GFAP) (Dako; 1:1000), or rabbit anti-aif1 (Wako Chemicals USA, Inc ; 1:500). Sections were washed with PBS and incubated with secondary antibodies, donkey anti-rabbit-alexa Fluor 488 1:500 (Life technologies, Paisley, UK) for fluorescent optical density determination. After washing, sections were mounted on superfrost plus coated microscope slides (Fisher Emergo, Landsmeer, Netherlands). The slides were then immediately coverslipped using EverBrite hardset mounting medium with DAPI (Biotium, Hayward, USA). For cell morphology assessment, the sections were incubated overnight with the primary antibody with the same dilution, followed by a secondary antibody 1:800 biotinylated donkey anti-rabbit (Jackson Immunoresearch Laboratories, West Grove, USA), and ABC-step (avidin–biotin-peroxidase complex, diluted 1:800, Elite ABC-kit, (Vestastain, Burlingame, CA, USA). To visualize the horseradish peroxide reaction product, the sections were incubated with DAB (3,30-diaminobenzidine tetrahydrochloride) with nickel chloride intensification. Slides were washed, dehydrated and coverslipped using Pertex (Histolab Products ab, Goteborg, Sweden). Optical density determination through fluorescence was performed on three coronal sections per mouse (5 AON treated vs 5 PVS treated) at 10x magnification using Image J software. Coronal sections of the striatum at 60x magnification were scored for Aif1 levels to assess microglia activation and for GFAP levels to assess astrocytes number and state of activation. Morphology of cells was assessed for cells in 5 images from three different sections per mouse. The scoring of microglia activation state was done based on morphology assessment from previous studies [27, 28]. Aif1 positive cells (microglia) were categorized as resting or active state. Resting state microglia were characterized by small and smooth-surfaced cell bodies with thin, ramified processes. Active microglia had an irregularly shaped cell body with thicker, ramified processes. Activation of astrocytes was assessed similar to previously described [29]. Resting state astrocytes had low levels of GFAP expression, with

stellate morphology and numerous spatially distinct, thin branched processes. Active astrocytes had increased GFAP expression, with a hypertrophic appearance and thicker, highly branched, overlapping processes. Images of AON distribution were obtained as described previously [26].

RNA isolation and sequencing

RNA was isolated from mouse striatum, cortex and cerebellum using the Trizol method and PureLink RNA mini kit (Ambion, Thermo Fisher scientific, Waltham, MA, USA). Genomic DNA was degraded using a DNAse incubation according to manufacturer's protocol, and concentration and purity of RNA was determined by Nanodrop spectrophotometry. Library preparation and RNA sequencing was done at deCode Genetics (Reykjavik, Iceland). Starting material was approximately 1 μg of total RNA, with an average RIN value of 7.6 (SD ± 0.3). Quality of RNA was determined using the LabChip GX (Perkin Elmer, Waltham, USA). Sample preparation was performed non-strand specifically, using the TruSeq Poly-A v2 kit (Illumina, San Diego, USA). Capture of mRNA was performed with magnetic poly-T beads, followed by fragmentation. Synthesis of cDNA was then performed with random hexamer primers using the SuperScript II kit (Invitrogen, Carlsbad CA, USA). Subsequently, 2nd strand cDNA synthesis was performed in conjunction with RNAse-H treatment. Indexing adapters were ligated to the ds-cDNA and amplification was performed using PCR. Insert size and sample diversity was assessed through pool sequencing on a MiSeq instrument (Illumina). Sequencing (read length 2x125 cycles) was then performed using the HiSeq 2500 with v4 SBS sequencing kits. Illumina scripts (bcl2fastq v1.8) were used for demultiplexing and FASTQ file generation. Counts were aligned to genes of the mouse reference genome build 10 (GRCm38/mm10).

Analysis of differential gene expression

Analysis of gene expression was performed only on genes exceeding an average of >4 counts per million (CPM). Gene counts were normalized using the trimmed mean of M-values (TMM) normalization method [30]. Differential gene expression was performed using the R package edgeR, version 3.14.0 [31]. A principal component analysis was performed to assess clustering of samples per brain region, and 6 out of 53 samples were excluded based on abnormal clustering (Fig. S2A). One additional sample was excluded based on the fact that there was a large percentage of reads originating from a single gene (Fig. S2B). The design model matrix for edgeR was described as model.matrix(~ treatment_group * brainregion) to allow for detection of AON treatment effects at the transcript level accounting for the different brain regions. Dispersion was estimated using the design matrix, after which a generalized linear model (GLM) was fitted using the glmFit function. Likelihood ratio test was performed using the glmLRT function on the coefficients of AON treatment and the interaction term treatment*brainregion. To assess the effect of the AON treatment within each brain region, a coefficient was assigned for each brain region and treatment group. The glmLRT function was then performed with contrast argument to allow pairwise treatment effect comparison for each brain region. Genes were considered significantly differentially expressed when the false discovery rate (FDR, Benjamini-Hochberg) was below 0.05. Data was plotted using ggplot 2 or graphpad Prism version 7.0.

Pathway analysis

Genes found to be significantly differentially expressed between PBS and AON treated mice at FDR < 0.01 were included for pathway analysis using Ingenuity (Ingenuity Systems Inc., Redwood City, CA; www.ingenuity.com). Functional annotation of genes was performed using DAVID bioinformatics resources 6.8 (https://david.ncifcrf.gov). Pathways and biological processes with corrected p-value < 0.05 (Benjamini–Hochberg) were considered significantly enriched in the dataset.

Validation with ddPCR

To validate the RNA sequencing results, droplet digital PCR (ddPCR) was performed on striatum RNA from the same samples as used for RNA sequencing for the FVB test cohort, and using RNA from a separate C57Bl/6 validation cohort. cDNA was generated as previously described [32] using Transcriptor First Strand cDNA Synthesis Kit (Roche, Mannheim, Germany) with random hexamer primers. The amount of cDNA that was used per reaction was the equivalent of 30 ng of RNA for ddPCR for genes of interest. Due to high expression, 5 ng of input was used for reference genes. PCR product sizes ranged between approximately 100 and 200 bp (primer sequences are listed in Table S1). PCR reactions were set up using QX200 ddPCR EvaGreen Supermix (Bio-Rad, Hercules, CA, USA), with 100 nM of forward and reverse primer in an end volume of 22 µl. Between 15,000 and 20,000 droplets were generated using an AugoDG droplet generator and DG32 cartridges (Bio-Rad). PCR was then performed as follows: 10 min denaturation at 95°C followed by 40 cycles of 30 sec at 94°C and 1 min at 58 °C. The reactions were ended for 5 min at 4°C, 5 min at 90°C and then cooled to 10°C. The ramp rate for all steps was 2°C/sec. Droplets were quantified using the QX200 droplet reader (Bio-Rad) and analysed with QuantaSoft analysis software (Bio-Rad). Expression was normalized to reference gene expression level, and copies of target transcript per µl are reported.

RESULTS

AONs lead to upregulation of the antiviral enzyme Oasl2

A total dose of 200 µg AON administered ICV did not result in any negative effect on the bodyweights of the mice in the FVB test cohort (Fig. 1B). However, in the C57Bl/6 validation cohort a significantly reduced bodyweight was observed already after 100 µg of AON, which persisted until the end of the study (Fig. S1). Despite this, epileptic seizures were sporadically observed directly after AON administration in our FVB test cohort, but not the C57Bl/6 validation cohort. This observation is consistent with previous reports of increased sensitivity to epileptic seizures in mice of FVB background [33]. Immunohistological staining for the PS backbone revealed widespread AON distribution throughout the isolated brain regions (Fig. 1C). Striatum, cortex and cerebellum tissue from mice treated ICV with either AON or PBS was collected for RNA sequencing (Fig. 1A).When analysing the 8 weeks (215 µg) and 2 weeks (665 µg) AON treatment groups from the FVB test cohort, no major differences in gene expression

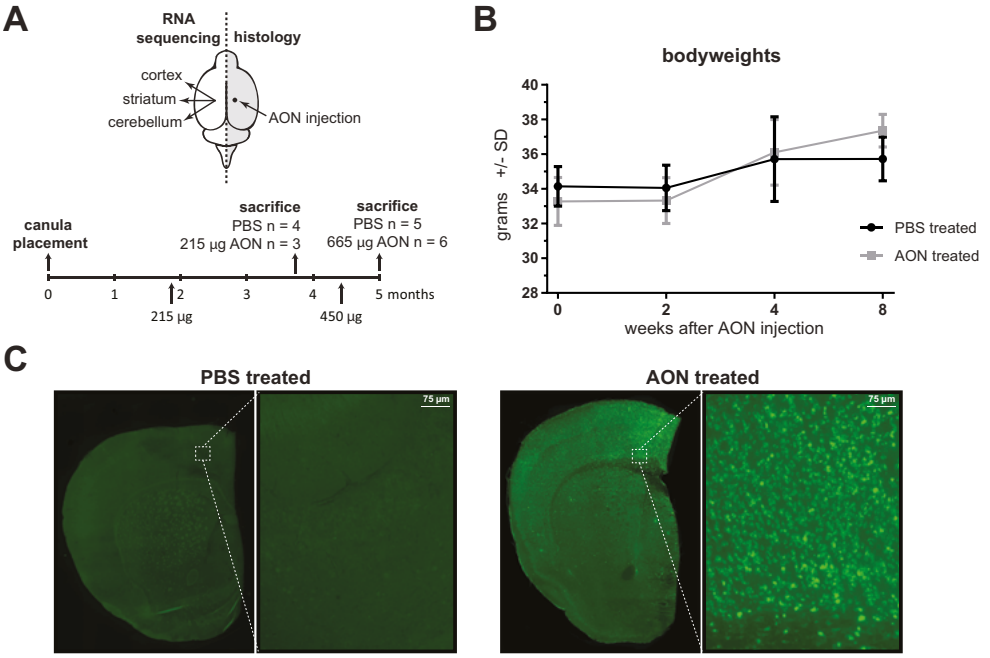

Figure 1. Study design and AON cellular uptake. A) During a 5 month period, FVB mice of the test cohort were injected intracerebroventricularly with a total of 215 µg AON (achieved with a total of 6 injections) or 625 µg AON (achieved with 2 additional injections). Two and 8 weeks after the last injection, mice were sacrificed and the right hemisphere was fixed for histology. Cortex, striatum and cerebellum were isolated from the left hemisphere for molecular analyses. **B**) Intracerebroventricular AON injection did not result in altered bodyweight compared to PBS injected mice in the FVB test cohort. Data depicted from mice treated with 215 µg AON (n = 4) or PBS (n = 5). **C**) Histological analysis showing AON distribution throughout the brain 2 weeks after the last injection.

were found between these dosage groups. For this reason it was decided to combine the 2- and 8 week time points groups for analysis of differential gene expression to obtain increased power for the comparison AON versus PBS treated. After exclusion of samples with low number of reads, poor alignment, or outliers in principal component analysis (Fig. S2A), a total of 44 samples were included for analysis of differential gene expression (Table 1). A median of 7.9 million reads per sample were aligned to the mouse reference genome (GRCm38/mm10). Genes with low expression (CPM < 4) were excluded, leading to inclusion of 12,160 genes for differential gene expression analysis. None of the mouse genes containing >16 nucleotide homology in BLAST[34] analysis were observed to be downregulated in the RNA sequencing analysis.

Gene expression analysis revealed a total of 925 genes differentially expressed (FDR <0.05) in at least one brain region of animals treated with AON. The top 10 differentially expressed genes and corresponding fold changes per brain region are depicted in Table 2. The largest and most consistent change observed for each brain region was an upregulation of 2'-5'-oligoadenylate synthase-like protein 2 *(Oasl2)* (Fig. 2A), which is an dsRNA-activated antiviral enzyme

Table 2. Top 10 significantly altered gene expression in brain after AON treatment

Gene	Name	FDR	Cerebellum log2 fold change	Cortex log2 fold change	Striatum log2 fold change	Protein function
Oasl2	2'-5'-oligoadenylate synthase-like protein 2	1.3E-07	2.2*	1.9	2.5*	Interferon-induced, dsRNA-activated antiviral enzyme
Sphkap	A-kinase anchor protein SPHKAP	1.3E-07	0.1	0.3	-0.9*	regulation of protein kinase A signaling
Lgals3bp	Galectin-3-binding protein	1.9E-07	1.4	1.5*	1.3*	scavenger receptor activity
Bst2	Bone marrow stromal antigen 2	1.2E-06	1.3	2.0	2.7*	defence response to virus
H2-Q4	Histocompatibility 2, Q region locus 4	3.9E-06	0.9	0.9	1.8*	antigen processing and presentation of peptide antigen via MHC class I
Ifit3	Interferon-induced protein with tetratricopeptide repeats 3	4.3E-06	1.4	1.4	1.8*	cellular response to interferon-alpha
Kcns1	Potassium voltage-gated channel subfamily S member 1	5.6E-06	0.0	-0.4	1.9*	potassium ion transport
Dgat2	Diacylglycerol O-acyltransferase 2	5.8E-06	0.1	0.2	0.9*	triacylglycerol biosynthesis
Kctd9	BTB/POZ domain-containing protein KCTD9	6.8E-06	-0.3	-0.1	-0.8*	adapter of E3 ubiquitin-protein ligase complex
Vipr1	Vasoactive intestinal polypeptide receptor 1	7.3E-06	-0.1	0.2	1.5*	cell surface receptor signalling pathway

* = gene is differentially expressed within individual brain region

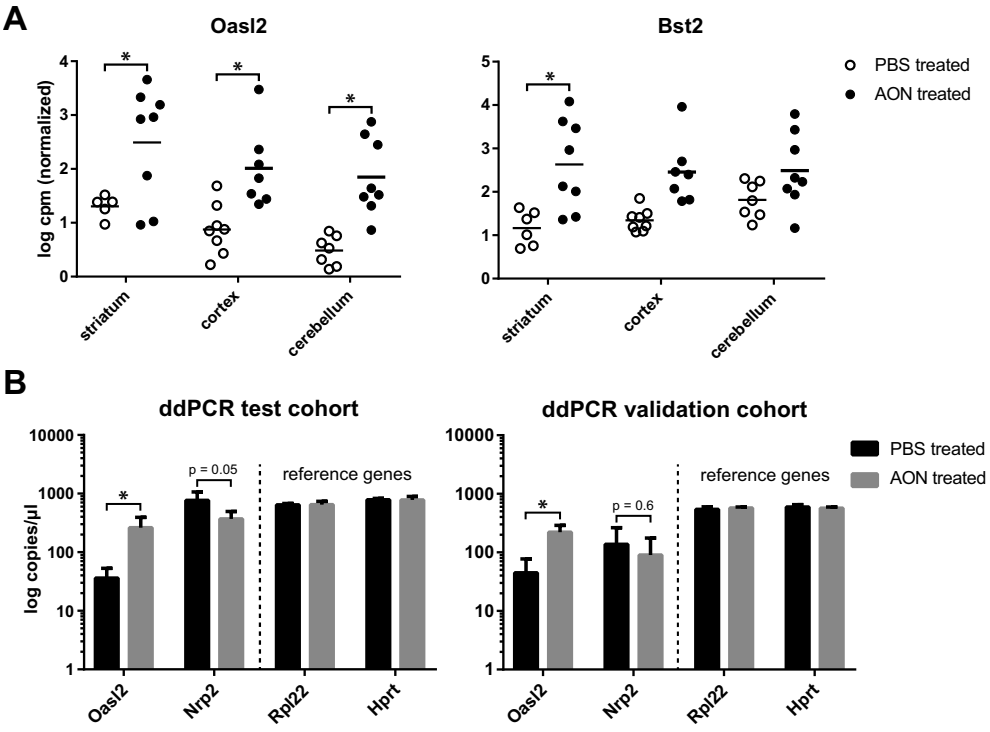

Figure 2. Increased expression of *Oasl2* in brain of AON treated mice. A) RNA sequencing shows expression of *Oasl2* and *Bst2* most strongly upregulated in response to AON, in particular in the striatum. * = FDR < 0.05, based on 8 vs 8 mice, analysis on samples of 2 weeks and 8 weeks after AON injection. **B**) ddPCR validation of top upregulated (*Oasl2*) and top downregulated (*Nrp2*) genes in striatum at 2 weeks after AON injection (FVB test cohort), and 4 months after AON injection (C57Bl/6 independent validation cohort). Based on ddPCR of 4 vs 4 mice. * = $p < 0.05$ using student's t-test.

involved in the innate antiviral response. Oasl2 requires double-stranded RNA as a co-factor [35], though the enzyme does not have a characteristic dsRNA binding motif [36].

Other top differentially upregulated genes were also involved in the immune and anti-viral response, such as Bone marrow stromal antigen 2 (*Bst2),* Histocompatibility 2, Q region locus 4 *(H2-Q4)* and Interferon-induced protein with tetratricopeptide repeats 3 *(Ifit3)*. In general, the upregulation of these genes was observed to a larger extent in the striatum than in the cortex and cerebellum, and were altered at both the 2 and 8 week time points after AON injection. Since AON uptake is comparable between striatum and cortex, it is unlikely that this difference is due to uptake efficiency of the AON. The top upregulated (*Oas*l2*)* and a downregulated (*Nrp2*) gene was validated using ddPCR on the same striatum RNA as was used for RNA sequencing. Both transcripts showed similar expression differences as detected in the RNA sequencing analysis, with *Oasl2* showing strong significant upregulation in AON treated mice (log2FC = 2.87) and *Nrp2* showing significant downregulation (log2FC = -1.05). A similar upregulation of

Oasl2 (Fig 2B) and several other immune system associated genes (Table S2) was also confirmed in the C57Bl/6 validation cohort through ddPCR. The immunostimulatory effect of the AON appears to be long lasting since mice of the validation cohort were sacrificed 4 months after the last AON administration (Fig. S1) and seems to be independent of the genetic background of the mice.

Immune system pathways are activated in AON treated brain

To determine which biological processes are altered in the mouse brain in response to AON administration, we performed pathway analysis using Ingenuity [37] and DAVID [38] on the significantly altered genes with FDR < 0.01 observed in the RNA sequencing analysis. This approach led to inclusion of 379 genes with relatively large changes that showed a most consistent change across the three brain regions. The significant canonical pathways and biological processes (KEGG) that are altered in response to the AON are listed in Table 3. Pathways involving the immune system, such as interferon and B-cell receptor signalling were activated in the AON treated mice.

Examination of the biological processes with DAVID showed that the most significant alteration in immune system associated genes. This process included 11 differentially expressed genes that were most strongly upregulated in striatum (Fig. 3). We validated 5 of these genes through ddPCR, (Fig. 2B and Table S2) which confirmed upregulation of the immune system associated genes *Oasl2, Ifit3, Bst2*, *Trim25* and *Lgals3bp* genes in striatum of AON treated mice in both the FVB test- and C57Bl/6 validation cohort. Together, these upregulated genes point to an innate immune response and complement activation, which constitutes the immediate defense in response to potential pathogens. In the context of the brain, this would suggest

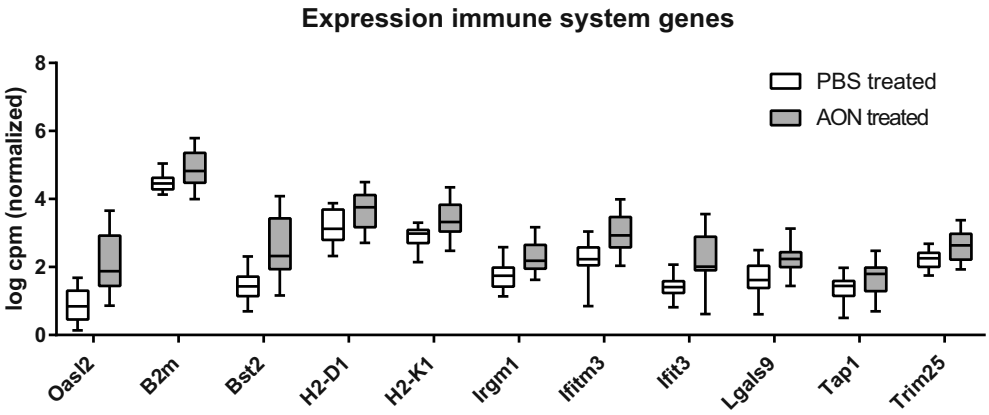

Figure 3. Immune system associated genes are upregulated in brain after AON injection. Expression of 11 significantly altered genes in brain belonging to immune system process (GO:0002376). Based on RNA sequencing analysis of cortex, cerebellum and striatum from 9 PBS treated vs 9 AON treated animals.

Table 3. Pathways and biological processes altered after AON treatment

	Number of genes	FDR	Activation z-score
Pathway (Ingenuity)			
Interferon Signaling	5	3.2E-04	2.0
G-Protein Coupled Receptor Signaling	13	7.9E-04	NA
GABA Receptor Signaling	6	1.1E-03	NA
B Cell Receptor Signaling	10	1.5E-03	2.3
IGF-1 Signaling	7	2.1E-03	NA
Leukocyte Extravasation Signaling	10	3.2E-03	2.3
Neuropathic Pain Signaling In Dorsal Horn Neurons	7	3.4E-03	1.9
Complement System	4	3.4E-03	2.0
Biological process (KEGG)	**Number of genes**	**FDR**	**Identifier**
Immune system process	11	2.8E-05	GO:0002376
Cellular response to interferon-beta	5	5.2E-04	GO:0035456
Antigen processing and presentation of peptide antigen via MHC class I	4	2.6E-03	GO:0002474
Defense response to virus	6	0.01	GO:0051607
Innate immune response	7	0.03	GO:0045087

microglia involvement. For this reason, we next performed histological analysis of microglial activation.

Microglia activation and increased astrocyte density

Based on the transcriptomic analysis, administration of the AON resulted in an immunologic response most strongly in the striatum of the mice. To further assess this innate immune response, immunohistological staining was performed on brain sections for the microglia marker allograft inflammatory factor 1 (Aif1) and for the astrocyte marker glial fibrillary acidic protein (GFAP). Microglia are brain resident macrophages that are widely expressed in the brain and constitute a major component of the innate arm of the brain immune system [39, 40]. In the RNA sequencing analysis, *Aif1* expression was significantly increased in the AON treated mouse brain. Mean optical density measurements in striatum did not reveal a significant change in the Aif1 levels in AON treated mice (Fig. 4B), indicating no significant increase in the number of microglia cells. However, when more closely examining the number of activated and resting state cells, an increase in activated microglia was observed in striatum of AON treated mice (Fig. 4C), similar to previously reported for CpG-containing AONs [41].

RNA sequencing results did not show significant alteration of *GFAP* transcript levels in AON treated mice. However, staining of GFAP in AON treated animals did reveal a small significant increase in mean optical GFAP density in striatum (Fig. 4B). GFAP is a marker for reactive astrocytes, which is a common cell type of the CNS with a wide range of functions.

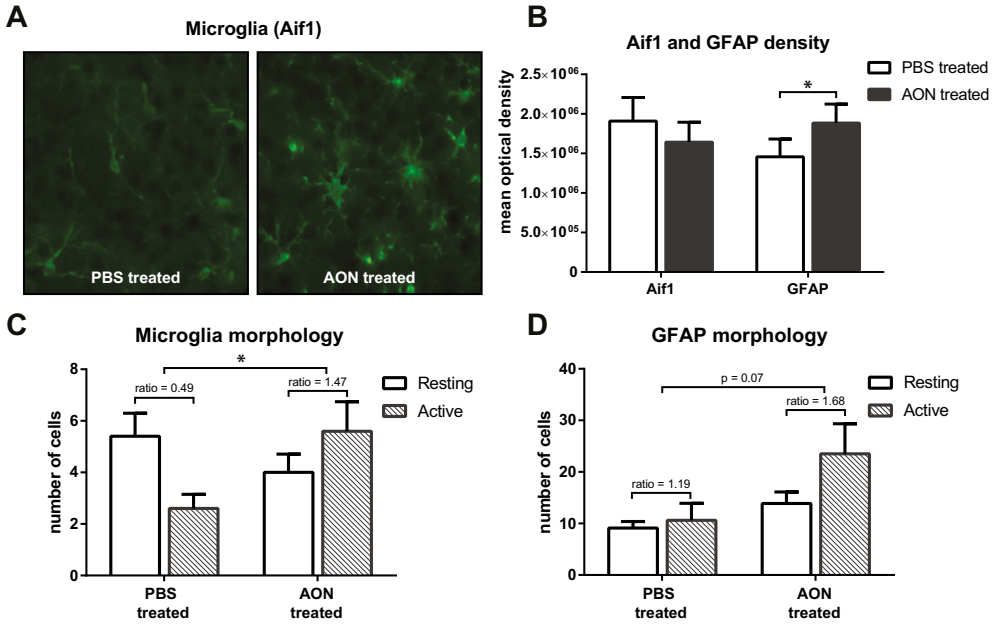

Figure 4. Assessment of astrocyte and microglia markers in striatum. Histological analysis of the microglia marker Aif1 and astrocyte marker GFAP was performed on 3 coronal striatum sections per mouse. **A**) Representative example of microglia staining with Aif1 of a PBS and AON treated mouse at 40x magnification. **B**) Quantification of the optical density revealed no observable change in Aif1 levels, but did show a significantly increased level of GFAP. **C**) Despite no increased number of Aif1 positive cells, the ratio of active to resting state microglia was significantly increased in striatum of AON treated mice. **D**) Scoring of GFAP morphology showed a general increase in astrocytes in AON treated mice, and a trend towards increased ratio of active over resting state cells. Based on 3 sections per mouse from 5 vs 5 mice. * $p < 0.05$ with student's t-test.

Astrocytes express Toll-like receptors (TLR) and are capable of producing several cytokines and chemokines [42]. Reactive astrogliosis is often a response to cytokines such as TGF-α or through indirect activation via neurons, microglia or endothelial cells [43]. When examining the activity state of astrocytes in the striatum, an increase in the number of active glia cells was observed in AON treated mice (Fig. 4D). To determine whether the immune stimulatory effect was not restricted to a single AON sequence, additional immunohistological stainings of brain tissue from a previous mouse study (described in [24]) was used. This AON was also a 2-'O-methyl PS-AON and was complementary to both the murine and human huntingtin mRNA, but showed no effect on the murine huntingtin transcript [24]. Similar to the AON used in the present study, this second AON resulted in increased astrocyte and microglia activation in the striatum of AON treated mice (Fig. S3), suggesting that the immune stimulation reported here is not restricted to a single AON sequence.

DISCUSSION

AONs are increasingly being used for treatment of CNS disorders, and have recently received FDA approval for treatment of SMA [44]. In this study we set out to determine the side effects of a uniformly modified 2-'O-methyl PS-AON in the mouse brain. This type of AON is typically implemented in steric blocking applications, such as exon inclusion or exon skipping [3].

The AON did not contain CpG motifs, which are known to be potent immunostimulatory agents [45]. A bolus ICV injection led to widespread distribution and cellular uptake throughout the mouse brain, in line with previous reports using similar AON chemistries [4, 6, 26]. Despite using the same AON, we observed different effects on bodyweight in our FVB test and C57Bl/6 validation cohort of mice. Mice in the validation cohort showed a reduction in bodyweight already after 100 µg ICV administration of AON, whilst our test cohort showed no discernible difference in bodyweight at a dose of 615 µg AON. This disparity may be the result of differences between the FVB and C57Bl/6 mouse background, or the differences in dosing schedule between the two cohorts.

Through RNA sequencing analysis, we found that the AON led to upregulation of several transcripts associated with the immune system. The largest upregulation was observed for *Oasl2*, *Bst2*, *Ifit3* and *H2-Q4*. These genes were upregulated in all brain regions tested (striatum, cortex and cerebellum), and generally showed a slightly larger fold change in the striatum compared to cortex and cerebellum. Given comparable AON uptake in striatum and cortex, this suggests the striatum is more sensitive to the immunostimulatory effects of the AON. The top differentially expressed genes were also found upregulated in the C57Bl/6 validation cohort, indicating that the immune system activation is not dependent on the genetic background of the mice.

It has been found that particular AON sequences, even without CpG motifs, can result in an atypical inflammatory response [46]. It is therefore important to consider that the immune stimulatory effects we describe here can potentially be confounded by the specific sequence of the AON used. However, we have confirmed the microglia and astrocyte activation for a different AON sequence of identical chemistry (Fig. S3), indicating that the results described here are not unique to one sequence.

The most strongly upregulated gene in response to the AON, *Oasl2,* belongs to the 2',5'-oligoadenylate synthetase gene family, of which a total of 11 have been identified in mouse, compared to 4 in human [47]. In the mouse brain, *Oasl2* is the most highly expressed of the enzyme family [47] and is an antiviral enzyme which through oligoadenylate synthetase activity activates ribonucleases, resulting in degradation of viral RNA. Oasl is one of the proteins upregulated in response to type I and II interferon (IFN) cytokines, and confers resistance to viral infection [48]. In response to virus infection, IFN induced upregulation of Oas activates the ribonuclease L, which leads to RNA degradation [49].

The second most upregulated gene observed in AON treated mice, the transmembrane protein *Bst2,* is also an IFN induced protein. Similar to Oasl2, Bst2 is a component of the innate defence response to viruses [50]. Bst2 is also known as tetherin, because it was identified as

a protein that caused retention of virions on infected cell surfaces [51]. Bst2 is able to tether these virions based on recognition of pathogen-associated molecular patterns (PAMPs), but is also able to act as a pattern-recognition receptor capable of signalling to the immune system through NFκB-dependent proinflammatory gene expression [52]. Indeed, double-stranded RNA is a known PAMP recognized by TLR3, which upon activation results in NF-κB and IFN-beta production [53]. Surprisingly however, Bst2 showed negligible ability to induce NF-κB response [52], suggesting this downstream signalling pathway may not have been activated in the mouse brain here. In line with this, we did not observe significant alteration in expression levels of *NFKB1* between PBS and AON treated mice. The increase in *Bst2* expression in this study (Log2FC = 2) is not substantially different from what was previously observed in transcriptional analysis of a mouse centrally injected with lippolysaccharide (LPS), where *Bst2* showed a Log2FC of 2.82 [54]. This observation indicates that the immune activation in response to the AON can be quite substantial at the dosages tested here, although expression changes of other immune response genes are more mildly affected in our study compared to LPS injection [54].

Another strongly upregulated gene in brain of the AON treated mice was *Ifit3*. Similar to Oasl2 and Bst2, Ifit3 is an anti-viral protein that is upregulated in response to IFN signalling [55]. Ifit3 restricts DNA and RNA virus replication, and evidence suggests that the Ifit family of proteins plays an important role in destruction of invasive RNA [56]. Ifit proteins are able to bind viral RNA and sequester viral proteins in the cytoplasm [57]. The observation that several IFN induced genes are upregulated in response to the AON suggest that the innate immune system is activated in response to the AON, resulting in IFN signalling. In line with this, we observed microglia activation based on significant *Aif1* transcript upregulation in RNA sequencing analysis, as well as increased active state microglia cells in histological examination. These observations are in concordance with previous reports, where doses higher than 100 μg of 2-'O-methyl PS-AON led to significant *Aif1* transcript upregulation [6]. Similarly, the observed increase in astrocyte activation in this study is indicative of a neuroprotective response in response to the AON [58]. Though the role of reactive astrocytes is still not well understood, it was recently found that A1 reactive astrocytes are induced by cytokines originating from activated neuroinflammatory microglia [59]. The observed astrocyte activation in striatum of AON treated mice may thus be a downstream result of microglial activation.

The mechanisms underlying the immune activation by RNA and AONs has been previously investigated, and a large portion of the immune activation originates from TLR stimulation (reviewed in [60]). This activation can be antagonized upon 2'-O-methylation of RNA [61, 62], which strongly reduces the immunostimulatory effects of the AON. Nonetheless, even in absence of CpG motifs and having 2'-metoxyethyl modifications, AONs are still capable of inducing an immune response [63]. In particular TLR3, 7 and 8 were shown to recognize single-stranded RNA [64-66]. Though the majority of TLRs sense stimulatory components on the cell surface, TLR3, 7 and 8 sense nucleic acids in endosomal compartments of the cell [65]. These three TLRs are expressed in microglia of mice [67], whilst astrocytes in contrast only express low levels of TLR2, 4, 5 and 9 in resting state [68]. This argues for an initiatory role of the microglia, which are able to sense the AONs through their TLRs, resulting in cytokine production and downstream

activation of the astrocytes. However, it is also known that human neurons express TLR3 [69] and TLR8 [70], and are able to initiate an anti-viral response characterized by cytokines (TNF-alpha, IL6), chemokines (CCL-5, CXCL-10) and antiviral molecules 2'5'OAS and IFN-beta [69].

Of note, the TLR receptors and general immune response is known to differ between mouse and human [71, 72]. For instance, CpG stimulatory sequences do not elicit TLR9 dependent TNF-alpha dependent toxicity in humans after pulmonary administration, while they do in mice [73]. This difference was hypothesized to be due to differential TLR9 expression patterns between rodents and primates, as monocyte/macrophage cells do not express TLR9 in primates [73]. Further, small interfering RNA (siRNA) was shown to be a ligand for the murine TLR3, whereas the human TLR3 was unresponsive to the siRNA [74]. It may therefore be difficult to extrapolate the murine immune response for AONs to the human situation.

However, also the use of monkeys as a model for AON tolerability has presented difficulties, as monkeys have a greater sensitivity to complement activation in response to second generation AONs compared to humans [75, 76]. As such, mouse models may overestimate the contribution of AON sequence specific effects, whilst experiments in monkeys appear to overestimate the AON induced complement activation aspect.

In conclusion, we show here that a 2-'O-methyl PS-AON of 19 nucleotide in length results in mild activation of the innate immune response when administered to the mouse brain. The immune activation is characterized by increased activation of microglia and astrocytes, likely resulting in IFN signalling. The resulting transcriptional changes in the brain are most strongly identified by upregulation of *Oasl2* and *Bst2*.

ACKNOWLEDGEMENTS

The authors want to thank Bharath Sampadi for performing Ingenuity analysis, Melvin Evers for advice on study design, Frank Rigo for providing antibody reagents, Peter-Bram 't Hoen and Szymon Kielbasa for advice on RNA sequencing analysis, and Ólafur Magnússon (Decode Genetics) for performing the RNA sequencing.

AUTHOR DISCLOSURE STATEMENT

The authors declare no competing financial interests.

REFERENCES

1. Lundin, KE, Gissberg, O, and Smith, CI (2015). Oligonucleotide Therapies: The Past and the Present. *Human gene therapy* **26**: 475-485.
2. Khvorova, A, and Watts, JK (2017). The chemical evolution of oligonucleotide therapies of clinical utility. *Nature biotechnology* **35**: 238-248.
3. Evers, MM, Toonen, LJ, and van Roon-Mom, WM (2015). Antisense oligonucleotides in therapy for neurodegenerative disorders. *Advanced drug delivery reviews* **87**: 90-103.
4. Casaca-Carreira, J, Temel, Y, Larrakoetxea, I, and Jahanshahi, A (2017). Distribution and Penetration of Intracerebroventricularly Administered 2'OMePS Oligonucleotide in the Mouse Brain. *Nucleic Acid Ther* **27**: 4-10.
5. Juliano, RL (2016). The delivery of therapeutic oligonucleotides. *Nucleic Acids Res* **44**: 6518-6548.
6. Rigo, F, Chun, SJ, Norris, DA, Hung, G, Lee, S, Matson, J, *et al.* (2014). Pharmacology of a central nervous system delivered 2'-O-methoxyethyl-modified survival of motor neuron splicing oligonucleotide in mice and nonhuman primates. *The Journal of pharmacology and experimental therapeutics* **350**: 46-55.
7. Chiriboga, CA (2017). Nusinersen for the treatment of spinal muscular atrophy. *Expert review of neurotherapeutics*: 1-8.
8. Hua, Y, Sahashi, K, Hung, G, Rigo, F, Passini, MA, Bennett, CF, *et al.* (2010). Antisense correction of SMN2 splicing in the CNS rescues necrosis in a type III SMA mouse model. *Genes Dev* **24**: 1634-1644.
9. Kordasiewicz, HB, Stanek, LM, Wancewicz, EV, Mazur, C, McAlonis, MM, Pytel, KA, *et al.* (2012). Sustained therapeutic reversal of Huntington's disease by transient repression of huntingtin synthesis. *Neuron* **74**: 1031-1044.
10. Smith, RA, Miller, TM, Yamanaka, K, Monia, BP, Condon, TP, Hung, G, *et al.* (2006). Antisense oligonucleotide therapy for neurodegenerative disease. *The Journal of clinical investigation* **116**: 2290-2296.
11. Miller, TM, Pestronk, A, David, W, Rothstein, J, Simpson, E, Appel, SH, *et al.* (2013). An antisense oligonucleotide against SOD1 delivered intrathecally for patients with SOD1 familial amyotrophic lateral sclerosis: a phase 1, randomised, first-in-man study. *Lancet Neurol* **12**: 435-442.
12. Sharma, VK, Sharma, RK, and Singh, SK (2014). Antisense oligonucleotides: modifications and clinical trials. *MedChemComm* **5**: 1454-1471.
13. Levin, AA (1999). A review of the issues in the pharmacokinetics and toxicology of phosphorothioate antisense oligonucleotides. *Biochimica et biophysica acta* **1489**: 69-84.
14. Brown, DA, Kang, SH, Gryaznov, SM, DeDionisio, L, Heidenreich, O, Sullivan, S, *et al.* (1994). Effect of phosphorothioate modification of oligodeoxynucleotides on specific protein binding. *The Journal of biological chemistry* **269**: 26801-26805.
15. Guvakova, MA, Yakubov, LA, Vlodavsky, I, Tonkinson, JL, and Stein, CA (1995). Phosphorothioate oligodeoxynucleotides bind to basic fibroblast growth factor, inhibit its binding to cell surface receptors, and remove it from low affinity binding sites on extracellular matrix. *The Journal of biological chemistry* **270**: 2620-2627.
16. Galbraith, WM, Hobson, WC, Giclas, PC, Schechter, PJ, and Agrawal, S (1994). Complement activation and hemodynamic changes following intravenous administration of phosphorothioate oligonucleotides in the monkey. *Antisense research and development* **4**: 201-206.

17. Bjersing, JL, Eriksson, K, Tarkowski, A, and Collins, LV (2004). The arthritogenic and immunostimulatory properties of phosphorothioate oligodeoxynucleotides rely on synergy between the activities of the nuclease-resistant backbone and CpG motifs. *Inflammation* **28**: 39-51.

18. Elepfandt, P, Rupprecht, S, Schoning-Burkhardt, B, Volk, HD, and Woiciechowsky, C (2002). Oligodeoxynucleotides induce brain inflammation in rats when infused intracerebroventricularly. *Neuroscience letters* **322**: 107-110.

19. Meng, W, Yamazaki, T, Nishida, Y, and Hanagata, N (2011). Nuclease-resistant immunostimulatory phosphodiester CpG oligodeoxynucleotides as human Toll-like receptor 9 agonists. *BMC biotechnology* **11**: 88.

20. Henry, S, Stecker, K, Brooks, D, Monteith, D, Conklin, B, and Bennett, CF (2000). Chemically modified oligonucleotides exhibit decreased immune stimulation in mice. *The Journal of pharmacology and experimental therapeutics* **292**: 468-479.

21. Monteith, DK, Henry, SP, Howard, RB, Flournoy, S, Levin, AA, Bennett, CF, *et al.* (1997). Immune stimulation--a class effect of phosphorothioate oligodeoxynucleotides in rodents. *Anti-cancer drug design* **12**: 421-432.

22. Zhao, Q, Temsamani, J, Iadarola, PL, Jiang, Z, and Agrawal, S (1996). Effect of different chemically modified oligodeoxynucleotides on immune stimulation. *Biochemical pharmacology* **51**: 173-182.

23. Peng Ho, S, Livanov, V, Zhang, W, Li, J, and Lesher, T (1998). Modification of phosphorothioate oligonucleotides yields potent analogs with minimal toxicity for antisense experiments in the CNS. *Brain research Molecular brain research* **62**: 1-11.

24. Casaca-Carreira, J, Toonen, LJ, Evers, MM, Jahanshahi, A, van-Roon-Mom, WM, and Temel, Y (2016). In vivo proof-of-concept of removal of the huntingtin caspase cleavage motif-encoding exon 12 approach in the YAC128 mouse model of Huntington's disease. *Biomedicine & pharmacotherapy = Biomedecine & pharmacotherapie* **84**: 93-96.

25. Evers, MM, Tran, HD, Zalachoras, I, Meijer, OC, den Dunnen, JT, van Ommen, GJ, *et al.* (2014). Preventing formation of toxic N-terminal huntingtin fragments through antisense oligonucleotide-mediated protein modification. *Nucleic Acid Ther* **24**: 4-12.

26. Toonen, LJA, Rigo, F, van Attikum, H, and van Roon-Mom, WMC (2017). Antisense Oligonucleotide-Mediated Removal of the Polyglutamine Repeat in Spinocerebellar Ataxia Type 3 Mice. *Molecular therapy Nucleic acids* **8**: 232-242.

27. Shitaka, Y, Tran, HT, Bennett, RE, Sanchez, L, Levy, MA, Dikranian, K, *et al.* (2011). Repetitive closed-skull traumatic brain injury in mice causes persistent multifocal axonal injury and microglial reactivity. *Journal of neuropathology and experimental neurology* **70**: 551-567.

28. Brown, GC, and Neher, JJ (2010). Inflammatory neurodegeneration and mechanisms of microglial killing of neurons. *Molecular neurobiology* **41**: 242-247.

29. VanGuilder, HD, Bixler, GV, Brucklacher, RM, Farley, JA, Yan, H, Warrington, JP, *et al.* (2011). Concurrent hippocampal induction of MHC II pathway components and glial activation with advanced aging is not correlated with cognitive impairment. *Journal of neuroinflammation* **8**: 138.

30. Robinson, MD, and Oshlack, A (2010). A scaling normalization method for differential expression analysis of RNA-seq data. *Genome Biology* **11**: R25.

31. Robinson, MD, McCarthy, DJ, and Smyth, GK (2010). edgeR: a Bioconductor package for differential expression analysis of digital gene expression data. *Bioinformatics* **26**: 139-140.

32. Toonen, LJ, Schmidt, I, Luijsterburg, MS, van Attikum, H, and van Roon-Mom, WM (2016). Antisense oligonucleotide-mediated exon skipping as a strategy to reduce proteolytic cleavage of ataxin-3. *Sci Rep* **6**: 35200.

33. Goelz, MF, Mahler, J, Harry, J, Myers, P, Clark, J, Thigpen, JE, *et al.* (1998). Neuropathologic findings associated with seizures in FVB mice. *Laboratory animal science* **48**: 34-37.

34. Altschul, SF, Gish, W, Miller, W, Myers, EW, and Lipman, DJ (1990). Basic local alignment search tool. *Journal of molecular biology* **215**: 403-410.

35. Eskildsen, S, Justesen, J, Schierup, MH, and Hartmann, R (2003). Characterization of the 2'-5'-oligoadenylate synthetase ubiquitin-like family. *Nucleic Acids Res* **31**: 3166-3173.

36. Justesen, J, Hartmann, R, and Kjeldgaard, NO (2000). Gene structure and function of the 2'-5'-oligoadenylate synthetase family. *Cellular and molecular life sciences : CMLS* **57**: 1593-1612.

37. Kramer, A, Green, J, Pollard, J, Jr., and Tugendreich, S (2014). Causal analysis approaches in Ingenuity Pathway Analysis. *Bioinformatics* **30**: 523-530.

38. Huang da, W, Sherman, BT, and Lempicki, RA (2009). Systematic and integrative analysis of large gene lists using DAVID bioinformatics resources. *Nature protocols* **4**: 44-57.

39. Prinz, M, and Priller, J (2014). Microglia and brain macrophages in the molecular age: from origin to neuropsychiatric disease. *Nat Rev Neurosci* **15**: 300-312.

40. Filiano, AJ, Gadani, SP, and Kipnis, J (2015). Interactions of innate and adaptive immunity in brain development and function. *Brain research* **1617**: 18-27.

41. Dalpke, AH, Schafer, MK, Frey, M, Zimmermann, S, Tebbe, J, Weihe, E, *et al.* (2002). Immunostimulatory CpG-DNA activates murine microglia. *Journal of immunology (Baltimore, Md : 1950)* **168**: 4854-4863.

42. Carpentier, PA, Begolka, WS, Olson, JK, Elhofy, A, Karpus, WJ, and Miller, SD (2005). Differential activation of astrocytes by innate and adaptive immune stimuli. *Glia* **49**: 360-374.

43. Hol, EM, and Pekny, M (2015). Glial fibrillary acidic protein (GFAP) and the astrocyte intermediate filament system in diseases of the central nervous system. *Current opinion in cell biology* **32**: 121-130.

44. Aartsma-Rus, A (2017). FDA Approval of Nusinersen for Spinal Muscular Atrophy Makes 2016 the Year of Splice Modulating Oligonucleotides. *Nucleic Acid Ther* **27**: 67-69.

45. Dalpke, AH, Zimmermann, S, Albrecht, I, and Heeg, K (2002). Phosphodiester CpG oligonucleotides as adjuvants: polyguanosine runs enhance cellular uptake and improve immunostimulative activity of phosphodiester CpG oligonucleotides in vitro and in vivo. *Immunology* **106**: 102-112.

46. Burel, SA, Machemer, T, Ragone, FL, Kato, H, Cauntay, P, Greenlee, S, *et al.* (2012). Unique O-methoxyethyl ribose-DNA chimeric oligonucleotide induces an atypical melanoma differentiation-associated gene 5-dependent induction of type I interferon response. *The Journal of pharmacology and experimental therapeutics* **342**: 150-162.

47. Kakuta, S, Shibata, S, and Iwakura, Y (2002). Genomic structure of the mouse 2',5'-oligoadenylate synthetase gene family. *Journal of interferon & cytokine research : the official journal of the International Society for Interferon and Cytokine Research* **22**: 981-993.

48. Chebath, J, Benech, P, Revel, M, and Vigneron, M (1987). Constitutive expression of (2'-5') oligo A synthetase confers resistance to picornavirus infection. *Nature* **330**: 587-588.

49. Silverman, RH (2007). Viral encounters with 2',5'-oligoadenylate synthetase and RNase L during the interferon antiviral response. *Journal of virology* **81**: 12720-12729.

50. Tokarev, A, Skasko, M, Fitzpatrick, K, and Guatelli, J (2009). Antiviral activity of the interferon-induced cellular protein BST-2/tetherin. *AIDS research and human retroviruses* **25**: 1197-1210.

51. Neil, SJ, Zang, T, and Bieniasz, PD (2008). Tetherin inhibits retrovirus release and is antagonized by HIV-1 Vpu. *Nature* **451**: 425-430.

52. Galão, Rui P, Le Tortorec, A, Pickering, S, Kueck, T, and Neil, Stuart JD (2012). Innate Sensing of HIV-1 Assembly by Tetherin Induces NFκB-Dependent Proinflammatory Responses. *Cell Host & Microbe* **12**: 633-644.

53. Matsumoto, M, Kikkawa, S, Kohase, M, Miyake, K, and Seya, T (2002). Establishment of a monoclonal antibody against human Toll-like receptor 3 that blocks double-stranded RNA-mediated signaling. *Biochemical and biophysical research communications* **293**: 1364-1369.

54. Bonow, RH, Aid, S, Zhang, Y, Becker, KG, and Bosetti, F (2009). The brain expression of genes involved in inflammatory response, the ribosome, and learning and memory is altered by centrally injected lipopolysaccharide in mice. *The pharmacogenomics journal* **9**: 116-126.

55. Schmeisser, H, Mejido, J, Balinsky, CA, Morrow, AN, Clark, CR, Zhao, T, *et al.* (2010). Identification of alpha interferon-induced genes associated with antiviral activity in Daudi cells and characterization of IFIT3 as a novel antiviral gene. *Journal of virology* **84**: 10671-10680.

56. Zhou, X, Michal, JJ, Zhang, L, Ding, B, Lunney, JK, Liu, B, *et al.* (2013). Interferon induced IFIT family genes in host antiviral defense. *International journal of biological sciences* **9**: 200-208.

57. Diamond, MS, and Farzan, M (2013). The broad-spectrum antiviral functions of IFIT and IFITM proteins. *Nat Rev Immunol* **13**: 46-57.

58. Pekny, M, Wilhelmsson, U, and Pekna, M (2014). The dual role of astrocyte activation and reactive gliosis. *Neuroscience letters* **565**: 30-38.

59. Liddelow, SA, Guttenplan, KA, Clarke, LE, Bennett, FC, Bohlen, CJ, Schirmer, L, *et al.* (2017). Neurotoxic reactive astrocytes are induced by activated microglia. *Nature* **541**: 481-487.

60. Dalpke, A, and Helm, M (2012). RNA mediated Toll-like receptor stimulation in health and disease. *RNA biology* **9**: 828-842.

61. Robbins, M, Judge, A, Liang, L, McClintock, K, Yaworski, E, and MacLachlan, I (2007). 2'-O-methyl-modified RNAs act as TLR7 antagonists. *Molecular therapy : the journal of the American Society of Gene Therapy* **15**: 1663-1669.

62. Sioud, M, Furset, G, and Cekaite, L (2007). Suppression of immunostimulatory siRNA-driven innate immune activation by 2'-modified RNAs. *Biochemical and biophysical research communications* **361**: 122-126.

63. Senn, JJ, Burel, S, and Henry, SP (2005). Non-CpG-containing antisense 2'-methoxyethyl oligonucleotides activate a proinflammatory response independent of Toll-like receptor 9 or myeloid differentiation factor 88. *The Journal of pharmacology and experimental therapeutics* **314**: 972-979.

64. Diebold, SS, Kaisho, T, Hemmi, H, Akira, S, and Reis e Sousa, C (2004). Innate antiviral responses by means of TLR7-mediated recognition of single-stranded RNA. *Science* **303**: 1529-1531.

65. Xagorari, A, and Chlichlia, K (2008). Toll-like receptors and viruses: induction of innate antiviral immune responses. *The open microbiology journal* **2**: 49-59.

66. Butchi, NB, Pourciau, S, Du, M, Morgan, TW, and Peterson, KE (2008). Analysis of the neuroinflammatory response to TLR7 stimulation in the brain: comparison of multiple TLR7 and/or TLR8 agonists. *Journal of immunology (Baltimore, Md : 1950)* **180**: 7604-7612.

67. Olson, JK, and Miller, SD (2004). Microglia initiate central nervous system innate and adaptive immune responses through multiple TLRs. *Journal of immunology (Baltimore, Md : 1950)* **173**: 3916-3924.

68. Bowman, CC, Rasley, A, Tranguch, SL, and Marriott, I (2003). Cultured astrocytes express toll-like receptors for bacterial products. *Glia* **43**: 281-291.

69. Lafon, M, Megret, F, Lafage, M, and Prehaud, C (2006). The innate immune facet of brain: human neurons express TLR-3 and sense viral dsRNA. *Journal of molecular neuroscience : MN* **29**: 185-194.

70. Ma, Y, Haynes, RL, Sidman, RL, and Vartanian, T (2007). TLR8: an innate immune receptor in brain, neurons and axons. *Cell cycle (Georgetown, Tex)* **6**: 2859-2868.

71. Bryant, CE, and Monie, TP (2012). Mice, men and the relatives: cross-species studies underpin innate immunity. *Open biology* **2**: 120015.

72. Ketloy, C, Engering, A, Srichairatanakul, U, Limsalakpetch, A, Yongvanitchit, K, Pichyangkul, S, *et al.* (2008). Expression and function of Toll-like receptors on dendritic cells and other antigen presenting cells from non-human primates. *Veterinary immunology and immunopathology* **125**: 18-30.

73. Campbell, JD, Cho, Y, Foster, ML, Kanzler, H, Kachura, MA, Lum, JA, *et al.* (2009). CpG-containing immunostimulatory DNA sequences elicit TNF-alpha-dependent toxicity in rodents but not in humans. *The Journal of clinical investigation* **119**: 2564-2576.

74. Weber, C, Muller, C, Podszuweit, A, Montino, C, Vollmer, J, and Forsbach, A (2012). Toll-like receptor (TLR) 3 immune modulation by unformulated small interfering RNA or DNA and the role of CD14 (in TLR-mediated effects). *Immunology* **136**: 64-77.

75. Shen, L, Frazer-Abel, A, Reynolds, PR, Giclas, PC, Chappell, A, Pangburn, MK, *et al.* (2014). Mechanistic understanding for the greater sensitivity of monkeys to antisense oligonucleotide-mediated complement activation compared with humans. *The Journal of pharmacology and experimental therapeutics* **351**: 709-717.

76. Henry, SP, Jagels, MA, Hugli, TE, Manalili, S, Geary, RS, Giclas, PC, *et al.* (2014). Mechanism of alternative complement pathway dysregulation by a phosphorothioate oligonucleotide in monkey and human serum. *Nucleic Acid Ther* **24**: 326-335.

SUPPLEMENTARY FIGURES

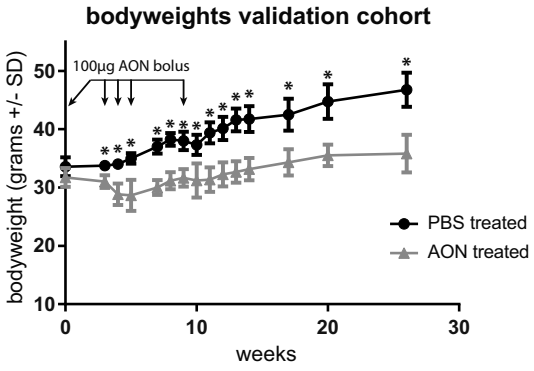

Supplementary Figure 1. Bodyweights of mice in validation cohort. C57BL/6 mice were injected intracerebroventricularly with a total of 500 µg AON during 10 weeks. Significantly reduced bodyweight was observed after each 100 µg AON injection. Mice were sacrificed approximately 4 months after the last AON injection for molecular analysis. Based on 4 PBS injected vs 8 AON injected mice.

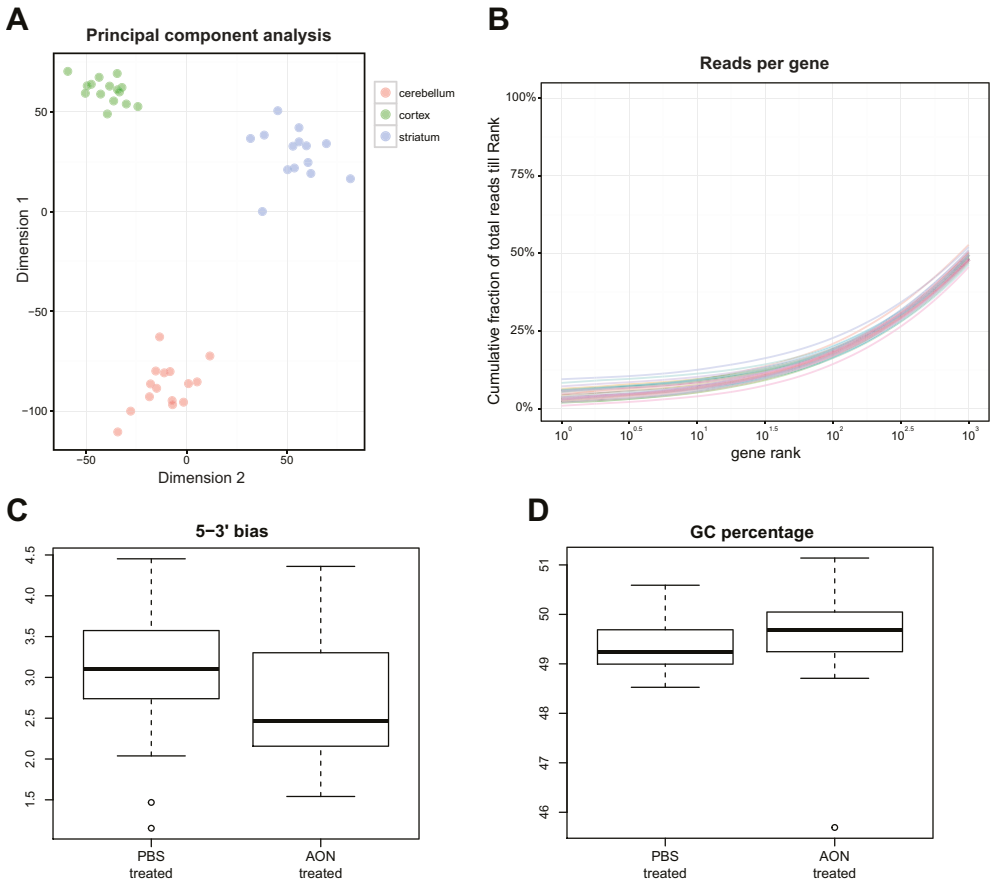

Supplementary Figure 2. RNA sequencing quality control. A) Principal component analysis was performed on normalized gene counts to determine clustering per brain region. Depicted is plot of samples used for differential gene analysis. B) Percentage of total reads per gene shows similar distribution for all 44 RNA sequencing samples. The first 1000 genes sorted on highest read counts are depicted, accounting for approximately 50% of total reads per sample. C) Average 5′ to 3′ read bias per treatment group. D) Average GC percentage of reads per treatment group.

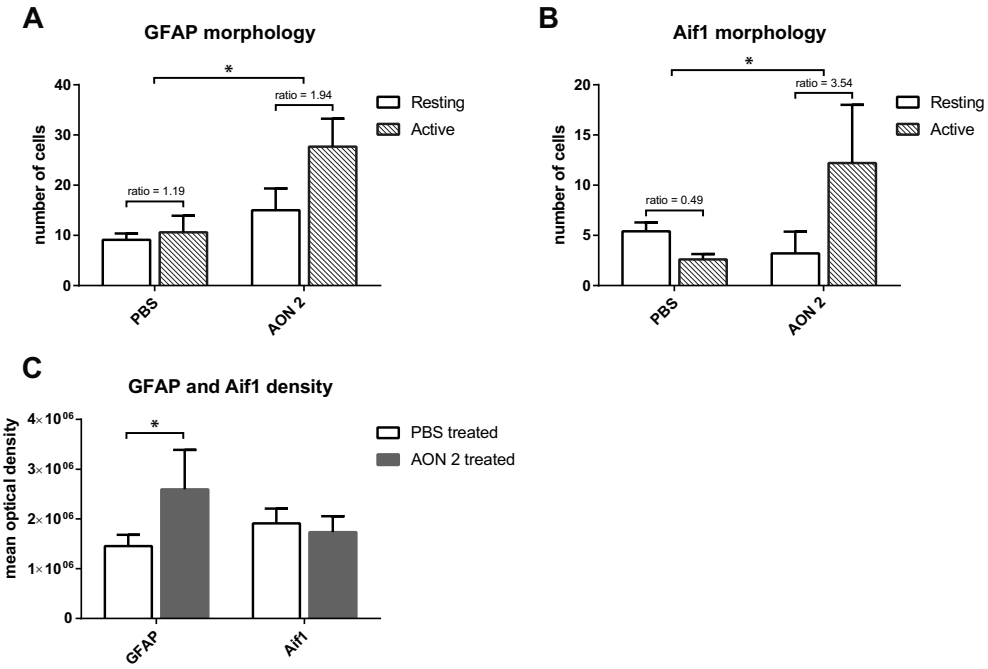

Supplementary Figure 3. Assessment of astrocyte and microglia markers in striatum of AON treated mice. Immunohistological staining was performed for an extra group of mice treated ICV with 665 µg of a different AON (AON 2) from a previous study [24]. AON 2 is also a fully PS backbone, 2'O-methyl modified 19-mer (sequence: GUCCCAUCAUUCAGGUCCAU), designed for splicing modulation of huntingtin, but was shown not to affect murine huntingtin [24]. The PBS treated group is identical as in figure 4. **A**) Based on GFAP based morphology scoring, a significantly increased ratio of activated astrocytes were present in striatum of AON 2 treated mice compared to PBS treated mice. **B**) Significantly increased levels of activated microglia were detected in striatum after treatment with AON 2. **C**) Optical density quantification showed increased levels of GFAP in striatum after AON 2 treatment. Based on 3 sections per mouse and 5 mice per treatment group. * $p < 0.05$ with student's t-test.

SUPPLEMENTARY TABLES

Supplementary Table 1. primers used for ddPCR and ddPCR

Target gene (mouse)	Primer name	Sequence (5′ to 3′)
Nrp2	mNrp2_ex9_fw	AGCCTAAATGGCAAGGACTG
Nrp2	mNrp2_ex10_rev	ATCGAACCTTCGGATGTCAG
Slfn5	mSlfn5_Qex4_Fw	ATGTGTGGAAGACCTGCAGAAG
Slfn5	mSlfn5_Qex5_Rev	AATCTGCGAAGAGGTCCTTG
Trim25	mTrim25_Qex4_Fw	ATGGCTCAGGTAACAAGGGAG
Trim25	mTrim25_Qex6_Rev	GGGAGCAACAGGGGTTTTCTT
Bst2	mBst2_Qex1_Fw	CACAGGCAAACTCCTGCAAC
Bst2	mBst2_Qex3_Rev	TGGTTCAGCTTCGTGACTTC
Ifit3	mIfit3_Qex1_Fw	TTTCCCAGCAGCACAGAAAC
Ifit3	mIfit3_Qex2_Rev	ACTTCAGCTGTGGAAGGATCG
Oasl2	mOASL2_Qex3_Fw	TGAAGAACCTCCTCCGGTTG
Oasl2	mOASL2_Qex4_Rev	TTTTGAGGGCAACACTGCAC
Lgals3bp	mLgals3bp_Qex1_Fw	TGCTGGTTCCAGGGACTCAA
Lgals3bp	mLgals3bp_Qex2_Rev	CCACCGGCCTCTGTAGAAGA
Hprt	mHprt_Qex6_fw	TCCCTGGTTAAGCAGTACAGCC
Hprt	mHprt_Qex7_rev	CGAGAGGTCCTTTTCACCAGC
Actb	mActb_Qex2_Fw	GGCTGTATTCCCCTCCATCG
Actb	mActb_Qex3_Rev	CCAGTTGGTAACAATGCCATGT
Rpl22	mRpl22ex3_fw1	AGGAGTCGTGACCATCGAAC
Rpl22	mRpl22ex3_rev1	TTTGGAGAAAGGCACCTCTG

Supplementary Table 2. Validation of expression changes in striatum

Gene	Log2FC RNA sequencing	Log2FC ddPCR test cohort	Log2FC ddPCR validation cohort
Slfn5	0.8	1.4	NT
Oasl	2.5	2.7	2.8
Ifit3	1.8	1.7	2.4
bst2	2.7	2.1	2.7
Trim25	0.8	1.0	1.2
Lgals3	1.3	0.9	1.4
Nrp2	-1.0	NT	-0.7

The Log2FC for the top differentially expressed genes in striatum of AON treated mice was validated using ddPCR using RNA from the test- and validation cohort. To allow for high throughput, cDNA from mice in the same treatment group were pooled. Test cohort: 4 PBS vs 6 AON treated mice. Validation cohort: 4 PBS vs 8 AON treated mice.

7

Discussion

In this thesis AONs were investigated as a potential therapy for the neurodegenerative disorder SCA3. Currently, only symptomatic treatment is available, and there is thus an immediate need for therapies preventing disease onset and disease progression. The monogenetic nature of SCA3 makes it a good candidate for generation of genetic therapies such as AONs. Additionally, AONs have proven versatile molecules that show particular promise for use in the CNS (chapter 2). In this thesis, we have investigated two different AON based exon skipping therapies for SCA3. In the first approach, the aim was to prevent the formation of toxic polyQ protein fragments by skipping exons encoding the proteolytic cleavage sites (chapter 3). In the second approach we directly targeted the CAG repeat containing exon of *ATXN3* for exclusion, and tested this approach in a SCA3 mouse model (chapter 5). Finally, we assessed potential side effects of phosphorothioate modified AON treatment in the mouse brain with RNA expression profiling (chapter 6). The results obtained in this thesis will be discussed both in the broader context of SCA3 molecular pathogenicity, and with regards to the use of AONs as a potential therapy for SCA3.

RECENT DISCOVERIES ON SCA3 PATHOLOGY

Gain of toxic protein function

Aggregation and formation of neuronal inclusion bodies containing the expanded polyQ protein region was one of the first pathologic hallmarks discovered in SCA3 brain material [1]. In part due to this observation, it was hypothesized that the expanded polyQ region of the mutant protein leads to gain of toxic function, perhaps due to sequestration of other proteins into the aggregates or through direct toxicity of the aggregates themselves. The opposing viewpoint has also been argued, namely that the polyQ expansion induces a loss of ataxin-3 protein function, in turn contributing to pathogenicity. A loss of the deubiquitinating activity of mutant ataxin-3 seems unlikely however, as we and others have shown that mutant ataxin-3 can both bind (chapter 3) and cleave (chapter 5) ubiquitin chains similar to wild-type ataxin-3. Similarly, mutant ataxin-3 can still interact with VCP [2], as well as the DNA damage response proteins RAD23 [3] and PNKP [4, 5]. Since interaction for these proteins with mutant ataxin-3 is retained, this argues against a "loss of wild-type function" pathologic model in SCA3.

In favor of the gain of toxic protein hypothesis, it was for instance recently discovered that mutant ataxin-3 inactivates PNKP, resulting in inefficient DNA repair and culminating in apoptosis [5]. Furthermore, an RNA expression profiling experiment compared a SCA3 mouse containing the mutant human ataxin-3 protein to an *ATXN3* knockout mouse, with the knockout mice showing fewer differentially expressed genes than SCA3 mice [6]. If a loss of ataxin-3 function underlies SCA3 pathogenesis, it would be expected that ataxin-3 knockout mice present with similar affected pathways as transgenic SCA3 mice. Hence, a gain of toxic protein function over loss of ataxin-3 function seems more likely to be the main source of pathogenicity in SCA3.

Role of toxic polyQ fragments

The aim of the experiments described in chapter 3 was to prevent proteolytic cleavage of ataxin-3, in order to reduce cellular toxicity. The reasoning behind this approach ties in with the toxic gain of protein function, as it has been shown that shorter protein fragments containing the polyQ expansion were in fact more toxic than full-length mutant ataxin-3 [7]. Besides displaying increased cellular toxicity, the polyQ fragments also appear to be central to initiation of the aggregation process and subsequent formation of inclusions in cells [8]. It remains to be determined whether the cellular toxicity can be attributed mostly to the ataxin-3 cleavage fragments themselves, or to their initiation of aggregate formation. The two main families of proteolytic enzymes associated with ataxin-3 cleavage are the caspases and calpains. As we reviewed in chapter 1, a greater body of evidence supports the role of calpain generation of toxic ataxin-3 protein fragments. Both the spontaneous generation of the polyQ fragments as well as the cytotoxic effects appear to be highly cell-type specific. In general, polyQ containing protein fragments are generated in non-neuronal cells only when perturbing the cells by artificially inhibiting autophagy or the proteasome. Using induced pluripotent stem cell (IPSc)-derived neurons, Koch and colleagues were able to show that only active neurons were prone to generation of the toxic ataxin-3 cleavage fragments due to calcium influx induced activation of calpains, with subsequent formation of aggregates [9]. As this process was not observed in fibroblasts or glia cells, these experiments provided a possible explanation as to why predominantly neurons are vulnerable to ataxin-3 aggregate formation. These results were however not replicated in more recent studies and thus require further validation [10]. The latest studies in cell models were however able to show that point mutations of 2 calpain sites abolished ataxin-3 fragmentation [11]. Also, transgenic mouse models were used to further establish the initiating role of the polyQ fragment in aggregate formation [12], and inhibition of calpains was shown to diminish mutant ataxin-3 cleavage, nuclear localisation and aggregation [13]. As such, the toxic fragment hypothesis of ataxin-3 is currently well supported, and a central role for calpain cleavage in this process still appears valid.

Recent findings suggest potential involvement of transcriptional dysregulation, as well as RAN and RNA toxicity in SCA3 pathogenicity

Other emerging disease mechanisms

The mechanisms through which ataxin-3 fragments and aggregates exert their cellular toxicity in the brain are still under investigation. Transcriptional dysregulation due to mutant ataxin-3 was already described over a decade ago in SCA3 cells and brain material, where inflammatory gene upregulation was shown [14]. Since this period, subsequent transcriptomic analysis in mouse models have identified potential involvement of glutamatergic neurotransmission, calcium

signalling and MAP kinase pathways [15]. Further, oligodendrocytes were found particularly affected by the process of transcriptional dysregulation, suggesting white matter vulnerability in SCA3 as well [6]. In our transcriptomic studies of the MJD84.2 mouse (chapter 4), we also found evidence suggestive of affected oligodendrocyte function and altered transcription of genes involved in myelination. Potential involvement of the immune system or calcium signalling was however not strong in our dataset. The observed differences between the studies may reflect distinct SCA3 disease stages, since the mice used for our study can be considered presymptomatic. Indeed, we did not detect signs of neurodegenerative or apoptotic processes taking place in the brain transcriptome of SCA3 mice, and we were unable to detect reduced performance in various motor coordination tests. Validation of the transcriptional changes in brain material of SCA3 patients would thus be useful to determine whether the transcriptional alterations we outline in chapter 4 are consistent with the human condition.

Another disease process associated to repeat disorders is repeat associated non-ATG (RAN) translation [16-19] and ribosomal slippage upon repeat translation [20]. Both these processes can result in translation of the CAG repeat in a different reading frame, generating either polySer or polyAla amino acid stretches, or even polyLeu and polyCys stretches for RAN translation of antisense transcripts [17]. These protein stretches, especially polyLeu [21], were shown to be more toxic and aggregation prone in cells compared to polyQ repeats [17]. Interestingly, the RAN proteins were detected in affected brain regions of HD patients, and polyAla accumulation and polySer aggregation were particularly abundant in cells expressing repeats >52 [17]. These findings are interesting when relating them to SCA3, as the repeat length required for RAN protein accumulation to occur in HD corresponds to the pathogenic repeat threshold for SCA3 (>54 CAGs). A logical next step is therefore to probe SCA3 mouse and patient material for presence of the alternative repeat protein stretches and establish whether they are present at levels that may contribute to neurodegeneration.

The aspect of RNA toxicity is also a disease mechanism that may be involved in SCA3. Ling-Bo and colleagues were the first to discover that interrupting the pure CAG repeat of ataxin-3 with CAA codons mitigated toxicity in *Drosophila* [22]. Since a CAA codon also encodes glutamine and the protein expression levels were similar, the observed neuronal degeneration in this experiment was attributed to an RNA effect. Additionally, it was shown that a pathogenic length of CAGs in an untranslated region also conveyed neuronal toxicity [22]. However, RNA foci typically arise for repeat expansion lengths that are beyond what is normally found in SCA3 patients, and hence involvement of RNA toxicity in SCA3 still remains to be reliably established.

SCA3 cell and mouse models

Due to the scarcity of human SCA3 brain material and the limitations this tissue presents in investigating molecular disease mechanisms, the vast majority of knowledge on pathogenic mechanisms have been obtained using SCA3 cell and mouse models. Cell models are typically useful for high throughput screening of therapeutics, as well as discovery of novel molecular effects in response to mutant ataxin-3 expression. Variation in cell culture experiments is

typically very low, due to strictly controlled culturing conditions and absence of cell type induced variation. Conversely, modelling of neurodegenerative disorders in cell culture experiments has been notoriously difficult due to complexity of the brain. As a result, predictive validity of cell culture to the *in vivo* situation is often limited. In case of SCA3, a good example of this limitation is aggregate formation, which must be artificially induced in cell culture and yet spontaneously occurs in SCA3 mouse brain. An important step forward in this regard has been the advent of IPS cells, which can be differentiated into neurons and glial cells hence offer a promising opportunity to more accurately study disease mechanisms of neurodegenerative diseases in cell culture [23]. IPS cell lines for SCA3 have been generated [9, 24], and studies with these cells are currently ongoing. In the research described in this thesis, we have typically used SCA3 patient derived fibroblast to screen AON efficacy. So far, results of *in vitro* AON efficacy has correlated well to the effects observed when infused in the mouse brain (chapter 5). However, a clear limitation of the fibroblasts is their inability to predict AON tolerability in the mammalian brain. As we show in chapter 6, intracerebroventricularly infused AONs in mouse brain can result in immune stimulation which is long lasting and can preclude dosing of AONs to therapeutic levels. Though the extent of AON-induced immune stimulation in the human CNS remains to be established, animal models remain imperative to establish pharmacokinetics and tolerability of new potential therapeutics.

Several SCA3 mouse models have been generated that can be useful for this type of research (reviewed by Gould [25]). Most of the mouse models are generated through exogenous gene expression, i.e. through integration of a human *ATXN3* construct in the mouse genome. To promote an early onset, the mice typically have repeat lengths of over 70 CAGs, and have wide-spread expression of mutant ataxin-3. Nonetheless, phenotypes between the mouse lines differ, and mild to severe phenotypes are reported. So far, SCA3 mouse models suggest a correlation between severity of behavioural abnormalities and presence of ataxin-3 cellular inclusions [25]. In our studies investigating the therapeutic potential of AONs, a SCA3 mouse model (MJD84.2) containing the human *ATXN3* gene with 84 repeats was used [26], as the human sequence as well as introns are required to assess splicing effects. In this mouse model, we did not detect the behavioural deficits (chapter 5 and 6) which were reported originally [26]. Correspondingly, we also did not observe nuclear ataxin-3 inclusions in the brain cells of these mice. We did, however, detect insoluble ataxin-3 protein using filter trap assays in all brain regions we have tested thus far (brainstem, cerebellum and cortex) (chapter 5). Further transcriptomic analysis of brainstem, cerebellum, striatum and cortex revealed that various signalling pathways were affected (chapter 4). However, in the transcriptomic analysis we showed larger transcriptional dysregulation in brainstem compared to cerebellum and cortex, whilst the levels of insoluble ataxin-3 protein was comparable between these brain regions. These observations hint toward brain region specific effects of mutant ataxin-3 at the transcript level, which may be unrelated to insoluble ataxin-3 levels. To further establish this relation a recently developed humanized SCA3 mouse model may thus be useful, though the reported behavioural phenotype appears mild [27]. Similarly, a recently developed knock in SCA3 mouse model where 82 CAGs were inserted into the murine *Atxn3* gene also displayed aggregate pathology, but did not present

with a behavioural phenotype [28]. It hence appears that the SCA3 mouse models most closely mimicking the human situation in terms of expression level and CAG repeat length, do not develop reliable motor phenotypes.

ADVANCES IN ANTISENSE OLIGONUCLEOTIDE THERAPEUTICS

In the research described here we have tested AON based therapies for SCA3. AONs have been used in research settings since the 1960's, but rapid degradation of the phosphodiester bonds by nucleases rendered these molecules initially unsuitable for therapeutic use. A solution to this problem was discovered in 1966 by Fritz Eckstein, who introduced the phosphorothioate (PS) backbone. The PS backbone rendered the AON remarkably resistant to nuclease degradation, and additionally conveyed protein binding properties favourable for *in vivo* use [29]. Together, these properties greatly improved therapeutic viability of the AONs, and the PS backbone is still one of the most commonly used AON modification to this day [30]. The second major step forward in AON modifications came in the form of the sugar group modifications, such as the 2'Ome and MOE modifications, which enhance target affinity, improve uptake and simultaneously reduce toxicity [31]. The drawback of these sugar group modifications, however, is that they are incompatible with RNAse-H target degradation [32], thereby impeding desired downregulation of a target transcript. This issue was subsequently circumvented using the "gapmer" strategy, where a few nucleotides in the central region of the AON contained unmodified sugar groups, hence recovering RNAse-H activation [33]. Making use of these modifications, AONs have proven a particularly useful molecule for application in the CNS (reviewed in chapter 2). In the research described in this thesis, we made use of the commonly used phosphorothioate backbone and both 2'Ome and MOE modifications. These chemistries resulted in similar potency in cell culture experiments following transfection, but the 2'Ome modification resulted in more side effects and lower potency when infused in the mouse brain, in line with previous reports [34]. Since completion of these studies, more recent AON modifications such as 2'Fluoro and Cet have gained traction, and may offer benefits for future clinical application. The potential of these latest AON modifications for use in CNS will be discussed below.

> Decades of research has resulted in an ever-expanding arsenal of AON modifications, which together hold exciting potential for clinical use for neurodegenerative disorders.

Bridged sugar ring modifications

Conformational constraints by bridging of the sugar ring of AONs can achieve similar properties as the other sugar group modifications; they result in an RNA-like structure, rendering them insensitive to RNAse-H, and increase nuclease resistance and especially binding affinity [35]. One of the older modifications belonging to this category is the locked nucleic acid (LNA) [36], but

more recently the 'constrained ethyl' (cET) [37] and Tricyclo DNA (tcDNA) [38] were discovered. The LNA modifications were confirmed to have increased potency, but suffered from significant toxicity [37, 39]. This increased toxicity appears to be a by-product of the high binding affinity, since hepatotoxicity was shown to be the result of off-target RNA degradation [40]. Subcutaneous injections of an LNA modified gapmer AON in a human patient confirmed the toxicity, as acute kidney injury occurred [41]. Due to high binding affinity, LNA efficacy typically occurs at short lengths, such as 13-mers [42]. The major advantage of the bridged ring modifications, their improved binding affinity, hence appears to be their downfall as well due to increased off-target effects. Compromises using so-called mixmers, where for instance LNA modifications are alternated with DNA nucleotides have also been designed, and these molecules show promise for splicing modulation [43]. In order to circumvent the reported toxicity, these mixmers may thus prove useful in future clinical application [44]. Clinical use of cET modified AONs for the treatment of lung cancer have shown good tolerability up to 3 mg/kg upon intravenous administration, but encountered dose limiting toxicity at 4 mg/kg likely due to on-target depletion of STAT3 [45]. Whether cET AONs provide additional clinical benefit compared to the other sugar group modifications thus still remains to be determined. Though already under investigation for almost two decades [46], tcDNA was recently demonstrated to have superior uptake in muscle tissue, be better tolerated than LNA, and was shown to be able to cross the blood brain barrier in modest amounts [47]. Future clinical trials should comprehensively establish tolerability and efficacy of these bridged ring AON modifications, as they offer potentially great benefits for AON efficacy [48]. An intriguing possibility is that AONs making use of the older 2'O-modifications can be combined with the newer bridged sugar ring modifications, in order to maximise the benefits of both chemistries in a single molecule.

Other strategies to improve AON efficacy

New strategies to improve the drug like properties of AONs are still being discovered. One well investigated way to improve the cellular delivery of AONs is by linkage to peptides [49]. In spite of the already favorable distribution and cellular uptake of naked AONs in the CNS, conjugation to peptides may still provide useful properties that improve AON efficacy. Peptides may for instance be of added value in improving endosomal escape of AONs [50], potentially providing better access to the nucleus of brain cells. The endosomal escape of the peptides themselves is currently still a challenging task, however [51]. Also, the added benefit of this strategy is still unclear, since the mechanisms underlying the favorable *in vivo* cellular uptake mechanisms of AONs in the brain are still largely unclear. A second intriguing application of the peptide conjugates may lie in assisting in the crossing of the blood brain barrier by AONs. Currently, AONs for neurodegenerative disorders are injected intrathecally in order to reach the brain [52, 53]. The invasive nature of this procedure as well as the required hospital visits are a burden for the patients, and efforts are therefore made to generate peptide conjugated AONs that can cross the blood brain barrier. For instance, a peptide linked splice modulating PMO for ataxia-telangiectasia showed uptake throughout the mouse brain following intravenous

injection [54]. Similarly, an internalizing peptide linked PMO (pip6a-PMO) was recently generated for potential treatment of spinal muscular atrophy (SMA). Intravenous administration of the pip6a-PMO showed effective splicing modulation of the SMN2 transcript in both peripheral as well as CNS tissue of SMA mice [55]. At present, peptide linked AONs show greater promise for improving uptake in peripheral tissues, such as muscle, rather than in effective crossing of the blood brain barrier. Nonetheless, optimization of peptides may in the future yield molecules capable of crossing the blood brain barrier with better efficiency, potentially warranting systemic administration of AONs targeting the CNS.

Recently 6 alternative genetic polymers, termed xeno-nucleic acids (XNAs), were generated based on nucleic acid architectures not found in nature [56]. These new synthetic polymers can be applied to other nucleic acid architectures and open new possibilities for incorporation of novel physicochemical properties of AONs [56]. Since their discovery XNAs have however not been studied extensively, and their therapeutic potential is thus unclear. Another interesting recent development is the control of AON chirality. For PS-modified siRNAs, a bias in stereochemistry during synthesis was noticed, which modulated siRNA activity [57]. An interesting feature of the PS backbone is that one isomer apparently provides better T_m and RNAse H activation, whilst the other isomer is better at improving nuclease stability [58]. When closely examined for AON gapmers, controlling PS chirality did not appear to provide benefits over stereo-random PS AONs obtained in conventional AON synthesis [59]. In contrast, a recent study did report a more durable *in vivo* response for a specific stereopure gapmer AON [60]. A phase 1b/2a clinical trial (NCT03225833) for HD using a intrathecally injected stereopure AON against a SNP in huntingtin was started in 2017 by Wave Life Sciences, with the expected completion date in September 2019.

In 2014, a strategy to incorporate neutral phosphotriester groups into the phosphate backbone of siRNAs was devised in order to create neutrally charged siRNAs [61]. Potential benefit of these molecules include increased serum stability and absence of innate immune response [61]. Together, the strategies listed above provide new avenues to improve AON drug like properties through a variety of chemical modifications and synthesis strategies. Benefits for CNS application of these strategies will first have to be determined in pre-clinical assessments in rodent and non-human primate experiments.

Recent clinical successes with use of AONs in the central nervous system pave the way for development of AON based treatments for other neurodegenerative disorders.

Lessons from clinical trials with AONs

The past few years have been a stimulating period in AON research for neurodegenerative disorders. Synthesis of AONs on a kilogram scale has become affordable, paving the way for

large clinical application of AONs. The forerunner of AON clinical development in the context of the CNS is undoubtedly the neuromuscular disorder SMA. An AON based splice modulating strategy to increase expression of survival of motor neuron (SMN) protein was devised as a therapeutic strategy for SMA [62]. Since then, increasing preclinical success in SMA mouse models have proved the validity of the strategy, and increasingly efficient AONs were developed to increase SMN protein expression in the CNS [63]. Approximately 10 years after being devised, the AON based therapy (Nusinersen) was successfully tested through intrathecal injection in the first phase 1 study with SMA affected children [64]. An encouraging safety profile and AON half-life in the CSF of 4-6 months warranted further clinical development of Nusinersen [64]. Subsequent phase 2 [65] and phase 3 [66] trials have shown unprecedented success in motor improvement and survival of Nusinersen treated SMA patients. The next landmark event was approval of the AON, now termed Spinraza, by the food and drug administration (FDA) at the end of 2016 [67] and is currently also approved by the European Medicines Agency (EMA). The story of Spinraza has underlined the fact that AONs are a very promising therapeutic tool for use in the CNS, and that meticulous preclinical research on AONs and their design can culminate in clinical success and benefit for patients. The successes obtained in SMA research open the door for other AON based therapies targeting the CNS to continue development, and provide hope for patients of several neurodegenerative disorders currently without treatment.

AON AND GENOME EDITING BASED THERAPY FOR SCA3

Following recent clinical successes with AONs for neuromuscular and CNS disorders, it is useful to consider the possibility of AON based treatment for SCA3 and other polyQ disorders. However, there are also other gene therapy strategies that can be potentially used for SCA3 treatment. Below, the potential of AONs and other gene therapies for the treatment of SCA3 will be discussed.

Potential of CRISPR/Cas treatment for SCA3

Without a doubt the most revolutionary discovery in genome editing in recent years has been the clustered, regularly interspaced, short palindromic repeat (CRISPR) technology. This technology allows RNA-guided nucleases, such as Cas9, to be targeted to specific DNA sequences. The flexibility in genome editing provided by CRISPR/Cas is a major improvement over previous technologies, as only a protospacer adjacent motif (PAM) consisting of NGG nucleotides is required in the target sequence [68]. A guide RNA (gRNA) can be designed to target the nuclease to the gene of interest, and depending on the specific nuclease or nickase used, a double stranded break can be introduced to induce non-homologous end joining or activate the homology directed repair pathways [69]. The system can hence be used to introduce insertions, deletions or frameshifts to induce gene knockout. In the case of homologous recombination, a repair template can be provided to introduce a sequence of interest in the target gene. In recent years a vast number of publications implementing CRISPR/Cas technology in research settings

have appeared [69]. An important question is hence whether this technology can be implemented in a clinical setting for treatment of hereditary neurodegenerative disorders such as SCA3. Since CRISPR/Cas targets the DNA, an important advantage of this technology over AONs is that one time treatment is sufficient to achieve a permanent treatment effect. One immediate difficulty for CRISPR/Cas in the context of the brain is that homology-directed repair is inefficient in G1 state cells [70], and hence in neurons. Non-homologous end joining based DNA repair is however active in post-mitotic cells, and AAV based delivery of Cas9 and guide RNAs in the mouse brain was successfully used to induce frame-shifts and subsequent protein depletion of several targets [71]. It is hence possible to achieve gene knockout *in vivo* in brain cells using this approach. Interestingly, it was recently shown that non-homologous end joining is a viable strategy for transgene insertion in neurons as well, opening the way for insertion strategies in neurons [72]. In the case of SCA3, CRISPR/Cas could most easily be implemented to knock down *ATXN3* expression. Non-allele specific downregulation of huntingtin was recently achieved through CRISPR/Cas in a Huntington mouse model, and successfully alleviated symptoms [73]. Targeting of the expanded CAG repeat of *ATXN3* directly through CRISPR/Cas does not seem possible at this time. It may however be possible to target SNPs associated with the mutant *ATXN3* allele, as SNP specific knockout through CRISPR/Cas is feasible [74]. Apart from similar complications associated with viral delivery as some of the RNAi strategies, the biggest hurdle for clinical application of CRISPR/Cas is currently the risk of off-target effects. In contrast to AONs, genome editing is permanent, and the risk of off-target effects is thus an important concern. Off-target effects of CRISPR/Cas has sparked an ongoing debate in the scientific community, with contradictive reports appearing [75, 76]. Nonetheless, improvements in CRIPR/Cas technology as well as the required delivery methods are continuously being developed, and the technology undoubtedly shows great promise for future therapeutic use.

AON based downregulation versus exon skipping

In this thesis, we have investigated two exon skipping based treatment strategies for SCA3. In the first strategy, we attempted to alleviate cleavage induced toxicity by removal of exons encoding known cleavage sites associated with mutant ataxin-3 toxicity (chapter 3). In the second strategy, we continued on a previously described exon skipping strategy [77] to remove the CAG repeat containing exon from *ATXN3* pre-mRNA. In the latter strategy, ataxin-3 is truncated just upstream of the polyQ repeat, resulting in a theoretically non-toxic protein (chapter 5). Among these two exon skipping strategies, we have concluded that skipping of the repeat containing exon is undoubtedly the preferred strategy for a number of reasons. Firstly, the cleavage sites within ataxin-3 that are associated with toxicity are encoded by the two exons that also encode the ubiquitin interacting motifs (exon 8) as well as the VCP binding site (exon 9). In contrast, skipping of exon 10 retains ataxin-3 ubiquitin binding function. Secondly, exon skipping of the CAG repeat containing exon was exceedingly more efficient than skipping of exons encoding the proteolytic cleavage sites. Thirdly, it is currently still unclear whether removal of the cleavage sites within mutant ataxin-3 truly alleviates toxicity *in vivo*. Lastly, in light of future clinical

application, the use of a single AON against exon 10 is more favourable than the two separate AON sequences required for removal of the cleavage sites from ataxin-3.

From our studies it is therefore clear that *ATXN3* exon 10 skipping is the preferred therapeutic approach. However, other research groups have shown successful downregulation of *ATXN3* transcripts *in vivo* by making use of gapmer AONs [78] or through lentivirus delivered shRNA [79]. A comprehensive evaluation of differences between AONs and RNAi based on viral delivery is beyond the scope of this thesis, but in brief, AONs have an advantage in their delivery and distribution [34], whereas lentiviral or adeno-associated virus (AAV) based delivery of RNAi molecules have the major advantage of requiring only one time or very infrequent treatments [80], though immune stimulation may be an concern [81]. Choosing the best RNAi based therapeutic strategy for SCA3 largely depends on a currently still unanswered question: is downregulation of ataxin-3 tolerated in the human brain for a prolonged period of time? As described in chapter 1, ataxin-3 downregulation or knockout is tolerated in mice, though protein ubiquitination is increased [82, 83]. On the other hand, intracellular signalling and cytoskeletal organisation was affected in human cell culture experiments upon ataxin-3 downregulation [84, 85]. Therefore, exon skipping based removal of the toxic polyQ tract in ataxin-3 is an interesting treatment option. Conversely, *in vivo* exon skipping occurred at higher AON dosages (chapter 5) than those required for downregulation through gapmer AONs [78]. Given these considerations, allele specific downregulation of mutant ataxin-3 may be a preferable therapeutic approach at this time, as in this case wild type ataxin-3 remains available to perform cellular functions, whereas the toxic entity is specifically removed. In this regard, perhaps the most interesting and safest possibility could be to induce preferential exon skipping of exon 10 of mutant *ATXN3* allele by targeting the CAG repeat, as was serendipitously shown in a large AON screening by Liu and colleagues [86]. A potential caveat to this strategy is that the human transcriptome contains many CAG repeat sequences, and off-target effects may thus occur.

Considerations for clinical implementation of SCA3 AONs

Recent successes in clinical trials for HD and especially SMA point to a promising future for clinical use of AONs for treatment of a range of neurodegenerative disorders. There are currently, however, still a few considerations regarding the therapeutic use of AONs. Firstly, clinical trials with AONs have shown good distribution and efficacy in the brains of SMA affected children, but no AON distribution data is as of yet available for the adult human brain. However, given that brain size and CSF flow does not differ greatly between children and adults [87], it is reasonable to assume comparable AON distribution and stability in the adult human brain. A second concern is that the long term effects of exposure of the CNS to AONs are as of yet unclear. Preclinical studies in animals are always comparatively short in duration, whilst treatment of SCA3 patients would in principle require repeated AON dosing during several decades. Currently, children have been treated with the AON drug Spinraza for a period of 15 months, and only adverse events related to the procedure of intrathecal injection were reported [66]. The safety profile of AONs in the brain thus is currently very promising, but long term side effects of continuous

treatment cannot be ruled out yet. Similarly, the actual on-target treatment effect of AONs, such as ataxin-3 protein depletion or truncation through exon skipping, may also induce side effects in the long term. With regards to exon skipping, the ataxin-3 polyQ domain was recently shown to be important in regulation of autophagy [88], and AON mediated removal could thus potentially affect cellular function as well. One advantage of AON mediated therapy in this regard is the fact that an "antidote" complementary AON can be designed in order to bind and inactivate the treatment AON that is already present in cells [89]. Given the reported AON half-life of months, this strategy can be useful if side effects related to AON functional effect arise, and is an advantage over other RNAi and CRISPR/Cas strategies. A last consideration specific to AON based therapy is the high cost of treatment. Treatment for disorders such as SCA3 should arguably be started before onset of symptoms, and would thus require repeated dosing during several decades. With reported costs of Spinraza currently being estimated around €600.000 for the first year and €300.000 for each subsequent year for each patient, insurance companies may not be capable of covering AON based treatments. Nonetheless, treatment prices will likely decline in the future and the many advantages of AONs for use in the CNS will likely assure a place for these molecules in treatment for neurodegenerative disorders.

REFERENCES

1. Paulson, HL, Perez, MK, Trottier, Y, Trojanowski, JQ, Subramony, SH, Das, SS, *et al.* (1997). Intranuclear inclusions of expanded polyglutamine protein in spinocerebellar ataxia type 3. *Neuron* **19**: 333-344.

2. Zhong, X, and Pittman, RN (2006). Ataxin-3 binds VCP/p97 and regulates retrotranslocation of ERAD substrates. *Human molecular genetics* **15**: 2409-2420.

3. Sutton, JR, Blount, JR, Libohova, K, Tsou, WL, Joshi, GS, Paulson, HL, *et al.* (2017). Interaction of the polyglutamine protein ataxin-3 with Rad23 regulates toxicity in Drosophila models of Spinocerebellar Ataxia Type 3. *Human molecular genetics* **26**: 1419-1431.

4. Chatterjee, A, Saha, S, Chakraborty, A, Silva-Fernandes, A, Mandal, SM, Neves-Carvalho, A, *et al.* (2015). The role of the mammalian DNA end-processing enzyme polynucleotide kinase 3'-phosphatase in spinocerebellar ataxia type 3 pathogenesis. *PLoS genetics* **11**: e1004749.

5. Gao, R, Liu, Y, Silva-Fernandes, A, Fang, X, Paulucci-Holthauzen, A, Chatterjee, A, *et al.* (2015). Inactivation of PNKP by mutant ATXN3 triggers apoptosis by activating the DNA damage-response pathway in SCA3. *PLoS genetics* **11**: e1004834.

6. Ramani, B, Panwar, B, Moore, LR, Wang, B, Huang, R, Guan, Y, *et al.* (2017). Comparison of spinocerebellar ataxia type 3 mouse models identifies early gain-of-function, cell-autonomous transcriptional changes in oligodendrocytes. *Human molecular genetics* **26**: 3362-3374.

7. Goti, D, Katzen, SM, Mez, J, Kurtis, N, Kiluk, J, Ben-Haiem, L, *et al.* (2004). A mutant ataxin-3 putative-cleavage fragment in brains of Machado-Joseph disease patients and transgenic mice is cytotoxic above a critical concentration. *The Journal of neuroscience : the official journal of the Society for Neuroscience* **24**: 10266-10279.

8. Haacke, A, Broadley, SA, Boteva, R, Tzvetkov, N, Hartl, FU, and Breuer, P (2006). Proteolytic cleavage of polyglutamine-expanded ataxin-3 is critical for aggregation and sequestration of non-expanded ataxin-3. *Human molecular genetics* **15**: 555-568.

9. Koch, P, Breuer, P, Peitz, M, Jungverdorben, J, Kesavan, J, Poppe, D, *et al.* (2011). Excitation-induced ataxin-3 aggregation in neurons from patients with Machado-Joseph disease. *Nature* **480**: 543-546.

10. Hansen, SK, Stummann, TC, Borland, H, Hasholt, LF, Tumer, Z, Nielsen, JE, *et al.* (2016). Induced pluripotent stem cell - derived neurons for the study of spinocerebellar ataxia type 3. *Stem Cell Res* **17**: 306-317.

11. Weber, JJ, Golla, M, Guaitoli, G, Wanichawan, P, Hayer, SN, Hauser, S, *et al.* (2017). A combinatorial approach to identify calpain cleavage sites in the Machado-Joseph disease protein ataxin-3. *Brain : a journal of neurology*.

12. Hsu, JY, Jhang, YL, Cheng, PH, Chang, YF, Mao, SH, Yang, HI, *et al.* (2017). The Truncated C-terminal Fragment of Mutant ATXN3 Disrupts Mitochondria Dynamics in Spinocerebellar Ataxia Type 3 Models. *Frontiers in molecular neuroscience* **10**: 196.

13. Simoes, AT, Goncalves, N, Koeppen, A, Deglon, N, Kugler, S, Duarte, CB, *et al.* (2012). Calpastatin-mediated inhibition of calpains in the mouse brain prevents mutant ataxin 3 proteolysis, nuclear localization and aggregation, relieving Machado-Joseph disease. *Brain : a journal of neurology* **135**: 2428-2439.

14. Evert, BO, Vogt, IR, Vieira-Saecker, AM, Ozimek, L, de Vos, RA, Brunt, ER, *et al.* (2003). Gene expression profiling in ataxin-3 expressing cell lines reveals distinct effects of normal and mutant ataxin-3. *Journal of neuropathology and experimental neurology* **62**: 1006-1018.

15. Chou, AH, Yeh, TH, Ouyang, P, Chen, YL, Chen, SY, and Wang, HL (2008). Polyglutamine-expanded ataxin-3 causes cerebellar dysfunction of SCA3 transgenic mice by inducing transcriptional dysregulation. *Neurobiology of disease* **31**: 89-101.

16. Zu, T, Gibbens, B, Doty, NS, Gomes-Pereira, M, Huguet, A, Stone, MD, *et al.* (2011). Non-ATG-initiated translation directed by microsatellite expansions. *Proceedings of the National Academy of Sciences of the United States of America* **108**: 260-265.

17. Banez-Coronel, M, Ayhan, F, Tarabochia, AD, Zu, T, Perez, BA, Tusi, SK, *et al.* (2015). RAN Translation in Huntington Disease. *Neuron* **88**: 667-677.

18. Buijsen, R (2016). Fragile X-associated Tremor/Ataxia Syndrome: RNA or RAN? Erasmus University Rotterdam.

19. Cleary, JD, and Ranum, LP (2013). Repeat-associated non-ATG (RAN) translation in neurological disease. *Human molecular genetics* **22**: R45-51.

20. Toulouse, A, Au-Yeung, F, Gaspar, C, Roussel, J, Dion, P, and Rouleau, GA (2005). Ribosomal frameshifting on MJD-1 transcripts with long CAG tracts. *Human molecular genetics* **14**: 2649-2660.

21. Dorsman, JC, Pepers, B, Langenberg, D, Kerkdijk, H, Ijszenga, M, den Dunnen, JT, *et al.* (2002). Strong aggregation and increased toxicity of polyleucine over polyglutamine stretches in mammalian cells. *Human molecular genetics* **11**: 1487-1496.

22. Li, LB, Yu, Z, Teng, X, and Bonini, NM (2008). RNA toxicity is a component of ataxin-3 degeneration in Drosophila. *Nature* **453**: 1107-1111.

23. Dolmetsch, R, and Geschwind, DH (2011). The human brain in a dish: the promise of iPSC-derived neurons. *Cell* **145**: 831-834.

24. Hansen, SK, Borland, H, Hasholt, LF, Tumer, Z, Nielsen, JE, Rasmussen, MA, *et al.* (2016). Generation of spinocerebellar ataxia type 3 patient-derived induced pluripotent stem cell line SCA3.A11. *Stem Cell Res* **16**: 553-556.

25. Colomer Gould, VF (2012). Mouse models of spinocerebellar ataxia type 3 (Machado-Joseph disease). *Neurotherapeutics : the journal of the American Society for Experimental NeuroTherapeutics* **9**: 285-296.

26. Cemal, CK, Carroll, CJ, Lawrence, L, Lowrie, MB, Ruddle, P, Al-Mahdawi, S, *et al.* (2002). YAC transgenic mice carrying pathological alleles of the MJD1 locus exhibit a mild and slowly progressive cerebellar deficit. *Human molecular genetics* **11**: 1075-1094.

27. Switonski, PM, Szlachcic, WJ, Krzyzosiak, WJ, and Figiel, M (2015). A new humanized ataxin-3 knock-in mouse model combines the genetic features, pathogenesis of neurons and glia and late disease onset of SCA3/MJD. *Neurobiology of disease* **73**: 174-188.

28. Ramani, B, Harris, GM, Huang, R, Seki, T, Murphy, GG, Costa Mdo, C, *et al.* (2015). A knockin mouse model of spinocerebellar ataxia type 3 exhibits prominent aggregate pathology and aberrant splicing of the disease gene transcript. *Human molecular genetics* **24**: 1211-1224.

29. Eckstein, F (1985). Nucleoside phosphorothioates. *Annual review of biochemistry* **54**: 367-402.

30. Eckstein, F (2014). Phosphorothioates, essential components of therapeutic oligonucleotides. *Nucleic acid therapeutics* **24**: 374-387.

31. Agrawal, S, Jiang, Z, Zhao, Q, Shaw, D, Cai, Q, Roskey, A, *et al.* (1997). Mixed-backbone oligonucleotides as second generation antisense oligonucleotides: in vitro and in vivo studies. *Proceedings of the National Academy of Sciences of the United States of America* **94**: 2620-2625.

32. Sproat, BS, Lamond, AI, Beijer, B, Neuner, P, and Ryder, U (1989). Highly efficient chemical synthesis of 2'-O-methyloligoribonucleotides and tetrabiotinylated derivatives; novel probes that are resistant to degradation by RNA or DNA specific nucleases. *Nucleic acids research* **17**: 3373-3386.

33. Monia, BP, Lesnik, EA, Gonzalez, C, Lima, WF, McGee, D, Guinosso, CJ, *et al.* (1993). Evaluation of 2'-modified oligonucleotides containing 2'-deoxy gaps as antisense inhibitors of gene expression. *The Journal of biological chemistry* **268**: 14514-14522.

34. Rigo, F, Chun, SJ, Norris, DA, Hung, G, Lee, S, Matson, J, *et al.* (2014). Pharmacology of a central nervous system delivered 2'-O-methoxyethyl-modified survival of motor neuron splicing oligonucleotide in mice and nonhuman primates. *The Journal of pharmacology and experimental therapeutics* **350**: 46-55.

35. Owczarzy, R, You, Y, Groth, CL, and Tataurov, AV (2011). Stability and mismatch discrimination of locked nucleic acid-DNA duplexes. *Biochemistry* **50**: 9352-9367.

36. Braasch, DA, and Corey, DR (2001). Locked nucleic acid (LNA): fine-tuning the recognition of DNA and RNA. *Chemistry & Biology* **8**: 1-7.

37. Seth, PP, Siwkowski, A, Allerson, CR, Vasquez, G, Lee, S, Prakash, TP, *et al.* (2009). Short antisense oligonucleotides with novel 2'-4' conformationaly restricted nucleoside analogues show improved potency without increased toxicity in animals. *Journal of medicinal chemistry* **52**: 10-13.

38. Ittig, D, Liu, S, Renneberg, D, Schumperli, D, and Leumann, CJ (2004). Nuclear antisense effects in cyclophilin A pre-mRNA splicing by oligonucleotides: a comparison of tricyclo-DNA with LNA. *Nucleic acids research* **32**: 346-353.

39. Swayze, EE, Siwkowski, AM, Wancewicz, EV, Migawa, MT, Wyrzykiewicz, TK, Hung, G, *et al.* (2007). Antisense oligonucleotides containing locked nucleic acid improve potency but cause significant hepatotoxicity in animals. *Nucleic acids research* **35**: 687-700.

40. Burel, SA, Hart, CE, Cauntay, P, Hsiao, J, Machemer, T, Katz, M, *et al.* (2016). Hepatotoxicity of high affinity gapmer antisense oligonucleotides is mediated by RNase H1 dependent promiscuous reduction of very long pre-mRNA transcripts. *Nucleic acids research* **44**: 2093-2109.

41. van Poelgeest, EP, Swart, RM, Betjes, MGH, Moerland, M, Weening, JJ, Tessier, Y, *et al.* (2013). Acute Kidney Injury During Therapy With an Antisense Oligonucleotide Directed Against PCSK9. *American Journal of Kidney Diseases* **62**: 796-800.

42. Shimo, T, Tachibana, K, Saito, K, Yoshida, T, Tomita, E, Waki, R, *et al.* (2014). Design and evaluation of locked nucleic acid-based splice-switching oligonucleotides in vitro. *Nucleic acids research* **42**: 8174-8187.

43. Touznik, A, Maruyama, R, Hosoki, K, Echigoya, Y, and Yokota, T (2017). LNA/DNA mixmer-based antisense oligonucleotides correct alternative splicing of the SMN2 gene and restore SMN protein expression in type 1 SMA fibroblasts. *Scientific Reports* **7**: 3672.

44. Bianchini, D, Omlin, A, Pezaro, C, Lorente, D, Ferraldeschi, R, Mukherji, D, *et al.* (2013). First-in-human Phase I study of EZN-4176, a locked nucleic acid antisense oligonucleotide to exon 4 of the androgen receptor mRNA in patients with castration-resistant prostate cancer. *British journal of cancer* **109**: 2579-2586.

45. Hong, D, Kurzrock, R, Kim, Y, Woessner, R, Younes, A, Nemunaitis, J, *et al.* (2015). AZD9150, a next-generation antisense oligonucleotide inhibitor of STAT3 with early evidence of clinical activity in lymphoma and lung cancer. *Sci Transl Med* **7**: 314ra185.

46. Steffens, R, and Leumann, CJ (1999). Synthesis and Thermodynamic and Biophysical Properties of Tricyclo-DNA. *Journal of the American Chemical Society* **121**: 3249-3255.

47. Goyenvalle, A, Griffith, G, Babbs, A, El Andaloussi, S, Ezzat, K, Avril, A, *et al.* (2015). Functional correction in mouse models of muscular dystrophy using exon-skipping tricyclo-DNA oligomers. *Nature medicine* **21**: 270-275.

48. Goyenvalle, A, Leumann, C, and Garcia, L (2016). Therapeutic Potential of Tricyclo-DNA antisense oligonucleotides. *Journal of neuromuscular diseases* **3**: 157-167.

49. Zou, LL, Ma, JL, Wang, T, Yang, TB, and Liu, CB (2013). Cell-penetrating Peptide-mediated therapeutic molecule delivery into the central nervous system. *Current neuropharmacology* **11**: 197-208.

50. Boisguerin, P, Deshayes, S, Gait, MJ, O'Donovan, L, Godfrey, C, Betts, CA, *et al.* (2015). Delivery of therapeutic oligonucleotides with cell penetrating peptides. *Advanced drug delivery reviews* **87**: 52-67.

51. Erazo-Oliveras, A, Muthukrishnan, N, Baker, R, Wang, TY, and Pellois, JP (2012). Improving the endosomal escape of cell-penetrating peptides and their cargos: strategies and challenges. *Pharmaceuticals (Basel, Switzerland)* **5**: 1177-1209.

52. Hache, M, Swoboda, KJ, Sethna, N, Farrow-Gillespie, A, Khandji, A, Xia, S, *et al.* (2016). Intrathecal Injections in Children With Spinal Muscular Atrophy: Nusinersen Clinical Trial Experience. *Journal of child neurology* **31**: 899-906.

53. Miller, TM, Pestronk, A, David, W, Rothstein, J, Simpson, E, Appel, SH, *et al.* (2013). An antisense oligonucleotide against SOD1 delivered intrathecally for patients with SOD1 familial amyotrophic lateral sclerosis: a phase 1, randomised, first-in-man study. *Lancet Neurol* **12**: 435-442.

54. Du, L, Kayali, R, Bertoni, C, Fike, F, Hu, H, Iversen, PL, *et al.* (2011). Arginine-rich cell-penetrating peptide dramatically enhances AMO-mediated ATM aberrant splicing correction and enables delivery to brain and cerebellum. *Human molecular genetics* **20**: 3151-3160.

55. Hammond, SM, Hazell, G, Shabanpoor, F, Saleh, AF, Bowerman, M, Sleigh, JN, *et al.* (2016). Systemic peptide-mediated oligonucleotide therapy improves long-term survival in spinal muscular atrophy. *Proceedings of the National Academy of Sciences of the United States of America* **113**: 10962-10967.

56. Pinheiro, VB, Taylor, AI, Cozens, C, Abramov, M, Renders, M, Zhang, S, *et al.* (2012). Synthetic genetic polymers capable of heredity and evolution. *Science* **336**: 341-344.

57. Jahns, H, Roos, M, Imig, J, Baumann, F, Wang, Y, Gilmour, R, *et al.* (2015). Stereochemical bias introduced during RNA synthesis modulates the activity of phosphorothioate siRNAs **6**: 6317.

58. Koziolkiewicz, M, Krakowiak, A, Kwinkowski, M, Boczkowska, M, and Stec, WJ (1995). Stereodifferentiation--the effect of P chirality of oligo(nucleoside phosphorothioates) on the activity of bacterial RNase H. *Nucleic acids research* **23**: 5000-5005.

59. Wan, WB, Migawa, MT, Vasquez, G, Murray, HM, Nichols, JG, Gaus, H, *et al.* (2014). Synthesis, biophysical properties and biological activity of second generation antisense oligonucleotides containing chiral phosphorothioate linkages. *Nucleic acids research* **42**: 13456-13468.

60. Iwamoto, N, Butler, DCD, Svrzikapa, N, Mohapatra, S, Zlatev, I, Sah, DWY, *et al.* (2017). Control of phosphorothioate stereochemistry substantially increases the efficacy of antisense oligonucleotides. *Nat Biotechnol* **35**: 845-851.

61. Meade, BR, Gogoi, K, Hamil, AS, Palm-Apergi, C, van den Berg, A, Hagopian, JC, *et al.* (2014). Efficient delivery of RNAi prodrugs containing reversible charge-neutralizing phosphotriester backbone modifications. *Nat Biotechnol* **32**: 1256-1261.

62. Singh, NK, Singh, NN, Androphy, EJ, and Singh, RN (2006). Splicing of a critical exon of human Survival Motor Neuron is regulated by a unique silencer element located in the last intron. *Molecular and cellular biology* **26**: 1333-1346.

63. Burghes, AH, and McGovern, VL (2010). Antisense oligonucleotides and spinal muscular atrophy: skipping along. *Genes & development* **24**: 1574-1579.

64. Chiriboga, CA, Swoboda, KJ, Darras, BT, Iannaccone, ST, Montes, J, De Vivo, DC, *et al.* (2016). Results from a phase 1 study of nusinersen (ISIS-SMN(Rx)) in children with spinal muscular atrophy. *Neurology* **86**: 890-897.

65. Finkel, RS, Chiriboga, CA, Vajsar, J, Day, JW, Montes, J, De Vivo, DC, *et al.* (2016). Treatment of infantile-onset spinal muscular atrophy with nusinersen: a phase 2, open-label, dose-escalation study. *Lancet* **388**: 3017-3026.

66. Finkel, R, Kuntz, N, Mercuri, E, Chiriboga, CA, Darras, B, Topaloglu, H, *et al.* (2017). Efficacy and safety of nusinersen in infants with spinal muscular atrophy (SMA): Final results from the phase 3 ENDEAR study. *European Journal of Paediatric Neurology* **21**: e14-e15.

67. Ottesen, EW (2017). ISS-N1 makes the First FDA-approved Drug for Spinal Muscular Atrophy. *Translational neuroscience* **8**: 1-6.

68. Mojica, FJ, Diez-Villasenor, C, Garcia-Martinez, J, and Almendros, C (2009). Short motif sequences determine the targets of the prokaryotic CRISPR defence system. *Microbiology (Reading, England)* **155**: 733-740.

69. Sander, JD, and Joung, JK (2014). CRISPR-Cas systems for editing, regulating and targeting genomes. *Nat Biotech* **32**: 347-355.

70. Orthwein, A, Noordermeer, SM, Wilson, MD, Landry, S, Enchev, RI, Sherker, A, *et al.* (2015). A mechanism for the suppression of homologous recombination in G1 cells. *Nature* **528**: 422-426.

71. Swiech, L, Heidenreich, M, Banerjee, A, Habib, N, Li, Y, Trombetta, J, *et al.* (2015). In vivo interrogation of gene function in the mammalian brain using CRISPR-Cas9. *Nat Biotech* **33**: 102-106.

72. Suzuki, K, Tsunekawa, Y, Hernandez-Benitez, R, Wu, J, Zhu, J, Kim, EJ, *et al.* (2016). In vivo genome editing via CRISPR/Cas9 mediated homology-independent targeted integration. *Nature* **540**: 144-149.

73. Yang, S, Chang, R, Yang, H, Zhao, T, Hong, Y, Kong, HE, *et al.* (2017). CRISPR/Cas9-mediated gene editing ameliorates neurotoxicity in mouse model of Huntington's disease. *The Journal of Clinical Investigation* **127**: 2719-2724.

74. Yoshimi, K, Kaneko, T, Voigt, B, and Mashimo, T (2014). Allele-specific genome editing and correction of disease-associated phenotypes in rats using the CRISPR–Cas platform **5**: 4240.

75. Cho, SW, Kim, S, Kim, Y, Kweon, J, Kim, HS, Bae, S, *et al.* (2014). Analysis of off-target effects of CRISPR/Cas-derived RNA-guided endonucleases and nickases. *Genome research* **24**: 132-141.

76. Schaefer, KA, Wu, W-H, Colgan, DF, Tsang, SH, Bassuk, AG, and Mahajan, VB (2017). Unexpected mutations after CRISPR-Cas9 editing in vivo. *Nat Meth* **14**: 547-548.

77. Evers, MM, Tran, HD, Zalachoras, I, Pepers, BA, Meijer, OC, den Dunnen, JT, *et al.* (2013). Ataxin-3 protein modification as a treatment strategy for spinocerebellar ataxia type 3: removal of the CAG containing exon. *Neurobiology of disease* **58**: 49-56.

78. Moore, LR, Rajpal, G, Dillingham, IT, Qutob, M, Blumenstein, KG, Gattis, D, *et al.* (2017). Evaluation of Antisense Oligonucleotides Targeting ATXN3 in SCA3 Mouse Models. *Molecular therapy Nucleic acids* **7**: 200-210.

79. Alves, S, Nascimento-Ferreira, I, Auregan, G, Hassig, R, Dufour, N, Brouillet, E, *et al.* (2008). Allele-specific RNA silencing of mutant ataxin-3 mediates neuroprotection in a rat model of Machado-Joseph disease. *PloS one* **3**: e3341.

80. Boudreau, RL, Rodriguez-Lebron, E, and Davidson, BL (2011). RNAi medicine for the brain: progresses and challenges. *Human molecular genetics* **20**: R21-27.

81. Hareendran, S, Balakrishnan, B, Sen, D, Kumar, S, Srivastava, A, and Jayandharan, GR (2013). Adeno-associated virus (AAV) vectors in gene therapy: immune challenges and strategies to circumvent them. *Reviews in medical virology* **23**: 399-413.

82. Schmitt, I, Linden, M, Khazneh, H, Evert, BO, Breuer, P, Klockgether, T, *et al.* (2007). Inactivation of the mouse Atxn3 (ataxin-3) gene increases protein ubiquitination. *Biochemical and biophysical research communications* **362**: 734-739.

83. Switonski, PM, Fiszer, A, Kazmierska, K, Kurpisz, M, Krzyzosiak, WJ, and Figiel, M (2011). Mouse ataxin-3 functional knock-out model. *Neuromolecular Med* **13**: 54-65.

84. Rodrigues, A-J, do Carmo Costa, M, Silva, T-L, Ferreira, D, Bajanca, F, Logarinho, E, *et al.* (2010). Absence of ataxin-3 leads to cytoskeletal disorganization and increased cell death. *Biochimica et Biophysica Acta (BBA) - Molecular Cell Research* **1803**: 1154-1163.

85. Neves-Carvalho, A, Logarinho, E, Freitas, A, Duarte-Silva, S, Costa Mdo, C, Silva-Fernandes, A, *et al.* (2015). Dominant negative effect of polyglutamine expansion perturbs normal function of ataxin-3 in neuronal cells. *Human molecular genetics* **24**: 100-117.

86. Liu, J, Yu, D, Aiba, Y, Pendergraff, H, Swayze, EE, Lima, WF, *et al.* (2013). ss-siRNAs allele selectively inhibit ataxin-3 expression: multiple mechanisms for an alternative gene silencing strategy. *Nucleic acids research* **41**: 9570-9583.

87. Cutler, RW, Page, L, Galicich, J, and Watters, GV (1968). Formation and absorption of cerebrospinal fluid in man. *Brain : a journal of neurology* **91**: 707-720.

88. Ashkenazi, A, Bento, CF, Ricketts, T, Vicinanza, M, Siddiqi, F, Pavel, M, *et al.* (2017). Polyglutamine tracts regulate beclin 1-dependent autophagy. *Nature* **545**: 108-111.

89. Crosby, JR, Zhao, C, Zhang, H, MacLeod, AR, Guo, S, and Monia, BP (2015). Reversing Antisense Oligonucleotide Activity with a Sense Oligonucleotide Antidote: Proof of Concept Targeting Prothrombin. *Nucleic acid therapeutics* **25**: 297-305.

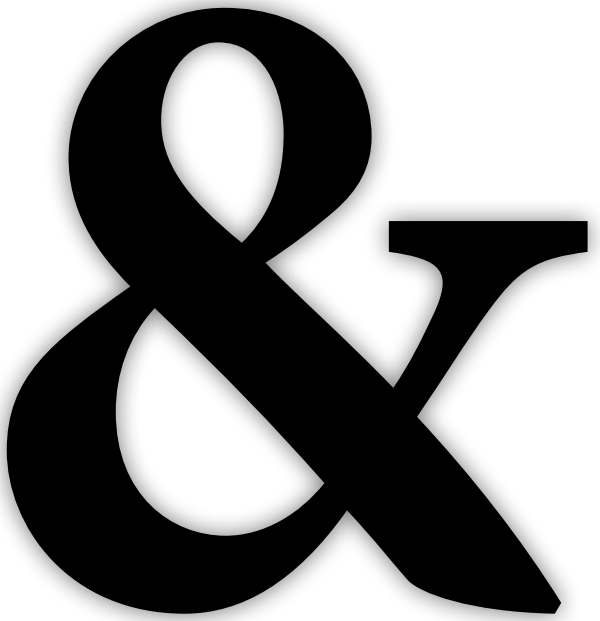

Nederlandse samenvatting
List of publications
Curriculum Vitae
Dankwoord

NEDERLANDSE SAMENVATTING

Spinocerebellaire ataxie type 3 (SCA3) is een erfelijke neurodegeneratieve aandoening waarbij de symptomen zich meestal tussen het 30e en 50e levensjaar presenteren. Met name de hersenstam en het cerebellum (de kleine hersenen) worden aangetast tijdens het SCA3 ziekteproces. Met een incidentie van ongeveer 1:100.000 is SCA3 vrij zeldzaam, maar komt wel over de gehele wereld voor. SCA3 is uiteindelijk fataal en er is momenteel geen medicijn dat de ziekte kan vertragen of voorkomen. Het onderzoek beschreven in dit proefschrift is gericht op het onderzoeken van antisense oligonucleotiden (AONs) als potentiële behandeling voor SCA3.

In **hoofdstuk 1** worden de ziekte veroorzakende mechanismen van SCA3 beschreven. SCA3 behoort tot de zogenaamde polyglutamine (polyQ) aandoeningen, welke veroorzaakt worden door eenzelfde soort verandering: een verlenging van een CAG herhaling in de coderende regio van een gen. Bij SCA3 ligt de verlengde CAG herhaling in het *ATXN3* gen en is deze verlengd tot meer dan 50 herhalingen. De CAG herhaling in het DNA wordt in de cel vertaald naar een glutamine aminozuur in het ataxine-3 eiwit. Het veranderde ataxine-3 eiwit zorgt met name in hersenencellen voor problemen, welke zich uiteindelijk manifesteren als de symptomen van SCA3. De exacte manier waarop het mutante ataxine-3 eiwit in de cel voor toxiciteit zorgt is nog niet achterhaald, maar er zijn wel een aantal mechanismen bekend. Zo is ontdekt dat het mutante ataxine-3 eiwit door enzymen in de cel wordt geknipt waardoor korte eiwitfragmenten, die de polyQ regio bevatten, vrijkomen. Deze korte eiwitfragmenten zijn schadelijker voor cellen dan het volledige ataxine-3 eiwit en spelen dus mogelijk een belangrijke rol bij het veroorzaken van de cellulaire toxiciteit. Daarnaast is bekend dat er in hersencellen van SCA3 patiënten ataxine-3 eiwitklonten ontstaan. Het is momenteel niet duidelijk of deze eiwitklonten bijdragen aan toxiciteit in de hersencellen, of dat de eiwitklonten juist ontstaan ter bescherming van de cel. Verder is gebleken dat mutant ataxine-3 leidt tot verstoring van de eiwitafbraak in de cel, door inhibitie van het proteasoom en autofagie, wat dus ook bij kan dragen aan de ophoping van ataxine-3 eiwitklonten.

Omdat SCA3 wordt veroorzaakt door een bekende genetische verandering, is de aandoening een goede kandidaat voor genetische therapieën. Een van de genetische therapieën waarvan de klinische toepassingen in de laatste jaren grote ontwikkelingen heeft doorgemaakt zijn de antisense oligonucleotiden (AONs). In **hoofdstuk 2** worden deze moleculen uitgebreid besproken in de context van het centrale zenuwstelsel. Het grote voordeel van het behandelen van het centrale zenuwstelsel met AONs is dat deze moleculen goed worden opgenomen door hersencellen en tevens maanden aanwezig en actief blijven in de cel. AONs bestaan uit kunstmatige stukjes DNA of RNA, welke op verschillende manieren met RNA kunnen interacteren. Zo kunnen AONs een bepaald RNA in de cel laten afbreken zodat het eiwit dat hieruit gecodeerd wordt, niet meer gevormd wordt. In dit proefschrift wordt echter onderzoek gedaan naar een AON toepassing waarbij de splicing van het RNA wordt beïnvloed. Bij het proces van splicing wordt bepaald welke exonen (de coderende regio's van het DNA) worden vertaald naar eiwit. AONs kunnen de splicingsignalen in exonen maskeren, zodat dit exon uit

het RNA wordt gespliced. Deze techniek, het zogenaamde exon skippen, kan er zo dus voor zorgen dat vorming van bepaalde eiwitregio's wordt voorkomen.

In **hoofstuk 3** hebben we een AON gebaseerde exon skip strategie onderzocht die erop gericht is om het enzymatisch knippen van ataxine-3 in de cel te verminderen. Wanneer het mutante ataxine-3 namelijk niet meer geknipt wordt, zullen de toxische polyQ fragmenten van ataxine-3 niet meer vrijkomen. Om dit teweeg te brengen, hebben we AONs ontworpen tegen exon 8 en 9 van het *ATXN3* gen, welke de toxische proteolytische kniplocaties in het ataxine-3 eiwit coderen. AON gemedieerde skip van exon 8 en 9 leidde inderdaad tot vorming van het verwachte gemodificeerde ataxine-3 eiwit. De AON efficiëntie was echter laag, dus de functionele tests met het gemodificeerde eiwit zijn met constructen en gezuiverd eiwit productie technieken onderzocht. Uit proteolytische reacties met caspase en calpaine-2 enzymen bleek dat het gemodificeerde ataxine-3 eiwit inderdaad resistenter was voor caspase degradatie, maar er werd geen effect op calpaine-2 proteolyse van ataxine-3 vastgesteld. Uit dit onderzoek concluderen we dan ook dat het skippen van exon 8 en 9 van *ATXN3* waarschijnlijk geen goede therapeutische strategie is.

Voordat AON gebaseerde therapeutische strategieën getest kunnen worden in patiënten, moet de validiteit van de aanpak eerst bewezen worden in diermodellen. Het eerste testmodel hiervoor is veelal een transgene muis en in **hoofdstuk 4** is dan ook een transgeen SCA3 muismodel onderzocht. Dit muismodel is reeds in 2001 gegenereerd en bevat het volledige humane *ATXN3* gen met 84 CAG herhalingen. Om het moleculaire ziekteproces van dit muismodel in kaart te brengen, hebben we gebruik gemaakt van een multi-omic aanpak. Hiervoor zijn verschillende hersenregio's en bloedmonsters van de muizen geïsoleerd en onderzocht door middel van RNA sequencing. Met RNA sequencing kan worden vastgesteld welke genen anders tot expressie komen door toedoen van het mutante ataxine-3 eiwit. Uit deze analyses bleek dat het striatum en de hersenstam veel genexpressie veranderingen lieten zien in de transgene SCA3 muizen, terwijl in cortex en cerebellum relatief weinig expressie verschillen plaatsvonden. De betrokken genexpressie veranderingen wijzen op aangetaste CREB en α-adrenergische signaling pathways. Deze twee pathways hebben een belangrijke rol in het functioneren van neuronale cellen en zouden dus deels ten grondslag kunnen liggen aan het SCA3 ziekteproces. Deze signaling pathways waren echter niet sterk genoeg aangetast om te leiden tot motorische evenwichtsproblemen in de muizen.

De transgene SCA3 muis is in **hoofdstuk 5** gebruikt voor het testen van een AON gebaseerde therapie waarmee de toxische polyQ regio uit het ataxine-3 eiwit wordt verwijderd. Hiervoor werden een viertal AONs ontworpen om exon 10 van het *ATXN3* gen te skippen. Door het skippen van dit exon wordt de toxische polyQ regio uit ataxine-3 verwijderd, echter zorgt het ook voor een frameshift waardoor een stopcodon wordt geïntroduceerd. Het ataxine-3 eiwit dat uit dit gemodificeerde transcript wordt gevormd (ataxine-3 Δ C-terminus) is dus verkort en bevat geen polyQ regio meer. Ataxine-3 Δ C-terminus zal dan ook naar verwachting niet toxisch zijn voor cellen. De meest efficiënte AON (10.4) werd herhaaldelijk in het laterale hersenventrikel van de SCA3 muizen geïnjecteerd. Uit analyse van het hersenweefsel van de muizen behandeld met AON 10.4 bleek dat de AON aanwezig was in alle hersenregio's. Ook

het behandeleffect, zijnde vorming van het ataxine-3 Δ C-terminus eiwit, werd aangetroffen in alle geteste hersenregio's. Behandeling met AON 10.4 resulteerde in verminderde hoeveelheid onoplosbaar ataxine-3, alsmede verminderde ataxine-3 lokalisatie in de celkern. Aangezien beide processen kenmerken zijn van ataxine-3 toxiciteit, lijkt exon 10 skippen een veelbelovende behandeling voor SCA3 te zijn.

AONs kunnen gemaakt worden met verschillende chemische modificaties. Uit verschillende pilot experimenten in ons lab is gebleken dat 2'Ome gemodificeerde AONs minder goed worden verdragen in de muizenhersenen dan MOE gemodificeerde AONs (zoals gebruikt in hoofdstuk 5). Om deze reden hebben we in **hoofdstuk 6** door middel van een RNA sequencing aanpak onderzocht welke processen ten grondslag liggen aan de bijwerkingen van 2'Ome AONs in muizenhersenen. In de hersenen van muizen behandeld met de 2'Ome AON was een duidelijke verhoogde expressie van immuunsysteemgenen waar te nemen, met name in het striatum. Daarnaast bleken de twee celtypes die belangrijk zijn voor een immuunreactie in de hersenen, microglia en astrocyten, geactiveerd te zijn in reactie op aanwezigheid van de AON. Uit deze studie valt dan ook te concluderen dat 2'Ome AONs leiden tot activatie van het immuunsysteem in muizenhersenen, wat wellicht een deel van de bijwerkingen verklaart.

In dit proefschrift hebben we aangetoond dat AONs veelbelovende eigenschappen hebben voor mogelijke behandeling van SCA3. In **hoofdstuk 7** worden de resultaten uit dit proefschrift besproken en gerelateerd aan de huidige kennis m.b.t. AON onderzoek en klinische trials. In dit proefschrift wordt beschreven dat exon skippen van het CAG-bevattende exon in ataxine-3 haalbaar is in hersencellen van een muis. Echter hebben andere onderzoeksgroepen gedemonstreerd dat het downreguleren van ataxine-3 met AONs eveneens mogelijk is. In tegenstelling tot exon skippen zorgt downregulatie ervoor dat het ataxine-3 eiwit in het geheel niet gevormd wordt. Het voordeel van exon skippen is dat de ataxine-3 eiwitfunctie behouden blijft, terwijl het voordeel van de downregulatie is dat er lagere concentraties AON nodig lijken te zijn voor een efficiënt therapeutisch effect. Er wordt momenteel ook onderzoek gedaan naar andere genetische therapieën voor SCA3, zoals bijvoorbeeld ataxine-3 downregulatie door middel van viraal toegediende microRNAs. Ook lijkt CRISPR/Cas gemedieerde knockout een veelbelovend toekomstperspectief te hebben voor SCA3 behandeling. Het voordeel van dit soort viraal toegediende behandelingen is dat deze slechts eenmalig, of in ieder geval erg infrequent, geïnjecteerd moeten worden. AON gemedieerde behandelingsstrategieën hebben echter het voordeel dat distributie via intrathecale injectie in de hersenen erg goed is. Daarnaast wordt erg veel onderzoek gedaan naar chemische modificaties van AONs, welke de pharmacokinetische en -dynamische eigenschappen aanzienlijk verbeteren. In de klinische trials voor spinale musculaire atrofie blijken AONs goed verdragen te worden in het centrale zenuwstelsel van mensen en de uitermate hoopgevende resultaten hebben dan ook geleid tot goedkeuring van het medicijn (Spinraza) in Amerika en Europa. Deze resultaten duiden dus op een goed perspectief voor toepassing van AONs in andere neurodegeneratieve aandoeningen zoals SCA3.

LIST OF PUBLICATIONS

Evers, M. M., **Toonen, L. J.**, & van Roon-Mom, W. M. (2014). Ataxin-3 protein and RNA toxicity in spinocerebellar ataxia type 3: current insights and emerging therapeutic strategies. *Mol Neurobiol, 49*(3), 1513-1531. doi:10.1007/s12035-013-8596-2

Evers, M. M., **Toonen, L. J.**, & van Roon-Mom, W. M. (2015). Antisense oligonucleotides in therapy for neurodegenerative disorders. *Adv Drug Deliv Rev, 87*, 90-103. doi:10.1016/j.addr.2015.03.008

Zalachoras, I., Verhoeve, S. L., **Toonen, L. J.**, van Weert, L. T., van Vlodrop, A. M., Mol, I. M., . . . Meijer, O. C. (2016). Isoform switching of steroid receptor co-activator-1 attenuates glucocorticoid-induced anxiogenic amygdala CRH expression. *Mol Psychiatry, 21*(12), 1733-1739. doi:10.1038/mp.2016.16

Toonen, L. J., Schmidt, I., Luijsterburg, M. S., van Attikum, H., & van Roon-Mom, W. M. (2016). Antisense oligonucleotide-mediated exon skipping as a strategy to reduce proteolytic cleavage of ataxin-3. *Sci Rep, 6*, 35200. doi:10.1038/srep35200

Casaca-Carreira, J., **Toonen, L. J. A.**, Evers, M. M., Jahanshahi, A., van-Roon-Mom, W. M. C., & Temel, Y. (2016). In vivo proof-of-concept of removal of the huntingtin caspase cleavage motif-encoding exon 12 approach in the YAC128 mouse model of Huntington's disease. *Biomed Pharmacother, 84*, 93-96. doi:10.1016/j.biopha.2016.09.007

Toonen, L. J.A., Rigo, F., van Attikum, H., & van Roon-Mom, W. M. C. (2017). Antisense Oligonucleotide-Mediated Removal of the Polyglutamine Repeat in Spinocerebellar Ataxia Type 3 Mice. *Mol Ther Nucleic Acids, 8*, 232-242. doi:10.1016/j.omtn.2017.06.019

Toonen, L. J. A., Casaca-Carreira, J., Pellisé-Tintoré, M., Mei, H., Temel, Y. Jahanshahi, A.,& van Roon-Mom, W. M. C. (2018). Intracerebroventricular administration of a 2-'O-methyl phosphorothioate antisense oligonucleotide results in activation of the innate immune system in mouse brain. *Nucleic Acid Ther*, doi: 10.1089/nat.2017.0705.

Toonen, L. J. A., Overzier, M., Evers, M. M., Leon, L. G., van der Zeeuw, S. A. J., Mei, H., . . . & van Roon-Mom, W. M. C. (2018). Transcriptional profiling and biomarker identification reveal tissue specific effects of expanded ataxin-3 in a spinocerebellar ataxia type 3 mouse model. *Mol Neurodegener,* in revision

CURRICULUM VITAE

Lodewijk Julius Anton Toonen is geboren op 18 mei 1988 te 's-Hertogenbosch. Hij begon in 2005 de studie Biologie en Medische Laboratorium Techniek aan de Avans Hogeschool te Breda. In 2008 en 2009 liep hij stage bij Johnson and Johnson Pharmaceuticals te Beerse (België), bij de afdeling Toxicologie en vervolgens bij de afdeling Neuroscience. In 2009 behaalde Lodewijk zijn Bachelor of Science diploma, waarna hij de studie Biomedische Wetenschappen begon bij het LUMC te Leiden. Tijdens deze studie liep hij stage onder begeleiding van dr. Thijs Houben en prof. dr. Joke Meijer, waar hij onderzoek deed naar elektrofysiologische veranderingen in migraine muismodellen. Zijn afstudeerstage deed hij in het LACDR te Leiden, onder begeleiding van dr. Ioannis Zalachoras en prof. dr. Onno Meijer. Tijdens deze stage assisteerde hij in een onderzoek waarbij antisense oligonucleotiden gebruikt werden om de mechanismen van stress adaptatie in het muizenbrein vast te stellen. In 2012 behaalde hij zijn Master diploma, waarna hij begon met zijn promotieonderzoek binnen de afdeling Humane Genetica van het LUMC, onder supervisie van dr. Willeke van Roon-Mom. De resultaten van dit onderzoek staan beschreven in dit proefschrift. Sinds 2017 is Lodewijk werkzaam in dezelfde onderzoeksgroep als postdoctoraal onderzoeker, waar hij betrokken is bij het testen van antisense oligonucleotiden voor SCA3 en de ziekte van Huntington.

DANKWOORD

Een promotieonderzoek is een omvangrijk leerproces dat bovenal wordt gekenmerkt door teamwork. Ik heb de afgelopen jaren veel hulp gehad van enthousiaste en kundige collega's, zonder wie dit proefschrift er nooit had kunnen zijn. Ik wil jullie dan ook allemaal hartelijk bedanken voor jullie grote bijdrage aan dit onderzoek!

Allereerst wil ik mijn co-promotor Willeke bedanken. Jouw optimistische, gezellige, enthousiaste en bovenal kundige begeleiding is zonder twijfel de hoeksteen van dit proefschrift. Je stond voortdurend paraat om experimenten en ideeën te bespreken, kwam altijd met goede suggesties en had manuscripten en presentaties binnen no-time van deskundig commentaar voorzien. Bedankt voor je voortdurende vertrouwen, professionele ondersteuning en vrijheid die je aan al je promovendi geeft.

Ook mijn directe collega's hebben een belangrijke bijdrage aan dit proefschrift geleverd. Ten eerste Melvin, jouw succesvolle onderzoek was de basis voor mijn promotietraject. Met veel enthousiasme (en humor) heb je me ingewerkt op het SCA3 onderzoek en we hebben samen mooie papers geschreven en met veel plezier de congressen bezocht. Ontzettend bedankt voor je hulp en veel succes in je verdere onderzoek! Barry, jij bent zonder twijfel de steunpilaar van onze onderzoeksgroep en houdt het lab soepel draaiende. Bedankt voor al je goede suggesties en praktische hulp die je de afgelopen jaren gegeven hebt. Iris, ik had veel geluk dat jij het SCA3 onderzoek kwam versterken en me hebt kunnen helpen met vele succesvolle qPCRs en blotjes. Maurice, de *in vivo* expert, jouw stereotact- en gedragstest vaardigheden hebben ons enorm verder geholpen, bedankt hiervoor! Menno, een van een handjevol die in staat is mooie huntingtine blots te maken, bedankt voor het delen van al je westernblot kennis en de gezelligheid die je bracht in het lab en onze kamer, alsook onze discussies over de pitfalls van het onderzoek doen. Tassos, thanks for your advice during my PhD and best of luck continuing your career in Greece! Recentelijk wordt ons team ook versterkt door Linda; bedankt voor je hulp en inzet voor het Huntington project, het is erg fijn samenwerken met jou!

Ook Nisha, Elena, Sarah, Ronald en Isabella wil ik graag bedanken voor sporadisch experimenteel advies maar vooral ook de goede sfeer, humor en gezelligheid die jullie ons kantoor brengen/gebracht hebben. Collega's als jullie maken het erg fijn werken in onze kamer!

Ik heb ook het geluk gehad om uitstekende ondersteuning te krijgen in het lab van gemotiveerde studenten. Amena, Anastassia en Robyn, heel erg bedankt voor jullie inzet in je eigen ataxine-3 subprojecten. Jullie hebben alle drie erg goed onderzoek uitgevoerd en mogen trots zijn op jullie stage! Een begeleider leert net zoveel van een student als andersom en ook hiervoor ben ik jullie dankbaar. Vanuit mijn eigen studententijd moet ik vooral Ioannis en Onno bedanken om mij wegwijs te maken in het exon-skip veld en me vervolgens te helpen om deze promotieplek te bemachtigen.

We zijn de afgelopen jaren ook goede samenwerkingen aangegaan met andere labs om zo expertise te delen. João, Ali and Yasin, thank you so much for the great collaboration on the Huntington AON project. We've undoubtedly encountered many setbacks, but together we were still able to get two good publications out of our efforts. Thanks a lot for the great collaboration and good luck in your future research efforts! Haico, Martijn en Wouter, de samenwerking met jullie is het bewijs van een succesvolle fusie tussen HG en Toxgen. Jullie suggesties en praktische hulp zijn een prachtige toevoeging gebleken aan het ataxine-3 exon skip onderzoek; dank hiervoor! Frank Rigo, your collaboration has been a great helping hand in achieving *in vivo* AON efficacy, thanks a lot for your support. We hebben de laatste jaren ook uitstekende bioinformatische ondersteuning gekregen bij onze multi-omics experimenten. Leticia and Peter-Bram, thanks a lot for performing the RNA seq analysis, it would not have been possible without you. Linda S, bedankt voor de hulp bij de mass spec! Hailiang, Olafur, Sander, Szymon, Kristina and Eleni, thanks a lot for assisting with the data processing, analysis and general sharing of expertise in the field of omics data!

Mijn promotor Johan wil ik graag bedanken voor de goede begeleiding en feedback, met name in de laatste fase van het promotietraject. Annemieke, jij ook heel erg bedankt voor al het advies over AON gerelateerde experimenten en je feedback op alle manuscripten. Ook jullie onderzoeksgroepen, het LGTC, de DMD groep en overige leden van Lab-J, helaas te veel om hier individueel op te noemen, zou ik graag willen bedanken voor de uitstekende samenwerking. Jullie stonden altijd paraat om advies te geven over technieken waarmee we nog geen ervaring hadden, reagentia te delen en bovenal te zorgen voor veel gezelligheid en een stimulerende werkomgeving. Babs, bedankt voor je hulp bij alle promotieregelingen. Ook de overige collega's van de afdeling Humane Genetica bedank ik graag voor hun hulp, suggesties en vooral ook de goede werksfeer. Dominique en René, bedankt dat jullie ons onderzoek mede mogelijk hebben gemaakt.

Tot slot moet ik ook mijn ouders bedanken voor de voortdurende ondersteuning. Zonder jullie was ik nooit zo ver gekomen, bedankt voor alles.